Spring 5-7-2016

The Role of DNA Methyltransferases in Normal and Malignant Hematopoiesis

Staci Haney
University of Nebraska Medical Center

THE ROLE OF DNA METHYLTRANSFERASES IN NORMAL AND MALIGNANT MOUSE HEMATOPOIESIS

By

Staci L. Haney

A DISSERTATION

Presented to the Faculty of

The University of Nebraska Graduate College

In Partial Fulfillment of the Requirements

For the Degree of Doctor of Philosophy

Genetics, Cell Biology, and Anatomy

Graduate Program

Under the Supervision of Professor Rene Opavsky

University of Nebraska Medical Center

Omaha, NE

April, 2016

Supervisory Committee:

Shantaram Joshi, Ph.D. Runqing Lu, Ph.D.

David Klinkebiel, Ph.D. Jenny Wang, Ph.D

ACKNOWLEDGEMENTS

First, I would like to thank my advisor, Rene Opavsky, for not only accepting me into his lab but for providing outstanding mentorship over the past 5 years. I am also eternally grateful to the other members of our lab, Ryan Hlady, Jana Opavska, and Michael Upchurch for all of their hard work.

Next, I would like to thank Dave Klinkebiel for his help with analyzing global methylation data. This project would not have been possible without his expertise.

I would also like to thank the other members of my committee: Dr. Jenny Wang, Dr. Shantaram Joshi, and Dr. Runqing Lu for their support and guidance over the years.

Lastly, I would like to thank my family, especially my husband, Ryan, for always believing me and encouraging me to do whatever makes me happy

THE ROLE OF DNA METHYLTRANSFERASES IN NORMAL AND MALIGNANT MOUSE HEMATOPOIESIS

Staci L Haney, Ph.D.

University of Nebraska Medical Center, 2016

Supervisor: Rene Opavsky, Ph.D.

DNA methylation is an epigenetic modification that regulates gene transcription. The addition of a methyl group to cytosine is catalyzed by a family of enzymes known as DNA methyltransferases (Dnmts). The three catalytically active Dnmts in humans and mice are Dnmt1, Dnmt3a, and Dnmt3b. DNA methylation is clinically relevant, as aberrations in the methylation landscape are a hallmark of nearly all human cancers. Cancer methylomes are typically characterized by genome wide hypomethylation and regional specific hypermethylation, both of which have been linked to alterations in gene expression. In order to understand the contribution of epimutations to the development of hematological malignancies we created several mouse models in which one or more Dnmt is deleted in hematopoietic stem cells and all downstream lineages. This allowed us to address the role of individual Dnmts in normal and malignant hematopoiesis. We found that Dnmts contribute to the cancer methylome through both *de novo* and maintenance methylation, and that activities of individual Dnmts seldom overlap with one another. We identified Dnmt1 as being critical for T cell development and maintenance of the tumor phenotype in T cell lymphomas. Furthermore, we identified Dnmt3a and Dnmt3b as critical tumor suppressor genes in the prevention of chronic lymphocytic leukemia in mice. Collectively, these studies provide insight into the effects of Dnmt deregulation in tumorigenesis.

TABLE OF CONTENTS

ACKNOWLEDGEMENTS..…….. i

ABSTRACT…… ii

TABLE OF CONTENTS……..……. iii

LIST OF FIGURES..……. v

LIST OF ABBREVIATIONS……. x

INTRODUCTION…….. 1

DNA methylation in mammalian cells…….…… 1

Methylation independent repressor function of Dnmts…….. 2

DNA methylation and cancer……. 3

The role of Dnmt3a in hematological malignancies……... 5

The role of Dnmt1 in tumorigenesis…….. 7

The role of Dnmt3b in tumorigenesis……. 8

Hypothesis…… 9

CHAPTER 1: Essential Role for Dnmt1 in the Prevention and Maintenance of MYC-Induced T-Cell Lymphomas

Introduction……... 11

Methods……. 13

Results…….. 18

Discussion……. 39

CHAPTER 2: Methylation-independent repression of Dnmt3b contributes to oncogenic activity of Dnmt3a in mouse MYC-induced T-cell lymphomagenesis

Introduction……... 45

Methods……. 48

Results…….. 51

Discussion……. 87

CHAPTER 3: Tumor suppressor functions of Dnmt3a and Dnmt3b in the prevention of malignant mouse lymphopoiesis

Introduction……... 92

Methods……. 93

Results…….. 95

Discussion……. 110

CHAPTER 4: Promoter hypomethylation and expression is conserved in mouse chronic lymphocytic leukemia induced by decreased or inactivated Dnmt3a

Introduction……... 112

Methods……. 114

Results…….. 120

Discussion……. 148

DISCUSSION…… 153

BIBLIOGRAPHY……... 164

LIST OF FIGURES

CHAPTER 1:

Figure 1. Loss of Dnmt1 delays MYC-induced T-cell lymphomagenesis….. 21

Figure 2. Loss of Dnmt1 results in decreased proliferation and is critical for tumor cell survival……. 24

Figure 3. Loss of *Dnmt1* impairs T-cell development…… 27

Figure 4. Impaired hematopoiesis in *MYC*; *Dnmt1*$^{-/-}$ mice…….. 29

Figure 5. Analysis of DNA methylation in Dnmt1-deficient tumors…….. 32

Figure 6. Significantly deregulated genes in *MYC*; *Dnmt1*$^{-/-}$ tumors……. 35

Figure 7. H2-Ab1 is a target of Dnmt1-mediated methylation in lymphomas 38

CHAPTER 2:

Figure 1. Ablation of Dnmt3a delays T-cell lymphomagenesis …..... 53

Figure 2. Dnmt3a inactivation decreases cellular proliferation during disease progression……. 57

Figure 3. Dnmt3a ablation results in genome-wide methylation changes in *MYC;Dnmt3a*$^{\Delta/\Delta}$ lymphomas…….. 64

Figure 4. Loss of Dnmt3a leads to deregulated transcription…….. 69

Figure 5. DNA methylation-independent upregulation of tumor suppressor genes in Dnmt3a-deficient lymphomas……. 73

Figure 6. Dnmt3a represses Dnmt3b expression independently of its catalytic activity……. 77

Figure 7. Loss of Dnmt3b accelerates lymphomagenesis in Dnmt3a-deficient mice…… 80

Supplementary Figure S1. MYC expression is similar between control and Dnmt3a-deficient lymphomas……. 54

Supplementary Figure S2. Tumor burden in control and Dnmt3a-deficient mice……. 55

Supplementary Figure S3. Loss of Dnmt3a does not effect T-cell development…….. 58

Supplementary Figure S4. EGFP expression in thymocytes from control and Dnmt3a-deficient mice……. 59

Supplementary Figure S5. Analysis of Annexin V staining by FACS…… 60

Supplementary Figure S5. Analysis of Annexin V staining by FACS 2…… 61

Supplementary Figure S7. Summary of differentially methylated genes in Dnmt3a-deficient tumors……. 65

Supplementary Figure S8. Global methylation profiling by MSCC using 1 tag analysis…… 66

Supplementary Figure S9. Summary of Ingenuity pathway analysis…… 70

Supplementary Figure S10. MSCC analysis of promoter methylation for the 17 gene signature obtained from IPA……. 73

Supplementary Figure S11. Quantification of total gene body methylation for the 17 gene signature obtained from IPA……... 74

Supplementary Figure S12. MSCC analysis of gene body methylation of four tumor suppressor genes……. 75

Supplementary Figure S13. Relative Dnmt3b protein levels in three cell lines after Dnmt3a expression…… 78

Supplementary Figure S14. Representative Annexin V and BrdU staining in control and DKO thymocytes…… 81

Supplementary Figure S15. Analysis of T-cell development in control and DKO mice…….. 82

Supplementary Figure S16. Summary of tumor burden in control and DKO mice…….. 83

Supplementary Figure S17. MYC expression is similar between control and DKO tumors…….. 84

Supplementary Figure S18. Summary of tumor immunophenotypes in control and DKO mice…….. 85

Supplementary Figure S19. Representative FACS analysis of T-cell lymphomas in control and DKO mice…… 86

CHAPTER 3:

Figure 1. Loss of Dnmt3a induces CLL in mice……. 99

Figure 2. Loss of Dnmt3b accelerates tumor development in *Dnmt3a*$^{-/-}$ mice and alters the disease spectrum…… 108

Figure S1. Analysis of EGFP and cell surface marker expression in *Dnmt3a*$^{+/+}$ and *Dnmt3a*$^{-/-}$ mice …… 101

Figure S2. Cellularity of Dnmt3a and Dnmt3a/Dnmt3b knockout mice…….. 102

Figure S3. Deletion efficiency of Dnmt3a conditional knockout allele in *Dnmt3a*$^{-/-}$ tumors ..……. 103

Figure S4. Histological analysis of *Dnmt3a*$^{-/-}$ splenic tumors …….. 104

Figure S5. *Dnmt3a*$^{-/-}$ splenic tumor cells induce splenomegaly and CLL disease in recipient mice…… 105

Figure S6. Methylation analysis of gene bodies and repetitive elements….. 106

Figure S7. Schematic representation of the genetic setting to delete conditional alleles of Dnmt3a and Dnmt3b in hematopoietic system…….. 109

CHAPTER 4:

Figure 1. Dnmt3a heterozygous mice develop CLL…… 122

Figure 2. *Dnmt3a*$^{+/-}$ mice also develop non-malignant myeloproliferative disorder……. 129

Figure 3. DNA methylome and transcriptome of normal mouse B-1a cells……... 132

Figure 4. DNA methylome of CLL induced by decrease or absence of Dnmt3a…….. 135

Figure 5. Dnmt3a has a cancer-specific maintenance function ……. 140

Figure 6. Decreased Dnmt3a levels result in deregulated transcription in Dnmt3a$^{+/\Delta}$ CLL similar to Dnmt3a$^{\Delta/\Delta}$ CLL ……... 142

Figure 6. Decreased Dnmt3a levels result in deregulated transcription in Dnmt3a$^{+/\Delta}$ CLL similar to Dnmt3a$^{\Delta/\Delta}$ CLL ……... 146

Figure S1. Dnmt3a heterozygous mice develop CLL…….. 124

Figure S2. Normal hematopoiesis in 6-week old *Dnmt3a*$^{+/-}$ mice …… 125

Figure S3. Deregulated methylation in *Dnmt3a*$^{\Delta/\Delta}$ and *Dnmt3a*$^{+/\Delta}$ CLL……. 137

Figure S4. Related to Figures 6 and 7. Ingenuity pathway analysis of differentially expressed genes…….. 147

LIST OF ABBREVIATIONS

4-OHT	4-hydroxytamoxifen
AML	acute myeloid leukemia
Bp	base pair
CLL	chronic lymphocytic leukemia
COBRA	combined bisulfite restriction analysis
DKO	double knockout
DMC	differentially methylated cytosine
DMR	differentially methylated region
Dnmts	DNA methyltransferases
EGFP	enhanced green fluorescent protein
FDR	false discovery rate
HDACs	histone deacetylases
HSC	hematopoietic stem cell
IPA	Ingenuity Pathway analysis
LSK	Lineage-negative, Sca1-positive, ckit-negative
MBL	monoclonal B cell lymphocytosis
MPD	myeloproliferative disorder
MSCC	methyl sensitive cut counting
MTCL	Myc-induced T cell lymphoma
PTCL	peripheral T cell lymphoma
RRBS	reduced representation bisulfite sequencing
TCLs	T cell lymphomas
TS	tumor suppressor

TSS	transcriptional start site
WGBS	whole genome bisulfite sequencing

INTRODUCTION

DNA methylation in mammalian cells.

DNA methylation plays a critical role in many biological processes, including regulating gene expression, silencing of retroviruses, X-chromosome inactivation, genomic imprinting, and differentiation (1). DNA methylation primarily occurs in the context of CpG dinucleotides, is asymmetrical and cell-type specific (1). In general, DNA methylation at promoter regions is associated with the inhibition of gene transcription (2), while increased gene body methylation is postulated to promote gene transcription (3). The three active mammalian DNA methyltransferases, Dnmt1, Dnmt3a, and Dnmt3b, are responsible for catalyzing the addition of a methyl group to the 5th position of the cytosine ring. All three Dnmts are critical for development, as demonstrated by knockouts generated in mice. Deletion of Dnmt1 and Dnmt3b are embryonically lethal, while loss of Dnmt3a results in death of mice around 4 months of age, likely due to multi organ failure (4, 5).

Dnmt3a and Dnmt3b are largely responsible for *de novo* methylation during early embryogenesis. While both enzymes are responsible for the establishment of methylation patterns, they each display non-overlapping functions during mouse embryonic development. Dnmt3b for example is almost exclusively involved in the methylation of minor satellite repeats at centromeres (5). The sequence-specificity of Dnmts is further demonstrated by findings in mouse embryonic stem cells (ES cells) in which the expression of only Dnmt1, and not Dnmt3a or Dnmt3b, results in a lack of methylation at imprinted genes and genomic repeats, suggesting that these loci are *de novo* methylated by either Dnmt3b or Dnmt3a (6). In contrast, Dnmt1 was initially classified as a maintenance enzyme, due to its high affinity for hemi-methylated sites (7).

The unique regulatory domain of Dnmt1 functions by binding to PCNA during cellular divisions, thus allowing it to read existing methylation patterns and duplicate them on the newly synthesized DNA strand (8). While the *de novo* and maintenance classifications are convenient, further investigation into the discrete roles of Dnmts has changed the way we think about the formation and maintenance of the methylation landscape.

Several reports suggest that Dnmt1 can also function as a *de novo* methyltransferase. For example, overexpression of Dnmt1 induced locus-specific *de novo* methylation in human fibroblasts that was associated with specific sequence motifs (9, 10). Additionally, knockout of Dnmt1 in ES cells suggests *de novo* activity for Dnmt1 at repeat elements and single-copy genes (11). We found that Dnmt3a and Dnmt3b function in the cancer-specific maintenance methylation of gene promoters (12, 13), while others showed that Dnmt3a maintained lowly methylated canyon regions (14). Despite an ever increasing body of research, a complete understanding of the individual roles of Dnmts in normal cells and various disease states remains elusive.

Methylation independent repressor function of Dnmts.

In addition to their roles as methyltransferases, Dnmts can function to repress gene transcription in a methylation independent manner (18). The methylation independent repressor activity has been well demonstrated for Dnmt3a. The conserved C-terminal domain of Dnmt3a mediates the addition of methyl groups to DNA, while the N-terminal regulatory domain mediates interactions with DNA and other proteins (15). While Dnmt3a can regulate transcription via methylation at CpG dinucleotides found in the promoter and other regulatory regions (15), it can also repress transcription in a methylation-independent manner through interaction with histone deacetylases (HDACs) and other repressor proteins via its ATRX-like domain (16). For instance, Dnmt3a interacts with the methyl CpG binding domain of Mbd3 and Brg1 to silence expression of

the metallothionein-I gene in mouse lymphosarcoma cells (17). Likewise, *in vitro* studies found that RP58, a transcriptional repressor, targeted Dnmt3a to a synthetic promoter to silence gene expression in a methylation-independent manner (16). In addition to Dnmt3a's ability to interact with transcriptional repressors, it may also interfere with the ability of transcription factors to bind to regulatory elements on chromosomes to activate transcription. For instance, p53-mediated transactivation of the *CDKN1A* gene was inhibited by direct Dnmt3a binding with p53 without changes in DNA methylation (18). Which proteins facilitate the recruitment of Dnmt3a to specific loci is difficult to predict, given that Dnmt3a can interact with at least 68 transcription factors (19). Overall, the methylation-independent activity of Dnmts is a lesser studied area and its prevalence and effects on physiological processes not fully known.

DNA methylation and cancer.

Due to its role in several critical biological processes, it is not surprising that aberrant DNA methylation is a hallmark of nearly all cancers. For decades the DNA methylation field has focused on the identification of tumor suppressors that become inactivated by promoter hypermethylation in tumors. The discovery that loci encoding tumor suppressors, p21 and p15, are both hypermethylated and silenced in human hematological malignancies (20, 21) led many to believe that all methyltransferases function as oncogenes. Since DNA methylation if reversible, removal of this hypermethylation could lead to the re-expression of tumor suppressor genes. These concepts lead to the creation of Dnmt inhibitors, such as 5-azacytidine and decitabine, which shows modest success in the treatment of myelodysplastic syndrome and acute myeloid leukemia (22). However, the use of such hypomethylating agents overlooks three important aspects: 1) the unique roles of individual Dnmts in the generation and maintenance of the cancer methylome, as methylation inhibitors are non-specific and

believed to inhibit all methyltransferases equally, 2) promoter hypomethylation and oncogene expression and 3) genomic instability induced by hypomethylation. Thus, further understanding of the role of individuals Dnmts in the generation and maintenance of the cancer epigenome, as well as the effect of inhibition of these enzymes is needed.

While the DNA methylation field has focused mainly on the identification of hypermethylated tumor suppressors, little attention has been paid to the role of promoter hypomethylation and expression of oncogenic modifiers. Studies in solid tumors found that putative oncogenes WNT5A, S100P, and CRIP1 are demethylated and overexpressed in human prostate cancer (23). Others found that promoter hypomethylation of protease urokinase results in its overexpression, which is associated with tumor progression in breast and prostate cancers (24, 25).

In addition to oncogene re-expression, DNA hypomethylation may also result in genomic instability and an increased susceptibility to spontaneous mutations, chromosomal breaks, and re-expression of normally silenced retroviral elements (26). Some suggest that as the genome increased in complexity and size the risk brought forth by unrestricted movable elements increased dramatically and that DNA methylation evolved as a way to protect the genome from the spread outside elements (27). Several reports in mice and humans support the idea that DNA methylation “protects” the genome. For instance, *in vivo* studies in mice carrying a hypomorphic allele of Dnmt1 were found to develop T-cell lymphomas, likely due to hypomethylation and genomic instability that resulted in the generation of oncogenic Notch1 (28). Studies in human prostate cancer found a significant correlation between alterations on chromosome 8 and genome wide hypomethylation (29), while a similar study noted an association between hypomethylated Sat2 sequences and 1q copy gain with a 1q12 breakpoint in hepatocellular carcinoma (30). Together, these studies demonstrate the importance of

hypomethylation in tumorigenesis and highlight the need for additional studies investigating the potential tumor suppressor role of Dnmts.

Hypomethylation in tumors may results from inactivation or reduction in the levels of Dnmts. To understand the role of Dnmts in tumorigenesis, numerous conditional Dnmt knockouts were created. For instance, *Dnmt1*$^{chip/-}$ mice which have drastically low levels of Dnmt1 develop T-cell lymphomas around 8 months of age, despite severely compromised T-cell development (31, 32). To gain deeper insight into the function of Dnmt1 in lymphoid malignancies, we genetically inactivated Dnmt1 in a mouse model of MYC-induced T-cell lymphomagenesis and found that Dnmt1 is critical for the prevention and maintenance of T-cell lymphomas (33). Using the same model, we demonstrated that loss of Dnmt3b accelerated tumorigenesis and lead to the hypomethylation and ovexpression of the oncogenic modifier Ment, suggesting that Dnmt3b functions as a tumor suppressor (13). The tumor suppressor activity for Dnmt3b is further supported in mouse models of B-cell malignancies, by us and others (34, 35). Work from our lab and others show that loss of Dnmt3a expression in hematopoietic stem cells is sufficient to induce a wide range of hematological malignancies in mice, including chronic lymphocytic leukemia, myelodysplastic syndrome, and T-cell lymphoma (34, 36, 37). Such results, coupled with the high mutation rates of DNMT3A in human hematological malignancies has led to profound interest into the tumor suppressor properties of Dnmt3a in malignant hematopoiesis.

The role of Dnmt3a in hematological malignancies.

Next generation sequencing of human tumors has identified DNMT3A as a mutational hotspot in human hematological malignancies. Mutations in the DNMT3A coding sequence have been reported in 22% of patients with acute myeloid leukemia (38), 8% of myelodysplastic syndrome (39), 7% of primary myelofibrosis (40), 7% of

chronic myelomonocytic leukemia (41) and 11% of T-cell lymphomas (42). Two studies have suggested that DNMT3A mutations occur very early in pre-leukemic cells and likely serve as an initiating mutation (43, 44). Importantly, pre-leukemic cells with DNMT3A mutations were found in the blood of patients in remission from AML, indicating they can survive chemotherapy treatment and upon acquisition of additional mutations may spur a relapse (43, 44). This idea is supported by the fact that Dnmt3a deficient hematopoietic stem cells (HSC) have an increased ability to cell renew and their expansion over time may lead to an increased ability to promote pre-leukemic cells (45).

While mutations have been found throughout the DNMT3A loci, they largely cluster in the c-terminal catalytic domain. Mutations are almost always heterozygous, and not homozygous (46). Arginine 882 is a mutational hotspot, accounting for 58% of mutations in AML and 23% of mutations in T-call acute lymphoblastic leukemia (46). In vitro studies showed that the R882H mutation functions in a dominate-negative manner by inhibiting the wild-type proteins ability to form tetramers (47). In mice, overexpression on the R882H DNMT3A mutant in hematopoietic stem cells resulted in the development of chronic myelomonocytic leukemia within 12 months (48). In patients with AML, the R882 mutation is associated with global hypomethylation (49). This loss of methylation is most prominent at promoters, with loci encoding HOX genes being significantly affected (49). These studies suggest that mutations found in human tumors, in particular R882H, disrupt normal Dnmt3a function which result in epimutations that likely play a role in tumorigenesis. Furthermore, understanding the functional consequence of these mutations may be of critical importance for the development of new therapies.

Due to the significant mutation rate of DNMT3A in human hematological malignancies, our lab was interested in further elucidating the role of Dnmt3a in malignant hematopoiesis. To do so we utilized a conditional knock out model, in which

Dnmt3a is deleted in hematopoietic stem cells and all downstream lineages (34). Surprisingly, all Dnmt3a-deficient mice developed a disease similar to chronic lymphocytic leukemia (CLL) by one year of age. Next, we asked whether Dnmt3a haploinsufficiency can induce a CLL-like disease or other hematologic malignancies by observing *Dnmt3a*$^{+/-}$ mice. Likewise, long-term Dnmt3a decrease results in the development of a CLL-like disease in 65% of mice and myeloproliferative disease in 15% of mice within 16 months. Whole-genome bisulfite sequencing (WGBS) revealed significant hypomethylation in tumors. Later studies performed by Mayle et al., and Celik et al., found that deletion of Dnmt3a in the hematopoietic compartment of mice resulted in the development of a wide-range of malignancies, including myelodysplastic syndrome, acute myeloid leukemia, primary myelofibrosis, and T- and B-cell acute lymphocytic leukemia. Altogether, these findings demonstrate that reduction in Dnmt3a levels has profound phenotypic consequence on both the cellular and molecular levels, and identify Dnmt3a as a tumor suppressor gene in the prevention of myeloid, B- and T-cell transformation.

The role of Dnmt1 in tumorigenesis.

While DNMT3A is heavily mutated in human tumors, DNMT1 is mutated less frequently. DNMT1 is mutated in about 7% of cases of colorectal adenocarcinoma and 1.6% of prostate cancer (50-53), while mutations in hematologic malignancies are very rare, with only one mutation found to date in AML (54). Studies in human T cell, B cell, and myeloid malignancies revealed an increase in the levels of DNMT1 in tumors, suggesting a possible role in tumor maintenance (55, 56). Functional studies in mice have provided profound insight in the roles of Dnmt1 in tumorigenesis. One study using a mouse model of colorectal cancer found that decreased levels of Dnmt1 in *Apc*$^{Min/+}$ mice resulted in an increased tumor incidence at early stages of colon cancer (57).

Dnmt1 was also found to function as a tumor suppressor in a simian virus 40 (SV40)-induced tumorigenesis model of prostate cancer (57, 58). In addition to its role in solid tumors, several reports suggested an important role for Dnmt1 in normal and malignant hematopoiesis. Using *Dnmt1*$^{chip/-}$ mice, near complete reduction in Dnmt1 levels in mice resulted in the development of CD4+CD8+ T cell lymphomas (31, 32). In an AML model driven by MLL-AF9 overexpression, a reduction in Dnmt1 delayed leukemogenesis and impaired leukemic stem cell self-renewal, indicating a key role for Dnmt1 in the maintenance and establishment of leukemia (59). To further elucidate the role of Dnmt1 in malignant hematopoiesis, we deleted Dnmt1 in a mouse model of MYC-induced T-cell lymphomagenesis (MTCL). Reduction in Dnmt1 delayed lymphomagenesis by suppression of normal hematopoiesis and by impairing proliferation of tumor cells. Collectively, these studies illustrate a critical role for Dnmt1 in both tumor development and maintenance for solid and hematological malignancies.

The role of Dnmt3b in tumorigenesis.

Despite similarities in sequence homology and function, unlike DNMT3A, DNMT3B is very rarely mutated in human tumors. While not linked with tumorigenesis, germline mutations in DNMT3B are associated with the very rare immunodeficiency-centromeric instability-facial anomalies (ICF) syndrome, which is characterized by global hypomethylation and chromosome instability (60). In addition, Shen et al., identified single-nucleotide polymorphisms (SNPs) in DNMT3B that were associated with increased risk of developing lung cancer (61).

Despite the lack of observed mutation, there are several lines of evidence to suggest that alterations in the levels or activity of Dnmt3b plays a role in tumorigenesis. In mice, two separate studies using MYC-induced models of T- and B-cell lymphoma identified Dnmt3b as a tumor suppressor gene (13, 35). Likewise, we found that loss of

Dnmt3b accelerated the development of CLL in Dnmt3a-deficient mice (34). In fact, additional evidence exists suggesting that Dnmt3b may play a role in CLL pathogenesis. Down-regulation of DNTM3B in CLL was first noted almost a decade ago (62). Furthermore, analysis of available microarray data from 448 human CLL samples revealed that DNMT3A and DNMT3B are in the top 1% of the most frequently under-expressed genes (63). Consistent with the down-regulation of Dnmts, whole-genome bisulfite sequencing of human CLL samples reveled massive hypomethylation of the genome, suggesting that loss of methylation may play a pivotal role in the pathogenesis of the disease (64). Furthermore, in the TCL1 transgenic mouse model of CLL, it was reported that Tcl1 binds Dnmt3a and Dnmt3b and inhibits their activity, resulting in hypomethylation even prior to leukemia onset, suggesting that inhibition of Dnmts is likely partially responsible for CLL pathogenesis in this model (65). Collectively, these findings suggest that suppression of Dnmt3b likely plays a critical role in the transformation of multiple hematopoietic lineages, including B cells.

There is also evidence to suggest an oncogenic role for Dnmt3b. One study found that the overexpression of Dnmt3b was responsible for the hypermethylation phenotype observed in breast cancer cells (66). Likewise, Dnmt3b and Dnmt1 were found to cooperate to maintain DNA methylation and gene silencing in human cancer cells (67). Such hypermethylation may result in the inactivation of tumor suppressor genes, whose absence could contribute to disease pathogenesis.

Hypothesis.

Given that aberrant DNA methylation is hallmark of virtually all human tumors, and that alterations in the methylation landscape can have a direct effect on gene transcription and genomic stability, we sought to further elucidate the roles of individual

Dnmts in tumorigenesis. To accomplish this, several tumor studies using various Dnmt knockout mice were generated.

In Chapter 1, to further elucidate the role of Dnmt1 in malignant hematopoiesis and to determine Dnmt1's contribution to aberrant DNA methylation in cancer, we used a conditional knockout approach to inactivate Dnmt1 in a mouse model of MYC-induced T-cell lymphomagenesis with the hypothesis that loss of Dnmt1 will accelerate tumorigenesis in mice. Conversely, we show that loss of Dnmt1 delayed lymphomagenesis by suppression of normal hematopoiesis and by impairing proliferation of tumor cells, illustrating that Dnmt1 is required for maintenance of the tumor phenotype (33).

In Chapter 2, to understand the role of Dnmt3a in lymphomagenesis, we again use the MYC-induced T-cell lymphoma model in conjunction with a *Dnmt3a*$^{-}$ allele. We hypothesized that Dnmt3a will function as a tumor suppressor in this model, given the broad range of human malignancies that harbor DNMT3A mutations. Surprisingly, loss of Dnmt3a extends the survival of mice due to a decrease in cellular proliferation and the upregulation of a subset of tumor suppressor genes likely regulated by Dnmt3a's methylation independent repressor function (12).

In Chapters 3 and 4, we use a conditional Dnmt3a knockout (in the absence of MYC), and conventional Dnmt3a-heterozygous mice to examine the role of Dnmt3a in normal and malignant hematopoiesis. We hypothesized that loss or decrease in Dnmt3a levels would have profound effect on long-term hematopoiesis, resulting in the development of hematological malignancies similar to those observed in humans with DNMT3A mutations. Interestingly, we found that Dnmt3a is a haploinsufficient tumor suppressor in the prevention of chronic lymphocytic leukemia and myeloproliferative disorder.

CHAPTER 1: Essential Role for Dnmt1 in the Prevention and Maintenance of MYC-Induced T-Cell Lymphomas[1]

Introduction

Cytosine methylation is an epigenetic mark that is abundant throughout intragenic and intergenic regions within the mammalian genome. The methylation of gene promoters has been associated with gene repression, while the methylation of gene bodies may promote proper transcription (68, 69). Due to its genome-wide distribution and effects on transcriptional regulation, DNA methylation plays a critical role in a wide range of physiological processes, including silencing of endogenous retroviral elements, X-chromosome inactivation, imprinting, proliferation, differentiation, and apoptosis (70, 71). The disruption of normal methylation patterns contributes to the pathogenesis of a variety of human diseases such as neurodegenerative, developmental, and autoimmune disorders (72, 73). In particular, global deregulation of cytosine methylation is apparent in cancer, where genome-wide hypomethylation is suggested to promote tumorigenesis by invoking genomic instability and upregulating oncogenes, whereas aberrant promoter hypermethylation supports tumorigenesis by silencing tumor suppressor genes (15).

Whereas the association of deregulated methylation with cancer is well established, the individual roles of the enzymes catalyzing DNA methylation, DNA methyltransferases (Dnmts), in the pathogenesis of human cancer are unclear. Three catalytically active Dnmts (Dnmt1, Dnmt3a, and Dnmt3b) are responsible for the

[1] The material presented in this chapter were previously published: Peters SL, Hlady RA, Opavska J, Klinkebiel D, Novakova S, Smith LM, et al. Essential role for Dnmt1 in the prevention and maintenance of MYC-induced T-cell lymphomas. Molecular and cellular biology. 2013;33(21):4321-33.

generation and maintenance of methylation patterns in the mammalian genome. While Dnmt3a and Dnmt3b are associated with de novo methylation because of their involvement in the establishment of normal methylation patterns (5, 74), Dnmt1 is

essential for maintenance of the methylation landscape due to its ability to recognize hemimethylated DNA and conserve methylation during somatic cellular division (75). However, the discrete roles of Dnmts in the formation and maintenance of the methylation landscape are more complex. Several studies have suggested that Dnmt1 may function as a de novo enzyme. For example, overexpression of Dnmt1 induced locus-specific de novo methylation in human fibroblasts that was associated with specific sequence motifs (9, 10). Additionally, knockout of Dnmt1 in embryonic stem cells suggests de novo activity for Dnmt1 at repeat elements and single-copy genes (11). Although the main function of Dnmt1 appears to be related to cytosine methylation, Dnmt1 also interacts with a large number of repressor proteins, such as histone deacetylases and DNA methyltransferase-associated protein 1 (DMAP1), to inhibit transcription in a methylation-independent manner (76-78).

Recent studies have identified somatic mutations in DNMT1 in cancer; however, they are infrequent. DNMT1 is mutated in about 7% of cases of colorectal adenocarcinoma and 1.6% of prostate cancer as well as a small subset of cases of acute myeloid leukemia (AML) (50-53). Furthermore, increased DNMT1 expression is observed in subsets of human T-cell, B-cell, and myeloid malignancies, suggesting that DNMT1 may be important for tumor maintenance (55, 56). Functional studies in mice have shown that decreased levels of Dnmt1 resulted in an increased tumor incidence at early stages of colon cancer in $Apc^{Min/+}$ mice and simian virus 40 (SV40)-induced tumorigenesis in the prostate, suggesting a tumor suppressor function for Dnmt1 in these models (57, 58). Mutations in hematologic malignancies are very rare, with only

one mutation found to date in AML (54). Studies in mice suggested an important role for Dnmt1 in myeloid malignant hematopoiesis. In an AML model driven by MLL-AF9 overexpression, a reduction in Dnmt1 delayed leukemogenesis and impaired leukemic stem cell self-renewal, indicating a key role for Dnmt1 in the maintenance and establishment of leukemia (59). In contrast, a severe reduction in levels of Dnmt1 clearly promotes transformation of T cells. A combination of a hypomorphic Dnmt1chip allele (expressing only 10% of Dnmt1 levels relative to the wild-type allele) with a conventional Dnmt1 knockout allele in Dnmt1chip/− mice resulted in the development of T-cell lymphomas (TCLs) by 8 months of age, despite severely impaired T-cell development (31, 32). To further elucidate the role of Dnmt1 in malignant hematopoiesis and to determine Dnmt1's contribution to aberrant DNA methylation in cancer, we used a conditional knockout approach to inactivate Dnmt1 in a mouse model of MYC-induced T-cell lymphomagenesis. Here we show that loss of Dnmt1 delayed lymphomagenesis by suppression of normal hematopoiesis and by impairing proliferation of tumor cells. Global approaches identified 730 gene promoters differentially methylated in normal thymocytes, MYC-induced T-cell lymphomas (MTCLs), and MTCLs deficient for Dnmt1, suggesting that Dnmt1 contributes to the cancer methylome by both de novo and maintenance activity. Thus, our studies not only provide a biological mechanism explaining delayed lymphomagenesis in the absence of Dnmt1 but also identify Dnmt1 target genes for the first time in the relevant in vivo setting.

Methods

Mouse studies: *EμSRα-tTA; Teto-MYC* and *Dnmt12lox* mice were acquired from D. W. Felsher (Stanford University, Stanford, CA) and R. Jaenisch (Whitehead Institute, Cambridge, MA), respectively. *ROSA26EGFP* mice (79) and *Teto-Cre* mice (80) were obtained from The Jackson Laboratory. All mice were back-bred for five generations into

the FVB/NJ background. Standard genetic crosses were performed to generate the appropriate transgenic mice for these experiments, and the results were confirmed by PCR-based genotyping. Genomic DNA for genotyping was obtained from mouse tails. Tumor-bearing mice were carefully monitored for their overall health and harvested when they became terminally ill.

Mice used for tumor studies were *EμSRα-tTA; Teto-MYC; Teto-Cre; Rosa26LOXP$^{EGFP/EGFP}$; Dnmt1$^{flox/flox}$ and EμSRα-tTA; Teto-MYC; Rosa26LOXP$^{EGFP/EGFP}$; Dnmt1$^{flox/flox}$* mice (referred to as *MYC; Dnmt1$^{-/-}$* and *MYC; Dnmt1$^{flox/flox}$* mice, respectively). Further studies were performed utilizing *EμSRα-tTA; Teto-MYC; Teto-Cre; ROSA26$^{EGFP/EGFP}$; Dnmt1$^{+/+}$, EμSRα-tTA; Teto-MYC; Teto-Cre; ROSA26EGFP/EGFP; Dnmt3a$^{flox/flox}$*, and *EμSRα-tTA; Teto-MYC; Teto-Cre; ROSA26$^{EGFP/EGFP}$; Dnmt3b$^{flox/flox}$* mice (referred to as M*YC; Dnmt1$^{+/+}$, MYC; Dnmt3a$^{-/-}$,* and *MYC; Dnmt3b$^{-/-}$* mice, respectively).

Fluorescence-activated cell sorter (FACS) analysis, proliferation, and apoptosis: Single-cell suspensions from in vitro cultures or from the thymus, spleen, lymph node, and bone marrow were prepared and stained with the appropriate antibodies. For bromodeoxyuridine (BrdU) incorporation assays, cells were incubated with BrdU and labeled using allophycocyanin (APC)-conjugated anti-BrdU (BrdU-Flow kit; BD Biosciences) according to the manufacturer's instructions and analyzed using BD FACSDiva analysis software after processing samples on the FACSCalibur II flow cytometer. Similarly, tumor cells were stained with annexin V-APC (eBioscience) antibody and events were acquired on the FACSCalibur II flow cytometer. Cell cycle analysis was performed utilizing Vybrant DyeCycle Orange stain (Invitrogen) according to standard protocols and acquired on the LSR II cytometer. Thymi, spleens, lymph nodes, and bone marrow from developmental and tumor studies were stained with the

following antibodies to analyze cell surface marker expression: CD4, CD8, CD11b, B220, CD3, TER119, Sca-1, c-kit, CD19, gamma-delta T-cell receptor (TCRγδ), and TCRβ conjugated to phycoerythrin (PE), PE-Cy5, or APC. All antibodies were obtained from eBioscience. Populations of Lin− Sca-1+ c-kit+ (LSK; negative for lineage markers CD4, CD8, CD11b, CD19, TER119, CD3, gamma-delta T-cell receptor [TCRγδ], and TCRβ and positive for Sca-1 and c-kit) cells were distinguished by gating against lineage markers (CD4, CD8, CD11b, B220, CD3, and TER119) and subsequent gating for Sca-1+ c-kit+ cells. Sorting of enhanced green fluorescent protein (EGFP)-positive CD4− CD8−, CD4+ CD8+, CD4+, and CD8+ thymocytes was performed on the FACSAria cell sorter.

MSCC and data analysis: Methyl sensitive cut counting was performed using methods developed by Ball et al. (81). This technique uses the methyl-sensitive restriction endonucleases HpaII and HpyCh4IV to cut genomic DNA at all unmethylated CCGG and ACGT sites, respectively. Libraries were generated by digesting 2 µg of gDNA with 20 U of the restriction enzymes. Next, an adapter containing an Mme1 recognition site was ligated to the fragmented DNA. Libraries were digested with Mmel enzyme, which cuts 18 bp downstream of its recognition site. The fragments were then ligated to a second adapter to allow PCR amplification, gel purified, and sequenced using a high-throughput sequencer. The resulting 18-bp sequence tags were aligned with the mouse genome (mm9) using the short read sequence aligner Bowtie (82). The method results in output of sequencing tags, in which a high nuber of reads (termed counts) correlates with low methylation and vice versa. Count data was batch analyzed by edgeR (a bioconductor package for R programming language), which uses Bayesian estimation and exact tests based on the negative binomial distribution to generate pairwise comparisons between groups (83). False discovery rates (FDR) were

generated using the Benjamini Hochberg method (FDR < 0.05 was considered significant).

The data in the methylation heat maps (see Figure 5C and D and Figure 6C) represent averages for raw counts of all statistically significant changes of 2-fold or greater within individual promoters between *MYC; Dnmt1*$^{flox/flox}$ and *MYC; Dnmt1*$^{-/-}$ mice. The promoter is defined as at bp −1500 to +350 relative to the transcription start site. All genes considered to be hypomethylated or hypermethylated included two or more independent HpaII/HpyCh4IV sites that showed changes of 2-fold or greater with a false discovery rate (FDR) of less than 0.05.

Tissue culture: Mouse *MYC; Dnmt1*$^{flox/flox}$ cells were maintained in RPMI 1640 (Invitrogen) containing 10% fetal bovine serum (Invitrogen) and 0.025 mM 2-mercaptoethanol. Cell lines were cultured at 37°C in a humidified 5% CO2 atmosphere. Cre-mediated deletion of Dnmt1 was achieved using an established *MYC; Dnmt1*$^{flox/flox}$ cell line infected with murine stem cell virus (MSCV)-internal ribosome entry site (IRES)-puro-CreERT2 (Addgene plasmid 22776 [35]). Retroviral infections were done as described previously (13). Cre-mediated excision of Dnmt1 was induced by addition of 4-hydroxytamoxifen (4-OHT; Sigma-Aldrich) at a concentration of 150 nM. DNA for PCR-based determinations of Dnmt1 deletion efficiency was prepared from cells harvested after 24 and 72 h. For the colony PCR genotyping analysis, cells from two primary *MYC; Dnmt1*$^{-/-}$ lymphomas were plated into 48-well culture plates in RPMI medium with 10% fetal calf serum (FCS) at dilutions of one cell or fewer per well and cultured for several weeks. DNA was extracted from individual cones and subjected to genotyping.

Total methylcytosine: Measurement of 5-methyl-2′-deoxycytidine levels was performed at the University at Buffalo Pharmaceutical Sciences Instrumentation Facility, as described previously (84).

Affymetrix microarray analyses: RNA was isolated using Trizol and RNAeasy kit (Invitrogen and Qiagen, respetively). A total of 200 ng of RNA was reverse transcribed using the Ambion WT Expression Kit (Ambion). The cRNA was then hybridized to the Affymetrix GeneChip Mouse Gene 1.0 ST Array and chips were scanned using a GeneChip 3,000 6G scanner by the UNMC DNA Microarray Core Facility. GCOS software was used to scale dataset and assess quality assurance parameters such as background, hybridization kinetics, and reverse transcription efficiency. Intensities were imported into Partek Genomics Suite software using Robust Multi-chip Averaging (RMA) background correction and quantile normalization on a linear scale. Regularized t test analysis of control versus treatment comparisons was performed using a Bayesian approach to estimate the within-treatment variation among replicates using Cyber-T software (85). This principle uses the weighted average of local standard deviations for genes with similar expression levels, resulting in a stabilized within-treatment variance estimate.

Heat maps were generated using the average levels of expression of three *MYC; Dnmt1*$^{flox/flox}$ tumors as a reference. Ingenuity pathway analysis (IPA) (Ingenuity Systems) core analysis was used to interrogate microarray data based upon their functions and association with canonical pathways. Significant gene expression changes (FDR < 0.05) between *MYC; Dnmt1*$^{flox/flox}$ and *MYC; Dnmt1*$^{-/-}$ mice were imported into IPA with a threshold of 1.75-fold change.

Statistics: The survival data in Figure 1B were analyzed using the Kaplan-Meier method for overall survival and the log-rank test for survival distributions. Continuous variables were compared using 2-sample Student's t tests, with error bars representing 1 standard error of the mean. Bisulfite sequencing data were analyzed using paired t tests. P values and FDR of less than 0.05 were considered statistically significant.

Western blot analysis: The following antibodies were used for Western blot analysis: Dnmt3b (52A1018; Imgenex), Dnmt1 (H-300; Santa Cruz), Dnmt3a (H-295; Santa Cruz), and γ-tubulin (H-183; Santa Cruz). For Western blotting, protein lysates were separated in SDS acrylamide gels and blotted into Immobilon P membranes (Millipore). Blots were incubated in blocking buffer (5% skim milk) at a concentration of 1 mg/mL. The primary

antibody was then detected using horseradish-peroxidase-conjugated secondary

antibodies and the ECL reagent as described by the manufacturer (Pierce).

Quantitative qRT-PCR: cDNA was prepared from RNA using Bio-Rad iScript according to the manufacturer's protocol. cDNA was combined with SYBR green Supermix (Bio-Rad) with a final volume of 20 μl, and experiments were done in duplicate. Reaction conditions were optimized by the use of standard curves for each primer pair. Thermocycling was performed using a CFX96 system (Bio-Rad). Threshold cycle (CT) values were normalized based upon the expression of ubiquitin.

Primer sequences: The primer sequences used in these experiments are listed below. For determinations of Dnmt1 deletion efficiency, GGGCCAGTTGTGTGACTTGG, ATGCATAGGAACAGATGTGTGC, and CTTGGGCCTGGATCTTGGGGA were used. For Akt3 quantitative real-time RT-PCR (qRT-PCR), CATCTGAAACAGACACCCGATA and GTTGTCCATGCCGTCCAT were used. For Nrbf2 qRT-PCR, TCTCTGAAGCCATGAAGCTG and GTGCTCTGCTGCGCTTTC were used. For Rasgef1a qRT-PCR, AGGACAGCTGGAAGGCACT and ATCTGTCGCAATGTCACCAA were used. For Upb1 qRT-PCR, TCTCTGCCAGCAGATCAATG and TAGTTGGGTTTGACCGCTTC were used. For H2-Ab1 combined bisulfite restriction analysis (COBRA) and bisulfite sequencing, TGGTTTTTTATTTGGGATTAATTTT and TAAACCCTACTATCTCCCCATACAC were used. For Abhd14a COBRA,

GTTAAGTTTGGTTATTAGGGAAGAA and ATAAATCTTTTACACCCTTCCTAAC were used.

Bisulfite sequencing and COBRA: Sodium bisulfite treatment of genomic DNA was carried out utilizing an EpiTect bisulfite kit (Qiagen). Primers for bisulfite PCR for both COBRA and bisulfite sequencing were designed through the use of MethPrimer (86). For COBRA, bisulfite PCR products were digested with TaqI (NEB). The resulting fragments were then loaded onto an 8% PAGE gel, separated by electrophoresis, and detected with SYBR green Gold (Invitrogen). Bisulfite PCR fragments were also processed for bisulfite sequencing by cloning into pGem-T Easy vector (Promega). DNA was purified from clones and sequenced at the University of Nebraska Medical Center High-throughput DNA Sequencing and Genotyping Core Facility.

Results

Loss of Dnmt1 delays MYC-induced T-cell lymphomagenesis.

In this study, we utilized the genetic setting outlined in Figure 1A and described previously (13). Briefly, the *E*μ*SR*α promoter is active in ~40% of all hematopoietic lineages, including stem cells, and drives the expression of the tetracycline transcriptional transactivator (tTA). Expression of tTA drives simultaneous expression of the *MYC* oncogene and Cre recombinase from the *Teto* promoter. Activation of Cre results in the excision of the “stop cassette” located upstream of the *Rosa26LOXP*^{EGFP} locus, leading to the synthesis of EGFP. Thus, EGFP allows monitoring of tTA/Cre-expressing cells by flow cytometry (fluorescence-activated cell sorter [FACS]) analysis. Importantly, Cre expression also results in the excision of the conditional knockout allele of Dnmt1 (referred to herein as *Dnmt1*^{flox}).

To assess the effects of Dnmt1 loss on MYC-induced lymphomagenesis, we compared levels of tumor development in cohorts of *E*μ*SR*α-*tTA*; *Teto-MYC*; *Teto-Cre*; *Rosa26LOXP*$^{EGFP/EGFP}$; *Dnmt1*$^{flox/flox}$ and *E*μ*SR*α-*tTA*; *Teto-MYC*; *Rosa26LOXP*$^{EGFP/EGFP}$; *Dnmt1*$^{flox/flox}$ mice (designated *MYC*; *Dnmt1*$^{-/-}$ and *MYC*; *Dnmt1*$^{flox/flox}$ mice, respectively). As shown in Figure 1B, lymphomagenesis was significantly delayed in the cohort of *MYC*; *Dnmt1*$^{-/-}$ mice relative to *MYC*; *Dnmt1*$^{flox/flox}$ mice (median survival, 166 and 90 days, respectively). Analysis of DNA and protein revealed that tumors arising in *MYC*; *Dnmt1*$^{-/-}$ mice retained ~50% of Dnmt1 levels (Figure 1C and D). Furthermore, analysis of individual clones grown *in vitro* from single cells isolated from *MYC*; *Dnmt1*$^{-/-}$ tumors revealed that a vast majority of cells had the *Dnmt1*$^{flox/-}$ genotype, suggesting that primary tumors mainly consisted of cells heterozygous for the Dnmt1 knockout allele (Figure 1E). Taken together, these data suggest that Dnmt1 is required for the survival of tumor cells.

Reduced Dnmt1 levels did not affect the levels of Dnmt3a and Dnmt3b, suggesting that these enzymes are unlikely to exert compensatory effects on the process of lymphomagenesis (Figure 1F). FACS analysis confirmed similar immunophenotypes of lymphomas developed in *MYC*; *Dnmt1*$^{-/-}$ and *MYC*; *Dnmt1*$^{flox/flox}$ mice. Specifically, MTCLs from both genetic groups consisted of cells that were either $CD4^+$ $CD8^+$ $CD44^+$ $CD25^-$ or $CD4^+$ $CD8^-$ $CD44^+$ $CD25^-$, suggesting that loss of Dnmt1 does not affect the immunophenotype of the tumors (Figure 1G and H). We previously observed no measurable effects of Cre and EGFP expression on the process of lymphomagenesis in this model (13, 87). In addition, loss of Dnmt1 had no measurable effects on *MYC* expression (data not shown). Therefore, these results suggest that differences in survival between cohorts of *MYC*; *Dnmt1*$^{-/-}$ and *MYC*; *Dnmt1*$^{flox/flox}$ mice

can be attributed to the loss of *Dnmt1* and that this loss does not result in an altered immunophenotype(s) in this mouse model.

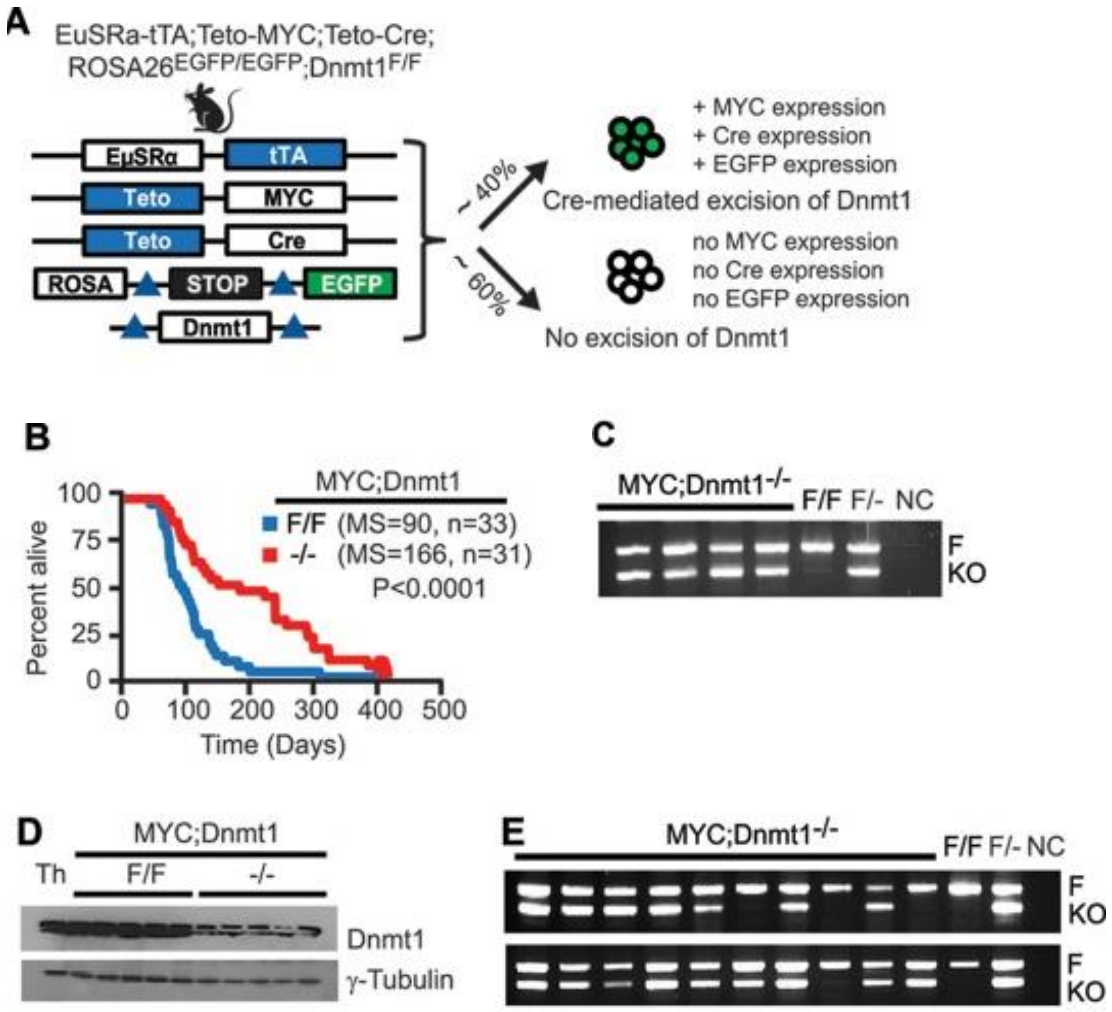

Figure 1. Loss of Dnmt1 delays MYC-induced T-cell lymphomagenesis. (A) Transgene schematic depicting genetic setting used in these studies. tTA is expressed in ~40% of cells and drives expression at the *Teto* promoter, resulting in transcription of the MYC oncogene and activating Cre-lox recombination to conditionally delete Dnmt1 and activate EGFP expression. (B) Kaplan-Meier survival curves MYC; *Dnmt1*$^{flox/flox}$ (F/F) and MYC; *Dnmt1*$^{flox/flox}$ (−/−) mice. Median survival rates (MS), numbers of mice (n), and *P* values (log-rank test) are shown. (C) PCR-based analysis of deletion efficiency of the *Dnmt1* conditional knockout allele in *MYC*; *Dnmt1*$^{-/-}$ tumors. F and KO indicate DNA fragments derived from the floxed and knockout alleles, respectively. *Dnmt1*$^{flox/flox}$ and *Dnmt1*$^{flox/-}$ genomic DNAs served as controls. NC indicates negative control (no DNA). (D) Immunoblot analysis of Dnmt1 expression in normal thymocytes (Th) and in *MYC*; *Dnmt1*$^{flox/flox}$ and *MYC*; *Dnmt1*$^{-/-}$ lymphomas. γ-Tubulin served as a loading control. (E) PCR-based analysis of deletion efficiency of the *Dnmt1* conditional knockout allele in cellular clones from *MYC*; *Dnmt1*$^{-/-}$ tumors. The top and bottom panels represent two tumors with 10 clones each. F and KO indicate floxed and knockout alleles, respectively. *Dnmt1*$^{flox/flox}$ and *Dnmt1*$^{flox/-}$ genomic DNAs served as controls. NC indicates negative control (no DNA).

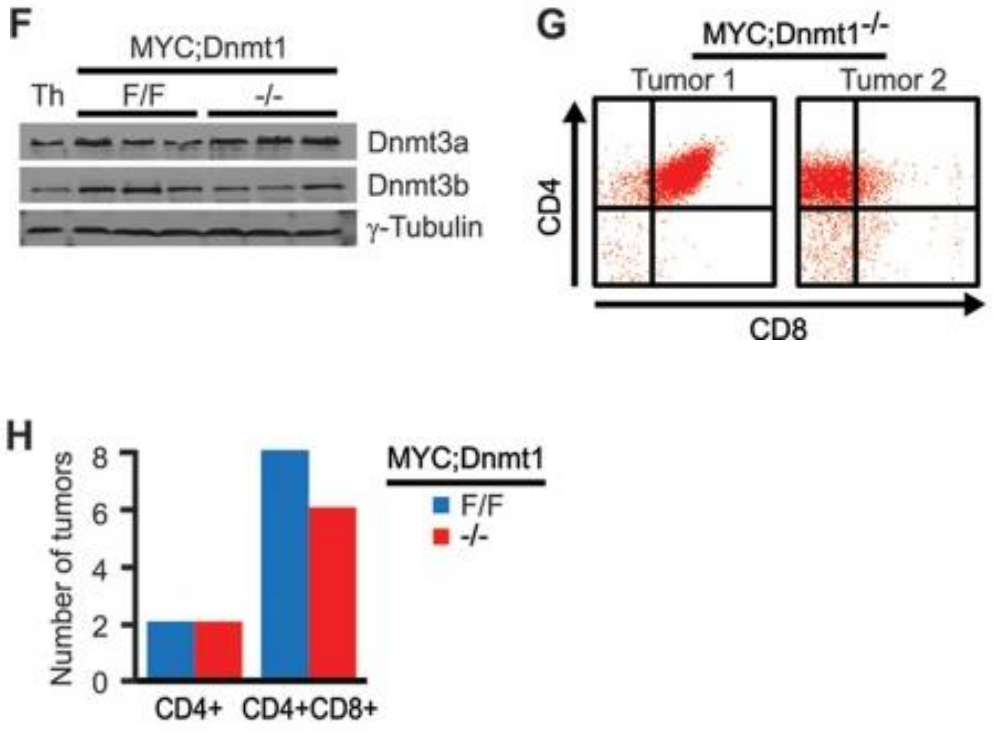

Figure 1 cont. Loss of Dnmt1 delays MYC-induced T-cell lymphomagenesis. (F) Immunoblot analysis of Dnmt3a and Dnmt3b expression in normal thymocytes (Th) and in *MYC*; *Dnmt1*$^{flox/flox}$ and *MYC*; *Dnmt1*$^{-/-}$ lymphomas. **(G)** Representative examples of FACS analysis from immunophenotyping of *MYC*; *Dnmt1*$^{-/-}$ tumors using anti-CD4 and anti-CD8 antibodies. Examples of CD4 single-positive and CD4/CD8 double-positive tumors are shown. **(H)** Summary of immunophenotypes for CD4 single-positive and CD4/CD8 double-positive tumors as determined by FACS analysis using CD4 and CD8 expression in *MYC*; *Dnmt1*$^{flox/flox}$ and *MYC*; *Dnmt1*$^{-/-}$ lymphomas.

Dnmt1 is required for cellular proliferation and maintenance of tumor phenotypes in MTCLs.

To examine the underlying cellular basis for the extended survival of *MYC*; *Dnmt1*$^{-/-}$ mice, we measured annexin V expression and bromodeoxyuridine (BrdU) incorporation in cell lines established from lymphomas of terminally sick *MYC*; *Dnmt1*$^{-/-}$ and *MYC*; *Dnmt1*$^{flox/flox}$ mice. Flow cytometry quantification of annexin V revealed similar expression levels for *MYC*; *Dnmt1*$^{flox/flox}$ and *MYC*; *Dnmt1*$^{-/-}$ mice. However, a modest but statistically significant reduction in BrdU incorporation was observed in cells from *MYC*; *Dnmt1*$^{-/-}$ lymphomas (Figure 2A and B). These data suggest that defective tumor cell proliferation may, in part, be responsible for the delayed tumorigenesis seen in *MYC*; *Dnmt1*$^{-/-}$ mice.

To determine whether Dnmt1 is required for maintenance of the tumor phenotype, we generated two inducible *MYC*; *Dnmt1*$^{flox/flox}$; *Cre-ER* cell lines, in which Cre-mediated excision of the Dnmt1 conditional allele is achieved by the addition of 4-hydroxytamoxifen (4-OHT) to cell cultures. Importantly, while the cellular viability of two *MYC*; *Dnmt1*$^{+/+}$; *Cre-ER* control cell lines treated with 4-OHT was not affected (data not shown), loss of Dnmt1 resulted in death of *MYC*; *Dnmt1*$^{flox/flox}$ *lymphoma* cells within 72 h (Figure 2C). As shown in Figure 2D, activation of Cre-ER *in vitro* yielded efficient deletion of the Dnmt1 conditional allele at as early as 24 h and remained high at 72 h. Collectively, these data support the idea of a requirement for Dnmt1 in the maintenance of the tumor phenotype *in vitro*.

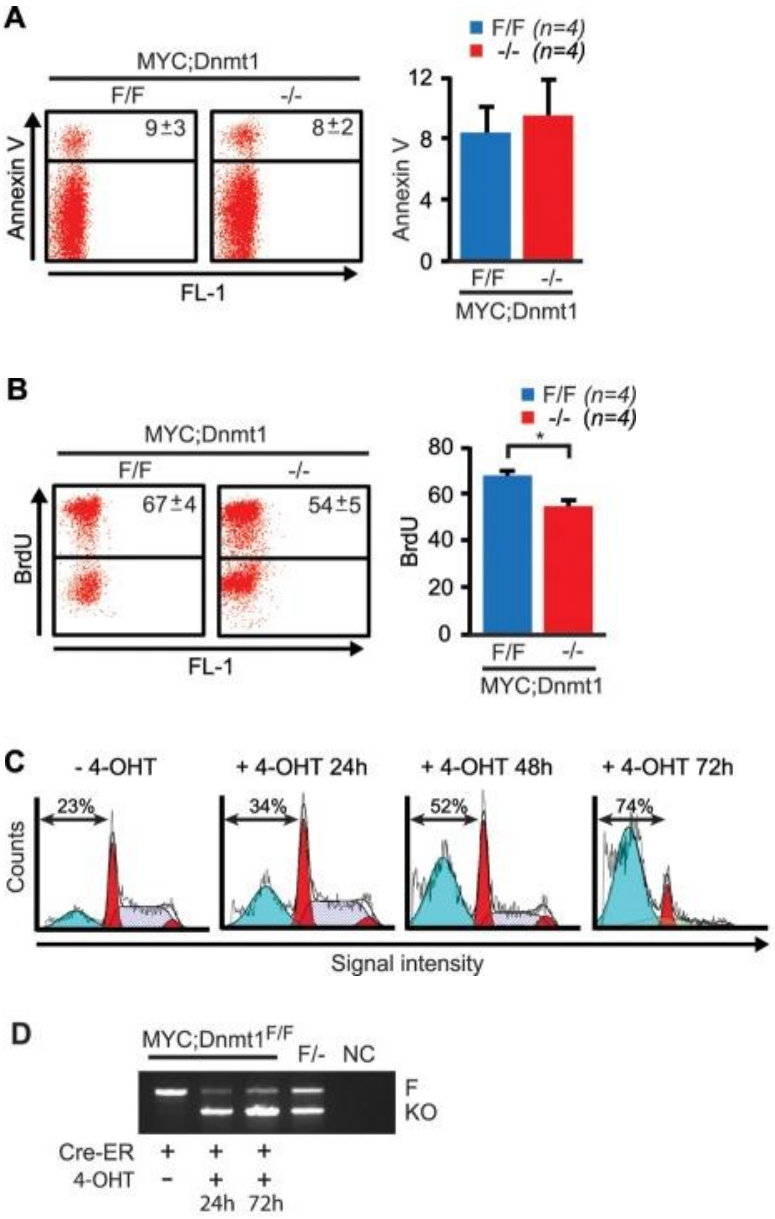

Figure 2. Loss of Dnmt1 results in decreased proliferation and is critical for tumor cell survival. (A and B) Analysis of apoptosis by annexin V staining (A) and BrdU incorporation assay (B) of four independent T-cell lines derived from *MYC*; *Dnmt1*$^{flox/flox}$ and *MYC*; *Dnmt1*$^{-/-}$ primary MYC-induced lymphomas. Representative FACS diagrams are shown with average percentages and standard deviations in the upper right quadrant ($P < 0.05$ (Student's *t* test). Quantification of obtained results for each assay is shown as an average value with error bars representing standard errors of the means (SEM). Statistically significant differences are indicated by an asterisk. (C) A representative example of cell cycle analysis of a *MYC*; *Dnmt1*$^{flox/flox}$ cell line expressing Cre-ER without 4-hydroxytamoxifen (4-OHT) and after 24, 48, and 72 h of incubation with 4-OHT. The cell cycle was measured by Invitrogen Vybrant DyeCycle Orange stain. The percentage of dead cells (blue) is indicated on FACS diagrams. (D) PCR-based analysis of deletion efficiency of the Dnmt1 conditional KO allele in *MYC*; *Dnmt1*$^{flox/flox}$ cell lines infected with Cre-ER and treated with 4-OHT at 24 and 72 h. F and KO indicate DNA fragments derived from the floxed and knockout alleles, respectively.

Loss of Dnmt1 impairs T-cell development.

The presence of the *Rosa26LOXP*^{EGFP} reporter transgene in *MYC*; *Dnmt1*$^{-/-}$ mice allows evaluation of biological and molecular events occurring in hematopoietic cells by FACS. To further investigate the processes responsible for delayed lymphomagenesis, we evaluated T-cell development in *MYC*; *Dnmt1*$^{-/-}$ mice by measuring levels of EGFP in thymi. Both percentages and numbers of EGFP-positive cells were decreased ~20-fold in *MYC*; *Dnmt1*$^{-/-}$ mice relative to thymi isolated from control *E*μ*SR*α-*tTA*; *Teto-MYC*; *Teto-Cre*; *Rosa26LOXP*$^{EGFP/EGFP}$; *Dnmt1*$^{+/+}$ mice (designated *MYC*; *Dnmt1*$^{+/+}$ mice) (Figure 3A and B). PCR-based genotyping revealed low levels of deletion efficiency of the conditional Dnmt1 allele in the thymi of *MYC*; *Dnmt1*$^{-/-}$ mice, whereas EGFP-positive thymocytes sorted by FACS analysis retained ~50% of the conditional Dnmt1 allele (Figure 3C). A marked decrease in cell numbers was evident at all stages of T-cell development in EGFP-positive *MYC*; *Dnmt1*$^{-/-}$ thymi, including DN1 to -4, CD4^{-} CD8^{-}, CD4^{+} CD8^{+}, CD4^{+}, and CD8^{+} cells (Figure 3D to F). Dnmt1 was particularly important for the transition from CD4^{-} CD8^{-} double-negative (DN1 to -4) cells to the CD4^{+} CD8^{+} double-positive (DP) stage during differentiation, since CD4^{+} CD8^{+} cells showed the highest fold reduction (Figure 3G). Consistently, the number of T cells in spleen and lymph nodes was substantially reduced (Figure 3G). PCR-based genotyping of sorted EGFP^{+} DN, DP, CD4^{+}, and CD8^{+} *MYC*; *Dnmt1*$^{-/-}$ cells showed the lowest level of Dnmt1 knockout efficiency in the DN population, with progressive increases in DP, CD4, and CD8 cells (Figure 3H), suggesting that the requirement of Dnmt1 for cellular survival during normal thymocyte

development is highest in the least-differentiated DN cells but becomes less stringent in the more-differentiated stages. This is consistent with the CD4^{+} CD8^{+} immunophenotype and deletion efficiency of Dnmt1 observed in the majority of *MYC*; *Dnmt1*$^{-/-}$ lymphomas

(Figure 1C and H). Altogether, these results suggest that T cells lacking Dnmt1 are selected against during T-cell development and that an efficient transition from the DN stage to the DP stage of thymocyte differentiation requires Dnmt1.

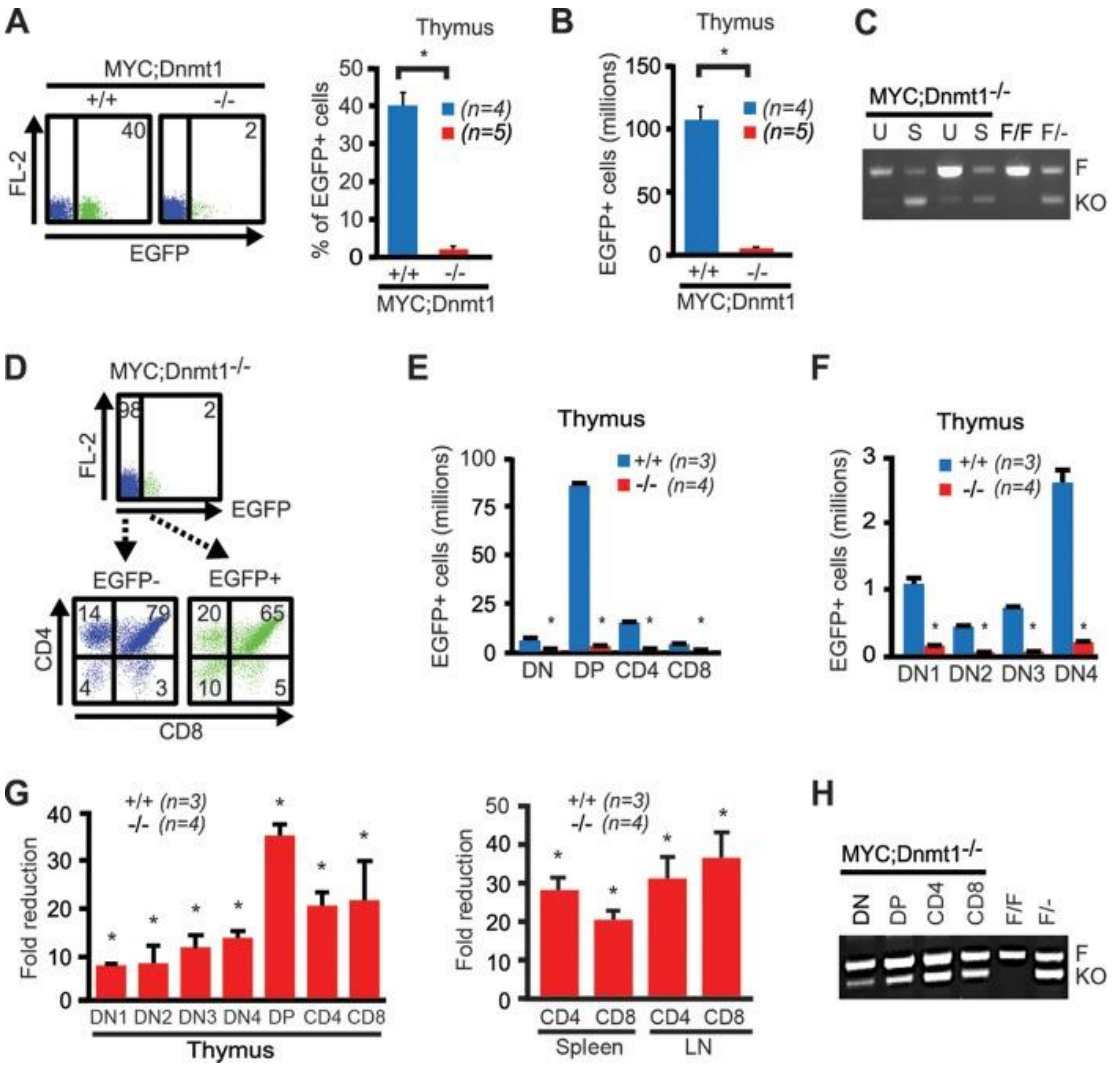

Figure 3. Loss of *Dnmt1* impairs T-cell development. (A) Representative FACS profiles with total percentages of EGFP expression. (B) Total numbers of EGFP+cells isolated from thymi of 24-day-old *MYC*;*Dnmt1*$^{+/+}$ and *MYC*;*Dnmt1*$^{-/-}$ mice. (C) PCR-based analysis of deletion efficiency of the Dnmt1 conditional KO allele in unsorted (U) and EGFP-positive sorted (S) cells isolated from thymi of *MYC*; *Dnmt1*$^{-/-}$ mice (n = 2). F and KO indicate DNA fragments derived from the floxed and knockout alleles, respectively. (D) CD4 and CD8 expression in EGFP+ and EGFP- cells from thymi of 24-day-old *MYC*; *Dnmt1*$^{-/-}$ mice. (E) The total number of EGFP+ T-cell populations within the thymus of *MYC*; *Dnmt1*$^{+/+}$ and *MYC*; *Dnmt1*$^{-/-}$ mice. Double-negative (DN), CD4/CD8 double-positive (DP), CD4 single-positive (CD4), and CD8 single-positive (CD8) cell results are shown. (F) Further analysis of thymocyte development within the CD4/CD8 double-negative population (DN1 to DN4) by FACS in *MYC*; *Dnmt1*$^{+/+}$ and *MYC*; *Dnmt1*$^{-/-}$ thymi. (G) The left bar graph shows the fold reduction of EGFP+ double-negative (DN1 to -4), CD4/CD8 double-positive (DP), CD4 single-positive, and CD8 single-positive cells in the thymi of 24-day-old *MYC*; *Dnmt1*$^{-/-}$ mice relative to EGFP-positive *MYC*; *Dnmt1*$^{+/+}$ cells. The right bar graph depicts fold reduction of EGFP+ CD4 and CD8 single-positive cells in the spleen and lymph node (LN) relative to EGFP+ *MYC*; *Dnmt1*$^{+/+}$ cells. Error bars represent SEM; (*) denotes $P < 0.05$ (Student's t test). n represents the number of biological replicates. (H) PCR-based analysis of deletion efficiency of the Dnmt1 conditional KO allele in FACS-sorted DN, DP, CD4, and CD8 single-positive EGFP-positive thymic cells from 24-day-old *MYC*; *Dnmt1*$^{-/-}$ mice. F and KO indicate DNA fragments derived from the floxed and knockout alleles, respectively. *Dnmt1*$^{flox/flox}$ and *Dnmt1*$^{flox/-}$ genomic DNA served as controls.

Ablation of Dnmt1 alters hematopoietic development.

We next investigated whether loss of Dnmt1 negatively impacted development of other hematopoietic lineages. Indeed, cell surface marker expression revealed decreased levels of EGFP-positive B -cells and myeloid cells in the spleen, lymph node, and bone marrow in *MYC*; *Dnmt1*$^{-/-}$ mice (Figure 4A and B). Interestingly, the fold reduction of B220^{+} cells was substantially greater than that of CD11b^{+} cells in all three tissues, indicating that the lymphoid lineage may be more sensitive to reductions in the Dnmt1 level. This finding is consistent with previous work in which Dnmt1 was found to be essential for normal B-cell differentiation but not myeloid differentiation (27). DNA isolated from the bone marrow and spleen showed low efficiency of Dnmt1 knockout (Figure 4C), further supporting the idea that Dnmt1 is required for normal hematopoiesis.

The *E*μ-*tTA* transgene that activates Cre-mediated excision of the conditional Dnmt1 allele is expressed in hematopoietic stem cells and early hematopoietic progenitor cells (HSC/HPCs), which are defined by a Lin^{-} Sca-1^{+} c-kit^{+} marker profile (LSK; cells negative for lineage markers CD4, CD8, CD11b, CD19, TER119, CD3, gamma-delta T-cell receptor [TCRγδ], and TCRβ and positive for Sca-1 and c-kit). Thus, the substantial decrease in EGFP-positive cells in hematopoietic organs of *MYC*; *Dnmt1*$^{-/-}$ mice could be caused by an essential role of Dnmt1 in either the differentiation or the maintenance of HSC/HPCs. To assess this, we analyzed LSK populations in the bone marrow. Numbers of EGFP-positive LSK cells in *MYC*; *Dnmt1*$^{-/-}$ mice were significantly lower than of those isolated from *MYC*; *Dnmt1*$^{+/+}$ mice (Figure 4D and E). The relative absence of EGFP-positive *MYC*; *Dnmt1*$^{-/-}$ LSK cells indicated these cells have a competitive disadvantage in comparison to their EGFP-negative counterparts with respect to maintenance of their physiological levels in the bone marrow and during

differentiation into hematopoietic lineages, likely due to the critical role of Dnmt1 in these processes.

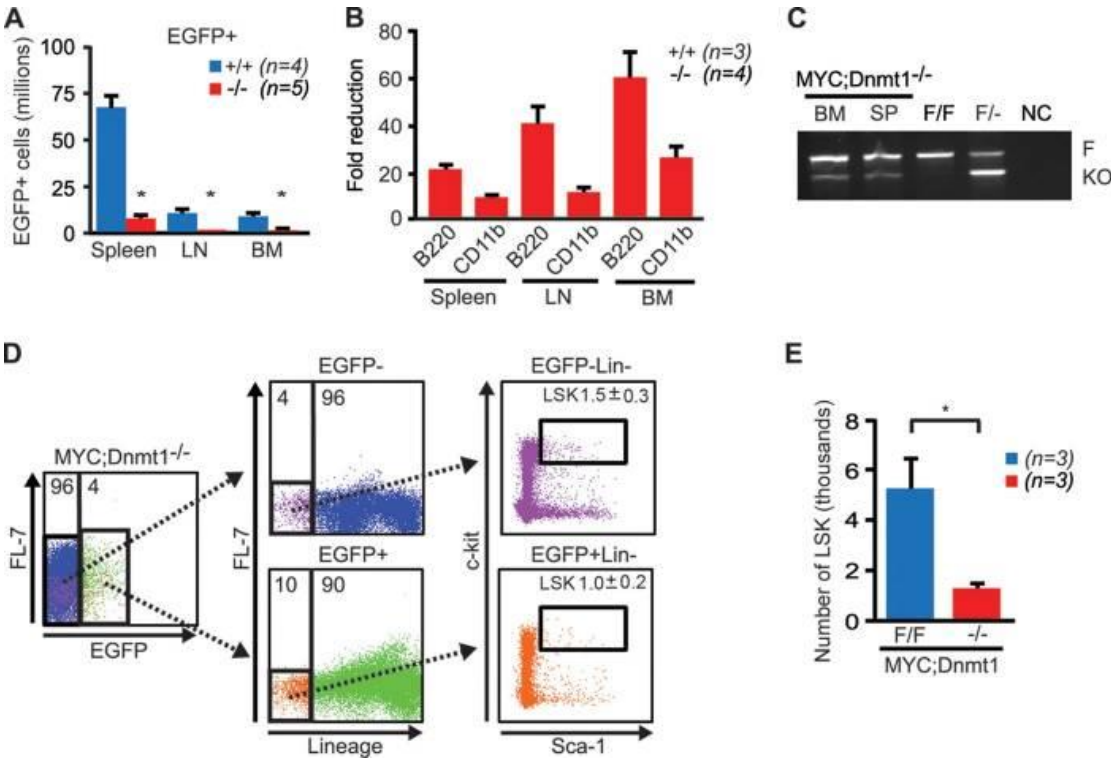

Figure 4. Impaired hematopoiesis in *MYC*; *Dnmt1*$^{-/-}$ mice. (A) The total numbers of EGFP-positive cells within the spleen, lymph node (LN), and bone marrow (BM) of *MYC*; *Dnmt1*$^{+/+}$ and *MYC*; *Dnmt1*$^{-/-}$ mice. (B) Fold reductions in total numbers of EGFP-positive B-lymphoid (B220) and myeloid (CD11b) cells relative to EGFP-negative B-lymphoid and myeloid cells in spleens, lymph nodes, and bone marrow of 24-day-old *MYC*; *Dnmt1*$^{-/-}$ mice. (C) PCR-based analysis of deletion efficiency of the *Dnmt1*^{F} allele in total DNA isolated from bone marrow (BM) and spleen (SP) of 24-day-old *MYC*; *Dnmt1*$^{-/-}$ mice. *Dnmt1*$^{flox/flox}$ and *Dnmt1*$^{flox/-}$ genomic DNA controls as well as a negative control (NC) are shown. F and KO indicate DNA fragments derived from the floxed and knockout alleles, respectively. (D) FACS analysis of c-kit and Sca-1 expression in lineage-negative (Lin^{-}) EGFP-negative and Lin^{-} EGFP-positive cells (LSK cells: Lin^{-} Sca1^{+} c-kit^{+}) in the bone marrow of *MYC*; *Dnmt1*$^{-/-}$ mice. Average percentages of LSK cells are indicated in the FACS diagrams. (E) The total numbers of LSK cells in EGFP-positive populations in bone marrow of *MYC*; *Dnmt*$^{flox/flox}$ and *MYC*; *Dnmt1*$^{-/-}$ mice. Error bars represent SEM; $P < 0.05$ (Student's *t* test). Statistically significant differences are indicated by an asterisk. The number of samples is indicated by *n*.

Reduction of Dnmt1 in MTCLs leads to altered locus-specific methylation.

To investigate how decreased levels of Dnmt1 affect DNA methylation in tumors, we first analyzed the content of 5-methyl-2′-deoxycytosine in DNA from primary mouse MTCLs using an established mass spectrometry method (84). *MYC*; *Dnmt1*$^{flox/flox}$ and *MYC*; *Dnmt1*$^{-/-}$ lymphomas had decreased levels of global 5-methylcytosine relative to normal thymocytes, suggesting that tumors underwent global DNA hypomethylation (Figure 5A). No significant differences between *MYC*; *Dnmt1*$^{flox/flox}$ and *MYC*; *Dnmt1*$^{-/-}$ lymphomas were observed. This result is consistent with the moderate effects observed in an HCT116 cell line with knockout of Dnmt1 alleles (88). To determine locus-specific effects of Dnmt1 on DNA methylation, we profiled the methylation status of HpaII and HpyCh4IV restriction sites using methyl-sensitive cut counting (MSCC) in genomic DNA isolated from *MYC*; *Dnmt1*$^{flox/flox}$ *and MYC*; *Dnmt1*$^{-/-}$ lymphomas as described previously (30). Analysis of *Line-L1*, *Line-L2*, and *Sine/Alu* repeat elements revealed hypomethylation in both tumor groups relative to normal thymocytes but no significant differences in repeat element methylation between tumor groups (Figure 5B).

We next analyzed MSCC data to determine how Dnmt1 affected the DNA methylation landscape in *MYC*; *Dnmt1*$^{flox/flox}$ tumors. A total of 24,236 promoters in the mouse genome have at least two restriction sites as seen from HpaII and/or HpyCh4IV digests. To rigorously assess the methylation status of promoters, we considered a change in methylation to be significant only if it occurred in two or more independent restriction sites in promoter areas at from bp −1500 to +350 relative to the transcription start site, with a 2-fold or greater change at a false discovery rate (FDR) of less than 0.05. A comparison of the methylation landscapes of *MYC*; *Dnmt1*$^{flox/flox}$ and *MYC*; *Dnmt1*$^{-/-}$ cells revealed that 730 promoters were differentially methylated between these

two tumor groups (Figure 5C; see also Data Set S1 in the supplemental material). Of these,

303 promoters showed increased levels of methylation in *MYC*; *Dnmt1*$^{-/-}$ lymphomas, possibly as a result of deregulation of DNA methylation machinery. Of the 427 promoters that showed decreased methylation levels in *MYC*; *Dnmt1*$^{-/-}$ lymphomas, 214 promoters were also hypomethylated in normal thymocytes, suggesting that these promoters might be *de novo* targets of Dnmt1 in tumorigenesis. The remaining 213 promoters were highly methylated in normal thymocytes and *MYC*; *Dnmt1*$^{flox/flox}$ lymphomas but hypomethylated in *MYC*; *Dnmt1*$^{-/-}$ lymphomas, suggesting that Dnmt1 is involved in the maintenance of methylation at these promoters.

Decreased levels of Dnmt1 resulted in methylation changes of 777 genes, with 440 hypomethylation and 337 hypermethylation events in gene bodies (Figure 5D). Additionally, we have seen a relatively small amount of overlap of genes that are hypomethylated in both the promoter and the gene body (~6%), suggesting that Dnmt1 activity is locus specific. Collectively, these data indicate that the contribution of Dnmt1 to the promoter methylation consists not only of maintenance methylation patterns but also of cancer-specific *de novo* activity. Since *MYC*; *Dnmt1*$^{flox/flox}$ tumors retain ~50% of Dnmt1 protein levels, our data also suggest that gene promoters require higher levels of Dnmt1 than gene bodies or intragenic regions to maintain proper methylation patterns.

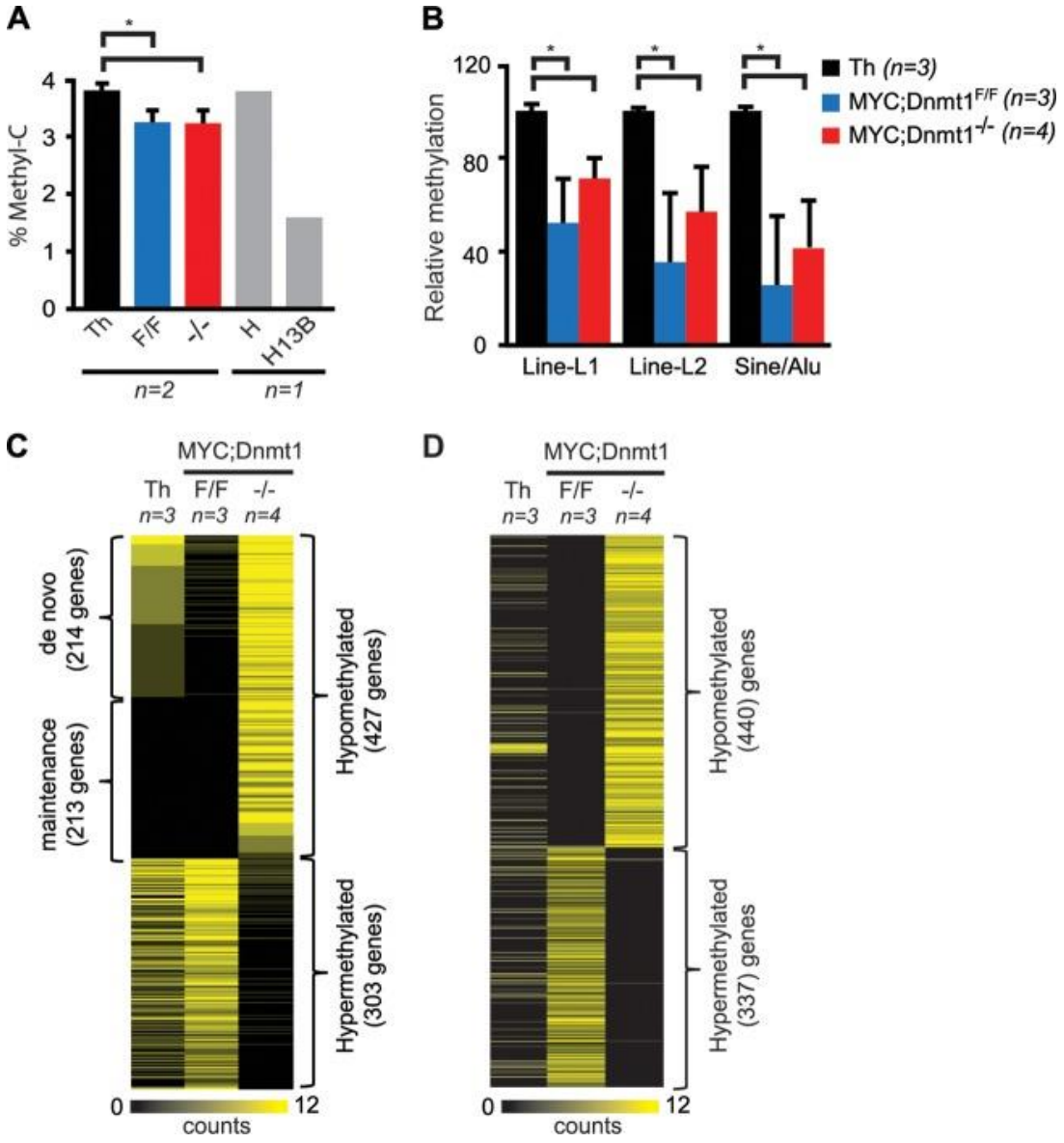

Figure 5. Analysis of DNA methylation in Dnmt1-deficient tumors. (A) Total 5-methylcytosine levels in normal thymocytes (Th), *MYC*; *Dnmt1*$^{flox/flox}$ (F/F) tumors, and *MYC*; *Dnmt1*$^{-/-}$ (−/−) tumors. The human colorectal carcinoma parental cell line HCT116 (H) and the HCT116 *DNMT1*$^{-/-}$; *DNMT3B*$^{-/-}$ cell line (H13B) served as controls. (B) *In silico* analysis of relative methylation levels of *Line-L1*, *Line-L2*, and *Sine/Alu* repeats in normal thymus (Th), *MYC*; *Dnmt1*$^{flox/flox}$ tumors, and *MYC*; *Dnmt1*$^{-/-}$ tumors by MSCC. (C) A heat map analysis of MSCC data displaying 427 hypomethylated and 303 hypermethylated promoters in *MYC*; *Dnmt1*$^{-/-}$ tumors relative to *MYC*; *Dnmt1*$^{flox/flox}$ tumors (FDR < 0.05 [negative binomial]). Genes proposed to have Dnmt1 *de novo* (214 genes) and Dnmt1 maintenance (213 genes) activity are labeled. A color bar is shown, with black representing a high degree of methylation and yellow representing lower levels. Th indicates normal thymocytes. *n* represents the number of biological replicates. (D) A heat map displaying the numbers of hypermethylated (*n* = 337) and hypomethylated (*n* = 440) gene bodies in *MYC*; *Dnmt1*$^{-/-}$ tumors relative to *MYC*; *Dnmt1*$^{flox/flox}$ tumors. Normal thymus (Th) levels are also shown. Changes represent a *P* of <0.05 with a 2-fold or greater change.

Deregulated transcription in Dnmt1-deficient lymphomas.

To further understand the molecular basis for increased survival of *MYC*; *Dnmt1*$^{-/-}$ mice, as well as the effects of Dnmt1 on gene transcription, we next compared microarray-based gene expression profiles of *MYC*; *Dnmt1*$^{-/-}$ lymphomas to those of normal thymocytes and MTCLs. We identified 1,260 genes whose expression levels were significantly different (1.75-fold; FDR < 0.05) between *MYC*; *Dnmt1*$^{flox/flox}$ *and MYC*; *Dnmt1*$^{-/-}$ lymphomas (Figure 6A; see also Data Set S2 in the supplemental material). Loss of Dnmt1 resulted in transcriptional upregulation of 780 genes, which is consistent with the function of Dnmt1 as a repressor protein. Although we cannot rule out the possibility that Dnmt1 plays a role in transcriptional activation, 480 genes downregulated in *MYC*; *Dnmt1*$^{-/-}$ lymphomas likely represent secondary changes rather than being a direct consequence of Dnmt1 inactivation. Real-time quantitative RT-PCR (qRT-PCR) confirmed that *Akt3*, *Nrfb2*, and *Rasgef1a* genes are upregulated whereas *Upb1* is downregulated in *MYC*; *Dnmt1*$^{-/-}$ lymphomas (Figure 6B). Unsupervised hierarchical clustering analysis using global gene transcription profiles of all genes resulted in perfect segregation of tumors in a Dnmt1-specific manner, with *MYC*; *Dnmt1*$^{flox/flox}$ tumors clustering closer to *MYC*; *Dnmt1*$^{-/-}$ lymphomas than to normal thymocytes (Figure 6A). Tight clustering of *MYC*; *Dnmt1*$^{-/-}$ lymphomas suggests that Dnmt1 plays an important role in regulating the transcriptome in MTCLs, likely through specific target genes.

To gain further insight into the pathogenesis of *MYC*; *Dnmt1*$^{-/-}$ lymphomas, we performed IPA using 780 genes whose transcription was significantly changed (upregulated 1.75-fold or more, FDR < 0.05) relative to *MYC*; *Dnmt1*$^{flox/flox}$ lymphomas. The top five disease groups associated with higher expression in *MYC*; *Dnmt1*$^{-/-}$ lymphomas relative to control *MYC*; *Dnmt1*$^{flox/flox}$ lymphomas were cancer, hematological disease, developmental disorders, immunological disease, and renal and urological

disease (data not shown). Of these, the most significant functional disease network was that of cancer. Eight genes (*Dcn*, *Rag1*, *Brca2*, *Cdkn1a*, *Zeb1*, *Ccnd3*, *Runx1*, and *Ssbp2*) from the hematologic disease network “tumorigenesis in thymic lymphomas” were overexpressed in Dnmt1-deficient lymphomas, and their upregulation was suggested by IPA to be involved in the suppression of T-cell lymphomagenesis (Figure 6C). In addition, IPA showed that negative regulators of cell cycle, such as retinoblastoma (*Rb1*), were upregulated in Dnmt1-deficient lymphomas. Considering all

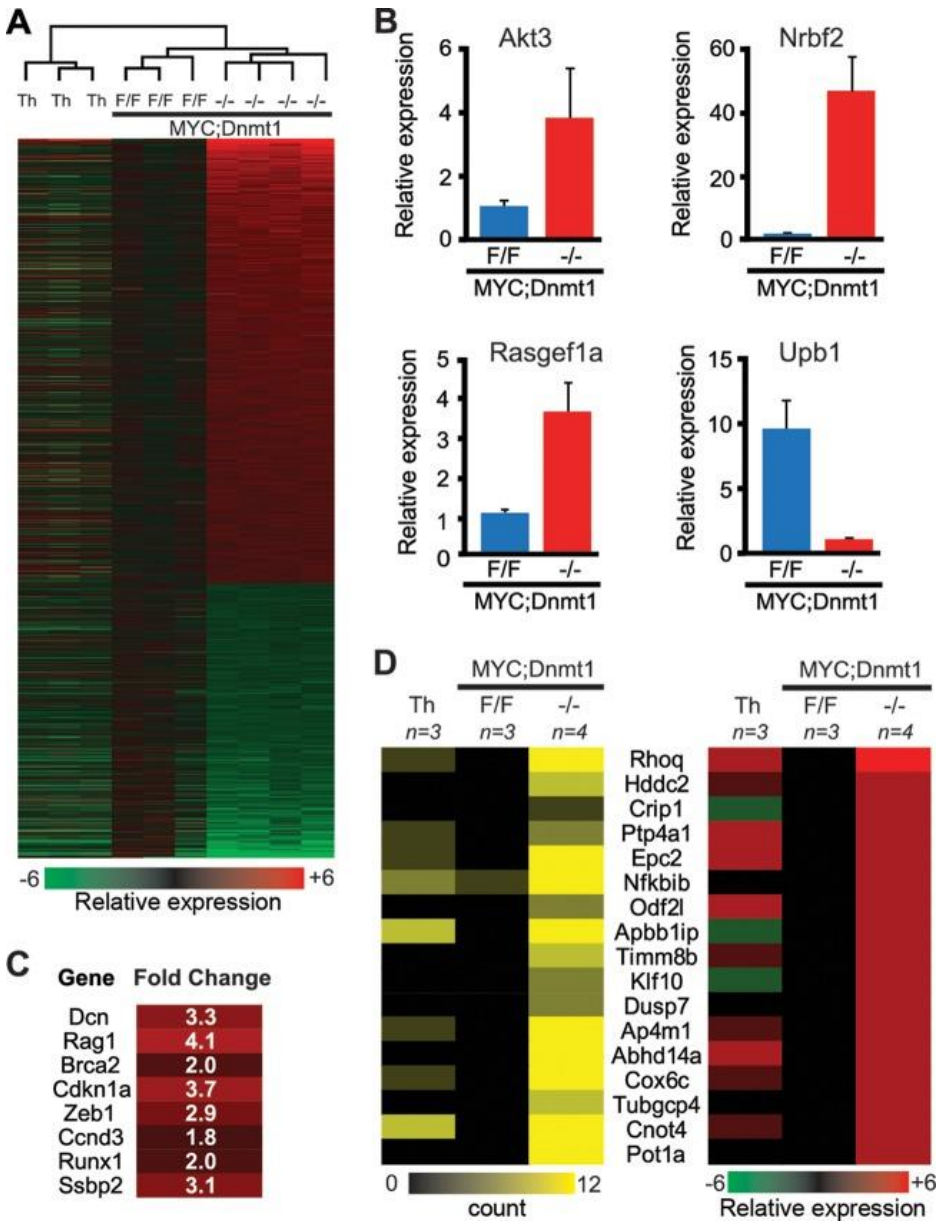

Figure 6. Significantly deregulated genes in *MYC*; *Dnmt1*$^{-/-}$ tumors. (A) A heat map derived from global transcription profiling by microarray displaying 1,260 genes that are 1.75-fold changed in *MYC*; *Dnmt1*$^{-/-}$ tumors relative to *MYC*; *Dnmt1*$^{flox/flox}$ tumors. A total of 780 genes show upregulation, while 480 show downregulation (FDR < 0.05 [Bayesian *t* test]). A color bar is shown to reference upregulation in red and downregulation in green. Above the heat map, an unsupervised hierarchical clustering of normal thymi (Th), *MYC*; *Dnmt1*$^{flox/flox}$ (F/F) tumors, and *MYC*; *Dnmt1*$^{-/-}$ (−/−) tumors is shown. (B) qRT-PCR displaying the relative mRNA levels of 4 differentially expressed genes in *MYC*; *Dnmt1*$^{flox/flox}$ and *MYC*; *Dnmt1*$^{-/-}$ tumors. The average results of two replicates are shown for $n = 2$ samples for each group. Error bars represent SEM. (C) The network tumorigenesis in thymic lymphomas derived from Ingenuity pathway analysis of 780 upregulated genes from *MYC*; *Dnmt1*$^{-/-}$ cells. All eight genes within the network are predicted to suppress thymic lymphomagenesis. (D) Heat maps for genes with at least a 2-fold decrease in promoter methylation as determined by MSCC and at least a 1.75-fold induction in expression as determined by microarray in *MYC*; *Dnmt1*$^{-/-}$ lymphomas. Average values from normal thymocytes (Th) and *MYC*; *Dnmt1*$^{flox/flox}$ and *MYC*; *Dnmt1*$^{-/-}$ tumors are shown.

these results together, these molecular events may contribute to the delayed lymphomagenesis observed in *MYC*; *Dnmt1*$^{-/-}$ mice.

To determine the effects of Dnmt1-dependent methylation on gene transcription, we next analyzed levels of gene expression in Dnmt1 target genes. This comparison revealed that expression of 17 of 427 hypomethylated genes correlated with promoter hypomethylation, suggesting that differential methylation affects a relatively small (~4.0%) subset of genes (Figure 6D).

H2-Ab1* is a target of cancer-specific *de novo* methylation by Dnmt1 *in vivo.

The major histocompatibility class 2 gene (*H2-Ab1*) is involved in antigen processing and presentation (89). Its locus encodes two distinct isoforms (Figure 7A). Our MSCC data showed that the promoter region driving expression of the longer H2-Ab1 isoform may be a target of Dnmt1, as it was consistently hypomethylated in *MYC*; *Dnmt1*$^{-/-}$ tumors (Figure 7B). To determine if H2-Ab1 is a maintenance or *de novo* target of Dnmt1, we performed combined bisulfite restriction analysis (COBRA) and bisulfite sequencing of the −43 to +471 region of this promoter in normal thymocytes and *MYC*; *Dnmt1*$^{flox/flox}$ and *MYC*; *Dnmt1*$^{-/-}$ tumors. In both assays, *MYC*; *Dnmt1*$^{flox/flox}$ tumors were consistently hypermethylated relative to normal thymocytes, while Dnmt1-deficient tumors showed near-complete ablation of promoter methylation (Figure 7C and D). These changes in methylation correlated with gene transcription of the major isoform of H2-Ab1, which was severely repressed in *MYC*; *Dnmt1*$^{flox/flox}$ tumors compared to normal thymocytes but was derepressed in *MYC*; *Dnmt1*$^{-/-}$ tumors (Figure 7E). Importantly, this potential *de novo* activity of Dnmt1 is independent of the presence of Dnmt3a and Dnmt3b, as levels of methylation of the *H2-Ab1* locus remained high in thymic lymphomas with genetic inactivation of either Dnmt3a or Dnmt3b (Figure 7D).

Importantly, a potential *de novo* activity of Dnmt1 is not limited to *H2-Ab1* since the promoter of the

Abhd14a gene is also hypermethylated in *MYC*; *Dnmt1*$^{flox/flox}$ but is unmethylated in *MYC*; *Dnmt1*$^{-/-}$ lymphomas (Figure 7E). Furthermore, global methylation profiling of *MYC*; *Dnmt1*$^{-/-}$ and *MYC*; *Dnmt3b*$^{-/-}$ tumors showed an overlap of only 3% in Dnmt1 target genes (Figure 7G, (13), and data not shown). In addition, only 35 of 780 (4%) Dnmt1 target genes were overexpressed in both *Dnmt1*$^{-/-}$ and *Dnmt3b*$^{-/-}$ MTCLs (Figure 7G). Thus, Dnmt1 appears to have cancer-specific target genes whose methylation and/or expression is largely independent of the presence of Dnmt3b and perhaps Dnmt3a.

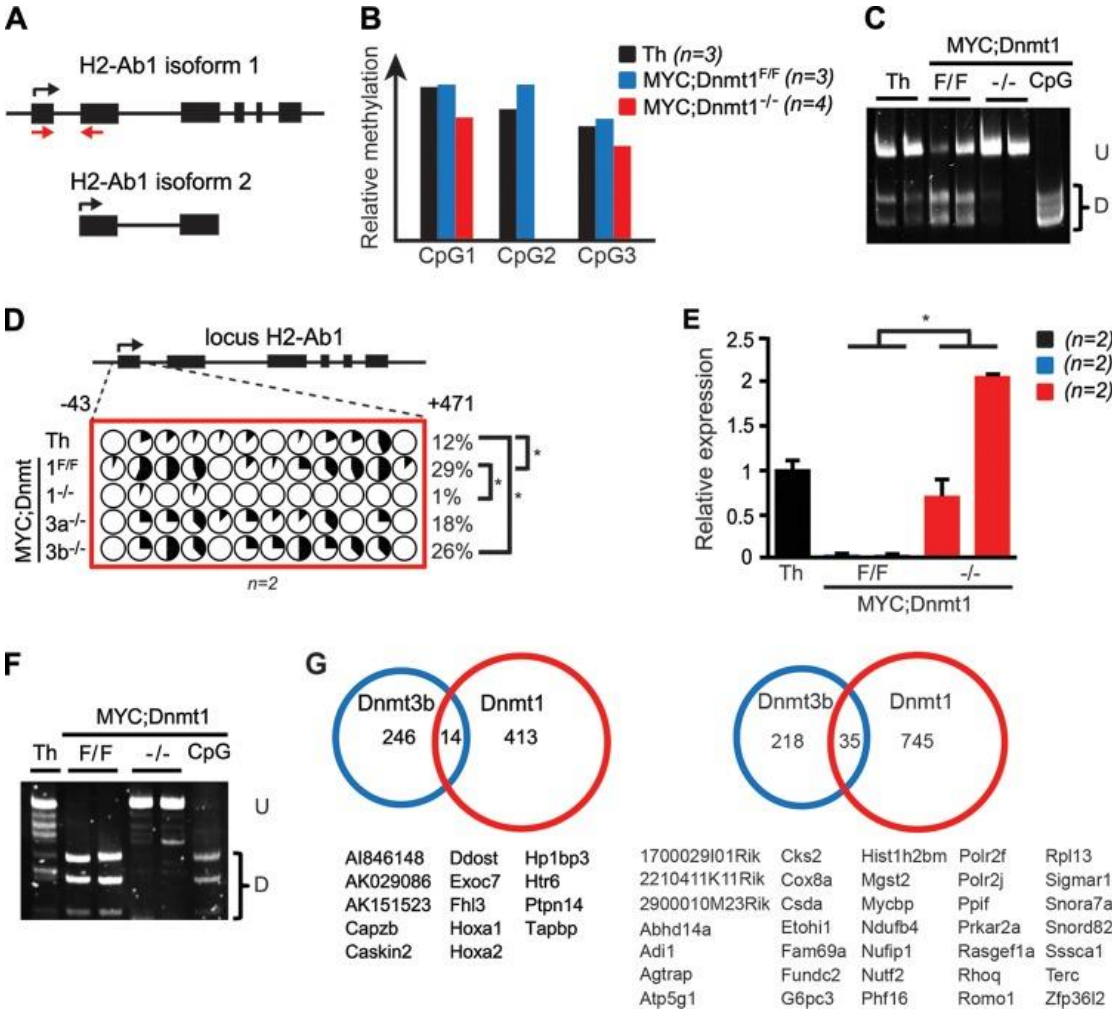

Figure 7. H2-Ab1 is a target of Dnmt1-mediated methylation in lymphomas. (A) An illustration of the exons and introns comprising the two *H2-Ab1* isoforms. Black arrows represent the transcription start site. Red arrows denote the location of qRT-PCR primers. (B) A methylation bar graph depicting average methylation levels across three CpG sites analyzed by MSCC in the promoter of *H2-Ab1* for normal thymocytes (Th) and *MYC*; *Dnmt1*$^{flox/flox}$ and *MYC*; *Dnmt1*$^{-/-}$ tumors. (C) COBRA of the *H2-Ab1* promoter in normal thymocytes and in *MYC*; *Dnmt1*$^{flox/flox}$ (F/F) and *MYC*; *Dnmt1*$^{-/-}$ lymphomas. Undigested (U) and digested (D) fragments correspond to unmethylated and methylated DNA, respectively. CpG indicates a fully methylated control. (D) Bisulfite sequencing of the *H2-Ab1* promoter in normal thymocytes (Th) and in *MYC*; *Dnmt1*$^{flox/flox}$, *MYC*; *Dnmt1*$^{-/-}$, *MYC; Dnmt3a*$^{flox/flox}$ (*3a*$^{-/-}$), and *MYC*; *Dnmt3b*$^{flox/flox}$ (*3b*$^{-/-}$) lymphomas. The dashed lines denote the location of the CpG dinucleotides within the locus. Each pie denotes an individual CpG dinucleotide within the locus, and each wedge of the pie represents the sequence of an individual allele. Black denotes the percentage of methylated alleles, while white represents unmethylated alleles. (E) qRT-PCR analysis of *H2-Ab1* longer-isoform expression in normal thymocytes, *MYC*; *Dnmt1*$^{flox/flox}$ tumors, and *MYC*; *Dnmt1*$^{-/-}$ tumors. Error bars represent SEM; (*) denotes $P < 0.05$ (Student's *t* test). (F) COBRA of the *Abhd14a* promoter in normal thymocytes (Th) and in *MYC*; *Dnmt1*$^{flox/flox}$ and *MYC*; *Dnmt1*$^{-/-}$ lymphomas. (G) Overlap of 260 genes identified in Dnmt3b-deficient MTCLs and 427 potential Dnmt1-dependent targets, as determined by MSCC, are shown in the left Venn diagram. The right Venn diagram shows 253 genes that were at least 1.75-fold upregulated in the absence of Dnmt3b in MTCLs overlaid with the 780 genes that were upregulated in *MYC*; *Dnmt1*$^{-/-}$ tumors. The overlapping genes are listed below each diagram.

Discussion

In the present study, we used a MYC model to characterize the role of Dnmt1 in T-cell lymphomagenesis. We show that Dnmt1 plays a crucial role in the prevention and maintenance of the tumor phenotype in MTCLs as well as in normal hematopoiesis. Importantly, we identified locus-specific maintenance and *de novo* activity for Dnmt1. Our results suggest that Dnmt1, in addition to its involvement in maintenance of DNA methylation patterns during cellular division, also plays an irreplaceable role in promoter and gene body methylation during tumorigenesis. This report represents the first in which the cancer-specific *de novo* and maintenance activity of Dnmt1 in the *in vivo* setting is presented.

Suppressed tumorigenesis in *MYC*; *Dnmt1*$^{-/-}$ mice is surprising in view of previous work that has suggested that T cells are particularly sensitive to low levels of Dnmt1. Whereas a global decrease in Dnmt1 levels is achieved in all cells in *Dnmt1*$^{chip/-}$ mice, these mice almost exclusively (91%) develop T-cell lymphomas over the course of 8 months, despite the fact that this all occurs in the context of reduced numbers of HSC/HPCs and thymocytes in *Dnmt1*$^{chip/-}$ mice. This is likely occurring through the induction of genomic instability and activation of oncogenes such as Notch by intracisternal A particles (28, 31, 32).

There are at least two biological processes that may explain the increased latency of Dnmt1 tumors in our model. First, deletion of Dnmt1 in *MYC*; *Dnmt1*$^{-/-}$ mice results in considerable defects in hematopoietic development which may limit the pool of cells susceptible to MYC-induced lymphomagenesis. Inefficient hematopoiesis is largely a consequence of a severe reduction in the number of HSC/HPCs. The total quantity of EGFP-positive LSK cells in *MYC*; *Dnmt1*$^{-/-}$ mice is decreased 4-fold relative to the EGFP-negative population, suggesting that HSC/HPCs encountering loss of Dnmt1 are

at a competitive disadvantage relative to EGFP-negative cells in terms of their ability to self-renew within the same microenvironment. Additionally, decreased cellularity of EGFP-positive cells of lymphoid and myeloid origins suggests that the differentiation potential of the remaining LSK cells—likely with only partial Dnmt1 expression—is also skewed. Our data are consistent with observations showing an essential role for Dnmt1 in the self-renewal and differentiation of HSCs (31, 90). c-Myc has been reported to be involved in differentiation of HSCs, as loss of c-MYC results in pooling of stem cells (91, 92). Since our data were obtained in a setting where high levels of transgenic MYC were present, it also appears that MYC overexpression is insufficient to rescue Dnmt1-driven defects in hematopoietic differentiation. Our results show an accumulation of Dnmt1-deficient T cells in the double-negative stage of T-cell differentiation, similar to what was observed in *Lck-Cre*; *Dnmt1*$^{-/-}$ mice, whereby Cre actively deletes Dnmt1 alleles at the DN2 stage of thymocyte differentiation and results in impaired differentiation (93). Altogether, these data indicate serious defects in hematopoiesis in the absence of Dnmt1, which ultimately diminishes the pool of hematopoietic cells available for MYC-induced transformation.

Second, a biological process that may contribute to increased survival of *MYC*; *Dnmt1*$^{-/-}$ mice is the decreased proliferation potential of *MYC*; *Dnmt1*$^{-/-}$ cells. This may reflect increases in the levels of key antiproliferative genes such as retinoblastoma (Rb) that were observed in *MYC*; *Dnmt1*$^{-/-}$ lymphomas. Rb is a negative regulator of cell cycle and is a tumor suppressor in hematopoietic cancers (94, 95). Another possibility is that a larger cadre of genes contributes to this phenomenon. For example, Ingenuity pathway analysis of genes upregulated in *MYC*; *Dnmt1*$^{-/-}$ lymphomas unveiled an eight-gene (*Dcn*, *Rag1*, *Brca2*, *Cdkn1a*, *Zeb1*, *Runx1*, *Ssbp2*, and *Ccnd3*) signature (tumorigenesis in thymic lymphomas) where all eight genes are predicted to decrease thymic

lymphomagenesis. Indeed, inactivation of seven of these eight genes has been functionally linked to promotion of thymic lymphomagenesis. Loss of *Ssbp2* or *Dcn* accelerated T-cell lymphomagenesis in *p53*$^{-/-}$ mice, while ablation of *Rag1* accelerated *E*μ-*MYC* tumorigenesis (96-98). Germ line inactivation of *Brca2*, *Cdkn1a*, *Runx1*, or *Zeb1* is sufficient to result in hematologic malignancies in mice (99-103). Thus, these putative Dnmt1 target genes have been independently linked to their ability to suppress lymphomagenesis in mouse tumor prevention settings.

Therefore, within one cellular compartment (T cells), Dnmt1 plays a dichotomous role by preventing tumorigenesis through maintaining the integrity of the genome and silencing oncogenes (*Dnmt1*$^{chip/-}$ studies [(28, 32)]) and promoting lymphomagenesis by retention of cells susceptible to transformation (*MYC*; *Dnmt1*$^{-/-}$ studies). This is likely due to the fact that low levels of Dnmt1 allow cells to survive and accumulate genetic and epigenetic changes promoting tumorigenesis whereas complete deletion of Dnmt1 is incompatible with the viability of normal hematopoietic cells. Thus, Dnmt1 may both promote and inhibit tumorigenesis even within the same tumor type, depending on the degree of its activity. At present, we cannot rule out the possibility that germ line inactivation of one Dnmt1 allele in *Dnmt1*$^{chip/-}$ mice promotes T-cell transformation in a non-cell-autonomous way. Thus, further studies are required to determine if microenvironments deficient for Dnmt1 can enhance T-cell lymphomagenesis.

This study also uncovered an important role for Dnmt1 in the maintenance of the tumor phenotype. For example, all tumors that developed in *MYC*; *Dnmt1*$^{-/-}$ mice retained ~50% of Dnmt1 levels and exhibited decreased proliferation, suggesting that Dnmt1 is crucial for the survival of tumor cells. This was further confirmed through functional inactivation of Dnmt1 in fully developed *MYC*; *Dnmt1*$^{flox/flox}$ lymphomas, which led to severely impaired cellular survival. In addition to being critical for the maintenance

of the tumor phenotypes either in AML induced by MLL-AF9 or in B-cell leukemia induced by combined overexpression of Myc and Bcl2 (31, 59), Dnmt1 function is also fundamental for the maintenance of mouse MTCLs.

Our data further indicate that even incomplete inactivation of Dnmt1 has a profound effect on the molecular landscape of MTCLs. By comparing methylation patterns of normal thymocytes, *MYC*; *Dnmt1*$^{flox/flox}$ lymphomas, and *MYC*; *Dnmt1*$^{-/-}$ lymphomas, we identified 427 promoters whose methylation appeared to depend upon Dnmt1. Of these, 214 promoters are likely targets of Dnmt1 *de novo* activity, as their methylation is low in normal thymocytes and *MYC*; *Dnmt1*$^{-/-}$ lymphomas but is increased in *MYC*; *Dnmt1*$^{flox/flox}$ tumors. The remaining 213 gene promoters are methylated in normal thymocytes and *MYC*; *Dnmt1*$^{flox/flox}$ lymphomas but hypomethylated in *MYC*; *Dnmt1*$^{-/-}$ lymphomas, suggesting that Dnmt1 is involved in maintenance of the methylation at these loci throughout tumorigenesis. Furthermore, Dnmt1 target loci appear to be largely independent of Dnmt3b, as a comparison with our previously published Dnmt3b targets (13) showed only a 3% overlap with newly unveiled Dnmt1 targets in this study. Along the same lines, locus-specific *de novo* methylation by Dnmt1 at the *H2-Ab1* target gene is independent of both Dnmt3a and Dnmt3b, as lymphomas deficient for either methyltransferase gain methylation at levels similar to those seen with *MYC*; *Dnmt1*$^{flox/flox}$ lymphomas. Results showing differing spectra of Dnmt1 and Dnmt3b target genes identified in MTCLs are consistent with the opposing effects of Dnmt1 and Dnmt3b on MYC-induced lymphomagenesis, during which, as our recent studies showed, Dnmt3b functions as a tumor suppressor gene (13). Our data also show increased methylation of 303 promoter regions in *MYC*; *Dnmt1*$^{-/-}$ lymphomas. At present, it is unclear why a decrease in Dnmt1 levels results in promoter hypermethylation. However, locus-specific increases in methylation levels have been

recently observed upon loss of methyltransferase activity of Dnmt3a in mouse hematopoietic stem cells (45).

The present knowledge base of target loci of Dnmt1 is minimal. Previous studies have identified targets of Dnmt1-dependent methylation and transcription in the HCT116 colon cancer cell line (93, 104). When we compared these target genes with Dnmt1 targets identified in this study, we observed only a 2% overlap (data not shown), suggesting that Dnmt1 may have tissue- or species-specific target loci. The apparent lack of a significant overlap in Dnmt1 target genes between the HCT116 cell line and MTCLs may also stem from the different growth conditions under which the cells were maintained. For example, the spectrum of Dnmt1 target genes in HCT116 cell line may reflect the different selection pressures that cells experience during *in vitro* culturing. In contrast, the methylation profiles of the MTCLs are more likely to faithfully reflect physiological patterns, as they were obtained from primary lymphomas grown *in vivo*. In any case, in addition to Dnmt1's canonical function as a maintenance methyltransferase during DNA replication, Dnmt1 may localize to specific loci in a cell- or tissue-specific manner.

Juxtaposition of 427 Dnmt1-dependent methylation targets and 780 genes upregulated in *MYC*; *Dnmt1*$^{-/-}$ tumors identified only a ~4% correlation of promoter methylation with the transcription status. This number is likely underestimated, perhaps due to limitations in MSCC analysis as well as in array-based gene transcription profiling. The use of two restriction enzymes (HpaII and HpyCh4IV) increased the coverage of DNA methylation profiling to ~16% of all CpGs in the mouse genome but still may not have been sufficient to fully reveal the effects of Dnmt1 on the cancer methylome (105). Similarly, Affymetrix gene transcription profiling is unable to reliably distinguish between the levels of expression of various gene isoforms. For example, the

Dnmt1 target gene *H2-Ab1* encodes at least two isoforms whose transcripts significantly overlap. As a result, global microarray profiling has not identified differences in expression of this gene between *MYC*; *Dnmt1*$^{flox/flox}$ *and MYC*; *Dnmt1*$^{-/-}$ lymphomas. However, isoform-specific qRT-PCR clearly showed upregulation of the longer isoform which is driven by a specific promoter upon hypomethylation in Dnmt1-deficient MTCLs. Thus, future studies will focus on the use of more-sensitive methods, such as whole-genome bisulfite sequencing for methylation profiling and transcriptome sequencing (RNA-seq) for transcriptional profiling, to further analyze the relationship of DNA methylation to transcription. It is possible that inhibitory effects of DNA methylation on transcription are limited in some biological settings. Indeed, recent studies have identified a low correlation between changes in promoter methylation and differential gene expression in mouse hematopoiesis and human AML (38, 45). Thus, additional discrete studies should be performed to address this point.

Our present findings highlight the importance of Dnmt1 in the prevention and maintenance of T-cell malignancies and complex activities of Dnmt1 in the tumor methylome and transcriptome.

CHAPTER 2: Methylation-independent repression of Dnmt3b contributes to oncogenic activity of Dnmt3a in mouse MYC-induced T-cell lymphomagenesis[2]

Introduction

Methylation of CpG dinucleotides in DNA is an essential epigenetic modification involved in X-chromosome inactivation, genomic imprinting and tissue-specific gene regulation (15).Three DNA methyltransferases (Dnmts) catalyze the addition of a methyl group to cytosine in mammalian cells: Dnmt1, Dnmt3a and Dnmt3b. Dnmt1 is primarily responsible for maintenance of methylation patterns during cellular divisions through its ability to read and transfer methylation groups to the newly synthesized DNA strand during replication (7). Consistently with the importance of maintaining epigenetic integrity in dividing cells, homozygous deletion of Dnmt1 is lethal at early stages of embryogenesis (4). Dnmt3a and Dnmt3b function primarily as *de novo* enzymes (5). Dnmt3b is responsible for early *de novo* methylation and repression of germ line genes (74), and its inactivation is embryonically lethal. Dnmt3a is dispensable for embryogenesis, but *Dnmt3a*-knockout mice die shortly after birth due to multiple organ failure (5). Emerging evidence suggests that all three enzymes may have a role in maintenance and *de novo* activity in a locus-specific manner (15), but their ability to affect promoter methylation in normal and pathological settings is still poorly understood.

[2] The material presented in this chapter were previously published: Haney SL, Hlady RA, Opavska J, Klinkebiel D, Pirruccello SJ, Dutta S, et al. Methylation-independent repression of Dnmt3b contributes to oncogenic activity of Dnmt3a in mouse MYC-induced T-cell lymphomagenesis. Oncogene. 2015;34(43):5436-46.

Dnmt3a and Dnmt3b share several sequence and structural similarities, including a conserved C-terminal domain, which mediates addition of methyl groups to DNA, and the N-terminal regulatory domain, which mediates interactions with DNA and other proteins (15). Methylation at CpG dinucleotides found in the promoter and other regulatory regions is often associated with transcriptional silencing (15). In addition to their methyltransferase activities, Dnmt3a and Dnmt3b can repress transcription in a methylation-independent manner. Critical to this process is their interaction with histone deacetylases (HDACs) and other repressor proteins via their ATRX-like domain (16). For instance, Dnmt3a interacts with the methyl CpG binding domain of Mbd3 and Brg1 to silence metallothionein-I transcription in mouse lymphosarcoma cells (17). However, how methylation-independent repressor activity affects physiological processes remains elusive.

Genome-wide deregulation of the DNA methylation landscape, including locus-specific hyper- and global hypo-methylation, is a consistently observed phenomenon in human tumors. This deregulation, in particular hypomethylation, likely comes from genetic alterations of DNMTs found in cancer. Although mutations in DNMTs were identified in a variety of human tumors, they are most often found in hematologic malignancies. For example, *DNMT3A* is one of the most frequently mutated genes in myeloid and T-cell malignancies with the frequency ranging from 8% cases of myelodysplastic syndrome to 33% of angioimmunoblastic T-cell lymphoma (38, 39, 106, 107). In T-cell malignancies, approximately two-third of mutations are missense, with the remainder being frame shifts, nonsense mutations and deletions (42, 106, 107). The majority of mutations cluster in the catalytic domain, suggesting that the change in methylase activity is important for tumor development. The substitution of arginine for histidine in the catalytic domain (R882H mutation) accounts for ~60% of the mutations in

acute myeloid leukemia. In addition to being hypomorphic, this mutant is believed to function as a dominant-negative protein (108). The effects of aberrations found outside the catalytic domain, and those common to T-cell malignancies, are not known. In contrast to *DNMT3A*, *DNMT3B* or *DNMT1* is rarely mutated in hematologic malignancies. Why in hematologic diseases genetic alterations are present in *DNMT3A* but not in other DNMTs is unclear.

Like mutations in *DNMT3A*, increased activity of the proto-oncogene MYC is frequently observed in human T-cell malignancies, either through mutations in oncogenes, such as NOTCH1 for which MYC is a transcriptional target, or through genetic alterations of the *MYC* locus itself (109). For example, a subset of peripheral T-cell lymphomas (TCLs) has a frequent gain of the *MYC* locus (8q24) with subsequent overexpression, suggesting that MYC has a role in the pathogenesis of the disease (110).

The sensitivity of T-cells to MYC-induced transformation was previously demonstrated using a bitransgenic *EμSRα-tTA;Teto-MYC* mouse model in which tetracycline transcriptional transactivator (tTA) drives *MYC* expression resulting in the development of immature TCLs (111). Using a model of MYC-induced T-cell lymphomagensis (MTCL), we recently demonstrated that conditional inactivation of Dnmt1 compromised normal and malignant hematopoiesis and delayed MYC-induced T-cell lymphomagenesis (33). In contrast, Dnmt3b functions as a tumor suppressor (TS) as its loss does not affect normal T-cell development but accelerates MTCL (13).

Utilizing a model of MTCL, we show that loss of Dnmt3a extends the survival of mice due to a decrease in cellular proliferation with no effect on the disease spectrum. Using genome-wide approaches, we observed upregulation of TS genes, including *Dnmt3b, E2f2* and *Pten,* whose expression is elevated in Dnmt3a-deficient lymphomas

without apparent changes in DNA methylation in their promoters or gene bodies. We further show that catalytically inactive Dnmt3a inhibits Dnmt3b *in vitro*. Finally, genetic inactivation of Dnmt3b accelerated MTCL, suggesting that delayed lymphomagenesis is at least in part mediated by Dnmt3b. Altogether, our data provide evidence for an unexpected oncogenic function of Dnmt3a in MTCL, through methylation independent repressor activity critical for the proliferation of tumor cells.

Methods

Mouse studies: *EμSRα-tTA;Teto-MYC* and *Dnmt3a*$^{F/F}$ mice were obtained from D.W. Felsher (Stanford University) and R. Jaenisch (Whitehead Institute), respectively. *ROSA26*^{EGFP} and *Teto-Cre* mice were purchased from The Jackson Laboratory (Bar Harbor, ME, USA). All experiments were performed using mice of FVB/NJ background. Genotypes were confirmed by PCR using genomic DNA isolated from mouse tails. For analysis of T-cell development (including cell surface marker analysis, EGFP expression, and weights and cellularity of thymus, lymph node and spleen), 21-day-old mice from the *EμSRα-tTA;Teto-MYC;Teto-Cre;Rosa26LOXP*$^{EGFP/EGFP}$*;Dnmt3a*$^{F/F}$ (*MYC*;*Dnmt3a*$^{Δ/Δ}$) and *EμSRα-tTA;Teto-MYC;Teto-Cre;ROSA26*$^{EGFP/EGFP}$*Dnmt3a*$^{+/+}$ (*MYC;Dnmt3a*$^{+/+}$) cohorts were used. FACS-sorted EGFP^{+} thymocytes isolated from 21-day-old *EμSRα-tTA;Teto-Cre;Rosa26LOXP*$^{EGFP/EGFP}$ *(Dnmt3a*$^{+/+}$) and *EμSRα-tTA;Teto-Cre;Rosa26LOXP*$^{EGFP/EGFP}$*;Dnmt3a*$^{F/F}$ mice (*Dnmt3a*$^{Δ/Δ}$) were used as controls for MSCC analysis. For tumor studies, the survival of *EμSRα-tTA;Teto-MYC;Rosa26LOXP*$^{EGFP/EGFP}$*;Dnmt3a*$^{F/F}$ mice (*MYC*;*Dnmt3a*$^{F/F}$) was compared with *MYC*;*Dnmt3a*$^{Δ/Δ}$ or *EμSRα-tTA;Teto-MYC;Teto-Cre;Rosa26LOXP*$^{EGFP/EGFP}$*;Dnmt3a*$^{F/+}$ (*MYC*;*Dnmt3a*$^{Δ/+}$) mice, and survival of *EμSRα-tTA;Teto-MYC;Rosa26LOXP*$^{EGFP/EGFP}$*;Dnmt3a*$^{F/F}$*;Dnmt3b*$^{F/F}$ (*MYC*;*Dnmt3a*$^{F/F}$*;Dnmt3b*$^{F/F}$) was compared with that of *EμSRα-tTA;Teto-MYC;Teto-*

Cre;Rosa26LOXP$^{EGFP/EGFP}$*;Dnmt3a*$^{F/F}$*;Dnmt3b*$^{F/F}$ (*MYC*; *Dnmt3a*$^{\Delta/\Delta}$*;Dnmt3b*$^{\Delta/\Delta}$). Full genotypes with abbreviations and genetic crosses to produce mice are listed in Supplementary Tables S1 and S2. Differences in survival were calculated using the Kaplan–Meier method and the log-rank test for survival distributions. A two-sided Student's *t*-test was used to analyze differences in tumor burden, EGFP percentage and cell surface marker expression.

MSCC and data analysis: MSCC library preparation, data collection and data analysis were performed as previously described (13, 33, 34, 81). The method results in an output of sequencing tags, or counts, which inversely correlate with the methylation status of a particular CpG. The R programming language and bioconductor package 'edgeR' was used for statistical analysis of count data (83, 112). An FDR was estimated using the Benjamini Hochberg method. To carefully assess the methylation status of promoters, we considered a change in methylation to be significant only if it occurred in two or more independent *Hpa*II and/or *HpyCh4*IV restriction sites, with a fold change 2, at an FDR of <0.05. The promoter was defined as −1500 to +500 base pairs relative to the transcription start site. Results were confirmed using COBRA as previously described (13, 33).

Affymetrix microarray analyses: Microarray was performed at the UNMC Microarray core facility as previously described (13). Statistical analysis was done using Cyber-T software (85). Genes differentially expressed (*P*<0.05 and fold change >1.5) in *MYC;Dnmt3a*$^{\Delta/\Delta}$ tumors relative to *MYC;Dnmt3a*$^{F/F}$ tumors were analyzed using IPA (Qiagen, Valencia, CA, USA) to identify common pathways and disease associations. Microarray data were deposited in NCBI's Gene Expression Omnibus (accession no. GSE59338).

Generation of retroviruses and infection of cell lines: Retroviral vectors were created by subcloning the coding sequences of wild-type *Dnmt3a* and catalytically dead *Dnmt3a* (*Dnmt3aCD*) into the *MSCV-IRES-RFP* vector (113). *Dnmt3a*$^{P705V/C706D}$ has two amino-acid substitutions in the catalytic domain, which eliminate methylase activity of the enzyme. Constructs were verified by sequencing. Tumor cells isolated from *MYC;Dnmt3a*$^{\Delta/\Delta}$ mice were cultured *in vitro* in RPMI 1640 medium supplemented with 10% FBS and 0.025 mM 2-mercaptoethanol. Retroviral infection of cells was performed as previously described (13). Cells were infected using one of three retroviral vectors (*MSCV-IRES-RFP*, *MSCV-IRES-Dnmt3a-RFP* or *MSCV-IRES-Dnmt3aCD-RFP*), and RFP+ cells were sorted 72 h after infection for RNA isolation and qRT–PCR analysis.

FACS analysis, proliferation, and apoptosis: Flow cytometry, BrdU, and Annexin V measurements were performed as previously described (13, 33). All antibodies were obtained from eBioscience (San Diego, CA, USA). BrdU was performed using the APC BrdU-Flow Kit (BD-Pharmigen, San Jose, CA, USA) according to the manufacturer's instructions and data was analyzed using BD-FACS Diva software. Apoptosis was measured using the Annexin V-APC antibody (eBioscience). A two-sided Student's *t* test was used to analyze differences in proliferation and apoptosis. Thymocytes isolated from 21 day old *Dnmt3a*$^{+/+}$ and *Dnmt3a*$^{\Delta/\Delta}$ (*EμSRα-tTA;Teto-Cre;Rosa26LOXP*$^{EGFP/EGFP}$ *and EμSRα-tTA;Teto-Cre; Rosa26LOXP*$^{EGFP/EGFP}$*;Dnmt3a*$^{F/F}$ *mice, respectively*) were sorted for EGFP^{+} cells using the FACS Aria.

Western blot: The following antibodies were used for Western blot: Dnmt3b (52A1018, Imgenex, Littleton, CO, USA), Dnmt3a (H-295, Santa Cruz, Santa Cruz, CA, USA), γ-Tubulin (H-183, Santa Cruz), and PCNA (PC10, Santa Cruz). Western blots were carried out as described previously (13). Briefly, For Western blotting, protein lysates were separated in SDS acrylamide gels and blotted into Immobilon P

membranes (Millipore). Blots were incubated in blocking buffer (5% skim milk) at a concentration of 1 mg/mL. The primary antibody was then detected using horseradish-peroxidase-conjugated secondary antibodies and the ECL reagent as described by the manufacturer (Pierce). For Figure 6d and Supplementary Figure S13 protein levels were quantified by measuring band density of Dnmt3b and normalized to PCNA and γ-tubulin, respectively (ImageJ software).

Real-time quantitative RT-PCR (qRT-PCR): RNA was converted to cDNA using oligo dT primers and Superscript reverse transcriptase per manufacturer's instruction (Invitrogen, Grand Island, NY, USA). qRT-PCR was carried out using SYBR Green Supermix (Bio-Rad, Hercules, CA, USA) at a final volume of 20 μl and performed in triplicates. Thermocycling was performed using the CFX96 cycler (Bio-Rad). *Gapdh* expression values were used for normalization of C_T values. Primer sequences are listed in Supplementary File S3.

Results

Oncogenic role of Dnmt3a in MTCL.

To evaluate the role of Dnmt3a in MTCL, we generated *EμSRα-tTA;Teto-MYC;Rosa26LOXP$^{EGFP/EGFP}$;Dnmt3a$^{F/F}$* (designated MYC;Dnmt3a$^{F/F}$or control mice), *EμSRα-tTA;Teto-MYC;Teto-Cre;Rosa26LOXP$^{EGFP/EGFP}$; Dnmt3a$^{+/F}$* (designated *MYC;Dnmt3a$^{+/Δ}$* or heterozygous mice) and *E*μ*SR*α*-tTA;Teto-MYC;Teto-Cre;Rosa26LOXP$^{EGFP/EGFP}$*; Dnmt3a$^{F/F}$ (designated *MYC;Dnmt3a$^{Δ/Δ}$* or Dnmt3a-deficient; Figure 1a) mice and measured survival. Although loss of one allele of *Dnmt3a* had no effect on MTCL, we found that the biallelic inactivation of *Dnmt3a* significantly extended the survival of mice relative to controls (Figure 1b). Analysis of protein and DNA confirmed the complete ablation of Dnmt3a in tumors arising in *MYC;Dnmt3a$^{Δ/Δ}$* mice

(Figures 1c and d). Loss of Dnmt3a had no effect on MYC expression (Supplementary Figure S1), suggesting that the delayed MTCL in Dnmt3a-deficient mice was not caused by downregulation of transgenic MYC. Tumor burden in various hematopoietic organs was similar between control and Dnmt3a-deficient mice, indicating that loss of Dnmt3a did not affect mouse survival in a tissue-specific manner (Supplementary Figure S2). Like control lymphomas, tumors from MYC;Dnmt3a$^{\Delta/\Delta}$ were either CD4+/CD8+ or CD4+, with no measurable differences in expression of other T-cell (CD3, TCRβ, TCRγδ), B-cell (B220, CD19), myeloid (CD11b, Gr-1) or erythroid (TER119) markers (Figure 1e and data not shown). Altogether, this suggests that loss of Dnmt3a did not affect the disease spectrum in this MTCL model. Thus, contrary to our expectations, these data show that loss of Dnmt3a suppresses MTCL, suggesting an oncogenic function for Dnmt3a in T-cells.

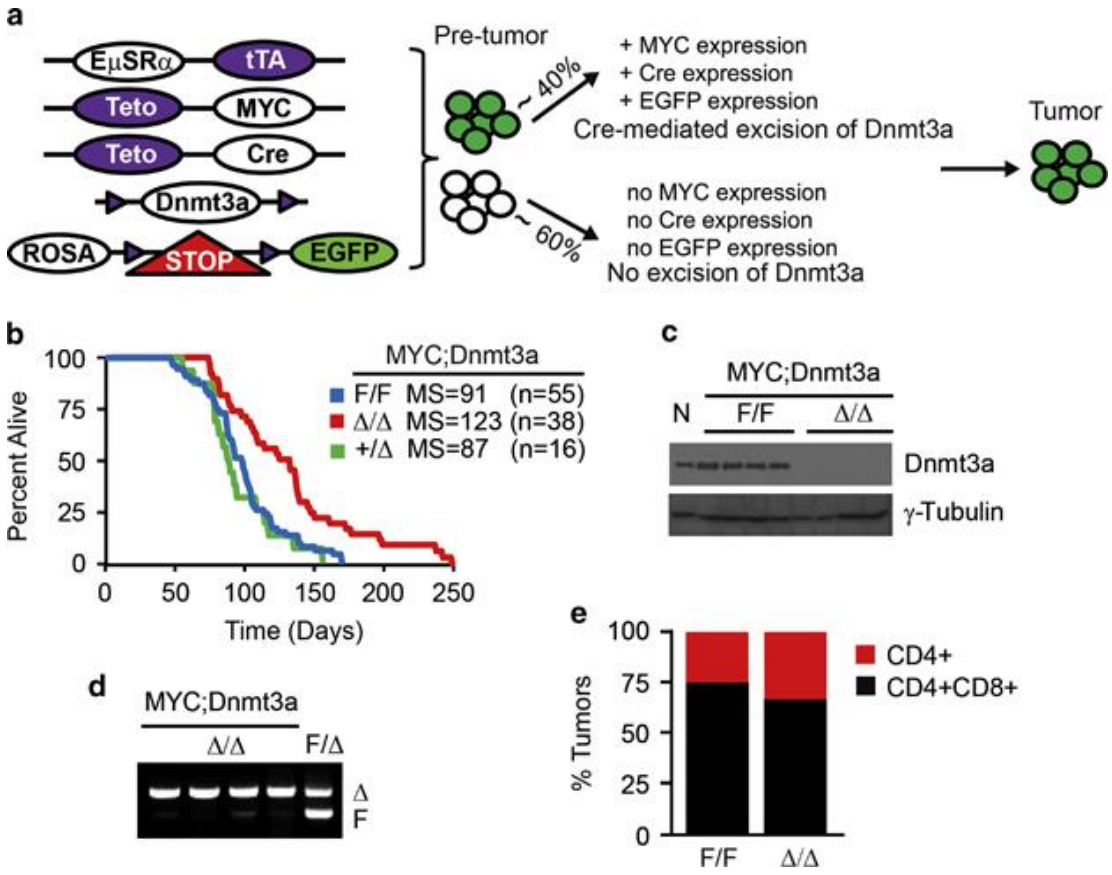

Figure 1. Ablation of Dnmt3a delays T-cell lymphomagenesis. (**a**) Genetic setting used to conditionally delete Dnmt3a. The tetracycline activator protein (tTA) is expressed and promotes simultaneous expression of the *Teto-MYC* and *Teto-Cre* transgenes. Expression of *Cre* results in excision of the stop cassette located upstream of the *Rosa26LOXPEGFP* reporter locus and deletion of Dnmt3a within the same subpopulation of cells. Thus, inclusion of the EGFP transgene allows for monitoring cells expressing *tTA, Cre* and *MYC*, as well as to identify cells deleted for Dnmt3a. In the pre-tumor stage (from birth to approximately day 21), the *EμSRα-tTA* transgene is expressed in 30–50% of cell in all hematopoietic lineages, including hematopoietic stem cells. During tumorigenesis, MYC-expressing cells expand rapidly, resulting in EGFP-positive tumors. (**b**) Kaplan–Meier survival curve for control (*MYC;Dnmt3a*$^{F/F}$, blue), Dnmt3a-deficient (*MYC;Dnmt3a*$^{Δ/Δ}$, red) and Dnmt3a heterozygous (*MYC;Dnmt3a*$^{+/Δ}$, green) mice. Number of mice (*n*) and median survival (MS) is shown. Comparison of *MYC;Dnmt3a*$^{F/F}$ with *MYC;Dnmt3a*$^{Δ/Δ}$ was statistically significant (*P*=0.0002). (**c**) Immunoblot showing Dnmt3a expression in normal thymocytes (N), control tumors (*MYC;Dnmt3a*$^{F/F}$) and Dnmt3a-deficient tumors (*MYC;Dnmt3a*$^{Δ/Δ}$). γ-Tubulin is shown as a loading control. (**d**) PCR-based deletion efficiency of Dnmt3a in *MYC;Dnmt3a*$^{Δ/Δ}$ tumors. *Dnmt3a*$^{F/Δ}$ served as a control. F and Δ indicate floxed and knockout alleles, respectively. (**e**) FACS analysis of immunophenotypes is plotted to show percentage of CD4+ and CD4+CD8+ malignanies in *MYC;Dnmt3a*$^{F/F}$ (F/F) and *MYC;Dnmt3a*$^{Δ/Δ}$ (Δ/Δ) mice.

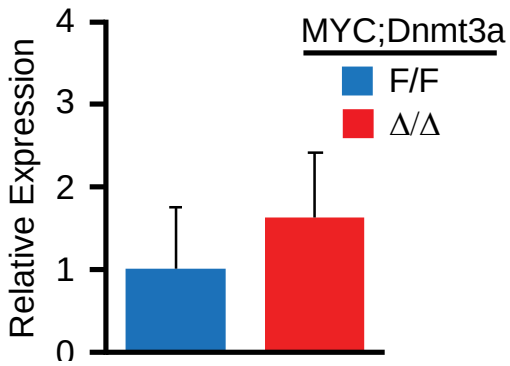

Supplementary Figure S1. MYC expression is similar between control and Dnmt3a-deficient lymphomas. qRT-PCR analysis of *MYC* levels in *MYC;Dnmt3a*$^{F/F}$ tumors (blue, n=4) and *MYC:Dnmt3a*$^{\Delta/\Delta}$ (red, n=4). Error bars denote ± SEM.

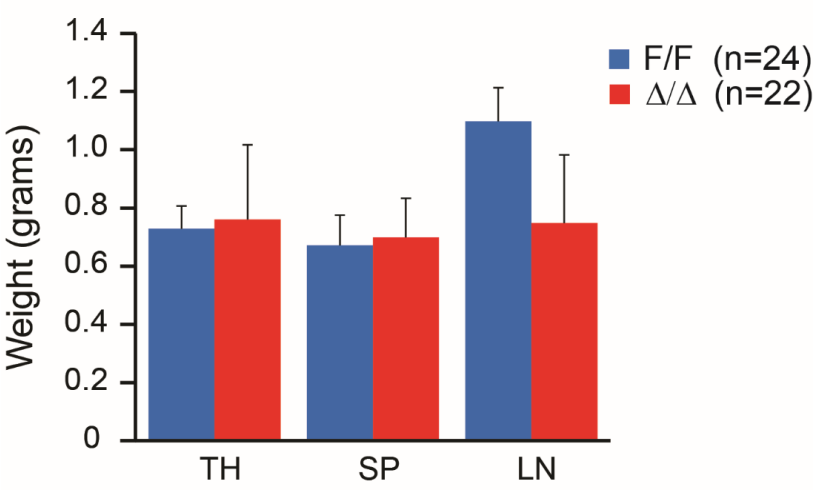

Supplementary Figure S2. Tumor burden in control and Dnmt3a-deficient mice. Analysis of tumor burden in *MYC;Dnmt3a*$^{F/F}$ (F/F, blue) and *MYC;Dnmt3a*$^{\Delta/\Delta}$ (Δ/Δ, red) terminally ill mice. Weights of thymus (TH), spleen (SP), and lymph node (LN) were averaged. Error bars denote ± SEM. Number of mice (n) used for each group is shown.

Dnmt3a inactivation decreases cellular proliferation during disease progression.

We next sought to determine the nature of biological processes affecting MTCL in the absence of Dnmt3a. We first looked at T-cell development in 21-day-old *EμSRα-tTA;Teto-MYC;Teto-Cre;ROSA26*$^{EGFP/EGFP}$;*Dnmt3a*$^{+/+}$ (*MYC;Dnmt3a*$^{+/+}$) and *MYC;Dnmt3a*$^{Δ/Δ}$ mice. Although Dnmt3a was efficiently deleted in EGFP^{+} cells isolated from the thymi of *MYC;Dnmt3a*$^{Δ/Δ}$ mice (Figure 2a), no substantial differences were found in size or cellularity of thymi and spleens when compared with *MYC;Dnmt3a*$^{+/+}$ in 21-day-old mice (data not shown). T-cell development evaluated by expression of CD4, CD8, CD25 and CD44 markers and the percentage of cells expressing EGFP was not affected by loss of Dnmt3a at 21 days (Figure 2b, Supplementary Figures S3 and S4). These data suggest that Dnmt3a is dispensable for T-cell development, consistent with our previous report (34). Similarly, no differences in the levels of apoptosis were observed between *MYC;Dnmt3a*$^{+/+}$ and *MYC;Dnmt3a*$^{Δ/Δ}$ mice at any stage of tumor development (Figure 2c). In contrast, whereas BrdU incorporation was similar at early stages of tumor development (21 days), a substantial decrease in cells incorporating BrdU was observed at later stages of tumor development (35 days and terminally ill mice; Figures 2d and e, Supplementary Figures S5 and S6). Together, these results imply that the extended survival of *MYC;Dnmt3a*$^{Δ/Δ}$ mice is caused by decreased proliferation during disease progression.

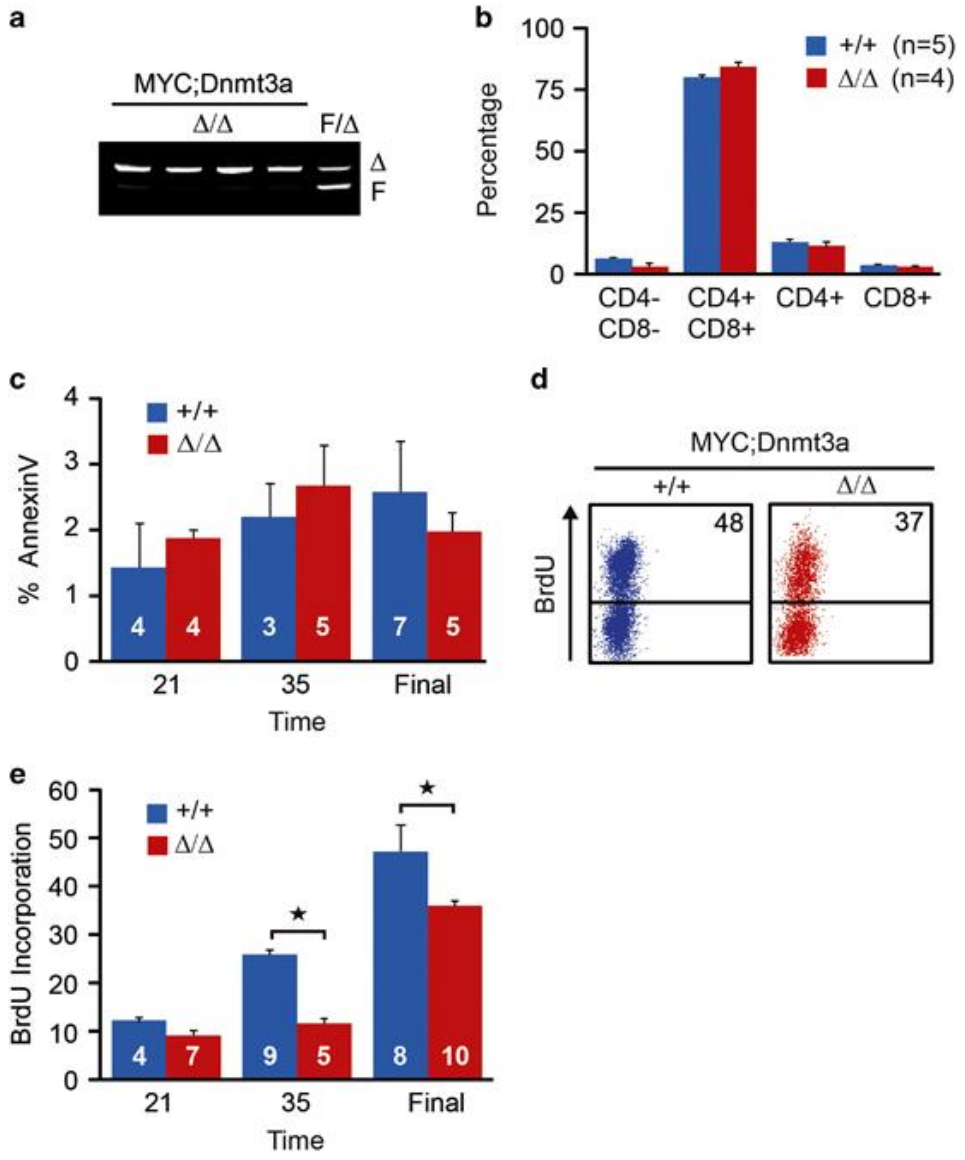

Figure 2. Dnmt3a inactivation decreases cellular proliferation during disease progression. (**a**) PCR-based deletion efficiency of Dnmt3a in EGFP^{+} sorted thymoctyes isolated from 21-day-old *MYC;Dnmt3a*$^{\Delta/\Delta}$ mice. *Dnmt3a*$^{F/\Delta}$ served as a control. F and Δ indicate floxed and knockout alleles, respectively. (**b**) FACS analysis of T-cell development in thymocytes isolated from 21-day-old *MYC;Dnmt3a*$^{+/+}$ (blue) and *MYC;Dnmt3a*$^{\Delta/\Delta}$ (red) mice. Number of mice (*n*) in each cohort is shown. Quantification of obtained results is shown as an average value with error bars representing±s.e.m. (**c**) Analysis of apoptosis by Annexin V staining in cells isolated from the thymi of 21-day-old, 35-day-old and final tumors in *MYC;Dnmt3a*$^{+/+}$ (blue) and *MYC;Dnmt3a*$^{\Delta/\Delta}$ (red) mice. Error bars denote±s.e.m. Number of mice used for each group is shown inside the bars. (**d**) Representative FACS diagrams showing BrdU labeling in *MYC;Dnmt3a*$^{+/+}$ (blue) and *MYC;Dnmt3a*$^{\Delta/\Delta}$ (red) final thymic tumors. The percentage of cells staining positive is shown. (**e**) Quantification of BrdU-positive cells isolated from the thymi of 21-day-old, 35-day-old and final tumors in *MYC;Dnmt3a*$^{+/+}$ (blue) and *MYC;Dnmt3a*$^{\Delta/\Delta}$ (red) mice. Quantification of results for each time point is shown as an average value with error bars representing±s.e.m. Number of mice used for each comparison is shown inside the bar. *P*<0.05 is denoted by a (*).

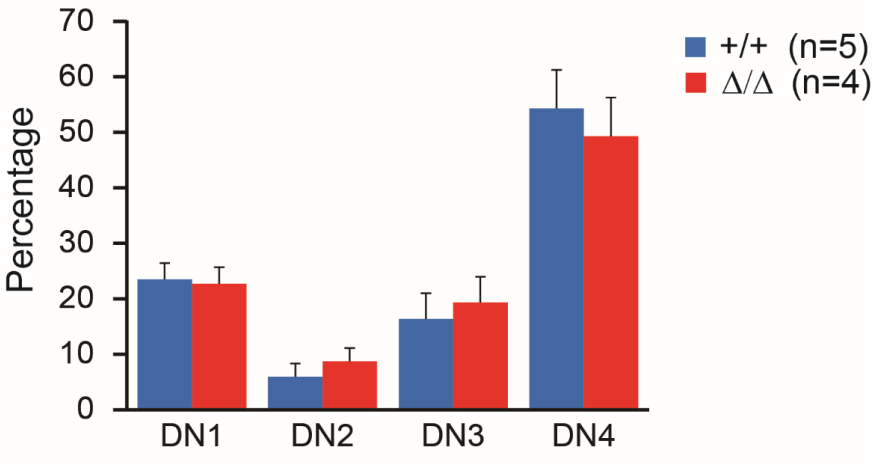

Supplementary Figure S3. Loss of Dnmt3a does not effect T-cell development. FACS analysis of T-cell development in $CD4^{neg}CD8^{neg}$ (double negative, DN) thymocytes populations isolated from 21 day old *MYC;Dnmt3a*$^{+/+}$ (+/+, blue) and *MYC;Dnmt3a*$^{\Delta/\Delta}$ (Δ/Δ, red) mice. Immunophenotypes of DN populations in thymocytes are as follows: $CD4^{neg}CD8^{neg}CD25^{neg}CD44^{+}$ (DN1), $CD4^{neg}CD8^{neg}CD25^{+}CD44^{+}$ (DN2), $CD4^{neg}CD8^{neg}CD25^{+}CD44^{neg}$ (DN3), and $CD4^{neg}CD8^{neg}CD25^{neg}CD44^{neg}$ (DN4). Number of mice (n) in each group is shown. Quantification of obtained results is shown as an average value with error bars representing ± SEM

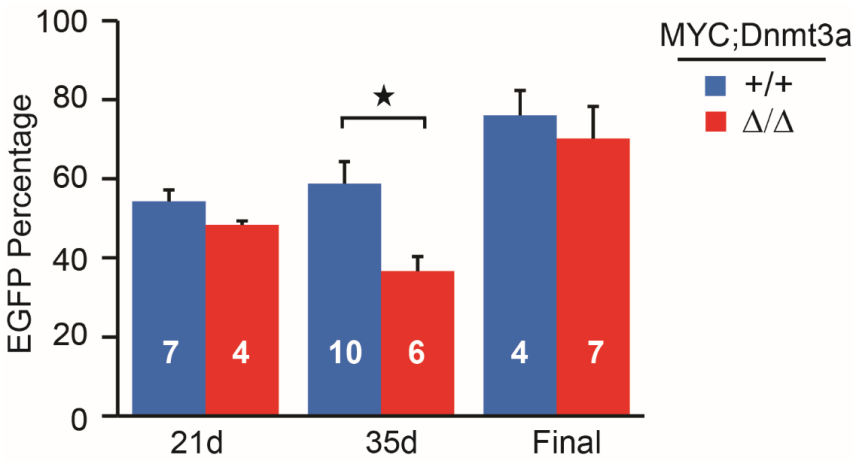

Supplementary Figure S4. EGFP expression in thymocytes from control and Dnmt3a-deficient mice. Average percentage of EGFP^{+} cells in the thymi of 21 day old, 35 day old, and final tumors in MYC;Dnmt3a$^{+/+}$ (blue) and MYC;Dnmt3a$^{\Delta/\Delta}$ (red) mice, as determined by FACS. Error bars represent ± SEM. Number of mice used for each group is shown inside the bars. (*) denotes $P<0.05$.

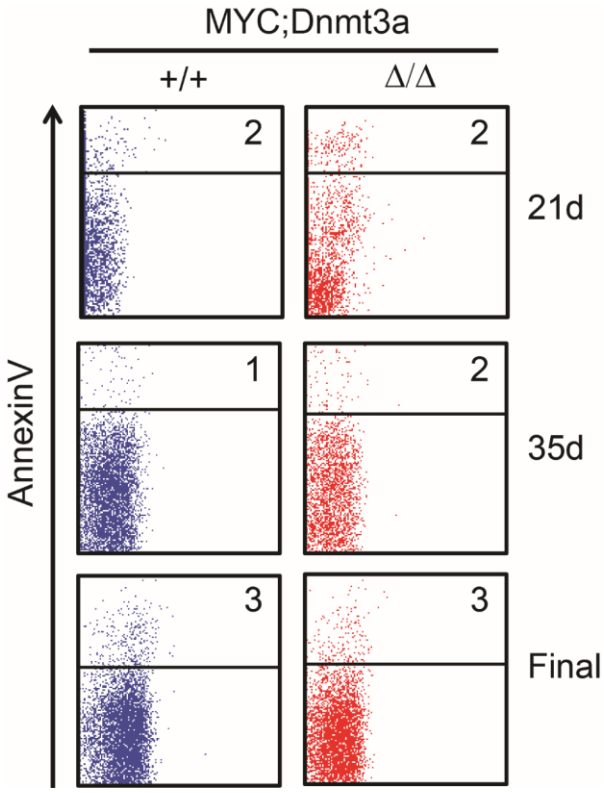

Supplementary Figure S5. Analysis of Annexin V staining by FACS. Representative FACS diagrams showing analysis of apoptosis by Annexin V staining in thymocytes isolated from 21 day old, 35 day old, and final tumors in *MYC;Dnmt3a*$^{+/+}$ (blue) and *MYC;Dnmt3a*$^{\Delta/\Delta}$ (red) mice. The percent of cells staining positive is shown in upper quadrant

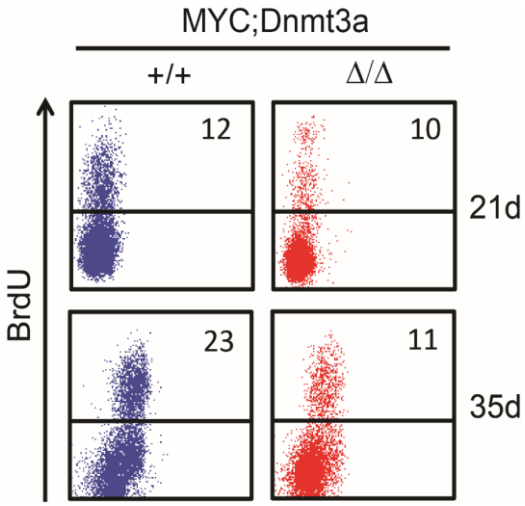

Supplementary Figure S6. Analysis of BrdU incorporation by FACS. Representative FACS diagrams showing BrdU labeling for thymocytes isolated from 21 day old and 35 day old *MYC;Dnmt3a*$^{+/+}$ (blue) and *MYC;Dnmt3a*$^{\Delta/\Delta}$ (red) mice.

Dnmt3a ablation results in genome-wide methylation changes in lymphomas.

To investigate the locus-specific effects of Dnmt3a on DNA methylation, we used methyl-sensitive cut counting (MSCC) to profile the methylation patterns of *MYC;Dnmt3a*$^{F/F}$ and *MYC;Dnmt3a*$^{\Delta/\Delta}$ lymphomas along with normal *Dnmt3a*$^{+/+}$ and *Dnmt3a*$^{\Delta/\Delta}$ thymocytes as previously described (13, 33, 34, 81). In this next-generation sequencing-based method, the methylation—evaluated based on the number of sequence tags (termed counts)—inversely correlates with the degree of methylation at *Hpa*II and *HpyCh4*IV sites (81). A total of 24 236 promoters in the mouse genome have at least two *Hpa*II and/or *HpyCh4*IV restriction sites. To rigorously assess the methylation status of promoters, we considered a change in methylation to be significant only if it occurred in two or more independent restriction sites in promoter areas from −1500 to +500 base pairs relative to the transcription start site (two fold, false discovery rate (FDR) <0.05). We first compared promoter-specific methylation between *MYC;Dnmt3a*$^{F/F}$ and *MYC;Dnmt3a*$^{\Delta/\Delta}$ lymphomas. This analysis revealed that 370 gene promoters were hypomethylated in *MYC;Dnmt3a*$^{\Delta/\Delta}$ lymphomas, suggesting that these promoters may represent potential targets of Dnmt3a-specific methylase activity (Figure 3a and Supplementary File S1). In contrast, the promoters of 64 genes were hypermethylated in *MYC;Dnmt3a*$^{\Delta/\Delta}$ lymphomas, likely as an indirect effect of Dnmt3a loss (Figure 3a).

Next, we analyzed the methylation status of these promoters in normal thymocytes and Dnmt3a-deficient thymocytes. Out of the 370 promoters hypomethylated in *MYC;Dnmt3a*$^{\Delta/\Delta}$ lymphomas, 353 were also hypomethylated when compared with either normal or *Dnmt3a*$^{\Delta/\Delta}$ thymocytes, implying that Dnmt3a is dispensable for their *de novo* methylation during normal development, but may have a role in their maintenance methylation during tumorigenesis (Figure 3a and Supplementary Figure S7). In contrast,

17 promoters were specifically hypermethylated in *MYC;Dnmt3a*$^{F/F}$ tumors, indicating that they may represent potential targets of Dnmt3a cancer-specific *de novo* methylation (Figure 3a and Supplementary Figure S7). Finally, promoters of 10 genes were hypomethylated in normal Dnmt3a-deficient thymocytes, suggesting that their methylation is already decreased during normal development and thus their hypomethylation in *MYC;Dnmt3a*$^{\Delta/\Delta}$ lymphomas is not tumor-specific (Supplementary Figure S7). Methylation read-outs from MSCC analysis were confirmed for selected promoters using locus-specific combined bisulfite restriction analysis (COBRA). For example, the predicted gene *AK046742* appeared to be a target of Dnmt3a's cancer-specific *de novo* activity, as its promoter region was not methylated in normal thymocytes and *MYC;Dnmt3a*$^{\Delta/\Delta}$ tumors but was methylated in *MYC;Dnmt3a*$^{F/F}$ tumors (Figure 3b). Conversely, *Leng1* may be a target of Dnmt3a maintenance activity as the area near its promoter was hypermethylated in normal thymocytes and *MYC;Dnmt3a*$^{F/F}$ lymphomas but not in *MYC;Dnmt3a*$^{\Delta/\Delta}$ lymphomas (Figure 3b). These data indicate that the contribution of Dnmt3a to the tumor-specific methylation patterns consists of both *de novo* and maintenance activities. It is worth noting that the magnitude of Dnmt3a effects on genome-wide methylation may be larger, as analysis of promoters using single *Hpa*II or *HpyCh4*IV sites showed 1854 hypomethylated promoters in *MYC;Dnmt3a*$^{\Delta/\Delta}$ lymphomas (Supplementary Figure S8). Thus, a higher resolution genome-wide methylation profiling studies—such as whole-genome bisulfite sequencing—may better address this point in future studies.

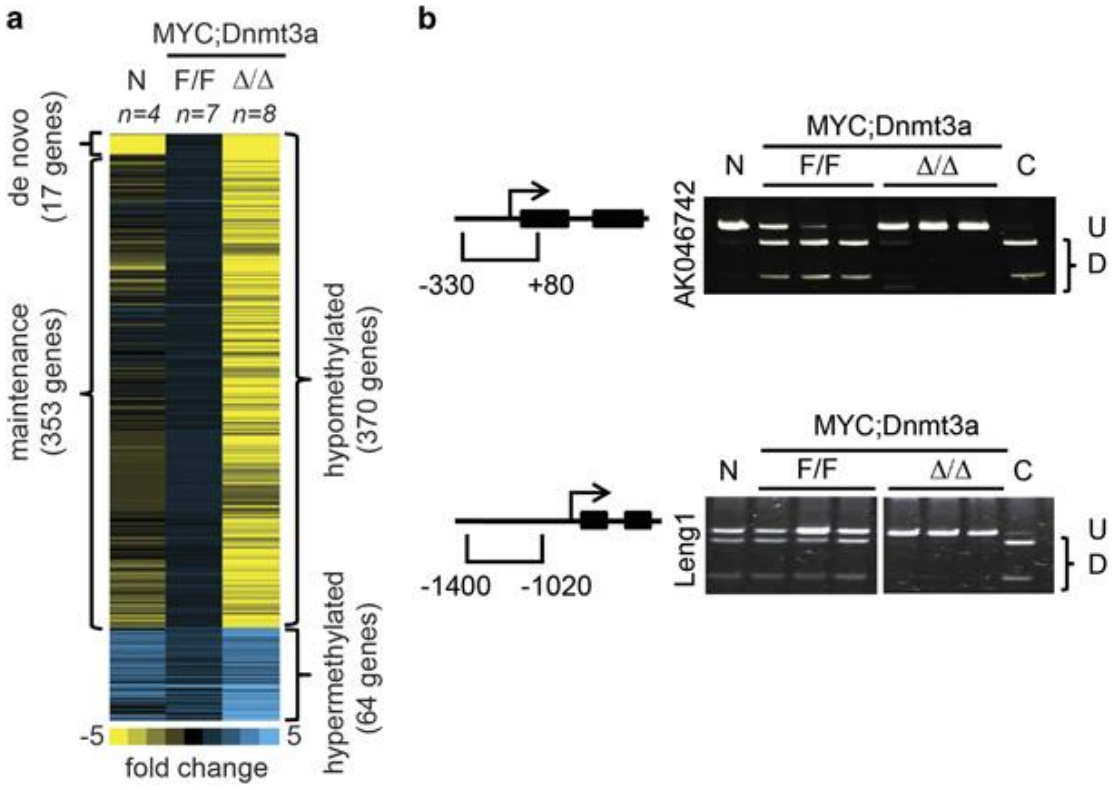

Figure 3. Dnmt3a ablation results in genome-wide methylation changes in *MYC;Dnmt3a*$^{\Delta/\Delta}$ lymphomas. (**a**) Analysis of MSCC data showing 370 hypomethylated and 64 hypermethylated promoters in *MYC;Dnmt3a*$^{\Delta/\Delta}$ tumors relative to *MYC;Dnmt3a*$^{F/F}$ tumors. Proposed *de novo* (17 genes) and maintenance (353 genes) targets are labeled. Methylation status of normal thymocytes (N) is also shown. Promoter is defined as +500 to −1500 relative to the transcription start site. Differentially methylated sites had a fold change of two or greater and an FDR<0.05 at two independent CpG sites. Number of samples per group (*n*) is shown. A color bar depicting fold change is shown with blue representing a high degree of methylation and yellow representing lower levels. (**b**) COBRA analysis of the *AK046742* and *Leng1* promoters in normal thymocytes (N), *MYC;Dnmt3a*$^{F/F}$ and *MYC;Dnmt3a*$^{\Delta/\Delta}$ tumors. PCR fragments were digested with the restriction enzyme *Bst*UI. Undigested {U} and digested {D} fragments correspond to un-methylated and methylated DNA, respectively. C indicates a fully methylated control. Position of primers relative to the transcription start site for each gene is shown in brackets to the left.

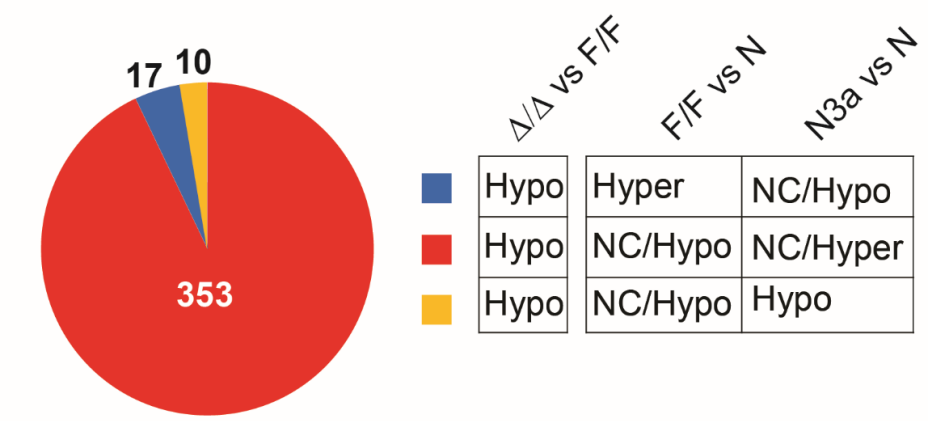

Supplementary Figure S7. Summary of differentially methylated genes in Dnmt3a-deficient tumors. Pie chart showing breakdown of differentially methylated genes in *MYC;Dnmt3a*$^{\Delta/\Delta}$ (Δ/Δ) tumors relative to *MYC;Dnmt3a*$^{F/F}$ (F/F) tumors as determined by analysis of MSCC data. Methylation changes for normal thymocytes (N) and Dnmt3a-deficient thymocytes (N3a) are also shown. All differentially methylated genes are based on 2 tag analysis, a fold change of 2 or greater and an FDR<0.05. Red denotes proposed maintenance targets and blue represents *de novo* targets.

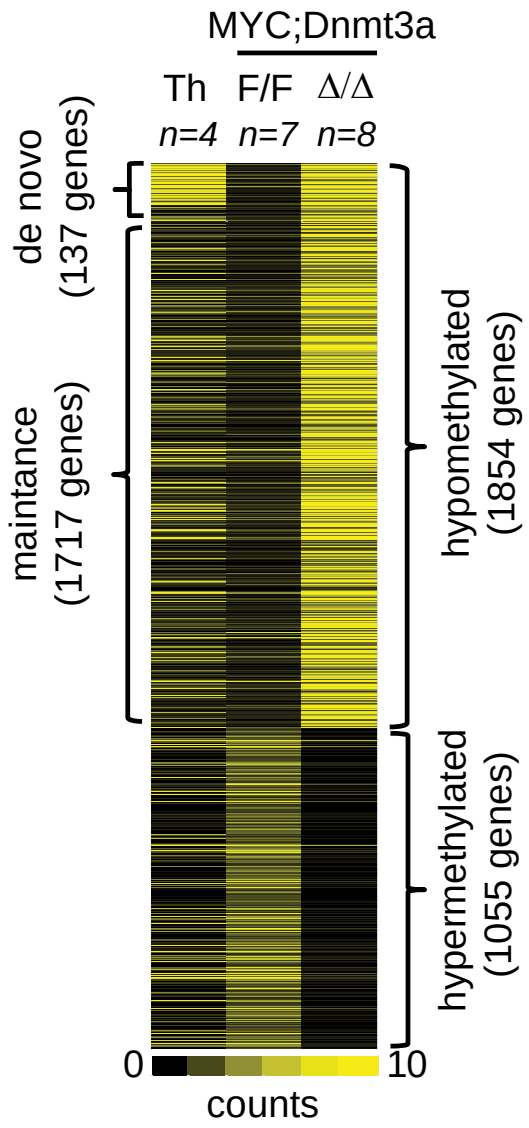

Supplementary Figure S8. Global methylation profiling by MSCC using 1 tag analysis. Analysis of MSCC data showing 1,854 hypomethylated and 1,055 hypermethylated promoters in *MYC;Dnmt3a*$^{\Delta/\Delta}$ tumors (Δ/Δ) relative to *MYC;Dnmt3a*$^{F/F}$ tumors (F/F). Proposed *de novo* (137 genes) and maintenance (1,717 genes) targets are labeled. Methylation status of normal thymocytes (Th) is also shown. Promoter is defined as +500 to -1,500 relative to the transcription start site. Differentially methylated sites had at least one tag with a fold change of 2 or greater and an FDR<0.05. Number of samples per group (n) is shown. A color bar depicting fold change is shown with black representing a high degree of methylation and yellow representing lower levels.

DNA methylation-independent upregulation of TS genes in Dnmt3a-deficient lymphomas.

To further understand the molecular basis for the extended survival of *MYC;Dnmt3a*$^{\Delta/\Delta}$ mice, we compared microarray-based gene expression profiles of *MYC;Dnmt3a*$^{\Delta/\Delta}$ lymphomas with those of normal thymocytes and *MYC;Dnmt3a*$^{F/F}$ lymphomas. We identified 2246 genes whose expression levels were significantly different (1.5-fold; $P<0.05$) between *MYC;Dnmt3a*$^{F/F}$ and *MYC;Dnmt3a*$^{\Delta/\Delta}$ lymphomas (Figure 4a, Supplementary File S2). Loss of Dnmt3a resulted in the transcriptional upregulation of 1421 genes, which is consistent with the function of Dnmt3a as a repressor protein. qRT–PCR confirmed that *Cd79b, E2f2* and *Pten* were upregulated in *MYC;Dnmt3a*$^{\Delta/\Delta}$ lymphomas (Figure 4b). Microarray analysis also identified 825 genes downregulated in *MYC;Dnmt3a*$^{\Delta/\Delta}$ tumors (Figure 4a). Although we cannot rule out the possibility that Dnmt3a has a role in transcriptional activation, these genes likely represent secondary changes resulting from deregulated transcription upon loss of Dnmt3a.

To gain further molecular insight into the pathogenesis of *MYC;Dnmt3a*$^{\Delta/\Delta}$ lymphomas, we performed Ingenuity Pathway Analysis (IPA) using the 1421 genes that were significantly upregulated relative to *MYC;Dnmt3a*$^{F/F}$ lymphomas. The top five disease groups associated with upregulated genes were immunological disease, cancer, inflammatory disease, infectious disease and hematological disease (Supplementary Figure S9). This search also identified a 17-gene signature under the disease network 'Lymphomagenesis' whose upregulation was predicted to suppress lymphomagenesis (Figure 5a). This signature consisted of *Bcl2l11*, *Brca2*, *Dna2*, *Dnmt3b*, *E2f1*, *E2f2*, *Exo1*, *Irf1*, *Irf8*, *Nqo1*, *Prdm2*, *Pten*, *Recql4*, *Smurf2*, *Ssbp2*, *Tyk2* and *Xrcc2*. In contrast, analysis using genes downregulated in *MYC;Dnmt3a*$^{\Delta/\Delta}$ lymphomas did not yield any significant change under the disease network 'Lymphomagenesis'. Surprisingly, both

promoter and gene body methylation was unaffected for all 17 genes (Figure 5b and Supplementary Figure S10), suggesting that the increased expression of these genes is independent of changes in DNA methylation. Furthermore, methylation of gene bodies (defined as +500 to the end of the gene) was largely unaffected by loss of Dnmt3a (Supplementary Figures S11 and S12). The 17-gene TS signature observed in Dnmt3a-deficient MTCLs may represent molecular events functionally contributing to the extended survival observed in *MYC*;*Dnmt3a*$^{\Delta/\Delta}$ mice.

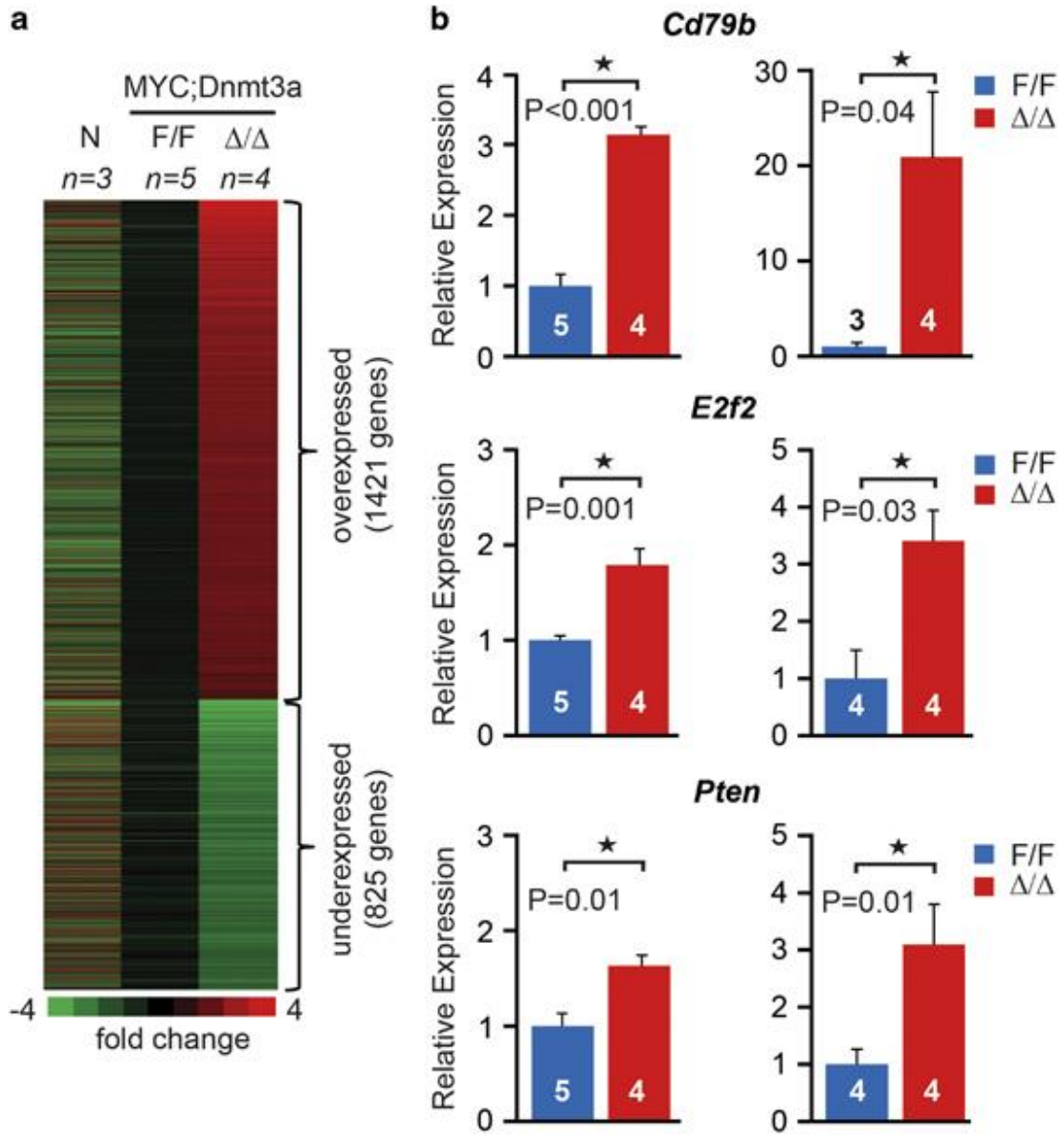

Figure 4. Loss of Dnmt3a leads to deregulated transcription. (a) A heat map derived from global transcription profiling by microarray displaying 1421 overexpressed and 825 under-expressed genes in *MYC;Dnmt3a*$^{\Delta/\Delta}$ tumors relative to *MYC;Dnmt3a*$^{F/F}$ tumors (fold changegreater than or equal to1.5 and P<0.05 by Bayesian t-test). Expression in normal thymocytes (N) is also shown. A color bar is shown to reference fold change with upregulation in red and downregulation in green. Number of samples (n) is shown. (b) On the left, expression data obtained from microarray for three differentially expressed genes in *MYC;Dnmt3a*$^{\Delta/\Delta}$ (red) relative to *MYC;Dnmt3a*$^{F/F}$ (blue) tumors are shown. On the right, qRT–PCR data displaying the relative mRNA levels of the three genes are shown. Quantification of obtained results is shown as an average value with error bars representing±s.e.m. Number of samples used for each comparison is shown inside the bars. P-values are shown with statistical significance denoted by a (*).

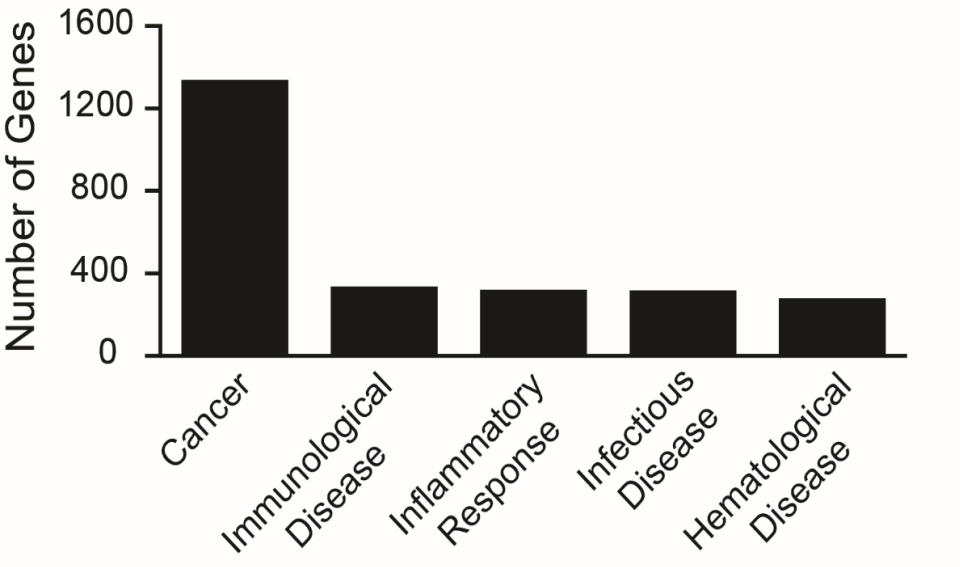

Supplementary Figure S9. Summary of Ingenuity pathway analysis. IPA core analysis was performed on 2,246 genes differentially expressed between *MYC;Dnmt3a*$^{\Delta/\Delta}$ and *MYC;Dnmt3a*$^{F/F}$ tumors.

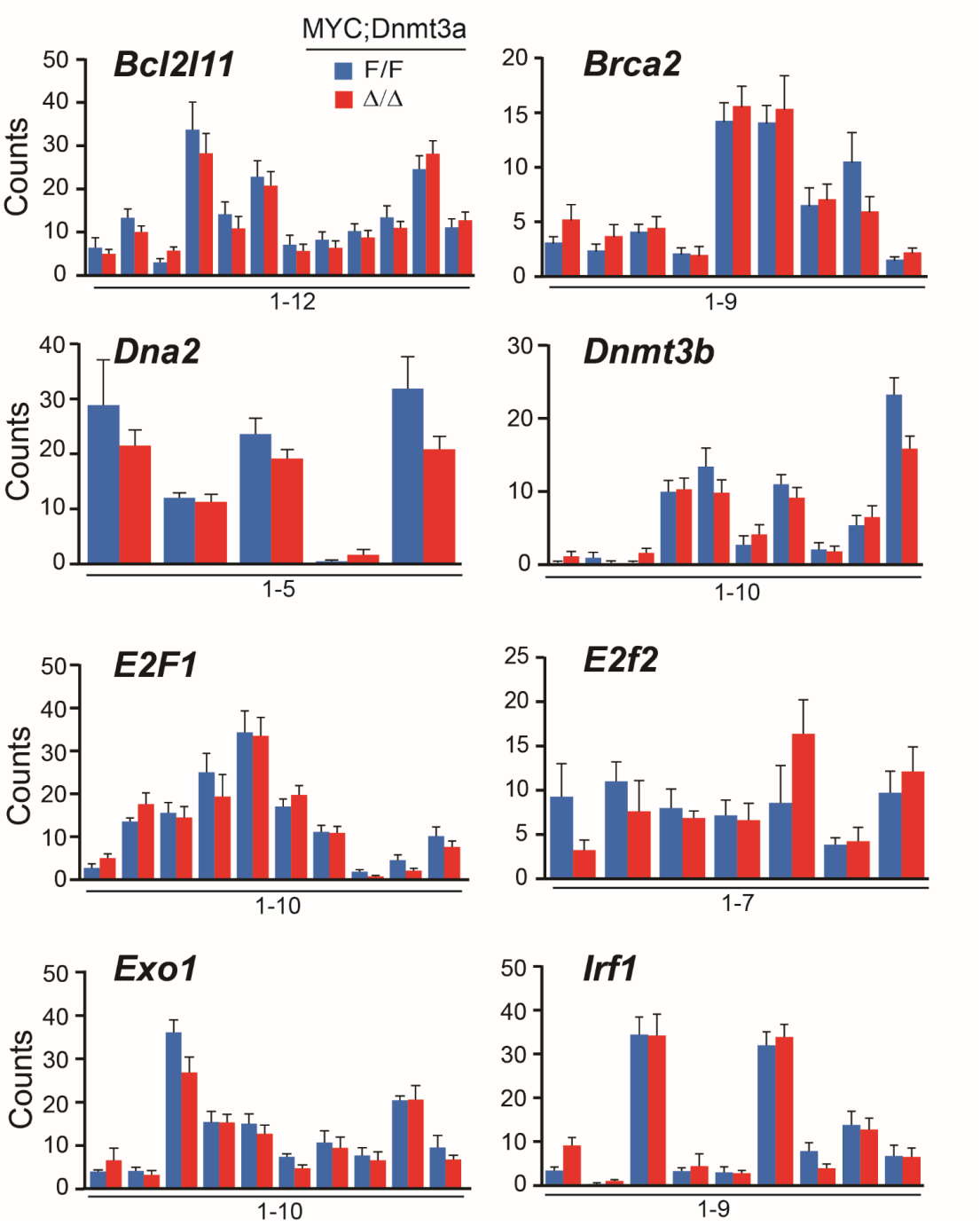
MYC;Dnmt3a
F/F
Δ/Δ
Bcl2l11
Brca2
Dna2
Dnmt3b
E2F1
E2f2
Exo1
Irf1
Counts
1-12
1-9
1-5
1-10
1-10
1-7
1-10
1-9

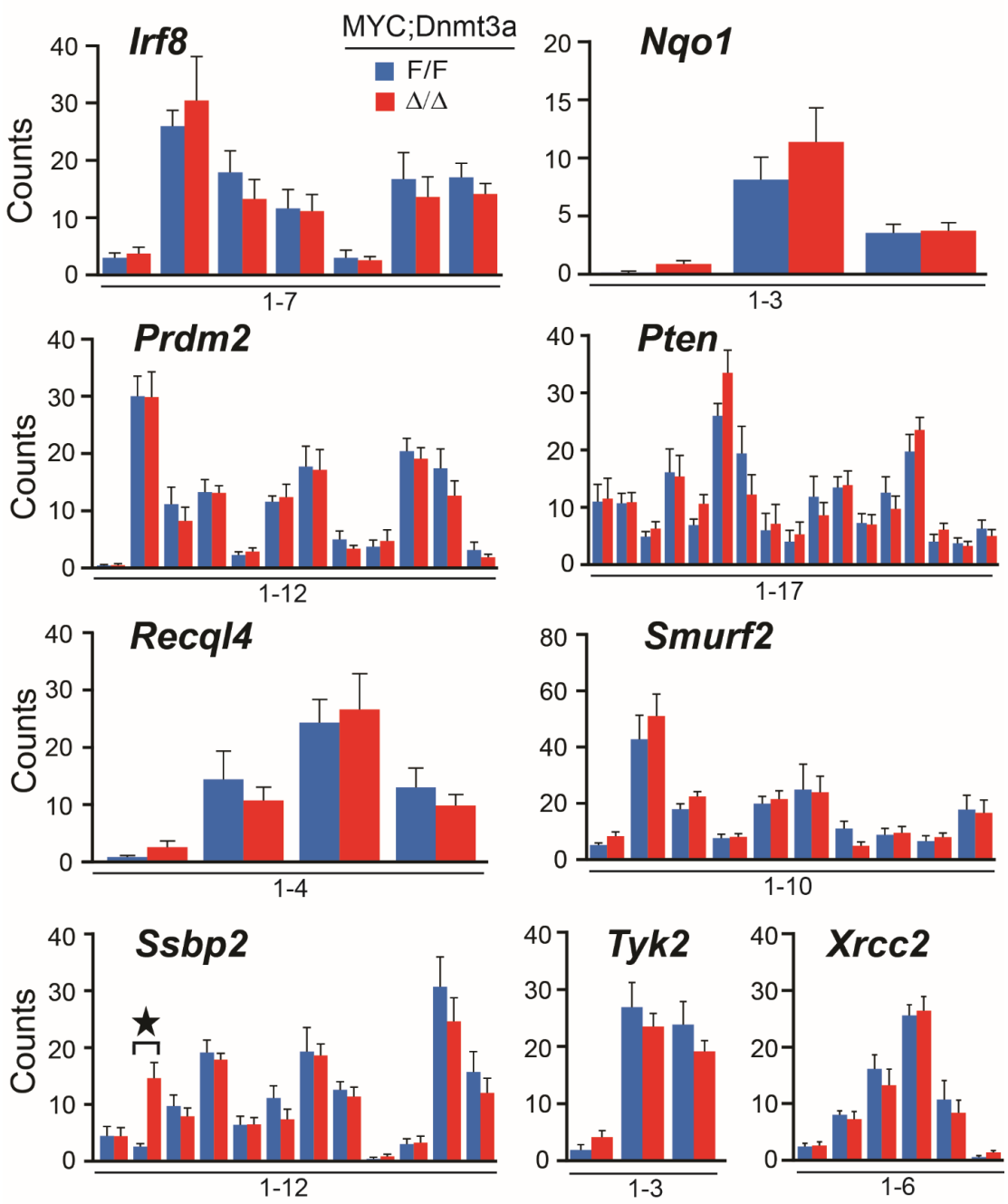

Supplementary Figure S10. MSCC analysis of promoter methylation for the 17 gene signature obtained from IPA. Analysis of methylation levels at individual CpGs present in the promoter regions of the 17 gene signature. Average counts from MSCC data in *MYC;Dnmt3a*$^{F/F}$ (blue) and *MYC;Dnmt3a*$^{\Delta/\Delta}$ (red) were used with error bars designating ± SEM. Counts inversely correlate with methylation status. Promoter is defined at -1,500 to +500 base pairs relative to the TSS. (*) denotes a P <0.05.

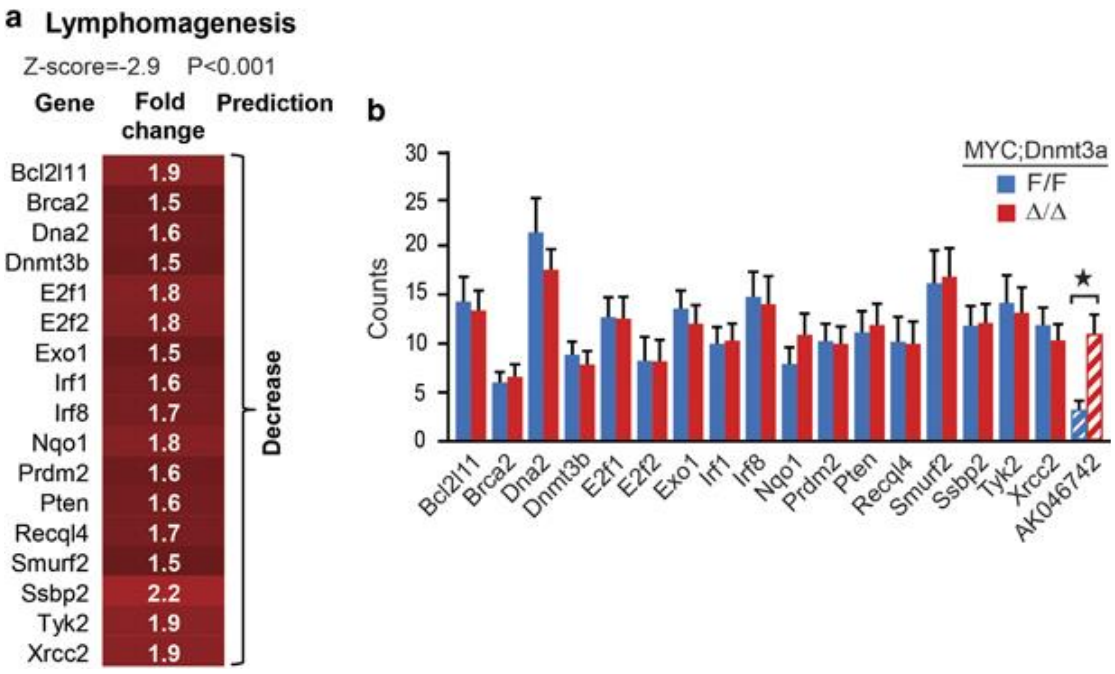

Figure 5. DNA methylation-independent upregulation of tumor suppressor genes in Dnmt3a-deficient lymphomas. (**a**) The 17-gene signature 'Lymphomagenesis' derived from Ingenuity Pathway Analysis (IPA) of 1421 upregulated genes in *MYC;Dnmt3a*$^{\Delta/\Delta}$ tumors. Upregulation of these 17 genes are predicted to suppress lymphomagenesis. Fold changes derived from microarray data, as well as Z-score and *P*-value generated by IPA, are shown. (**b**) Bar graph showing quantification of promoter methylation for the 17 genes using average counts from MSCC data in *MYC;Dnmt3a*$^{F/F}$ (blue) and *MYC;Dnmt3a*$^{\Delta/\Delta}$ (red) tumors. Proposed Dnmt3a target gene, *AK046742,* is shown as a positive control. The promoter is defined as −1500 to +500 relative to the transcription start site. Error bars denote±s.e.m. *P*<0.05 is shown by a (*).

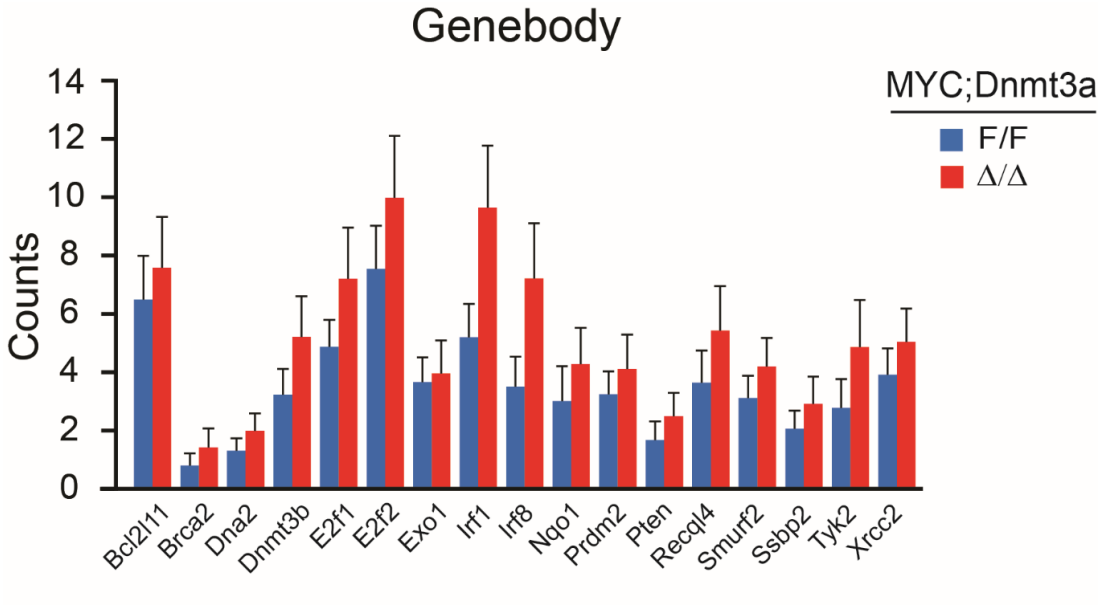

Supplementary Figure S11. Quantification of total gene body methylation for the 17 gene signature obtained from IPA. Counts from MSCC data for *MYC;Dnmt3a*$^{F/F}$ (blue) and *MYC;Dnmt3a*$^{\Delta/\Delta}$ (red) tumors were averaged. Error bars denote ± SEM. Counts inversely correlate with methylation status

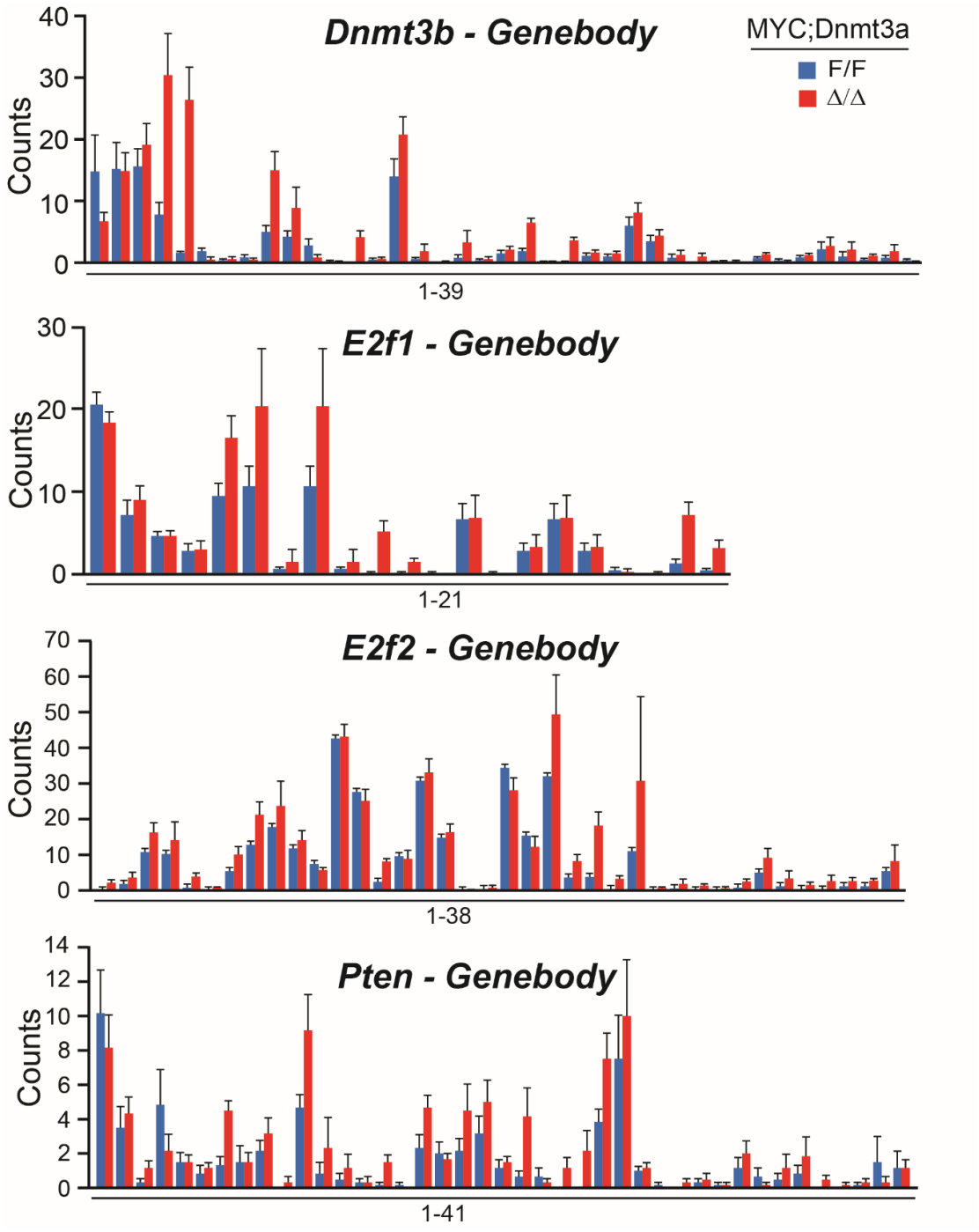

Supplementary Figure S12. MSCC analysis of gene body methylation of four tumor suppressor genes. Bar graph showing quantification of methylation levels for individual CpGs present in the gene body *of Dnmt3b, E2f1*, *E2f2*, and *Pten*. Average counts from MSCC data in *MYC;Dnmt3a*$^{F/F}$ (blue) and *MYC;Dnmt3a*$^{\Delta/\Delta}$ (red) were used and error bars represent ± SEM. Counts inversely correlate with methylation status.

Dnmt3a represses Dnmt3b expression independently of its catalytic activity.

Our global approach identified TS genes under the disease network 'Lymphomagenesis' whose increased expression is associated with little-to-no changes in DNA methylation. Thus, their increased expression could either be in a direct response to loss of Dnmt3a repressor function or could be an indirect consequence of lymphomagenesis.

We have recently reported that a close relative of Dnmt3a, Dnmt3b, is a TS gene in this MTCL model due to its ability to negatively regulate cellular proliferation during disease progression (13). As our data indicate that a key biological process behind delayed MTCL is decreased proliferation and our global gene expression data showed upregulation of Dnmt3b in *MYC;Dnmt3a*$^{\Delta/\Delta}$ tumors, we wondered whether Dnmt3a regulates Dnmt3b expression. To address this we first looked at the expression of Dnmt3b in *MYC;Dnmt3a*$^{\Delta/\Delta}$ lymphomas. This analysis revealed upregulation of mRNA and protein levels of Dnmt3b, suggesting that Dnmt3a may repress Dnmt3b (Figures 6a and b). Re-introduction of wild-type Dnmt3a into cell lines derived from *MYC;Dnmt3a*$^{\Delta/\Delta}$ lymphomas resulted in moderate but significant decrease in Dnmt3b RNA and protein levels (Figures 6c–e, Supplementary Figure S13). As we did not detect differences in methylation levels of the *Dnmt3b* promoter or gene body, we asked whether Dnmt3a inhibition of Dnmt3b could be independent of its methylase activity. To test this directly we infected *MYC;Dnmt3a*$^{\Delta/\Delta}$ lymphoma cells with Dnmt3a in which two key amino acids in the catalytic domain were mutated to produce a catalytically dead Dnmt3a protein (Dnmt3aCD (113)). Overexpression of Dnmt3aCD repressed Dnmt3b expression to a similar extent as wild-type Dnmt3a. Altogether, these data suggest that Dnmt3a represses Dnmt3b in a methylation-independent manner (Figures 6c–e).

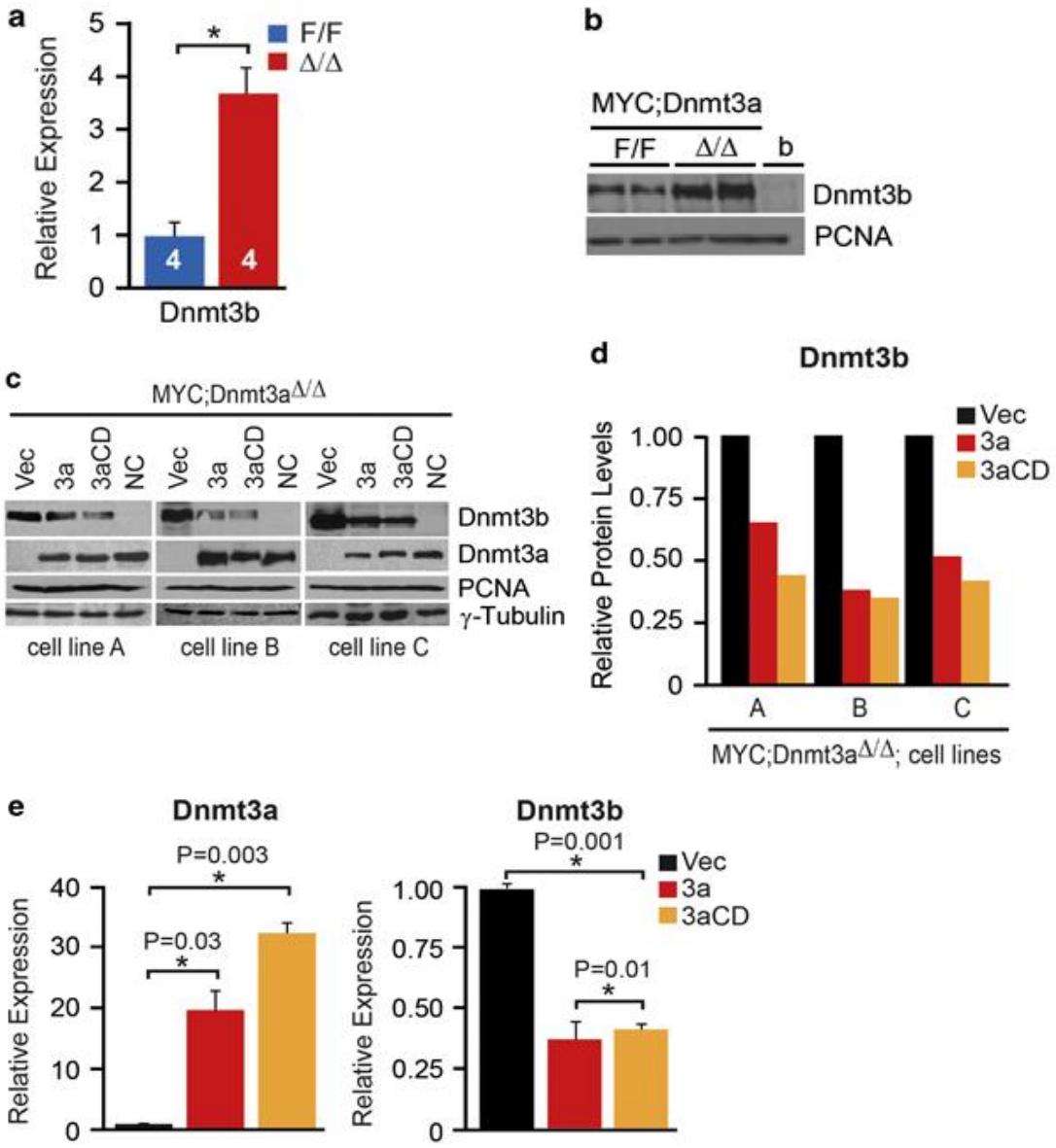

Figure 6. Dnmt3a represses Dnmt3b expression independently of its catalytic activity. (**a**) qRT–PCR analysis of *Dnmt3b* transcript levels in control *MYC;Dnmt3a*$^{F/F}$ tumors (blue) and *MYC;Dnmt3a*$^{\Delta/\Delta}$ tumors (red). The number of samples used for each group is shown inside the bars. Error bars denote±s.e.m. *P*<0.05 is shown by a (*). (**b**) Immunoblot showing Dnmt3b protein levels in *MYC;Dnmt3a*$^{F/F}$ tumors, *MYC;Dnmt3a*$^{\Delta/\Delta}$ tumors, and a Dnmt3b-deficient control (b). PCNA served as a loading control. (**c**) Immunoblot analysis showing Dnmt3b and Dnmt3a expression in three independent *MYC;Dnmt3a*$^{\Delta/\Delta}$ cell lines (A, B, C) infected with empty vector (Vec), wild-type Dnmt3a (3a) or catalytically dead Dnmt3a (3aCD). Lane 4 shows a Dnmt3b-deficient control (NC). PCNA and γ-Tubulin are shown as loading controls. (**d**) Quantification of Dnmt3b protein levels in *MYC;Dnmt3a*$^{\Delta/\Delta}$ cell lines (A, B, C) for (**c**). Dnmt3b levels were normalized to PCNA. Relative protein levels were calculated by adjusting values for empty vector control (Vec) to one and using this as a baseline for all other comparisons. (**e**) qRT–PCR analysis of *Dnmt3a* (left) and *Dnmt3b* (right) transcript levels in cell lines derived from *MYC;Dnmt3a*$^{\Delta/\Delta}$ tumors infected with empty vector control (black), wild-type Dnmt3a (red) or catalytically dead Dnmt3a (yellow).

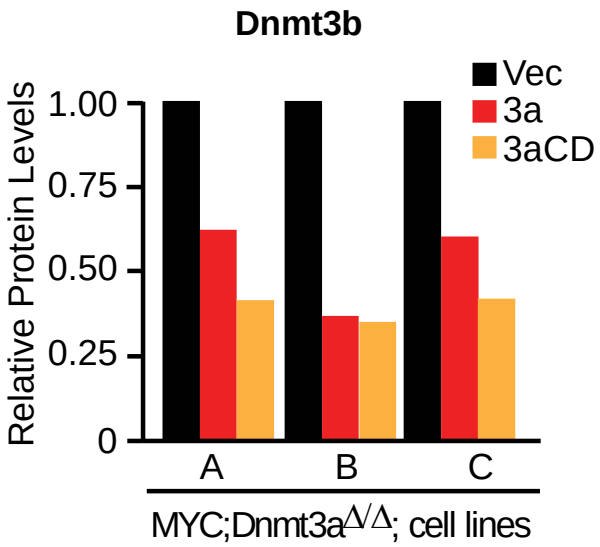

Supplementary Figure S13. Relative Dnmt3b protein levels in three cell lines after Dnmt3a expression. Quantification of Dnmt3b protein levels in *MYC;Dnmt3a*$^{\Delta/\Delta}$ cell lines (A, B, C) infected with empty vector (black), Dnmt3a (red) or catalytically dead Dnmt3a (3aCD). Dnmt3b levels were normalized to γ-Tubulin. Relative protein levels were calculated by adjusting values for empty vector control (Vec) to one and using this as a baseline for all other comparisons

Loss of Dnmt3b accelerates lymphomagenesis in Dnmt3a-deficient mice.

We next hypothesized that upregulation of Dnmt3b may be an important molecular event inhibiting MTCL in the absence of Dnmt3a. To test this directly, we generated and compared the survival of *MYC;Dnmt3a*$^{\Delta/\Delta}$;*Dnmt3b*$^{\Delta/\Delta}$ (Double-knockout; DKO) mice with *MYC;Dnmt3a*$^{F/F}$;*Dnmt3b*$^{F/F}$ mice (Figure 7a). In contrast to the prolonged survival seen in *MYC;Dnmt3a*$^{\Delta/\Delta}$ mice, DKO mice displayed indistinguishable survival compared with *MYC;Dnmt3a*$^{F/F}$;*Dnmt3b*$^{F/F}$ control mice (Figure 7b). Both Dnmt3a and Dnmt3b were efficiently inactivated in DKO lymphomas (Figures 7c and d). Apoptosis, T-cell development, tumor burden, transgenic *MYC* expression and tumor spectrum were similar between terminally sick control and DKO mice (Supplementary Figures S14–19), indicating that the additional loss of Dnmt3b did not impact these processes. Interestingly, proliferation of lymphoma cells, a process impaired in *MYC;Dnmt3a*$^{\Delta/\Delta}$ mice, was similar between terminally sick control and DKO mice (Figure 7e), which is consistent with the decreased survival of DKO mice relative to Dnmt3a-deficient mice. The distinct roles of Dnmt3a and Dnmt3b in MTCL are consistent with molecular changes observed in Dnmt3a- or Dnmt3b-deficient lymphomas. Out of 370 promoters hypomethylated in *MYC;Dnmt3a*$^{\Delta/\Delta}$ lymphomas, only 3% were hypomethylated in Dnmt3b-deficient lymphomas (13), indicating that Dnmt3a and Dnmt3b have distinct targets *in vivo* (Figure 7f). Similarly, only 11% of genes upregulated in Dnmt3a-deficient lymphoma were also overexpressed in Dnmt3b-deficient lymphomas (Figure 7f (13)). Collectively, these data illustrate both cellular and molecular differences between Dnmt3a and Dnmt3b in MTCL.

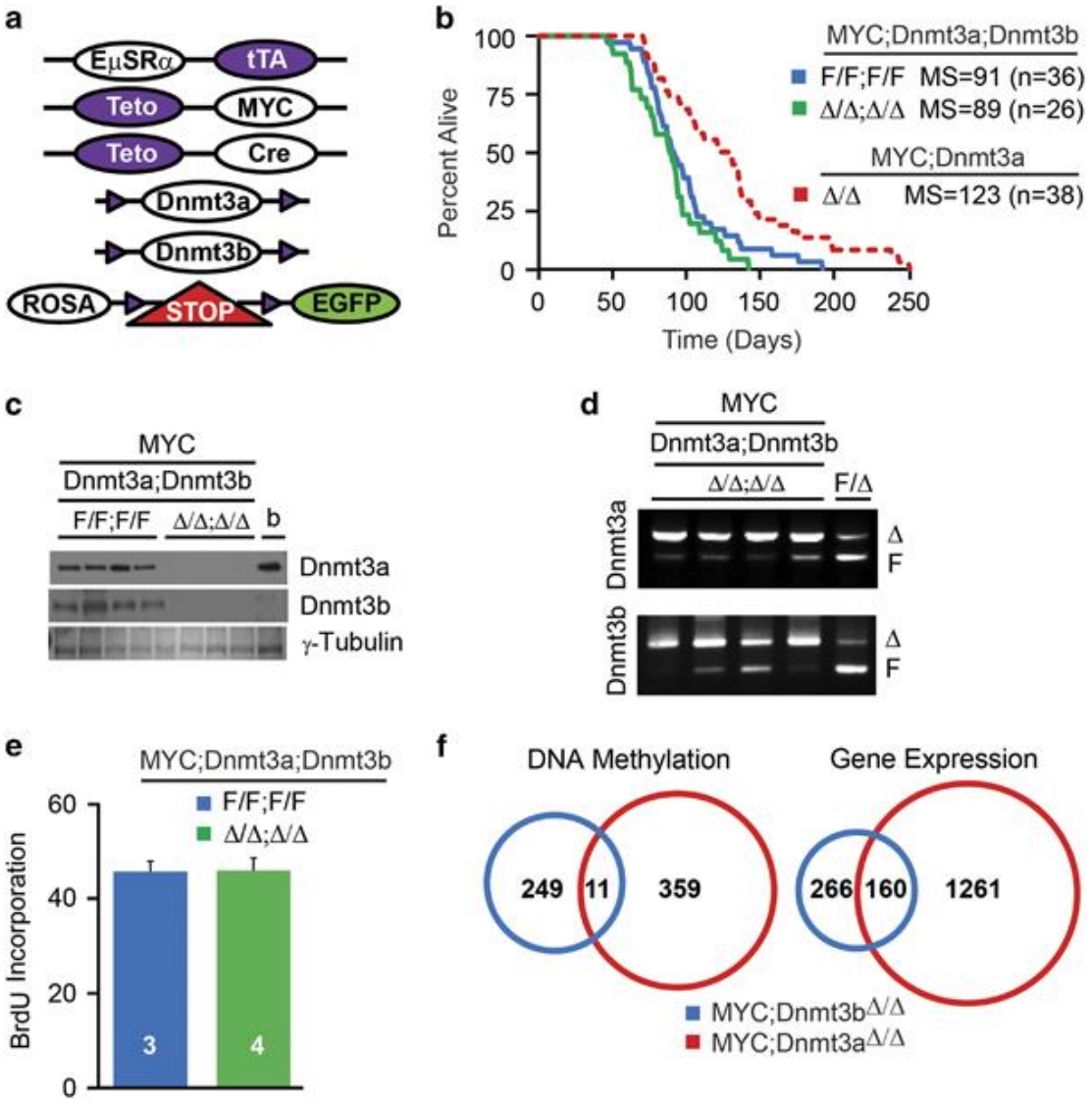

Figure 7. Loss of Dnmt3b accelerates lymphomagenesis in Dnmt3a-deficient mice. (**a**) Genetic setting used to delete conditional alleles of Dnmt3a and Dnmt3b. (**b**) Kaplan–Meier survival curve for *MYC;Dnmt3a*$^{F/F}$*;Dnmt3b*$^{F/F}$ (blue), *MYC;Dnmt3a*$^{Δ/Δ}$*;MYC;Dnmt3b*$^{Δ/Δ}$ (green) and *MYC;Dnmt3a*$^{Δ/Δ}$ (red, also shown in Figure 1b) mice. Median survival (MS) and number of mice (*n*) is shown. (**c**) Immunoblot showing Dnmt3a and Dnmt3b expression in control tumors (*MYC;Dnmt3a*$^{F/F}$*;Dnmt3b*$^{F/F}$), Dnmt3a;Dnmt3b-deficient tumors (*MYC;Dnmt3a*$^{Δ/Δ}$*;MYC;Dnmt3b*$^{Δ/Δ}$) and a Dnmt3b-deficient control (b). γ-Tubulin is shown as a loading control. (**d**) PCR-based deletion efficiency of Dnmt3a and Dnmt3b in *MYC;Dnmt3a*$^{Δ/Δ}$*;Dnmt3b*$^{Δ/Δ}$ tumors. *Dnmt3a*$^{F/Δ}$ and *Dnmt3b*$^{F/Δ}$ served as controls. F and Δ indicate floxed and knockout alleles, respectively. (**e**) Quantification of BrdU-positive cells isolated from final thymic tumors in *MYC;Dnmt3a*$^{F/F}$;*Dnmt3b*$^{F/F}$ (blue) and *MYC;Dnmt3a*$^{Δ/Δ}$;*Dnmt3b*$^{Δ/Δ}$ (green) mice. Error bars represent±s.e.m. Number of mice used for each comparison is shown inside the bars. (**f**) Venn diagrams displaying the overlap between genes hypomethylated (left) and overexpressed (right) in both Dnmt3b- and Dnmt3a-deficient tumors. The number of genes identified by methylation analysis usingMSCC (fold change 2, FDR<0.05, Benjamini Hochberg) and expression analysis using microarray (fold change 1.5, *P*<0.05, Bayesian *t* -test) are shown.

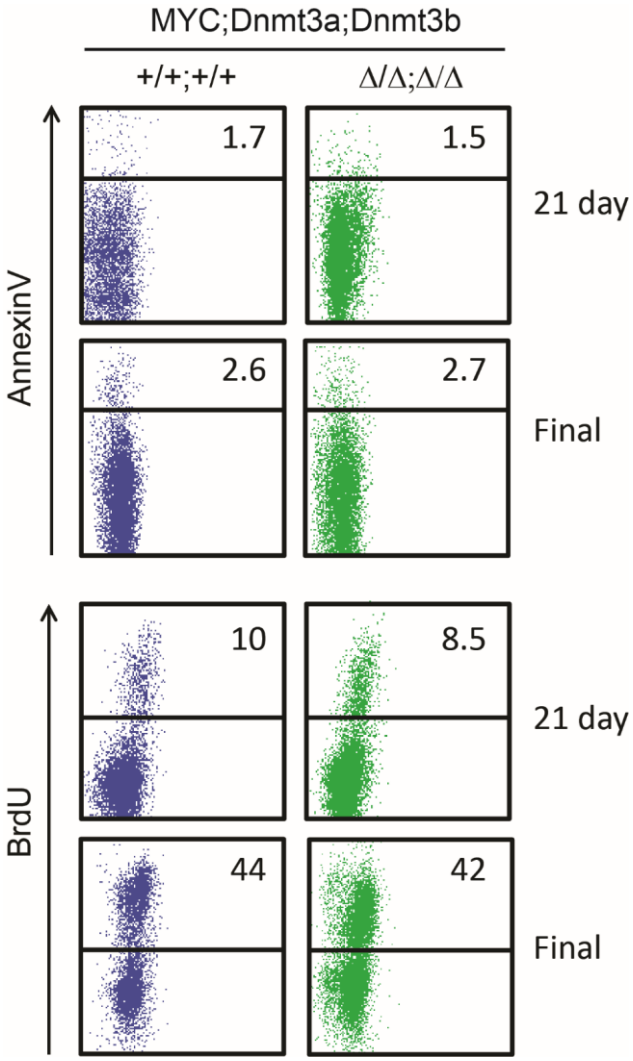

Supplementary Figure S14. Representative Annexin V and BrdU staining in control and DKO thymocytes. Cells were isolated from the thymi of 21 day old, and final tumors in *MYC;Dnmt3a*$^{+/+}$;*Dnmt3b*$^{+/+}$ (blue) and *MYC;Dnmt3a*$^{\Delta/\Delta}$; *Dnmt3b*$^{\Delta/\Delta}$ (green) mice. Percent of cells staining positive is shown in the upper quadrant.

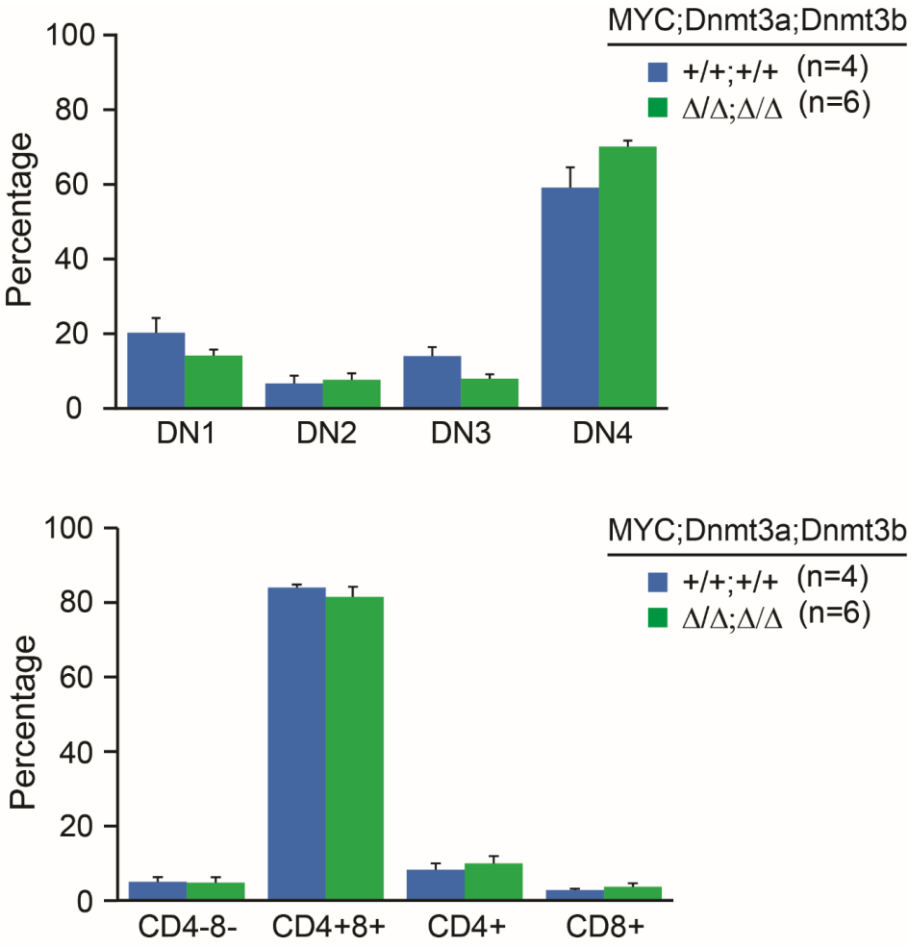

Supplementary Figure S15. Analysis of T-cell development in control and DKO mice. Top panel shows FACS analysis of T-cell development in $CD4^{neg}CD8^{neg}$ (DN) thymocytes populations isolated from 21 day old *MYC;Dnmt3a*$^{+/+}$;*Dnmt3b*$^{+/+}$ (blue) and *MYC;Dnmt3a*$^{\Delta/\Delta}$;*Dnmt3b*$^{\Delta/\Delta}$ (green) mice. Immunophenotypes of DN populations in thymocytes are as follows: $CD4^{neg}CD8^{neg}CD25^{neg}CD44^{+}$ (DN1), $CD4^{neg}CD8^{neg}CD25^{+}CD44^{+}$ (DN2), $CD4^{neg}CD8^{neg}CD25^{+}CD44^{neg}$ (DN3), and $CD4^{neg}CD8^{neg}CD25^{neg}CD44^{neg}$ (DN4). Bottom panel shows quantification of CD4 and CD8 labeling in thymocytes. Number of mice (n) in each cohort is shown. Quantification of obtained results is shown as an average value with error bars representing ± SEM.

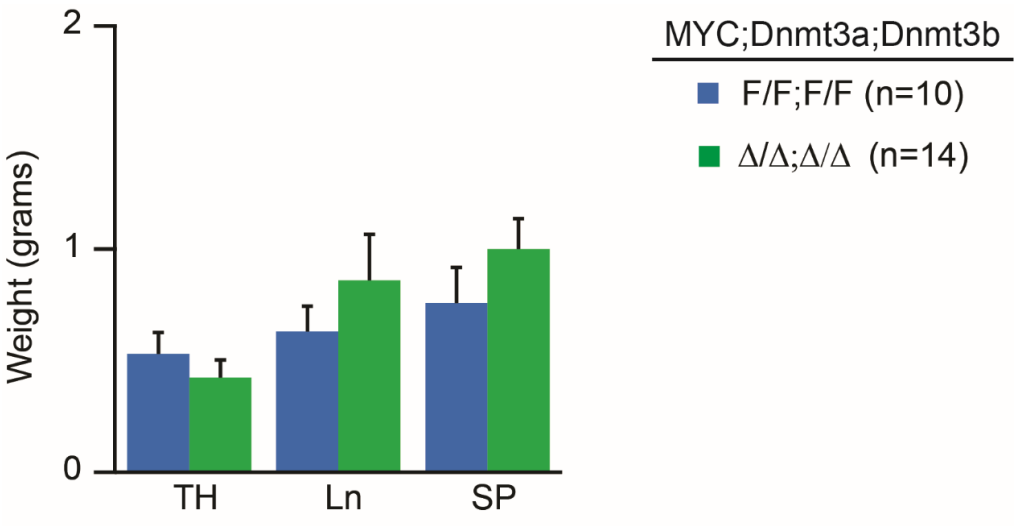

Supplementary Figure S16. Summary of tumor burden in control and DKO mice. Organs were isolated from *MYC;Dnmt3a*$^{F/F}$;*Dnmt3b*$^{F/F}$ (blue) and *MYC;Dnmt3a*$^{\Delta/\Delta}$;*Dnmt3b*$^{\Delta/\Delta}$ (green) terminally ill mice. Weights of thymus (TH), lymph node (Ln) and spleen (SP) were averaged and error bars represent ± SEM. Number of mice (n) used for each group is shown.

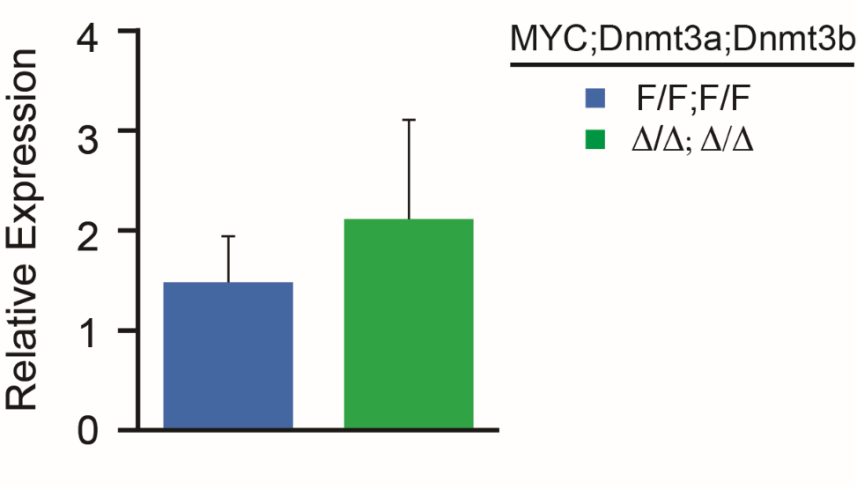

Supplementary Figure S17. MYC expression is similar between control and DKO tumors. qRT-PCR analysis of *MYC* levels in *MYC;Dnmt3a$^{F/F}$;Dnmt3b$^{F/F}$* tumors (blue, n=4) and *MYC;Dnmt3a$^{Δ/Δ}$;Dnmt3b$^{Δ/Δ}$* (green, n=3). Error bars denote ± SEM.

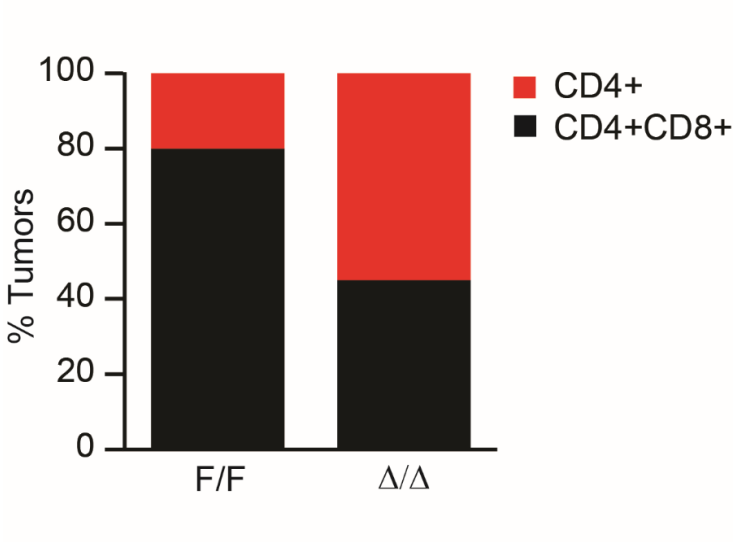

Supplementary Figure S18. Summary of tumor immunophenotypes in control and DKO mice. Immunophenotypes of tumors in *MYC;Dnmt3a*$^{F/F}$;*Dnmt3b*$^{F/F}$ (F/F) and *MYC;Dnmt3a*$^{\Delta/\Delta}$;*Dnmt3b*$^{\Delta/\Delta}$ (Δ/Δ) mice. Relative percentage of CD4+ and CD4+CD8+ malignancies is shown.

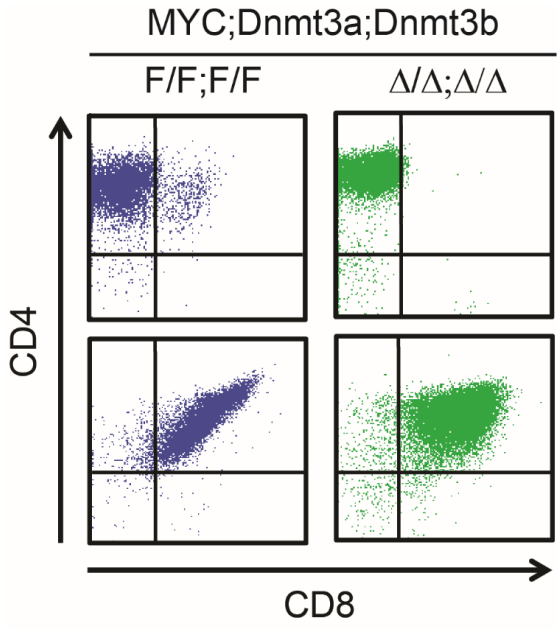

Supplementary Figure S19. Representative FACS analysis of T-cell lymphomas in control and DKO mice. Flow diagrams showing CD4 and CD8 staining in thymic tumors isolated from *MYC;Dnmt3a*$^{F/F}$;*Dnmt3b*$^{F/F}$ (blue) and *MYC;Dnmt3a*$^{\Delta/\Delta}$;*Dnmt3b*$^{\Delta/\Delta}$ (green) mice.

Discussion

Since the discovery of DNMT3A mutations in myelodysplastic syndrome and acute myeloid leukemia (38, 39) a number of alterations in DNMT3A were found in other human hematologic malignancies, including T-cell leukemias and lymphomas (42, 106, 107). In both myeloid and lymphoid malignancies, mutations in DNMT3A primarily occur in the catalytic domain (38, 39, 42, 106, 107), suggesting that inactivation of the methyltransferase activity contributes to transformation. A recent biochemical analysis showed that the most common mutation, DNMT3A R882H, decreases methylase activity by ~80% at least partially by disrupting the ability of Dnmt3a to homotetramerize (47). Overexpression of mouse R878H mutant (analogous to human R882H) in embryonic stem cells decreased the activity of wild-type Dnmt3a and Dnmt3b likely by functioning as a dominant-negative and forming complexes with wild-type Dnmt3a and Dnmt3b (108). Ectopic expression of DNMT3A R882H in hematopoietic stem cells followed by transplantation into lethally irradiated mice induced a disease resembling chronic myelogenous leukemia within 1 year, demonstrating direct functional involvement of mutated DNMT3A in the development of myeloid leukemia.

Here we used a mouse genetic model that allowed us to evaluate the effects of Dnmt3a inactivation along with *MYC* overexpression in all hematopoietic lineages. Although overexpression of *MYC* typically results in the development of TCLs, the development of acute myeloid leukemia in this model was reported in 13% of mice (111). We observed that Dnmt3a inactivation did not alter normal hematopoietic development, tumor spectrum or tumor type. Rather, Dnmt3a deficiency inhibited MTCL due to inhibitory effects on proliferation during disease progression and in tumor cells.

Several interesting implications arise from these studies. For instance, Dnmt3a functions as both an oncogene and TS in the hematopoietic compartment. This finding is

surprising in view of our recent study that long-term loss of Dnmt3a in hematopoietic cells results in B-cell transformation and the development of chronic lymphocytic leukemia (CLL) in mice (34). Thus, the *Dnmt3a* locus harbors both oncogenic (promotion of MTCL due to its pro-proliferative function) and TS (prevention of CLL development) functions in the hematopoietic compartment. What is the molecular basis for such different activities in similar cell types? We speculate that the differences may stem from two biological functions of Dnmt3a, methylation-independent and methylation-dependent repressor activities, respectively. This concept is supported in the MTCL model by IPA of microarray data, which identified 17 genes under the category of 'Lymphomagenesis' whose upregulation in Dnmt3a-deficient lymphomas was predicted to suppress lymphomagenesis. Importantly, whereas all of these genes were overexpressed in *MYC;Dnmt3a*$^{\Delta/\Delta}$ tumors, we have not observed changes in their promoters or gene body methylation. The lymphomagenesis signature consisted of genes whose TS functions were either reported in spontaneous B- and T-cell lymphomagenesis (*Brca2*, *Dna2*, *Exo1*, *Prdm2*, *Smurf2* and *Ssbp2* (99, 114-117)), p53-deficient or oncogene-provoked lymphomagenesis (*Bcl2l11*, *E2f1*, *Xrcc2*, *Recql4* and *Tyk2* (118-122)), including MTCL (*Pten*, *E2f2 and Dnmt3b* (13, 87, 123)), or other aspects of lymphomagenesis (*Nqo1*, *Irf1 and Irf8 (124-126)*). Whether upregulation of any of these genes is involved in MTCL in the absence of Dnmt3a remains to be seen; however, individual inactivation of E2f2 or Pten accelerated MTCL (87, 123). Furthermore, given that Xrcc2 deficiency accelerated lymphomagenesis induced by loss of p53 (120), and Brca2 deficiency results in the development of TCLs (99), other TS genes may be contributing to the extended survival of *MYC;Dnmt3a*$^{\Delta/\Delta}$ mice.

In contrast to MTCL, loss of Dnmt3a induces CLL and is associated with widespread promoter hypomethylation in this context (34). In view of these data, coupled

with recently reported extensive promoter and gene body hypomethylation in human CLL (64), it seems that the basis for Dnmt3a TS function in CLL is its methyltransferase activity. Such a conclusion is further supported by the recent finding that the Tcl1 oncoprotein, whose overexpression induces CLL in mice, inhibits Dnmt3a catalytic activity, which likely contributes to disease development (65). An alternative possibility is that methylation-dependent and independent repressor activities of Dnmt3a have opposing roles in T- and B-cell transformation, but T-cells are differentially sensitive due to cell-type-specific differences. Dnmt3a was reported to function as a TS in lung cancer and as an oncogene in colorectal carcinoma (127, 128), further supporting that the role of Dnmt3a in tumorigenesis is highly complex and likely context specific. Here we show that Dnmt3a functions as an oncogene in MTCL, likely through the methylation-independent repression of TS genes.

Another conclusion from our studies is that Dnmt3a and its close relative Dnmt3b have distinct functions in MTCL. We have recently reported that loss of Dnmt3b, unlike Dnmt3a, accelerated MTCL (13). Others have shown that Dnmt3b haploinsufficiency promoted MYC-induced B-cell lymphomagenesis (35), clearly demonstrating a TS role for Dnmt3b. It was reported that loss of Dnmt3a results in exhaustion of stem cell self-renewal and defective differentiation (45). However, our data presented here and previously, point to a lack of differences of Dnmt3a or Dnmt3b deficiency on thymocyte development, likely due to different biological settings (13, 34). Thus, opposing roles of Dnmt3a and Dnmt3b on MTCL cannot be explained by changes in hematopoiesis. Rather, Dnmt3a and Dnmt3b seem to have contrasting effects on proliferation of TCLs, with Dnmt3a promoting and Dnmt3b inhibiting proliferation of tumor cells. Molecularly, the scope of tumor-specific changes in methylation and gene expression are larger for Dnmt3a compared with Dnmt3b. Consistent with the differential effects of these

enzymes on MTCL, out of the 17 genes in the Dnmt3a-specific 'Lymphomagenesis' signature, only one gene (*Bcl2l11*) is upregulated in Dnmt3b-deficient MTCLs, further supporting the idea that at least some of these genes are responsible for the extended survival in *MYC;Dnmt3a*$^{\Delta/\Delta}$ mice. Whether these broader molecular effects of Dnmt3a in MTCL reflect different protein levels or qualitative differences in the functions of Dnmt3a and Dnmt3b remains to be seen.

Importantly, we present genetic evidence that the oncogenic function of Dnmt3a is at least in part due to the negative regulation of the TS Dnmt3b. The lack of methylation changes in the promoter and gene body, coupled with the ability of both wild-type and a catalytically dead mutant of Dnmt3a to repress Dnmt3b *in vitro,* suggests that methylation-independent repressor activity is important for its oncogenic functions. We show that repression is likely relevant *in vivo,* as genetic inactivation of Dnmt3b accelerates MTCL.

One critical question that remains to be answered is how the methylation-independent activity of Dnmt3a represses Dnmt3b. Dnmt3a interacts with a number of repressor proteins, including HDAC1, Rb and Daxx (16, 77, 129). Thus, recruitment of Dnmt3a to the *Dnmt3b* promoter could bring repressors that inhibit Dnmt3b transcription. Direct binding of Dnmt3a to sequences in the *Dnmt3b* promoter seems unlikely given that no clear Dnmt3a binding site has been identified, although weak consensus sequences were reported (19). Instead, interaction of Dnmt3a with transcription factors and subsequent recruitment to the *Dnmt3b* promoter seems more likely. Indeed, it was previously reported that the transcriptional repressor RP58 targeted Dnmt3a to a synthetic promoter to silence gene expression in a methylation-independent manner (16). Dnmt3a could also interfere with the ability of transcription factors to activate transcription. For example, p53-mediated transactivation of the *CDKN1A* gene was

suppressed by direct Dnmt3a interaction with p53 without changes in DNA methylation (18). Which protein mediates the potential recruitment of Dnmt3a to the *Dnmt3b* promoter is difficult to predict, given that Dnmt3a can interact with at least 68 transcription factors (19), including c-Myc, Ets1, Gata1, Creb and NF-KappaB, all of which have predicted binding sites in the *Dnmt3b* promoter region. Thus, future studies need to address this point.

It is also possible that rather than interacting with transcription factors, Dnmt3a interacts with histone-modifying enzymes to induce repressive histone modifications. For examples, the N terminal of Dnmt3a interacts with the histone methyltransferase SETDB1 to form a complex, which binds at a synthetic promoter region, and methylation of H3-K9 histones, but not of DNA, results in promoter inactivation (130).

Finally, Dnmt3a was shown to directly interact with chromatin-remodeling factor Brg1, a subunit of the SWI/SNF complex that has a role in both activation and repression of gene transcription (17). Thus, this interaction could induce nucleosomal rearrangement in the *Dnmt3b* promoter that would inhibit gene transcription in a DNA methylation-independent manner.

Whatever the precise mechanism of Dnmt3a-mediated repression is, the unexpected role of Dnmt3a in MTCL raises the possibility that some of the mutations in *DNMT3A* located outside of the methyltransferase domain may enhance biological processes contributing to methylation-independent repression. To our knowledge, this is the first report highlighting the distinct but interconnected roles of Dnmt3a and Dnmt3b in cancer through methylation-independent repressor activity of Dnmt3a.

CHAPTER 3: Tumor suppressor functions of Dnmt3a and Dnmt3b in the prevention of malignant mouse lymphopoiesis[3]

Introduction

DNA methyltransferases 3a (DNMT3A) and 3b (DNMT3B) are enzymes catalyzing the formation of methylcytosine in mammalian genomic DNA. Mutations in the coding sequence of DNMT3A are frequently found in human myeloid and lymphoid malignancies (131, 132). Allelic losses were recently reported in 48% of non-Hodgkin lymphomas (131). Long-term DNMT3A inactivation in mice impaired differentiation of hematopoietic stem cells (HSCs), resulting in accumulation of undifferentiated cells (45). Such findings indicate that DNMT3A loss may promote tumorigenesis in multiple hematopoietic lineages.

Unlike DNMT3A, DNMT3B is rarely mutated in human hematologic malignancies. However, transcription of aberrant isoforms (for example, DNMT3B7) acting as negative regulators of Dnmt3b activity has been reported (133). Consistently, DNMT3B7 overexpression accelerated MYC-induced B-cell lymphomas (133). Importantly, we and others have identified a tumor suppressor function for Dnmt3b in mouse T- and B-cell lymphomagenesis (13, 35).

[3] The material presented in this chapter were previously published: Peters SL, Hlady RA, Opavska J, Klinkebiel D, Pirruccello SJ, Talmon GA, et al. Tumor suppressor functions of Dnmt3a and Dnmt3b in the prevention of malignant mouse lymphopoiesis. Leukemia. 2014;28(5):1138-42.

Methods

Mouse Studies: *EμSRα-tTA, Dnmt3a^{2loxP}, and Dnmt3b^{2LoxP}* mice were obtained from, D.W. Felsher (Stanford University, Stanford, California, USA) R. Jaenisch (Whitehead Institute, Cambridge, Massachusetts, USA), and E. Li, (Novartis Institutes for Biomedical Research, Cambridge, Massachusetts, USA), respectively. *ROSA26^{EGFP}* (79) and *Teto-Cre* mice (80) were acquired from The Jackson Laboratory. Mice were back-crossed onto the FVB/NJ background for five generations. Transgenic mice used for these experiments were obtained by standard genetic crosses and genotypes were confirmed by PCR-based genotyping using gDNA from tails (13, 134). Mice were carefully monitored for signs of tumor formation and harvested when terminally ill.

Western Blot: Western blots were performed using the following antibodies: Dnmt3a (H-295, Santa Cruz), γ-Tubulin (H-183, Santa Cruz). Protein lysates were separated in SDS acrylamide gels and blotted into Immobilon P membranes (Millipore). Blots were incubated in blocking buffer (5% skim milk) at a concentration of 1 mg/mL. The primary antibody was then detected using horseradish-peroxidase-conjugated secondary antibodies and the ECL reagent as described by the manufacturer (Pierce).

FACS analysis: All antibodies were obtained from eBioscience with the exception of Ig kappa and Ig lambda (Southern Biotech). Cell counts were performed using Count Bright Absolute Counting Beads (Invitrogen). Flow cytometry was performed using the LSR II (BD Biosciences) and analyzed using BD FACSDiva (BD Biosciences). Identification of fetal liver HCSs was performed using lineage markers against B220, CD3, CD5, CD8, Gr-1 and Ter119, followed by subsequent gating for Thy1.1^{lo},Sca-1+,CD11b+ cells.[5] For experiments in mouse bone marrow lineage cocktails included antibodies against CD4, CD8, CD11b, B220, CD3, and TER119 to

define lineage positive populations. Sorting of the following population was accomplished used the FACS Aria: LSK cells (Lineage negative, Sca-1+,c-kit+), Pre-Pro B-cells (CD43+, CD25-, IgM-, B220+), immature B-cells (CD43+, CD25-, IgM-, B220+), mature B-cells (CD43-, CD25-, IgM+, B220+), B-cells (B220+), CD11b cells (CD11b+), Ter119 cells (Ter119+), CD4 cells (CD4+), CD8 cells (CD8+). For methylation analysis, control B1 cells from 2 *Dnmt3a*$^{+/+}$ mice were isolated by FACs sorting using B220, CD19 and CD5 antibodies.

Histology: H&E staining was performed using standard protocols by the University of Nebraska Medical Center Tissue Science Facility.

Methyl-sensitive Cut Counting (MSCC) and data analysis: MSCC was performed as previously described (13, 81). Briefly, two independent enzymes, *Hpa*II and *HpyCh4*IV, were used to assess the methylation landscapes. Next generation sequencing results in an output of tags where a higher number of counts correlate with hypomethylation and lower counts indicate hypermethylation. The R programming language bioconductor package “edgeR” was used for all statistical analysis (83, 112). Genes were only considered to by hypomethylated or hypermethylated if two or more independent *Hpa*II/*HpyCh4*IV sites showed a 2-fold change or greater with a false discovery rate <0.05. The methylation heat map was generated by taking the averages for raw counts of all 2-fold or greater statistically significant changes within individual promoters between *Dnmta3a*$^{+/+}$ B1 cells and *Dnmt3a*$^{-/-}$ tumors. The promoter is defined as -1500 to +500 base pairs relative to the transcription start site.

Analysis of Sine and Line elements in was performed as previously described.[3] In brief, MSCC tags associated with SINE and LINE elements were identified using a perl script (UNMC Center for Bioinformatics and Systems Biology and the Institute for System Biology [http://www.repeatmasker.org; *mm9*, July 2007, RepeatMasker, 3.2.8,

Repeat Library 20090604]). The total number of tags specific to gene body (defined as 500 base pairs from transcription start site to the 3' end) or repeat elements obtained from next generation sequencing of MSCC libraries were summed. Average counts for control *Dnmt3a*$^{+/+}$ B1 samples were used for normalization. As the number of MSCC tags inversely correlates with methylation levels the inverse values represent relative methylation levels. MSCC data is available upon request.

Combined Bisulfite Restriction Analysis (COBRA): COBRA analysis was performed as previously described.[3,6] Briefly, sodium bisulfite treatment of genomic DNA was carried out utilizing an EpiTect bisulfite kit (Qiagen). Primers for bisulfite PCR for both COBRA and bisulfite sequencing were designed through the use of MethPrimer (86). For COBRA, bisulfite PCR products were digested with TaqI, TaiI, or BstuI (NEB). The resulting fragments were then loaded onto an 8% PAGE gel, separated by electrophoresis, and detected with SYBR green Gold (Invitrogen). Primer sequences for promoter analysis are listed below: Hus1b: TTTTTTTATTAAAAGATTTGGAGTTTG (forward), AAAAAACACATTCATAACTTACTTTATCTC (reverse) Nfam1: GAAAAGGGTTAAAAGAAATTTTAGTTT (forward), CCCAATAAATAACTTATCACCTACAA (reverse)

Quantitative Real-Time RT-PCR: cDNA was prepared from RNA using Bio-Rad iScript according to the manufacturer's protocol. cDNA was combined with SYBR green Supermix (Bio-Rad) with a final volume of 20 µl, and experiments were done in duplicate. Reaction conditions were optimized by the use of standard curves for each primer pair. Thermocycling was performed using a CFX96 system (Bio-Rad). Threshold cycle (CT) values were normalized based upon the expression of Gapdh. Primer sequences used in these experiments are as follows: Hus1b: GCAAACCTCAATGGCAGAAT (forward), AAGGCCATTGTGGGGTTTAT (reverse)

Nfam1: GACGGAGGTCTACGCCTGTA (forward), CAAGTCTCGGAGCCTGTAGAA (reverse)

Results

To determine the impact of Dnmt3a on malignant hematopoiesis we utilized an *EμSRα-tTA;Teto-Cre;Rosa26LOXP*$^{EGFP/EGFP}$ tri-transgenic system (Figure 1a). In this system, the enhanced green fluorescent protein (EGFP) reporter is activated by Cre-mediated excision of a transcriptional STOP cassette allowing for monitoring of tTA- and Cre-expressing cells by fluorescence activated cell sorting (FACS). Using this system we detected EGFP in HSCs (Lineage− Thy1.1^{lo},Sca-1+,CD11b+) in fetal liver cells from E15.5 embryos (Supplementary Figure 1a). Importantly, EGFP was expressed in bone marrow-derived LSK cells (Lineage^{neg},Sca-1+,c-kit+), a population enriched in hematopoietic cells and early progenitors (Supplementary Figure 1b and c). EGFP was also detected in 30–50% of hematopoietic lineages in the spleen and thymus (Supplementary Figure 1d). Altogether, these data suggest that *EμSRα-tTA* drives expression of *Teto-Cre* in both embryonic and adult stem and progenitor cells and thus—in connection with a conditional knockout allele—is capable of generating hematopoietic lineages deficient for the gene of interest.

Using this system along with a conditional allele of DNMT3A (*Dnmt3a*^{F} (134) we generated *EμSRα-tTA;Teto-Cre;Rosa26LOXP*$^{EGFP/EGFP}$;*Dnmt3a*$^{+/+}$ (*Dnmt3a*$^{+/+}$) and *EμSRα-tTA;Teto-Cre;Rosa26LOXP*$^{EGFP/EGFP}$*;Dnmt3a*$^{F/F}$ mice (*Dnmt3a*$^{-/-}$). No significant difference in EGFP expression in LSK cells or hematopoietic lineages was observed among 21-day-old *Dnmt3a*$^{+/+}$ and *Dnmt3a*$^{-/-}$ mice (Figure 1b and Supplementary Figure 1b and c). Similarly, short-term loss of Dnmt3a had no impact on marker expression or cell numbers (Supplementary Table S1 and Supplementary Figure 2) despite efficient deletion of Dnmt3a in EGFP-positive LSK cells as well as lymphoid, myeloid and

erythroid cells from *Dnmt3a*$^{-/-}$ mice (Figure 1c). However, whereas control *Dnmt3a*$^{+/+}$ mice remained healthy over 500 days, 100% of *Dnmt3a*$^{-/-}$ mice died, with a median survival of 371 days (Figure 1d). Terminally ill mice were lethargic and had enlarged abdomens due to splenomegaly (Figures 1e and f). Dnmt3a was efficiently deleted in splenic cells of terminally ill mice (Figure 1g and Supplementary Figure 3). Analysis of spleens from 10 terminally ill mice showed that splenomegaly was largely caused by expansion of EGFP+ mature B1 B cells. Cells expressed the surface markers B220, CD5, CD19, CD43, CD11b and immunoglobulin light chain kappa or lambda (Figures 1h and i, and Supplementary Table 1). These cells were also present in the peripheral blood, bone marrow and, occasionally, liver (Figure 1h and data not shown). Consistently, sections of the spleen showed diffuse involvement by a monomorphic population of small neoplastic lymphocytes, similar in size to resting lymphocytes (Supplementary Figure 4). The tumor cell nuclei had slightly irregular borders with clumped chromatin and indistinct nucleoli, morphologically similar to the cells of small lymphocytic lymphoma/chronic lymphocytic leukemia (CLL). Two of the B1 populations expressed only immunoglobulin lambda light chain, whereas the remaining eight expressed purely kappa light chain, indicating that the B-cell expansions are most likely clonal (Figure 1i). Sequencing analysis from two independent tumors showed identical rearrangement of V_H alleles, further indicating clonal B-cell expansions (not shown). Upon intraperitoneal injection into FVB mice, splenic cells from terminally ill *Dnmt3a*$^{-/-}$ mice induced a phenotypically indistinguishable disease from donor mice over the course of 3 months, suggesting that *Dnmt3a*$^{-/-}$ cells have tumorigenic potential (Supplementary Figure 5a-c). Similarly, splenic cells from primary transplants induced disease in secondary FVB recipients, and the process could be successfully repeated at least five times, suggesting a long-term capability of these cells to self-renew and induce disease (Figure 1j and not shown). Altogether, our data indicate that, although loss of

Dnmt3a is insufficient to immediately induce cellular transformation of hematopoietic cells, long-term Dnmt3a deficiency results in the development of a B-cell malignancy.

The obvious disease parallel in humans to the phenotype observed in the *Dnmt3a*$^{-/-}$ mouse model is CLL, which is the most common type of chronic leukemia in adults in the Western hemisphere. Owing to Dnmt3a's role as a methyltransferase, we performed genome-wide methylation profiling in mouse CLL of *Hpa*II and *HpyCh4*IV sites using methyl-sensitive cut counting, as described previously (13, 33). Comparison of *Dnmt3a*$^{-/-}$ CLL samples with B220+, CD19+, CD5+ splenocytes isolated from control *Dnmt3a*$^{+/+}$ mice revealed promoter hypomethylation in 428 and hypermethylation in 37 genes (Figure 1k). Combined bisulfite restriction analysis (COBRA) confirmed promoter hypomethylation of two randomly selected genes (*Nfam1* and *Hus1b)* in CLL that was accompanied by upregulation of gene expression (Figures 1l and m). In addition to promoter hypomethylation, we observed an ~20% decrease in overall gene body methylation, as well as hypomethylation of repetitive elements (Supplementary Figures 6a and b). Altogether these data suggest that inactivation of Dnmt3a results in profound methylation changes manifested mainly by hypomethylation, similar to that observed in human CLL, which effects expression in at least some genes. The effect of aberrant methylation on global transcription in CLL remains to be seen.

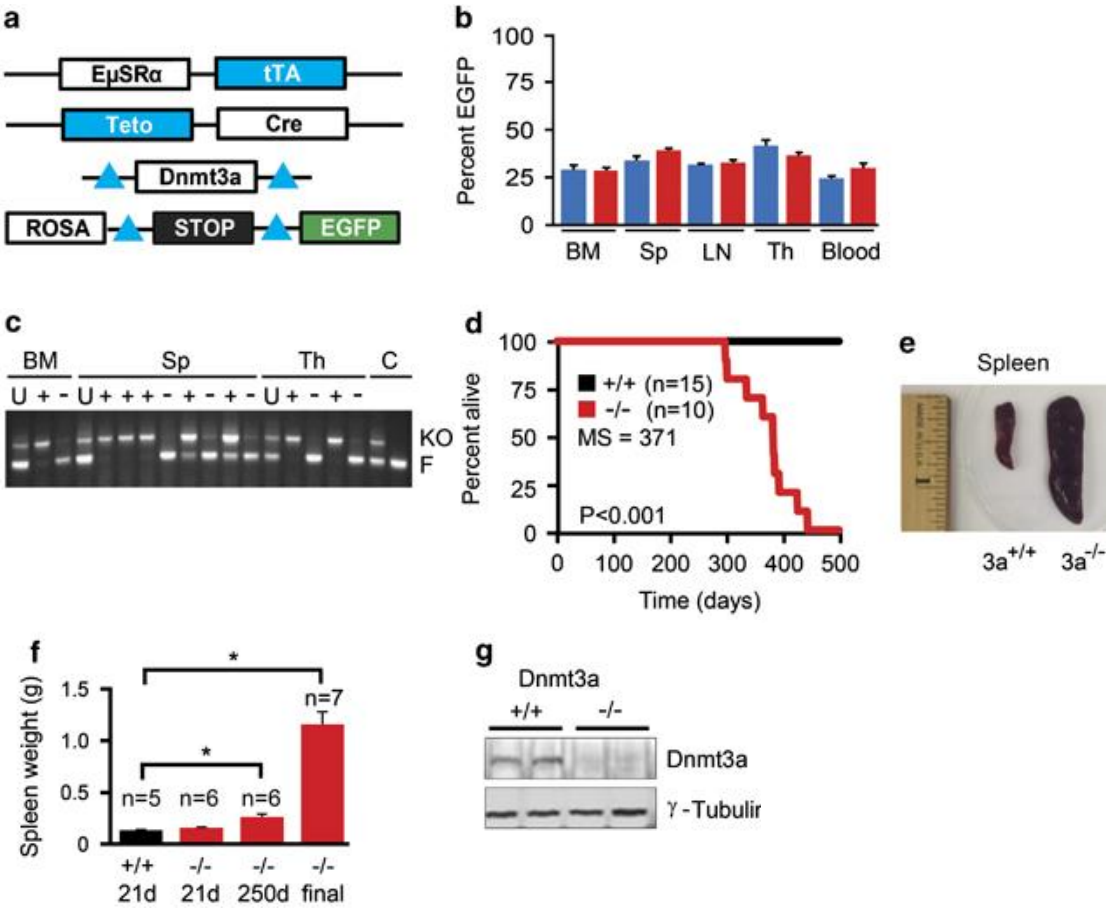

Figure 1. Loss of Dnmt3a induces CLL in mice. (**a**) The genetic setting for deleting a conditional allele of Dnmt3a. (**b**) EGFP expression as determined by FACS analysis of cells isolated from bone marrow, spleen, lymph node, thymus and blood of *Dnmt3a*$^{+/+}$ (blue, *n*=5) and *Dnmt3a*$^{-/-}$ (red, *n*=4) 21-day-old mice. Data were analyzed by Student's *t*-test and are presented as average percentages with error bars representing±s.e.m. (**c**) PCR-based genotyping of DNA isolated from unsorted (U) or FACS-sorted EGFP-positive (+) and EGFP-negative (−) populations of cells obtained from the bone marrow (BM), spleen (Sp) and thymus (Th) of 6-week-old *Dnmt3a*$^{-/-}$ mouse. PCR reactions were perfomed on samples in the following order: U BM, +LSK BM, −LSK BM, U Sp, +Sp Pre-Pro B-cells, +Sp immature B-cells, +Sp mature B-cells, −Sp B-cells, +Sp CD11b,−Sp CD11b, +SP Ter119, −Sp Ter119, U Th, +Th CD4, −Th CD4, +Th CD8, −Th CD8. Immunophenotypes of sorted populations are as follows: LSK cells (Lineage negative, Sca-1+, c-kit+), Pre-Pro B-cells (CD43+, CD25−, IgM−, B220+), immature B-cells (CD43+, CD25−, IgM−, B220+), mature B-cells (CD43−, CD25−, IgM+, B220+), B-cells (B220+), CD11b cells (CD11b+), Ter119 cells (Ter119+), CD4 cells (CD4+), CD8 cells (CD8+). Fragments from floxed (F) and knockout (KO) alleles are shown. Dnmt3a$^{-/+}$ and Dnmt3a$^{F/F}$ genomic DNA served as a control. (**d**) Kaplan–Meier survival curves for *Dnmt3a*$^{+/+}$ (black line) and *Dnmt3a*$^{-/-}$ (red line) mice. Median survival (MS), number of mice (*n*) and P-value (log-rank test) are indicated. (**e**) Representative spleens and average weight (**f**) of age-matched *Dnmt3a*$^{+/+}$ (black) and *Dnmt3a*$^{-/-}$ (red) mice at 21 days (21 d), 250 days (250 d) and at the terminally ill stage of disease (final). * denotes P<0.05. (**g**) Dnmt3a expression in spleens of *Dnmt3a*$^{+/+}$ and *Dnmt3a*$^{-/-}$ mice as determined by immunoblot using anti-Dnmt3a antibody. *γ*-Tubulin serves as a loading control.

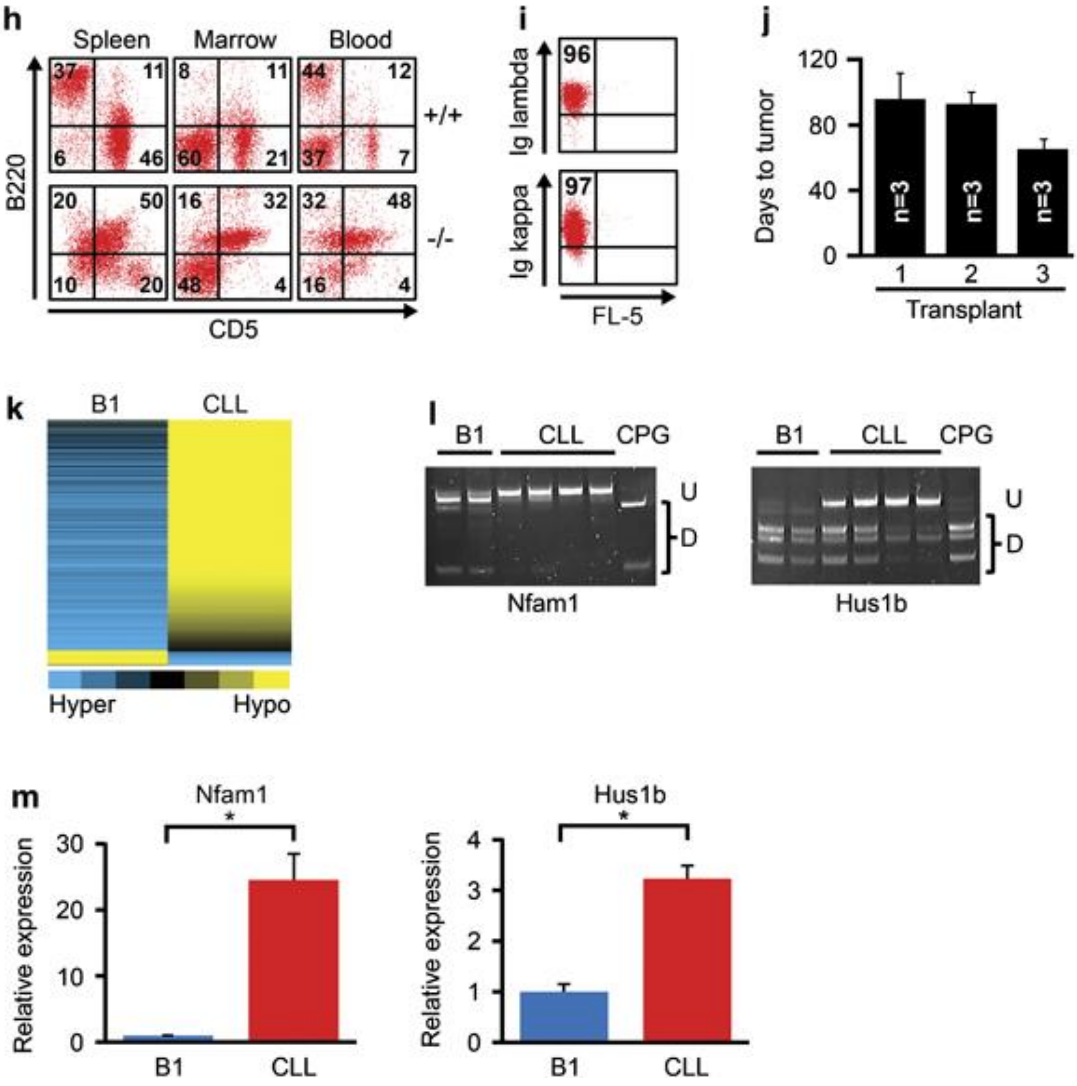

Figure 1 cont. Loss of Dnmt3a induces CLL in mice. (**h**) Expression of CD5 and B220 markers as determined by FACS analysis in indicated tissues isolated from *Dnmt3a*$^{+/+}$ mice (top panels) and terminally ill *Dnmt3a*$^{-/-}$ mice (bottom panels). **(i)** Expression of lambda and kappa light chains in selected CLL cases. (**j**) The time to CLL development for primary (1), secondary (2) and tertiary (3) serially transplanted FVB-recipient mice injected with *Dnmt3a*$^{-/-}$ CLL cells. Data are presented as average time to tumor development and were derived from three independent *Dnmt3a*$^{-/-}$ CLL samples. The number of mice (*n*) is shown. Error bars represent ±s.e.m. (*P*<0.05). (**k**) A heatmap displaying 428 hypomethylated and 37 hypermethylated promoters in *Dnmt3a*$^{-/-}$ CLL samples (*n*=3) relative to control B1 cells (*n*=2) as determined by analysis of MSCC data (FDR<0.05, edgeR). A color bar is shown with blue representing a high degree of methylation and yellow representing lower levels. B1 indicates control B220+,CD19+ and CD5+ splenocytes isolated from *Dnmt3a*$^{+/+}$ mice, whereas CLL denotes *Dnmt3a*$^{-/-}$ tumors. (**l**) COBRA analysis of the Nfam1 and Hus1b promoters using gDNA The percentage of positive cells for representative samples is indicated within the FACS quadrants isolated from splenic *Dnmt3a*$^{+/+}$ B1 cells and *Dnmt3a*$^{-/-}$ CLL samples. PCR fragments were digested with restriction enzyme TaqI. Undigested {U} and digested {D} fragments correspond to unmethylated and methylated DNA, respectively. CpG indicates a fully methylated control. (**m**) qRT-PCR analysis of Nfam1 and Hus1b expression in splenic *Dnmt3a*$^{+/+}$ B1 and *Dnmt3a*$^{-/-}$ CLL samples. Error bars represent ±s.e.m., *P*<0.05 (*).

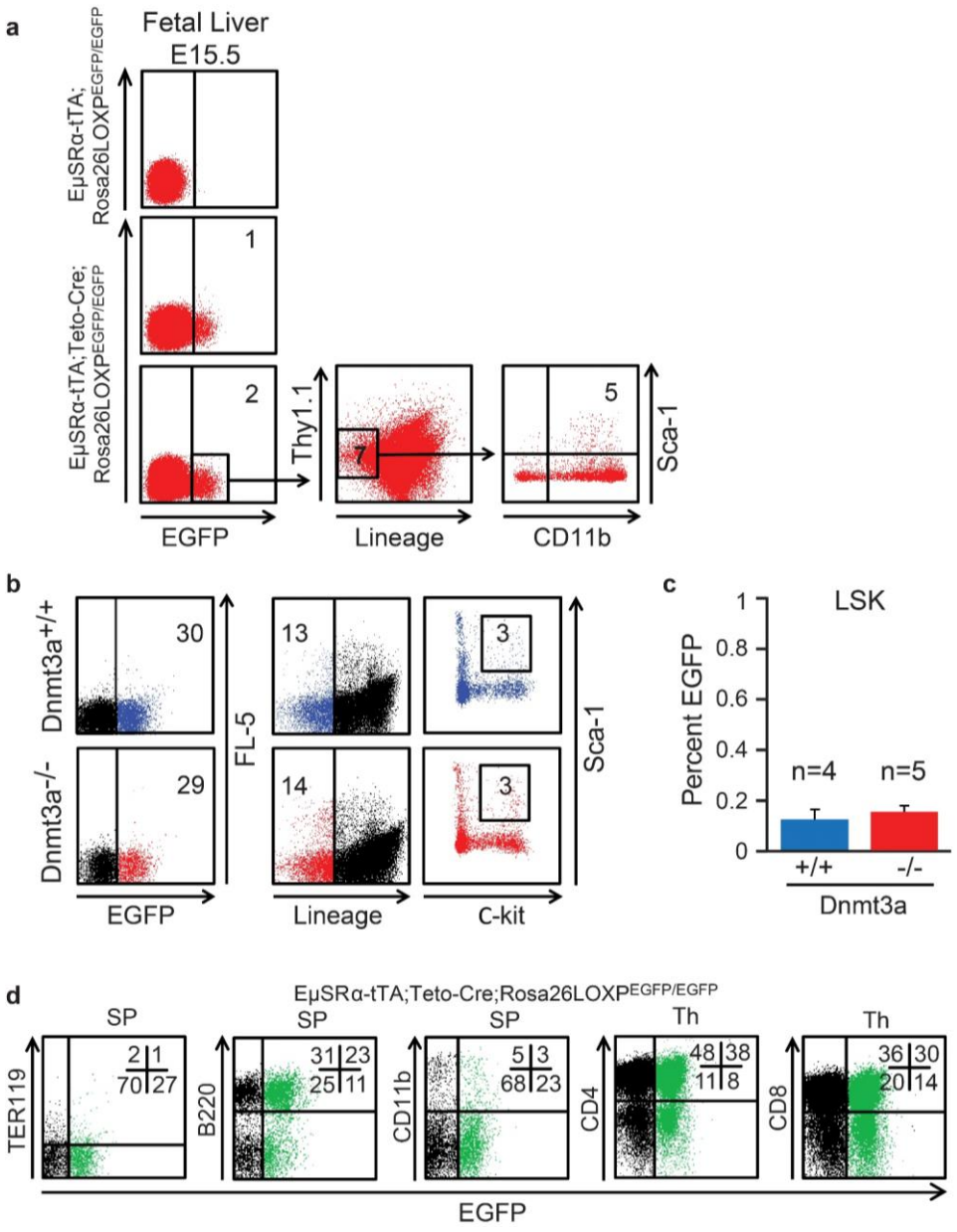

Figure S1. Analysis of EGFP and cell surface marker expression in *Dnmt3a*$^{+/+}$ and *Dnmt3a*$^{-/-}$ mice. (**a**) FACS analysis of EGFP expression in fetal liver cells isolated from 15.5 day embryos with indicated genotypes. EGFP-positive cells were further analyzed for expression of B220, CD3, CD5, CD8, Gr-1, Ter119 lineage markers to define lineage-positive cells. Lineage-negative cells were analyzed for expression of Thy1.1, CD11b and Sca-1. Lineage-negative, Thy1.1^{lo}, CD11b^{+}, Sca-1^{+} represent fetal liver HSCs. The percentage of positive cells is indicated in the FACS diagrams. (**b**) Representative FACS analysis of EGFP+ LSK cells in the bone marrow of 21days old *Dnmt3a*$^{+/+}$ and *Dnmt3a*$^{-/-}$ mice. Representative FACS diagrams show percentage of EGFP+ LSK cells identified as Lineage-negative,Sca1^{+},c-kit^{+}. Lineage-negative populations were identified by CD4, CD8, CD11b, B220, CD3, TER119 lineage marker expression. (**c**) Total percentage of EGFP+ LSK cells in the bone marrow of 21 days old *Dnmt3a*$^{+/+}$ (n=4) and *Dnmt3a*$^{-/-}$ (n=5) mice. Error bars represent the SEM. (**d**) Representative FACS diagrams showing expression of EGFP, Ter119, B220, CD11b, CD4 and CD8 in spleens (SP) and thymi (Th) of *Dnmt3a*$^{+/+}$ mice.

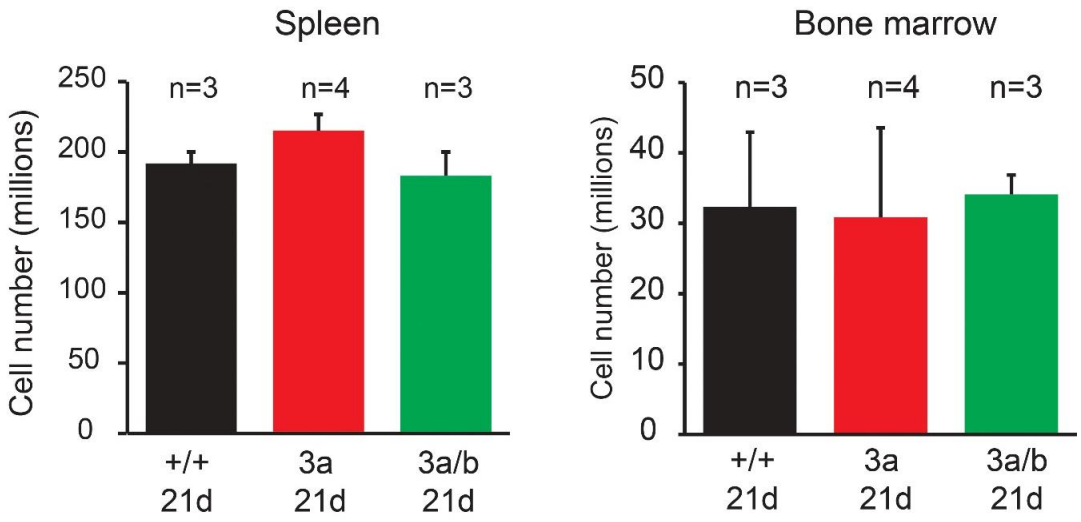

Figure S2. Cellularity of Dnmt3a and Dnmt3a/Dnmt3b knockout mice. The average cell counts of aged-matched *Dnmt3a*$^{+/+}$ (black), *Dnmt3a*$^{-/-}$ (red) *Dnmt3a*$^{-/-}$;*Dnmt3b*$^{-/-}$ (green) spleens and bone marrow at age 21 days (21d). Error bars represent the SEM.

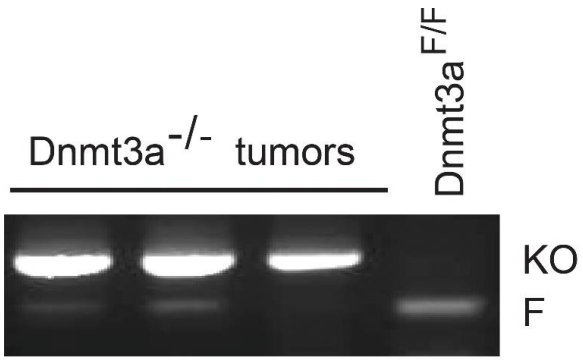

Figure S3. Deletion efficiency of Dnmt3a conditional knockout allele in *Dnmt3a*$^{-/-}$ tumors. PCR-based analysis of deletion efficiency of the *Dnmt3a* conditional knockout allele in DNA from splenic cells isolated from *Dnmt3a*$^{-/-}$ mice with CLL. Fragments derived from floxed (F) and knockout (KO) alleles are shown. *Dnmt3a*$^{F/F}$ genomic DNA served as a control.

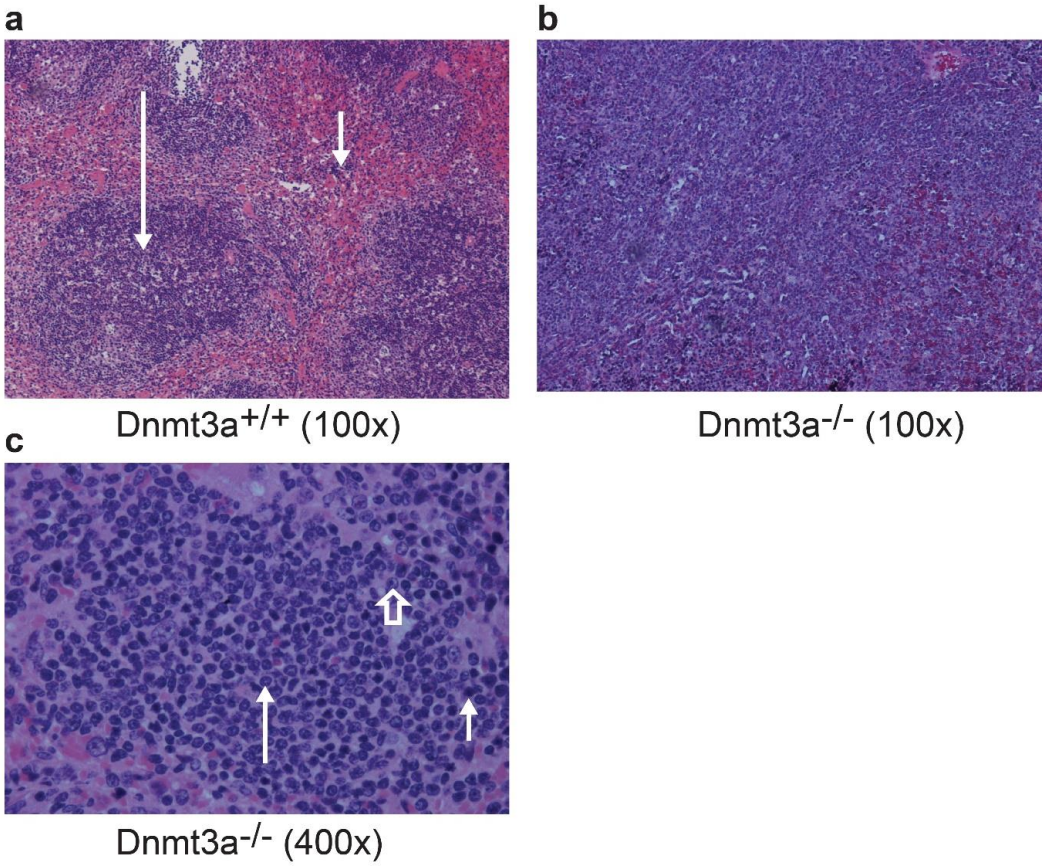

Figure S4. Histological analysis of *Dnmt3a*$^{-/-}$ splenic tumors. (**a**) A spleen from a *Dnmt3a*$^{+/+}$ mouse with normal architecture. White pulp (long arrow) and red pulp (short arrow) are indicated (H&E 100x). (**b**) *Dnmt3a*$^{-/-}$ tumors showing diffuse effacement of the splenic architecture with expansion of the white pulp (H&E 100x). (**c**) *Dnmt3a*$^{-/-}$ tumor showing neoplastic cell populations (long arrow), resting lymphocytes (short arrow) and prolymphocytes (block arrow) (H&E 400x).

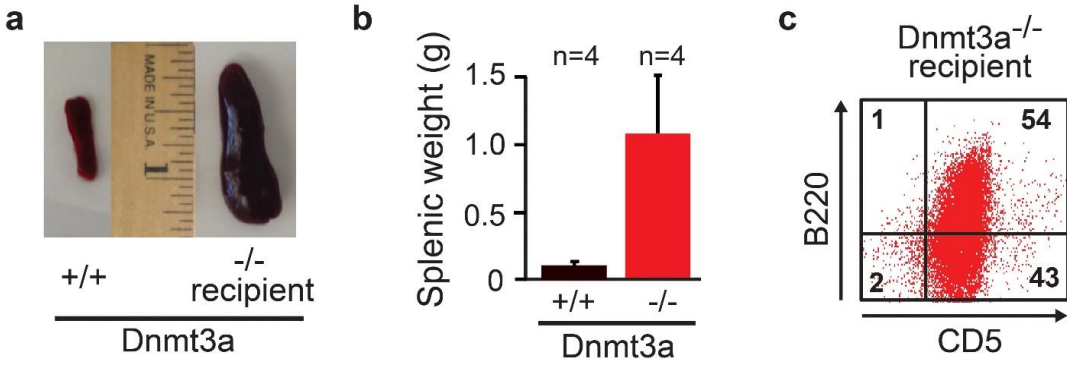

Figure S5. *Dnmt3a*$^{-/-}$ splenic tumor cells induce splenomegaly and CLL disease in recipient mice. (**a**) A picture showing spleens from a *Dnmt3a*$^{+/+}$ control and a *Dnmt3a*$^{-/-}$ recipient at 90 days post intraperitoneal injection. (**b**) A bar graph representing the average spleen weight in grams from *Dnmt3a*$^{+/+}$ controls and *Dnmt3a*$^{-/-}$ recipients at 90 day post i.p. injection. n denotes the number of mice. Error bars represent the SEM. (**c**) A representative flow diagram depicting B220 and CD5 expression in splenic tumor cells from *Dnmt3a*$^{-/-}$ recipient at 90 day post i.p. injection.

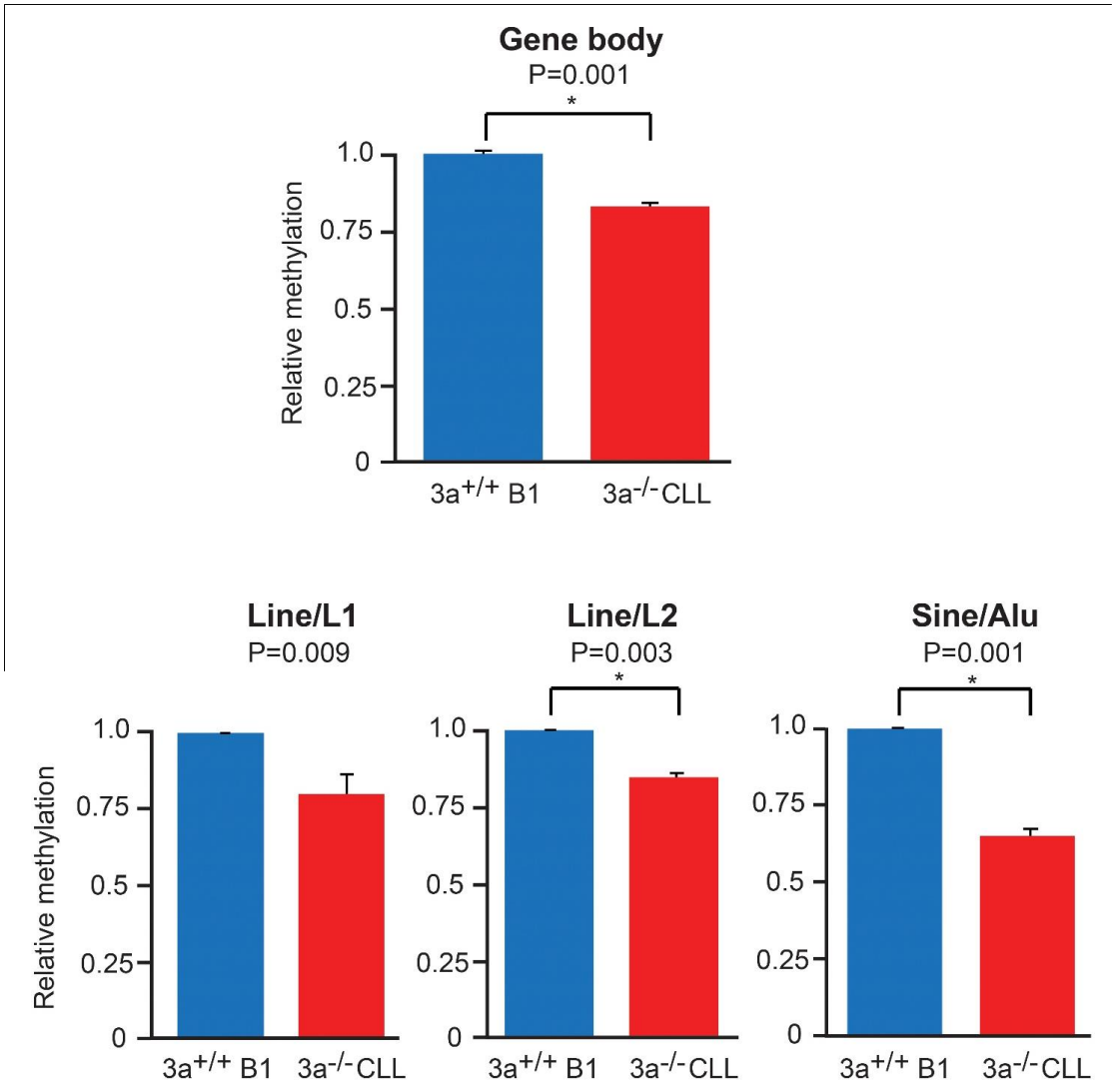

Figure S6. Methylation analysis of gene bodies and repetitive elements. Bar graphs depicting *in silico* analysis of relative methylation of gene body, *Line/L1*, *Line/L2*, and *Sine/Alu* repeats in *Dnmt3a*$^{+/+}$ B1 cells and *Dnmt3a*$^{-/-}$ tumors (CLL) as determined by MSCC. The total number of tags obtained from next generation sequencing of MSCC libraries (*Hpa*II and *HpyCh4*IV) generated from *Dnmt3a*$^{+/+}$ B1 cells (n=2) and *Dnmt3a*$^{-/-}$ CLL samples (n=3) specific to gene body (defined as +500 base pairs from transcription start site to the end of the gene) or repeat elements were summed. Averages of B1 tags were used for normalization of the data. As the number of MSCC tags inversely correlates with methylation levels the inverse values represent relative methylation levels. Error bars represent ± SEM (* denotes P<0.05).

Loss of Dnmt3b accelerates CLL development in *Dnmt3a*$^{-/-}$ mice.

In our previous studies, we have not observed any hematopoietic defects associated with long-term Dnmt3b deficiency (Figure 2a (13)). To determine whether loss of Dnmt3b affects CLL development in *Dnmt3a*$^{-/-}$ mice, we generated and *monitored a cohort of EμSRα-tTA;Teto-Cre;Rosa26LOXP*$^{EGFP/EGFP}$*;Dnmt3a*$^{F/F}$*;Dnmt3b*$^{F/F}$ mice (*Dnmt3a*$^{-/-}$;*Dnmt3b*$^{-/-}$, Supplementary Figure 7). The median survival of these mice (322 days) was significantly decreased relative to *Dnmt3a*$^{-/-}$ mice (371 days) (Figure 2a). Consistent with decreased survival, 10-month-old *Dnmt3a*$^{-/-}$;*Dnmt3b*$^{-/-}$ mice had more profound splenomegaly than *Dnmt3a*$^{-/-}$ mice, unlike 21-day-old mice that had no difference in spleen sizes, cell counts or marker expression (Figures 2b and c, Supplementary Figure 1 and Supplementary Table S1). Both Dnmt3a and Dnmt3b were efficiently deleted, as demonstrated by PCR-based genotyping (Figure 2d). Five out of eight analyzed *Dnmt3a*$^{-/-}$;*Dnmt3b*$^{-/-}$ mice developed a CLL disease immunophenotypically identical to that observed in *Dnmt3a*$^{-/-}$ mice (Figures 2e and f and Supplementary Table S1). Importantly, the remaining three *Dnmt3a*$^{-/-}$;*Dnmt3b*$^{-/-}$ mice developed CD8+, CD3+ and TCRβ+ T-cell malignancies (Figures 2e and f) that were also serially transplantable (not shown). Altogether, these data indicate that, in the absence of Dnmt3a, Dnmt3b functions as a tumor suppressor in CLL and T-cell malignancies.

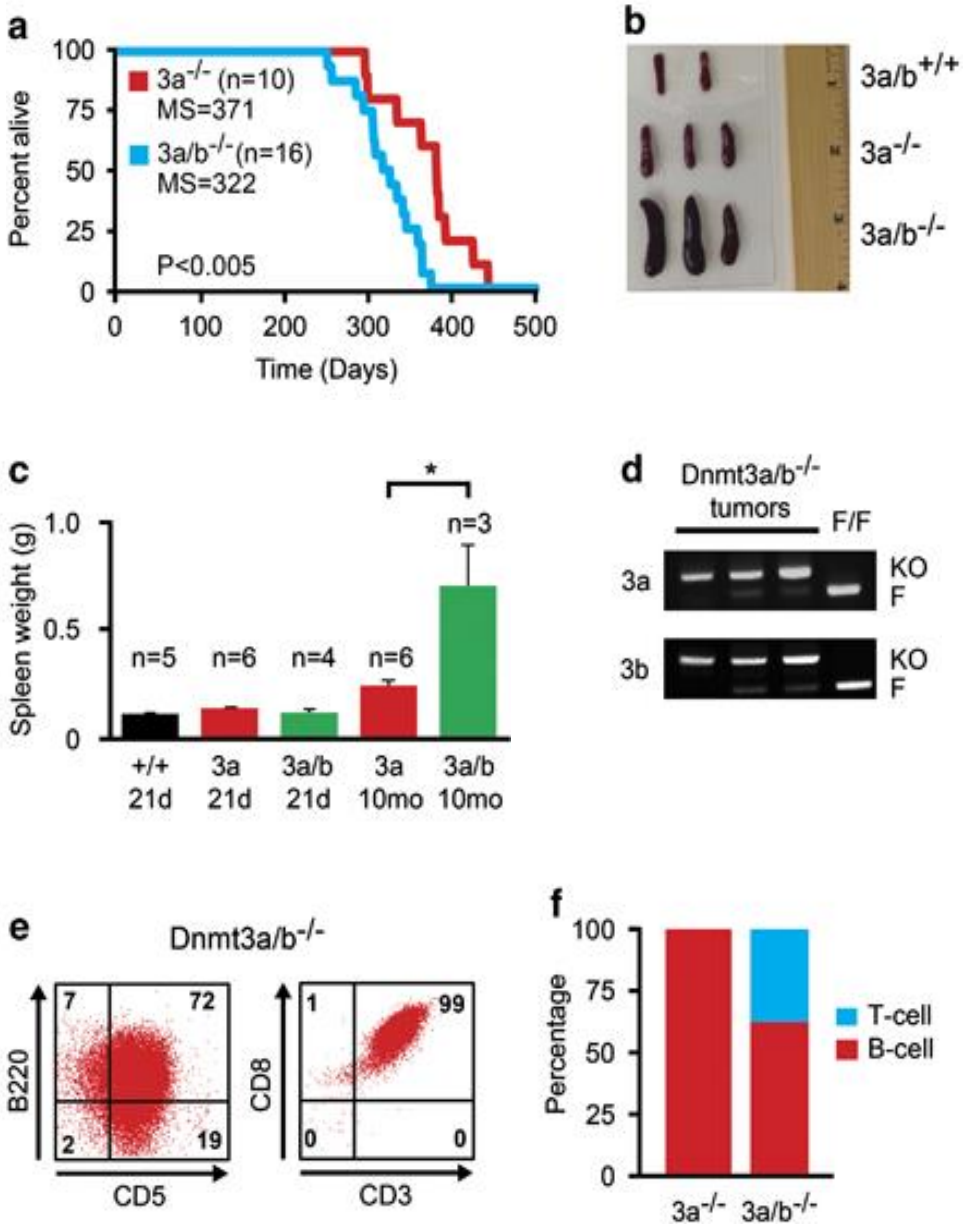

Figure 2. Loss of Dnmt3b accelerates tumor development in *Dnmt3a*$^{-/-}$ mice and alters the disease spectrum. (**a**) Kaplan–Meier survival curves for *Dnmt3a*$^{-/-}$ mice (red line) and *Dnmt3a*$^{-/-}$*; Dnmt3b*$^{-/-}$ mice (blue line). Median survival (MS), number of mice (*n*) and P-value (log-rank test) are indicated. The red line denoting *Dnmt3a*$^{-/-}$ mice is the same used in Figure 1d. (**b**) Representative spleen images from *Dnmt3a*$^{+/+}$;Dnmt3b$^{+/+}$, *Dnmt3a*$^{-/-}$ and *Dnmt3a*$^{-/-}$*;Dnmt3b*$^{-/-}$ mice at 10 months. (**c**) The average weight of age-matched *Dnmt3a*$^{+/+}$ (black), *Dnmt3a*$^{-/-}$ (red) *Dnmt3a*$^{-/-}$*;Dnmt3b*$^{-/-}$ (green) mice at 21 days (21 d) and 10 months (10 mo). * denotes *P*<0.05. *n* denotes the number of mice. (**d**) Deletion efficiency of conditional Dnmt3a^{F} and Dnmt3b^{F} knockout alleles as determined by PCR-based genotyping. Dnmt3a$^{F/F}$ and Dnmt3b$^{F/F}$ served as controls. (**e**) Representative flow cytometric profiles of surface marker expression for B- and T-cell malignancies from *Dnmt3a*$^{-/-}$*;Dnmt3b*$^{-/-}$ mice. (**f**) Graphical presentation of the percentage of T- and B-cell malignanies in *Dnmt3a*$^{-/-}$ and *Dnmt3a*$^{-/-}$*;Dnmt3b*$^{-/-}$ mice.

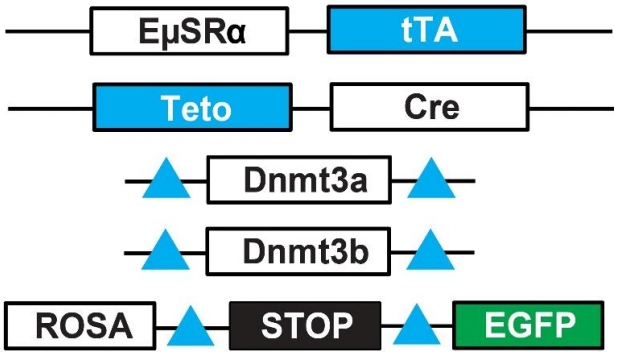

Figure S7. Schematic representation of the genetic setting to delete conditional alleles of Dnmt3a and Dnmt3b in hematopoietic system.

Discussion

Our data suggest that lymphoid cells are more sensitive to Dnmt3a and Dnmt3b levels than are myeloid cells, perhaps because deregulation of cytosine methylation has a higher transformation potential in B- and T-cells. Indeed, genome-wide studies identified a higher number of differentially methylated regions during the development of lymphoid relative to myeloid lineages (135). As a result, their deregulation may preferentially promote transformation of lymphoid cells. Tumor suppressor functions of Dnmt3a and Dnmt3b in the prevention of mouse CLL are consistent with observations that both genes are in the top 1% of underexpressed genes, as determined by global gene expression profiling of 448 human CLL samples (63). Consistent with low Dnmt3a and Dnmt3b expression in CLL, recent genome-wide bisulfite sequencing of human CLL samples revealed a massive decrease in CpG methylation relative to normal control samples, suggesting that hypomethylation may play a role in the pathogenesis of CLL (64). A recent study also showed that the Tcl1 protein, whose transgenic overexpression induces CLL in *Eμ-TCL1* mice, functions as an inhibitor of DNA methyltransferases Dnmt3a and Dnmt3b, resulting in hypomethylation in the early stages of CLL (65). These studies, along with our demonstration that loss of Dnmt3a alone or with Dnmt3b is sufficient to induce CLL in mice, which is characterized by large-scale genome-wide hypomethylation, suggest that CLL to a large extent is an epigenetic disease. Further functional studies will need to be perfomed to identify epigenetic drivers involved in the pathogenesis of CLL.

Interestingly, we have not observed the development of myeloid malignancies in this model, despite the fact that Dnmt3a and Dnmt3b are conditionally ablated in all hematopoietic lineages and that Dnmt3a mutations are most common in the myeloid compartment (39). The preferential presence of Dnmt3a mutations in human acute

myeloid leukemia may reflect a necessity for tight collaboration with *NPM1*, *FLT3* and *IDH1* genes, which are co-mutated with Dnmt3a (136). Alternatively, such mutations in Dnmt3a may result not only in inactivation of methyltransferase activity but possibly also in gain of function.

In studies performed by Challen *et al.* (45), a critical role for Dnmt3a in the differentiation of HSCs was observed utilizing *Mx1-Cre*-mediated excision of Dnmt3a. Although some bias toward B-cell differentiation was observed in *Dnmt3a*$^{-/-}$ cells, no tumor development was reported. Although the genetic settings in both studies are similar in the sense that Cre-mediated excision is achieved in HSCs/early progenitors, several differences may explain the development of CLL in *EμSRα-tTA;Teto-Cre; Rosa26LOXP*$^{EGFP/EGFP}$; *Dnmt3a*$^{F/F}$ mice but not in *Mx1-Cre;Dnmt3a*$^{F/F}$ mice. First, we used FVB rather than C57BL/6 mice to inactivate Dnmt3a. As mouse strains differ in levels of gene expression, the Dnmt3a phenotypes may be strain specific. Second, we utilized a conditional Dnmt3a knockout allele targeting exons 18–20 (134) rather than exon 19 (137). Although in principle Cre-mediated excision of both alleles results in inactivation of Dnmt3a, we cannot rule out the possibility of allele-specific effects. Other differences may come from different experimental approaches—for example, use of primary *Dnmt3a*$^{-/-}$ mice versus recipients receiving *Dnmt3a*$^{-/-}$ cells in adoptive transfer experiments, length of observational period, etc. Despite differences in our studies, for the first time we provide evidence that Dnmt3a and Dnmt3b function as tumor suppressor genes in the prevention of lymphoid malignancies in mice. Thus, this mouse model will be a particularly useful tool for studying the acquired epimutations that functionally contribute to CLL development.

CHAPTER 4: Promoter hypomethylation and expression is conserved in mouse chronic lymphocytic leukemia induced by decreased or inactivated Dnmt3a

Introduction

DNA methyltransferase 3a (Dnmt3a) is an enzyme important for the generation and maintenance of 5-methyl-cytosine in mammalian genomic DNA. The methylation of gene promoters is typically associated with gene repression and plays an important role in silencing of endogenous retroviral elements, X-chromosome inactivation, imprinting and differentiation. In particular, cytosine methylation plays a critical role in hematopoiesis and its deregulation contributes to hematologic malignancies (138). This is highlighted by the presence of mutations in the *DNMT3A* gene in a wide variety of human hematologic malignancies of myeloid and T cell origin (138). Although the precise biological and molecular functions by which DNMT3A prevents cellular transformation are poorly understood, functional studies in mice have begun to uncover the role of Dnmt3a in hematopoiesis. Long-term Dnmt3a deficiency inhibits the ability of hematopoietic stem cells (HSCs) to differentiate into hematopoietic lineages, promoting the development of various hematologic malignancies, including myelodysplastic syndrome, acute myeloid leukemia, and acute lymphoblastic leukemia of T and B cell origin (37, 45, 139). Introduction of genetic alterations found in hematologic malignancies into a Dnmt3a deficient background often results in enhanced phenotypes. For example, Dnmt3a deficiency in combination with c-kit overexpression induces acute T and B cell leukemia (36), and when associated with $Kras^{G12D/+}$ promotes progression of juvenile and chronic myelomonocytic leukemia (140). Given the multiple genome-wide activities associated with Dnmt3a, such as *de novo* methylation (5), maintenance methylation (14), and methylation-independent repression (17), it is not surprising that

under some circumstances Dnmt3a may promote the development of hematologic malignancies. For example, upregulation of Dnmt3a promotes AML/ETO induced leukemia through *de novo* hypermethylation (141) and methylation-independent repressor function enhances T cell lymphomagenesis (12). Such studies highlight the importance of context-dependent activities of Dnmt3a in hematologic malignancies. DNMT3A mutations in human hematologic malignancies are usually heterozygous and most commonly occur at amino acid 882. DNMT3A R882H mutants show both decreased methyltransferase activity (47) and dominant negative functions as its overexpression results in hypomethylation (108). Therefore, a partial, rather than complete inactivation of DNMT3A is likely more relevant in the pathogenesis of human hematologic malignancies. The effects of decreased levels of Dnmt3a in prevention of hematologic malignancies, however, are poorly understood.

We have previously utilized *EμSRα-tTA;Teto-Cre;Dnmt3a*$^{fl/fl}$*;Rosa26 LOXP* $^{EGFP/EGFP}$ quadruple transgenic mice (designated here as *Dnmt3a*$^{\Delta/\Delta}$ mice) to conditionally inactivate Dnmt3a in hematopoietic stem cells and hematopoietic lineages (34). Surprisingly, all *Dnmt3a*$^{\Delta/\Delta}$ mice developed disease similar to chronic lymphocytic leukemia (CLL) with a median survival of 371 days characterized by an expansion of EGFP+ mature B220+CD19+CD5+ B cells (B-1a cells) in hematopoietic organs. Here we asked whether Dnmt3a haploinsufficiency can result in the development of a CLL-like disease or other hematologic malignancies by observing *Dnmt3a*$^{+/-}$ mice. We show that whereas a decrease in Dnmt3a levels is insufficient to immediately induce cellular transformation of hematopoietic cells, long-term Dnmt3a decrease results in the development of a CLL-like disease in 65% of mice and myeloproliferative disease in 15% of mice within 16 months. Whole-genome bisulfite sequencing (WGBS) and RNA-seq revealed that a significant cohort of methylation and expression changes were

conserved in *Dnmt3a*$^{+/-}$ and *Dnmt3a*$^{\Delta/\Delta}$ CLL. Ingenuity Pathway Analysis (IPA) analysis revealed a signature of putative oncogenes that may drive CLL development. Altogether, our data demonstrate that a small reduction of Dnmt3a levels has profound phenotypic consequence on both cellular and molecular levels, identifying Dnmt3a as a critical gene preventing B-1a cell transformation.

Methods

Mouse Studies: All mice used in these studies were of the FVB/N background and were generated using standard genetic crosses. To obtain mice with a germline transmission of the *Dnmt3a*$^{-}$ allele, we crossed *EμSRα-tTA;Teto-Cre;Dnmt3a*$^{fl/fl}$ mice with FVB mice, taking advantage of our observation that the *EμSRα-tTA* transgene is expressed in germ cells (data not shown). To generate *Dnmt3a*$^{+/-}$ we subsequently bread out transgenes by crossing obtained mice with FVB mice). PCR-based genotyping of genomic DNA isolated from the tails was used to confirm genotypes. Mice were harvested at the experimental end point of 16 months. Transgenic mice used in these studies were obtained from the following laboratories: EμSRα-tTA (D.W. Felsher at Standford University), Dnmt3a^{2loxP} (R. Jaenisch at the Whitehead Institute), ROSA26EGFP and Teto-Cre (The Jackson Laboratory). Transplantation studies were carried out by injecting splenic cells isolated from 16 month old *Dnmt3a*$^{+/-}$ mice into the intraperitoneal cavity of FBV/N mice.

FACS analysis: FACS analysis was performed at the UNMC Flow Cytometry Facility. All antibodies used in these studies were purchased from eBioscience. Data was collected using the LSR II (BD Biosciences) and analyzed using BD FACSDiva software (BD Biosciences). B-1a cells used for methylation and expression analysis were isolated from the spleens of either FVB/N (controls), *Dnmt3a*$^{+/\Delta}$, *Dnmt3a*$^{+/-}$ or *Dnmt3a* $^{\Delta/\Delta}$ mice and sorted for CD19, B220, and CD5 positivity using the FACS Aria II

(BD Bioscience). Mice diagnosed with MBL had between 2 to 20% B-1a in the blood at time of harvest, while those diagnosed with CLL had greater than 20% B-1a in the blood. Mice diagnosed with MPD had profound expansion of CD11b+Gr-1+ cells in the blood (>70%), and spleen (>40%).

Whole genome Bisulfite sequencing (WGBS)*:* Splenic B-1a cells were isolated by FACS sorting from *Dnmt3a*$^{+/+}$, *Dnmt3a*$^{+/\Delta}$ tumor, and *Dnmt3a* $^{\Delta/\Delta}$ tumor samples (n=1 per genetic group). WGBS data is available for download through the NCBI Gene Expression Omnibus. Details regarding the number of aligned sequencing reads per sample can be found in Table S9. Splenic B-1a cells (EGFP+CD5+CD19+B220+) were isolated by FACS sorting from *Dnmt3a*$^{+/\Delta}$ and *Dnmt3a* $^{\Delta/\Delta}$ suffering from with CLL (n=1 per genetic group). Age-matched control B-1a cells were FACS-sorted from spleens of *EμSRα-tTA;Teto-Cre;Dnmt3a*$^{+/+}$;*Rosa26LOXP*$^{EGFP/EGFP}$ mice (n=1). Genomic DNA was isolated using standard protocols. The WGBS libraries were prepared and sequenced in DNA Services facility at the University of Illinois at Urbana-Champaign, Roy J. Carver Biotechnology Center / W.M. Keck Center using two lanes for each sample on the Illumina HiSeq2500 sequencer with paired-end 160bp reads. Each lane produced over 310 million reads. Sequence tags were aligned with the mouse genome (Dec. 2011 *mus musculus* assembly mm10, Build 38) using the methylated sequence aligner Bismark (142) by the University of Nebraska Epigenomics Core facility. The resulting data file contains the percent methylation at each CpG measured. Each individual CpG was retained and percent methylation determined only if it was represented by ≥ 5 individual sequences. Correlation based, average linkage hierarchical clustering of genome location matching CpG methylation percentages per sample was performed using the R software package RnBeads (143). Genome location matching differentially methylated loci (DMLs) and differentially methylated regions (DMRs) were determined using the R

software package DSS (144). DMLs were determined by first smoothing the raw percent methylation values based on a moving average algorithm and smoothing span of 500 bases. DMRs were then determined based on average DML methylation change of 30 percent or greater, at least 50 percent or greater individual DML P-values less than 0.05, minimum base pair length of 100, minimum of three DMLs represented, and the resulting DMRs were aveaged if they were closer than 50 bases. Circos plots (145) were generated to visualize DMRs that had at least a 100 base overlap with genomic promoters defined as 1500 bases upstream of the transcription start site (TSS) to 500 bases downstream of the TSS. DMRs were aligned with the mouse genomic repeats. Genomic repeats were acquired from the UCSC Genome table browser based on the RepeatMasker program (Smit et al., 1996-2000). The repeat was retained if the overlap between the DMR and repeat was more than 25 percent of the length of the repeat. WGBS data is available for download through the NCBI Gene Expression Omnibus.

FACS and BrdU: Cell counts were obtained using Count Bright Absolute Counting Beads from Invitrogen. B-1 cells (B220+CD19+CD5+) B-2 cells (B220+CD19+CD5-), CD4+ T cell (CD4+CD3+), CD8+ T cells (CD8+CD3+), and myeloid cells (Cd11b+), were isolated from the spleens of 6 week old FVB mice and sorted for their corresponding marker expression using FACS. BrdU labeling of B-1a cells was performed by injecting BrdU (100 mg/g per body weight) into the IP cavity of mice 2 hours prior to harvest. B-1a cells were stained with fluorescently conjugated antibodies against CD19, B220, and CD5, and BrdU-positive cells were quantified using APC-conjugated anti-BrdU and FACS analysis.

Western Blot: Western blots were performed as previously described (13) with use of the following antibodies: Dnmt3a (H-295, Santa Cruz), γ-Tubulin (H-183, Santa Cruz).

Combined Bisulfite Restriction Analysis (COBRA) and Bisulfite sequencing: COBRA and Bisulfite sequencing analysis were carried out as described previously (13, 33). Briefly, genomic DNA from tumor and sorted cell populations was treated with sodium bisulfite and isolated using the Qiagen Epitech Bisulfite Kit. PCR amplified products were digested with the restriction enzymes *Tai*I (Fermentas), *TaqA*I, or *BstU*I (New England Bioscience). Digests were run on a TBE-polyacrylamide gel and stained with SYBR Gold (Invitrogen). COBRA primers used in this study are presented in Table S10.

RNA-seq: RNA was isolated as previously described (Hlady et al., 2012) from sorted splenic B-1a cells of FVB/N mice (n=2) and *Dnmt3a* $^{+/\Delta}$ (n=1), *Dnmt3a*$^{+/-}$ (n=3) and *Dnmt3a* $^{\Delta/\Delta}$ (n=8) tumor mice. Library generation (TruSeq mRNA kit) and sequencing were performed by SeqMatic (Fremont, CA). The resulting libraries were sequenced on the Illumina HiSeq 2000 platform using paired-end 100bp runs . The sequencing data was first aligned using TopHat (version 1.0.0) and mapped to the Mus musculus UCSC mm10 reference genome using the TopHat 2 aligner. Cufflinks 2 was used to estimate FPKM of known transcripts, perform de novo assembly, of novel transcripts, and calculate differential expression. For differentially expressed genes, we considered those genes with a fold change ≥ 2 and a q-value < 0.05 to be significant. RNA-seq data is available for download through the NCBI Gene Expression Omnibus.

RNA-seq analysis of human CLL data: Publically available RNA-seq data generated using human CLL (n=10) and normal B cells (n=5) samples was downloaded from the NCBI GEO database (GSE70830). These data were used to identify

significantly overexpressed HOC genes in Figure 7B. Only those genes with a p-value <0.05 (CuffDiff) were considered significant.

Reduced Representation Bisulfite Sequencing (RRBS): Splenic B-1a cells were isolated by FACS sorting from two *Dnmt3a*$^{\Delta/\Delta}$ mice with CLL. Age-matched control B-1a cells were FACS-sorted from spleens of FVB/N mice (n=2). Genomic DNA was isolated using standard protocols. The RRBS libraries were prepared and sequenced at the Medical Genome Facility at the Mayo Clinic and ran on an Illumina HiSeq2500 sequencer. The Streamlined Analysis and Annotation Pipeline for RRBS data (SAAP-RRBS) was specifically designed to analyze RRBS data (Sun et al., 2012). This software was used to align and determine the methylation status of CpGs associated with this type of restriction digest high throughput method. Sequences were initially aligned with genome mm9 then converted to mm10 using the UCSC Genome Browser Batch Coordinate Conversion (liftOver) utility. Details regarding the number of sequencing read alignments can be found in Table S9. The methylation heat map was generated by taking the averages for all differentially methylated CpGs for a promoter (-1500 to +500 base pairs relative to the transcription start site). Promoters were only considered to be differentially methylated if one or more CpG sites showed a 30% change in methylation.

Methyl Sensitive Cut Counting (MSCC): Libraries were generated using gDNA from FACS sorted *Dnmt3a*$^{+/+}$ splenic B-1a cells (n=2), and *Dnmt3a*$^{\Delta/\Delta}$ CLL cells (n=3) and ran on an Illumina HiSeq2500 sequencer at the Univeristy of Nebraska Medical Center Sequencing Core. Data were analyzed as described previously (13, 33). In brief, promoters were only considered to be differentially methylated if one or more independent HpaII/HpyCh4IV sites showed a 2-fold change or greater with a P-value <0.05. The methylation heat map was generated by taking the averages for raw counts for all significant change and calculating a fold change in methylation between

Dnmta3a$^{+/+}$ B1 cells and Dnmt3a-deficient tumors. The promoter is defined as -1500 to +500 base pairs relative to the transcription start site.

Quantitative Real-Time qRT-PCR: qRT-PCR was performed as previously described (13, 33). Primer sequences used in experiments presented here are as follows: mouse Dnmt3a: GCAAAGTGAGGACCATTACCA (forward), CTGTGTAGTGGACGGGGAAG (reverse). Human DNMT3A: CAATGACCTCTCCATCGTCAAC (forward), CATGCAGGAGGCGGTAGAA (reverse). Mouse Nfam1: GAAAAGGGTTAAAAGAAATTTTAGTTT (forward), CCCAATAAATAACTTATCACCTACAA (reverse).

cDNA sequencing of Dnmt3a: RNA from three independent FACS sorted Dnmt3a$^{+/-}$ CLL tumors and pooled wild-type FVB splenic B1 cells was reverse transcribed into cDNA (BioRad iScript). Using Phusion DNA polymerase (Thermo Scientific) and primers spanning the translational start and stop codons, Dnmt3a was PCR amplified. The 2.7kb band representing the full length wild-type allele was gel extracted and sequenced. Tumor sample sequences were compared to wild-type B1 and NCBI reference cDNA gene sequences. The following primer sequences were used for amplification of the transcript from cDNA: ATGCCCTCCAGCGG (forward), TTACACACAAGCAAAATATTCCTTCAG (reverse), and confirmation by sequencing: TCGATGTTGGTCTGCTTCTG (reverse 1), CAGGAGAGGGCAAAGAACAG (forward 1), ACCAGGCCACCTACAACAAG (forward 2), GAACTGCTTCTTGGAGTGTGC (forward 3), AGGGTACTGGCCGCCTCT (forward 4).

Histology: H&E staining was performed using standard protocols by the University of Nebraska Medical Center Tissue Science Facility.

Results

The majority of *Dnmt3a*$^{+/-}$ mice develop a CLL-like disease.

During the course of our studies utilizing *Dnmt3a*$^{\Delta/\Delta}$ mice (Peters et al., Leukemia 2014) we also observed an *EμSRα-tTA;Teto-Cre;Dnmt3*$^{+/fl}$*;Rosa26LOXP*$^{EGFP/EGFP}$ mouse in which only one allele of Dnmt3a was conditionally inactivated (referred herein as *Dnmt3a*$^{+/\Delta}$ or conditional heterozygous mouse). This mouse became moribund at 16 months and analysis of the organs revealed expansion of EGFP-positive (EGFP+) B220+CD19+CD5+ (B-1a) cells in the spleen, suggesting that this mouse developed a CLL-like disease (Figure 1A). Serial transplantation of *Dnmt3a*$^{+/\Delta}$ splenic cells induced CLL within 4 months in primary, secondary and tertiary transplanted mice, illustrating their selective advantage to grow and induce disease (Figures S1A and S1B). *Dnmt3a*$^{+/\Delta}$ CLL cells showed reduced Dnmt3a protein and mRNA levels (Figures 1B and 1C), suggesting that decreased Dnmt3a dosage is sufficient to promote B-1a cell transformation. *Dnmt3a*$^{+/\Delta}$ tumor cells incorporated BrdU *in vivo* less efficiently than *Dnmt3a*$^{\Delta/\Delta}$ cells (Figure S1C). These data suggest that Dnmt3a haploinsufficiency in hematopoietic cells, like full Dnmt3a inactivation, might be sufficient to induce a less aggressive CLL-like disease in mice. To test this we generated *Dnmt3a*$^{+/-}$ mice harboring a conventional Dnmt3a knockout allele (referred to herein as *Dnmt3a*$^{-}$) via germline cre-mediated excision of Dnmt3a exons 18-20 (Figure S2A) (*Dnmt3a*^{fl}; Nguyen et al., 2007). Generation of the *Dnmt3a*$^{-}$ allele was confirmed by PCR-based genotyping (Figure S2B). Analysis of protein levels in normal thymus and spleen isolated from 6 week-old *Dnmt3a*$^{+/-}$ mice showed ~50% reduction in Dnmt3a protein levels (Figure 1D). This decrease had no measurable effect on hematopoiesis in 6 week old *Dnmt3a*$^{+/-}$ mice (Figures S2C-2G).

At 16 months of age, all *Dnmt3a*$^{+/+}$ control mice were healthy with no signs of deregulated hematopoiesis. In contrast, only 20% of *Dnmt3a*$^{+/-}$ mice were disease-free at 16 months (Figure 1E and data not shown). Five out of 20 *Dnmt3a*$^{+/-}$ mice developed a CLL-like disease, characterized by B-1a cell expansion greater than 20% in the blood, spleen and bone marrow (Figures 1E-1I, and data not shown). Eight *Dnmt3a*$^{+/-}$ mice showed signs of monoclonal B cell lymphocytosis (MBL) – a less progressed form of CLL – in which the percentage of B-1a cells in the blood are between 2% to 20%, with simultaneous expansion in the spleen and bone marrow (Figures 1E-1I and data not shown). Importantly, splenic cells either from mice with MBL or CLL were able to induce disease in recipient mice (Figures 1I-1J), demonstrating that both populations contain true leukemic cells. Therefore, we refer to both conditions as CLL-like disease. Similar to *Dnmt3a*$^{+/\Delta}$ CLL, leukemic B-1a cells isolated from *Dnmt3a*$^{+/-}$ mice retained approximately 50% expression of Dnmt3a, suggesting that the remaining allele is expressed in fully transformed cells (Figures 1K-L). Importantly, sequencing analysis of cDNA generated from three independent *Dnmt3a*$^{+/-}$ CLL revealed no mutations in the coding sequence of Dnmt3a (data not shown), demonstrating that the expressed Dnmt3a allele is in the wild-type configuration. Altogether these data suggest that Dnmt3a is a haploinsufficient tumor suppressor gene in prevention of CLL in mice.

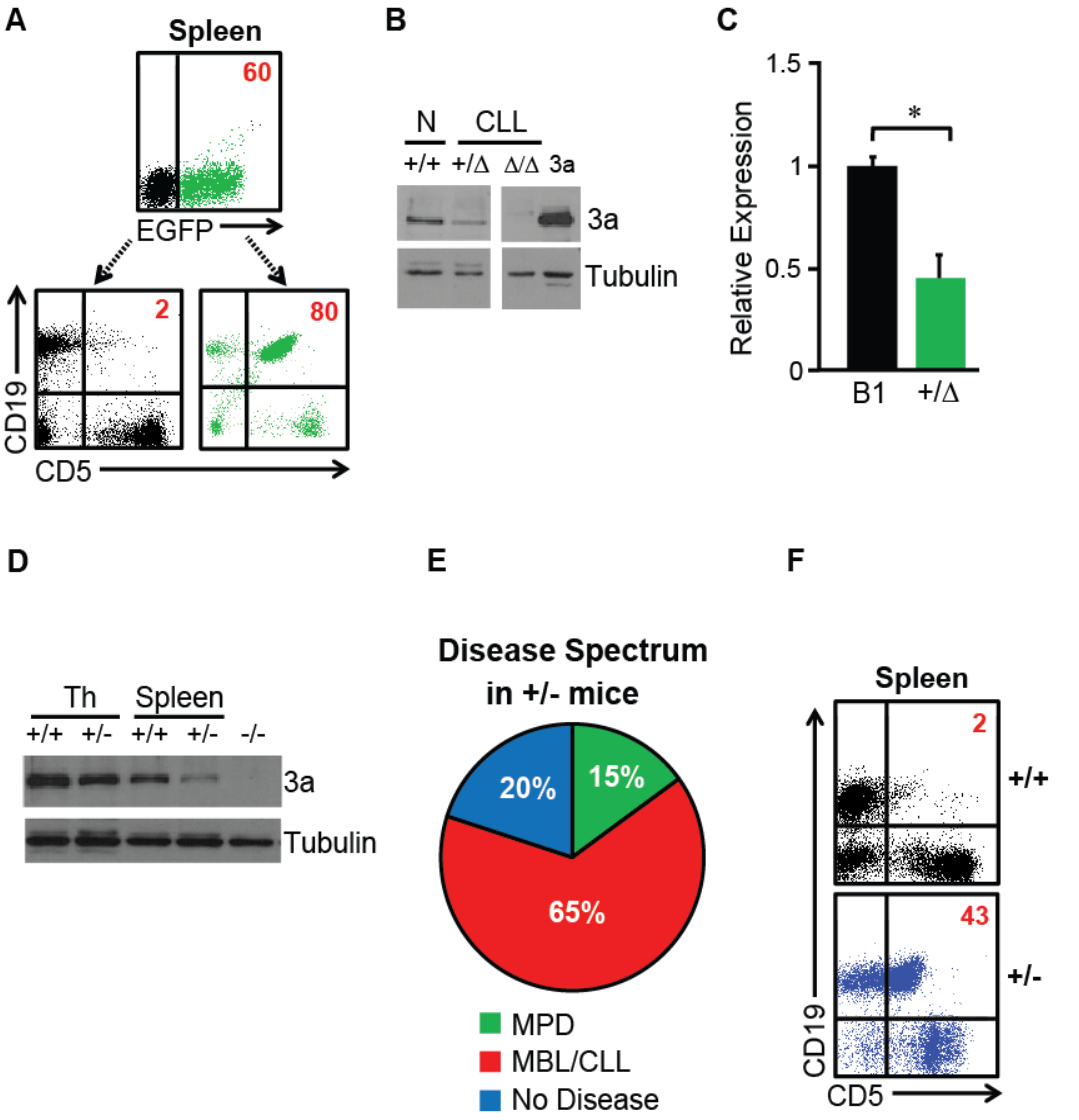

Figure 1. Dnmt3a heterozygous mice develop CLL. A. Flow diagram of CD5 and CD19 expression is shown for EGFP-negative (black) and EGFP-positive (green) cells from a Dnmt3a$^{+/\Delta}$ spleen. The percentage of positive cells is indicated in quadrants. **B.** Dnmt3a expression in Dnmt3a$^{+/\Delta}$ spleen as determined by immunoblot using anti-Dnmt3a antibody. N indicates Dnmt3a$^{+/+}$ CD19+ splenic cells. +/Δ and Δ/Δ indicate splenic CLL cells from Dnmt3a$^{+/\Delta}$ and Dnmt3a$^{\Delta/\Delta}$ mice, respectively. 3a represents a positive control in which Dnmt3a protein was overexpressed in Dnmt3a$^{-/-}$ cells. γ-tubulin served as a loading control. **C.** qRT-PCR analysis of Dnmt3a expression in normal splenic B-1a (B1) cells and Dnmt3a$^{+/\Delta}$ (+/Δ) CLL. Average of two independent experiment is presented. Error bars represent ± standard deviation (SD). P<0.05, Student's t-test. Statistically significant difference is indicated by (*). **D.** Dnmt3a expression in thymi (Th) and spleens of 6 week old Dnmt3a$^{+/+}$ (+/+) and Dnmt3a$^{+/-}$ (+/-) mice as determined by immunoblot using anti-Dnmt3a antibody. (-/-) represents Dnmt3a-defficient cells. γ-tubulin served as a loading control. **E.** Disease spectrum observed in ~16 months old Dnmt3a$^{+/-}$ mice (n=20). MBL/CLL – monoclonal B cell lymphopoiesis/CLL-like disease, MPD – myeloproliferative disease, no disease – disease free mice. **F.** Flow diagram of CD5 and CD19 expression in spleens of Dnmt3a$^{+/-}$ (+/-) and aged-matched Dnmt3a$^{+/+}$ (+/+) mice.

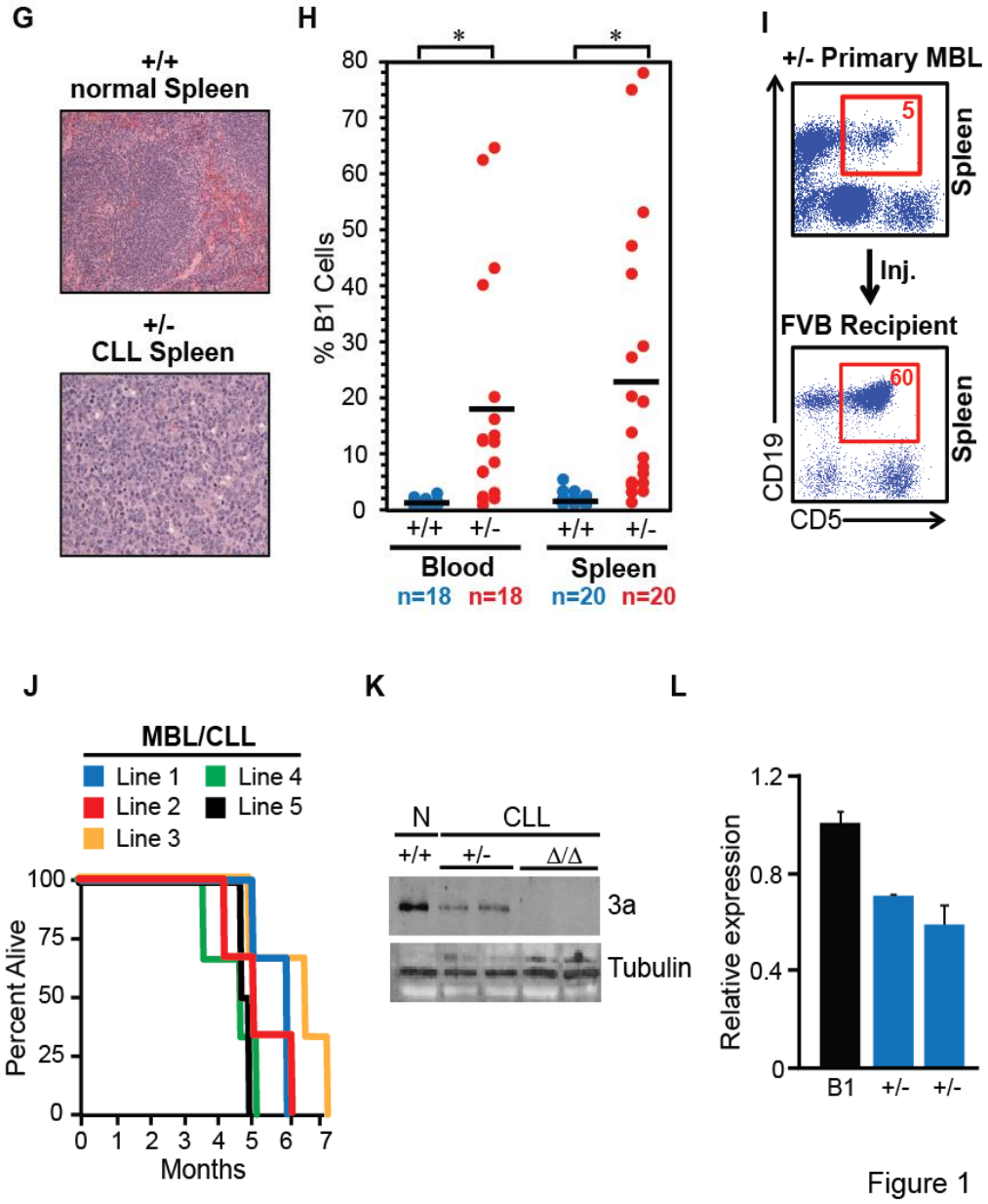

Figure 1

Figure 1 cont. Dnmt3a heterozygous mice develop CLL.
G. H&E stained sections of *Dnmt3a*$^{+/+}$ (normal) and *Dnmt3a*$^{+/-}$ **(**CLL) spleens (200X). **H.** Percentage of B-1a cells in the spleens and blood of ~16 months old Dnmt3a$^{+/+}$ (blue) and Dnmt3a$^{+/-}$ (red) mice as determined by FACS. Number of mice (n) is shown. $P<0.05$ is indicated by (*), Student's t-test. **I.** Flow diagram of CD5 and CD19 expression in the spleen of a *Dnmt3a*$^{+/-}$ mouse with Monoclonal B cell lymphopoeisis (MBL) (top) and terminally ill FVB recipient mouse injected with MBL splenic cells. **J.** Kaplan-Meier survival curves for FVB mice injected with *Dnmt3a*$^{+/-}$ MBL/CLL splenic cells (3 mice per line). Five primary MBL/CLL mice are shown. **K.** Dnmt3a expression in spleens of Dnmt3a$^{+/-}$ (+/–) and Dnmt3a$^{\Delta/\Delta}$ (Δ/Δ) mice as determined by immunoblot using anti-Dnmt3a antibody. N indicates Dnmt3a$^{+/+}$ CD19+ splenic cells. γ-tubulin served as a loading control. **L.** qRT-PCR analysis of Dnmt3a expression in normal and leukemic Dnmt3a$^{+/-}$ B-1a cells. Average of two independent experiment is shown.

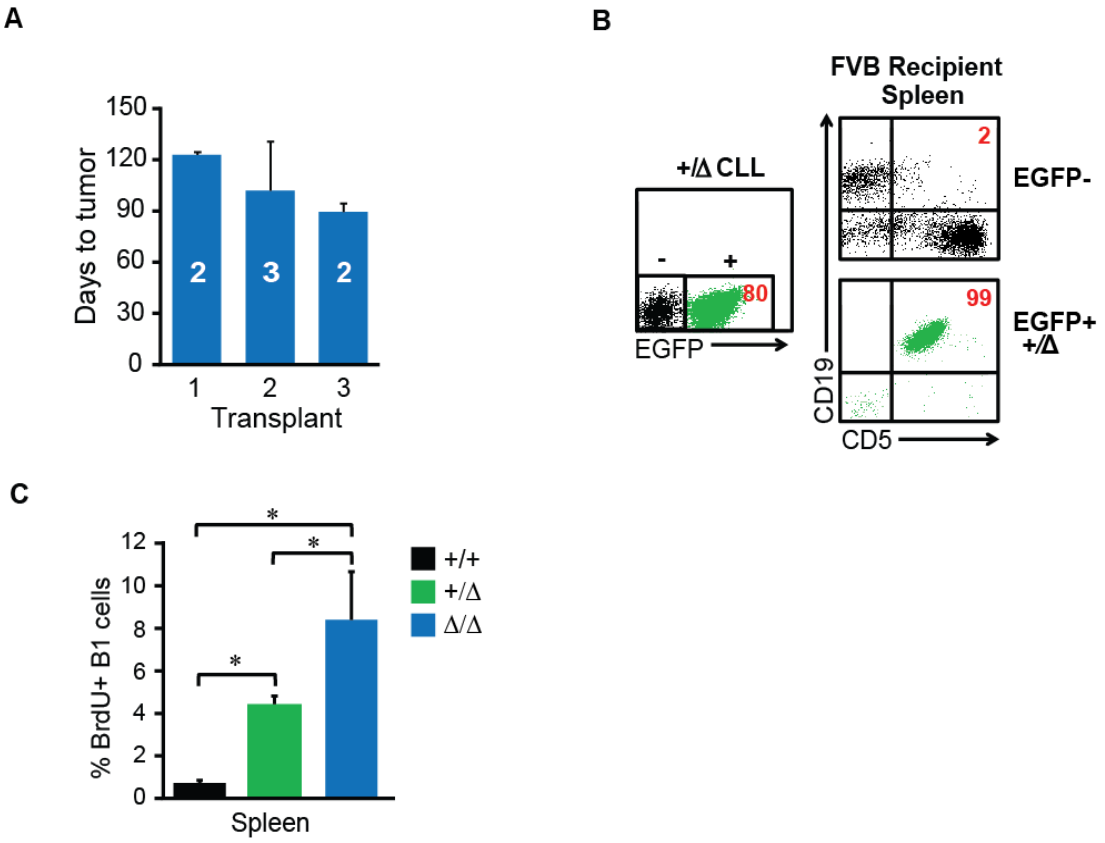

Figure S1. Dnmt3a heterozygous mice develop CLL. A. The time to CLL development for primary (1), secondary (2) and tertiary (3) serially transplanted FVB-recipient mice injected with splenic cells isolated from a terminally sick Dnmt3a$^{+/\Delta}$ mouse. Data are presented as average time to tumor development. The number of recipient mice is indicated within bars. **B.** FACS analysis of EGFP expression in splenic cells of a terminally sick primary FVB-recipient mouse injected with splenic cells from a *Dnmt3a*$^{+/\Delta}$ mouse. Expression of CD5 and CD19 is shown for EGFP-negative (black) and EGFP-positive (green) cells. **C.** BrdU incorporation assay, as determined by FACS analysis, of B-1a splenic cells isolated from normal *Dnmt3a*$^{+/+}$ (n=3), terminally sick *Dnmt3a*$^{\Delta/\Delta}$ (n=3) and *Dnmt3a*$^{+/\Delta}$ (n=3) mice. Error bars represent ± standard deviation (SD).

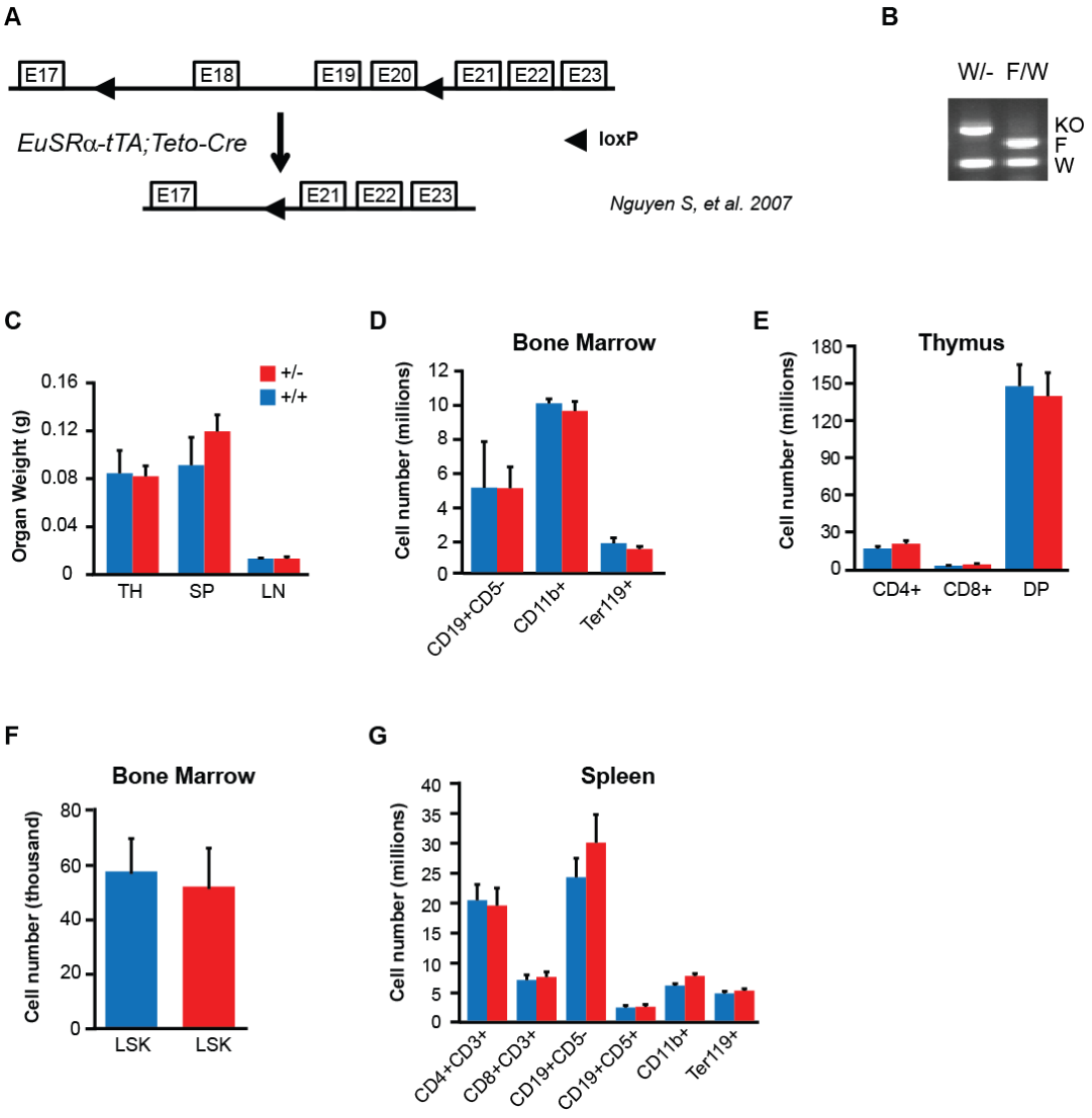

Figure S2. Normal hematopoiesis in 6-week old *Dnmt3a*$^{+/-}$ mice. **A.** A graphical presentation of a generation of a conventional knockout allele of Dnmt3a using *EμSRα-tTA*; *Tet-o-Cre*; *Dnmt3*$^{fl/fl}$ x FVB cross. A conditional knockout allele of Dnmt3a has exons 18 (E18) through exon 20 (E20) flanked by LoxP sites (*Nguyen et al, Dev Dyn 2007)*. *EμSRα-tTA*; *Tet-o-Cre* mice express Cre in germ cells. Cre-mediated excision of DNA between LoxP sites results in the generation of a conventional Dnmt3a knockout allele that lacks E18-E20. **B.** PCR of genomic DNA obtained from offspring of *EμSR*α*-tTA;Teto-Cre;Dnmt3a*$^{fl/fl}$ crossed with FVB. KO indicates a DNA fragment obtained from Dnmt3a conventional knockout allele, F indicates a DNA fragment obtained from Dnmt3a conditional knockout allele and W indicates a DNA fragment obtained from Dnmt3a wild-type allele. For **C-G,** cells were isolated from the organs of 6-weeks-old *Dnmt3a*$^{+/+}$ (n=4) and *Dnmt3a*$^{+/-}$ (n=4) and analyzed by FACS. No significant differences were observed in any of comparisons shown on this figure. Data were analyzed using Student's t test. The average number of cells is shown with $\pm$ SEM. **C.** Organ weights of thymi (TH), spleens (SP) and lymph nodes (LN). **D.** The number of CD19+CD5- (B-cells), CD11b+ (Myeloid), and Ter119+ (erythroid) cells isolated from bone marrow of 6-weeks-old *Dnmt3a*$^{+/+}$ (n=4) and *Dnmt3a*$^{+/-}$ (n=4).

Figure S2 cont. Normal hematopoiesis in 6-week old *Dnmt3a*$^{+/-}$ mice. E. The number of cells with CD4+CD8-, CD4-CD8+ or CD4+CD8+ (DP) immunophenotypes isolated from thymi of 6-weeks-old *Dnmt3a*$^{+/+}$ (n=4) and *Dnmt3a*$^{+/-}$ (n=4). **F.** The number of cells with Lineage^{neg}, Sca-1+, c-kit+ (LSK) immunophenotypes isolated from bone marrow of 6-weeks-old *Dnmt3a*$^{+/+}$ (n=4) and *Dnmt3a*$^{+/-}$ (n=4). **G.** The number of cells with CD4+CD3+ (T-cells); CD8+CD3+ (T-cells); CD19+CD5- (B-cells), CD19+CD5+ (B-1a cells), Gr-1+CD11b+ (Myeloid cells), Ter119+ (erythroid cells) immunophenotypes isolated from spleens of 6-weeks-old *Dnmt3a*$^{+/+}$ (n=4) and *Dnmt3a*$^{+/-}$ (n=4).

Dnmt3a$^{+/-}$ mice also develop myeloproliferative disease.

In addition to CLL, we also observed the development of a myeloproliferative disease (MPD) in 15% of _Dnmt3a_$^{+/-}$ mice (Figure 1E). These mice showed expansion of Gr-1+CD11b+ myeloid cells in the blood, spleen and bone marrow (Figure 2A-2C and data not shown). In contrast to CLL-like cells, Gr-1+CD11b+ splenic cells did not induce disease upon injection into sublethally irradiated FVB recipient mice, suggesting that this population of cells do not contain leukemia initiating cells (Figure 2D-E). Thus, our studies of _Dnmt3a_$^{+/-}$ mice show that long-term mono-allelic loss of Dnmt3a can induce a frank B cell malignancy, non-malignant myeloproliferative disorder with a combined 80% penetrance by 16 months of age. In order to understand why Dnmt3a heterozygosity affects primarily B-1a and myeloid cells, we measured Dnmt3a mRNA levels in FACS-sorted normal _Dnmt3a_$^{+/+}$ B-1a, B2, T cells and myeloid cells and found that Dnmt3a expression was lower in B-1a cells when compared to B2 cells and relatively equal when compared to T cells (Figure 2F). Thus, the preferential transformation of B-1a cells or myeloid cells does not seem to be associated with significantly different Dnmt3a levels relative to other normal hematopoietic cells. The reason why B-1a and, to some extent, myeloid cells are in particular sensitive to transformation upon decreased Dnmt3a levels therefore remains unclear.

Given that _Dnmt3a_$^{+/-}$ mice develop CLL, we next asked whether or not DNMT3A deficiency is observed in human CLL. Previous analysis of available gene expression data (Haferlach et al., 2010) identified DNMT3A as belonging to the top 1% of under-expressed genes in CLL (Peters et al., 2014). Our further analysis showed that in 4/5 cases of primary human CLL, DNMT3A expression was significantly decreased relative to normal human CD19+ B cells (Figure 2G). These data support the idea that

decreased DNMT3A may promote the development of human CLL. Further investigation is needed to more carefully address this point.

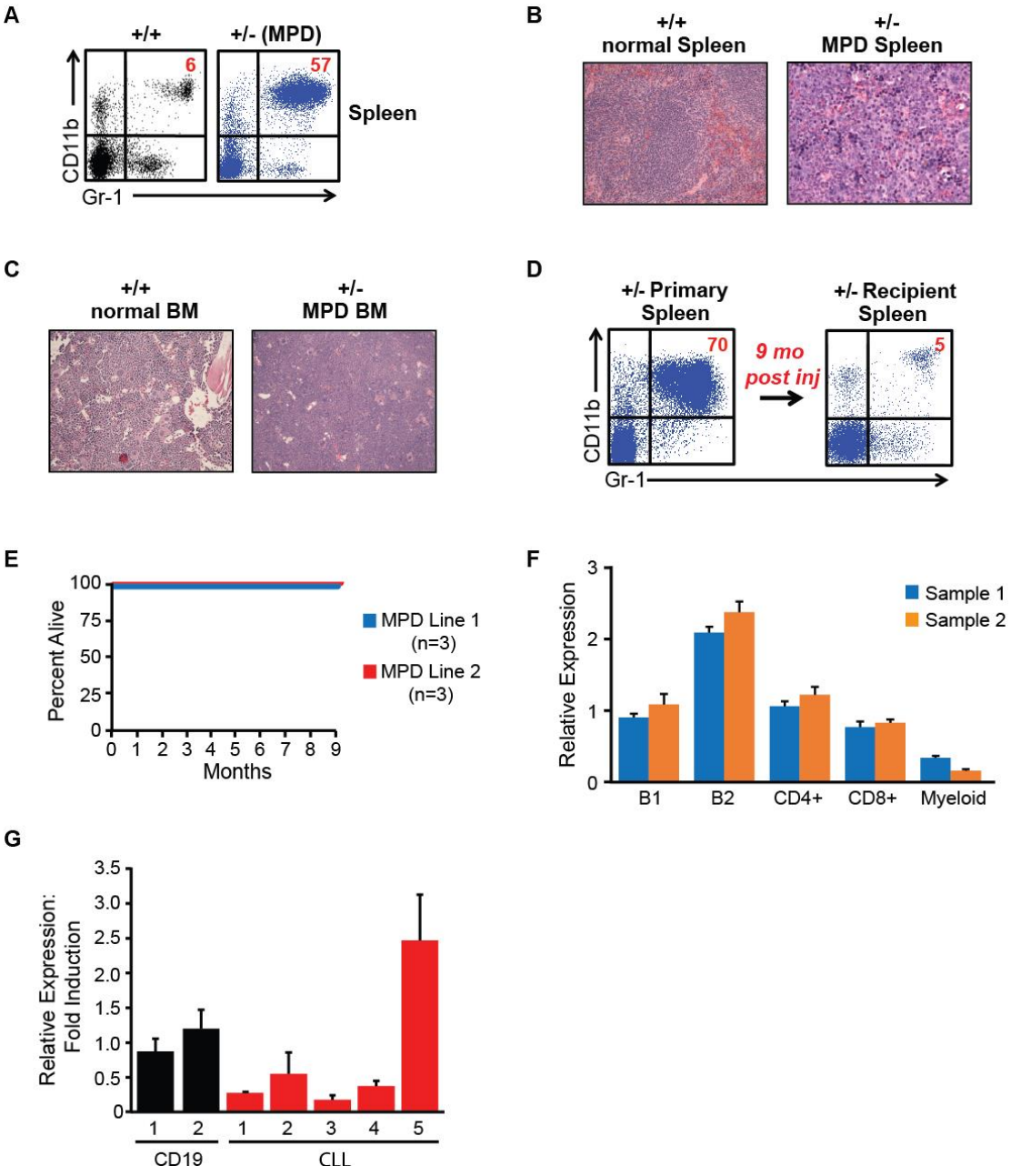

Figure 2. *Dnmt3a*$^{+/-}$ mice also develop non-malignant myeloproliferative disorder. A. Flow diagram of CD11b and Gr-1 expression in spleens of normal Dnmt3a$^{+/+}$ (+/+) and Dnmt3a$^{+/-}$ (+/-) mice with MPD. **B.** H&E stained sections of *Dnmt3a*$^{+/+}$ and *Dnmt3a*$^{+/-}$ spleens (200x). **C.** H&E stained sections of *Dnmt3a*$^{+/+}$ and *Dnmt3a*$^{+/-}$ femurs (200x). **D.** Flow diagram of Gr-1 and CD11b expression in spleen of *Dnmt3a*$^{+/-}$ mouse with MPD (left). Gr-1 and CD11b expression 9 months post injection (right). **E.** Kaplan-Meier survival curves for FVB recipients injected with two independent *Dnmt3a*$^{+/-}$ MPD lines (3 mice per line). **F.** qRT-PCR analysis of Dnmt3a expression in sorted B-1a, B2, CD4+ T cells, CD8+ T cells, and myeloid cells isolated from FVB spleen. Two biological replicates are shown. Data was normalized to Gapdh and error bars represent ± SD. **G.** qRT-PCR analysis of DNMT3A expression in five human CLL samples (1-5). Two biological replicates for CD19+ peripheral blood from healthy donors were used as controls. Average of two independent experiments is shown. Error bars represent ± SD.

DNA methylome and transcriptome of normal mouse B-1a cells.

To identify DNA methylation and transcriptional changes associated with CLL development, we performed global methylation profiling by WGBS and gene expression profiling by RNA-seq of B-1a cells isolated from normal *Dnmt3a*$^{+/+}$ spleens, as this cellular population is immunophenotypically the closest normal counterpart of CLL cells. We focused on splenic B-1a cells rather than B-1a cells residing in the intraperitoneal cavity because: a.) the observed CLL disease consistently presented with splenomegaly and the spleen served as a source of tumor cells b.) the microenvironment can effect gene expression and presumably methylation patterns. WGBS analysis of normal B-1a cells revealed that out of 22,452,960 CpG dinucleotides covered by our analysis 20,316,133 CpGs were methylated > 50%, whereas only 2,136,827 CpGs were methylated < 50% and only 133,765 CpGs ≤ 20% (Figure 3A). When we analyzed only CpG dinculeotides that aligned to core promoter regions (-300 to +150bp relative to transcription start site; TSS) we found that from the 25,742 promoters analyzed, 15,203 were methylated at > 50%. (Figure 3B; Table S1) and only 7,436 promoters were methylated at ≤ 20%. A combined analysis of gene expression and methylation revealed that 50% of genes with ≤ 20% promoter methylation were expressed (FPKM > 5; Figure 3C, Table S2). In contrast, 84% of genes with promoter hypermethylation (≥ 50%) were not expressed (FPKM ≤ 5; Figure 3C, Table S2). Consistently, the degree of promoter methylation inversely correlated with gene expression (Figure 3D). For example, promoters with less than 25% methylation were expressed at significantly higher levels than promoters with higher levels of methylation (Figure 3D). IPA of 3,700 highly expressed genes (FPKM ≥ 10) revealed a significant enrichment in genes relating to hematopoiesis and lymphoid tissue structure and development (Figure 3E). Altogether, these data demonstrates that most gene promoters in normal splenic B-1a cells are

hypermethylated and silenced whereas promoters that are hypomethylated are largely expressed and their physiological relevance is linked to the hematopoietic system.

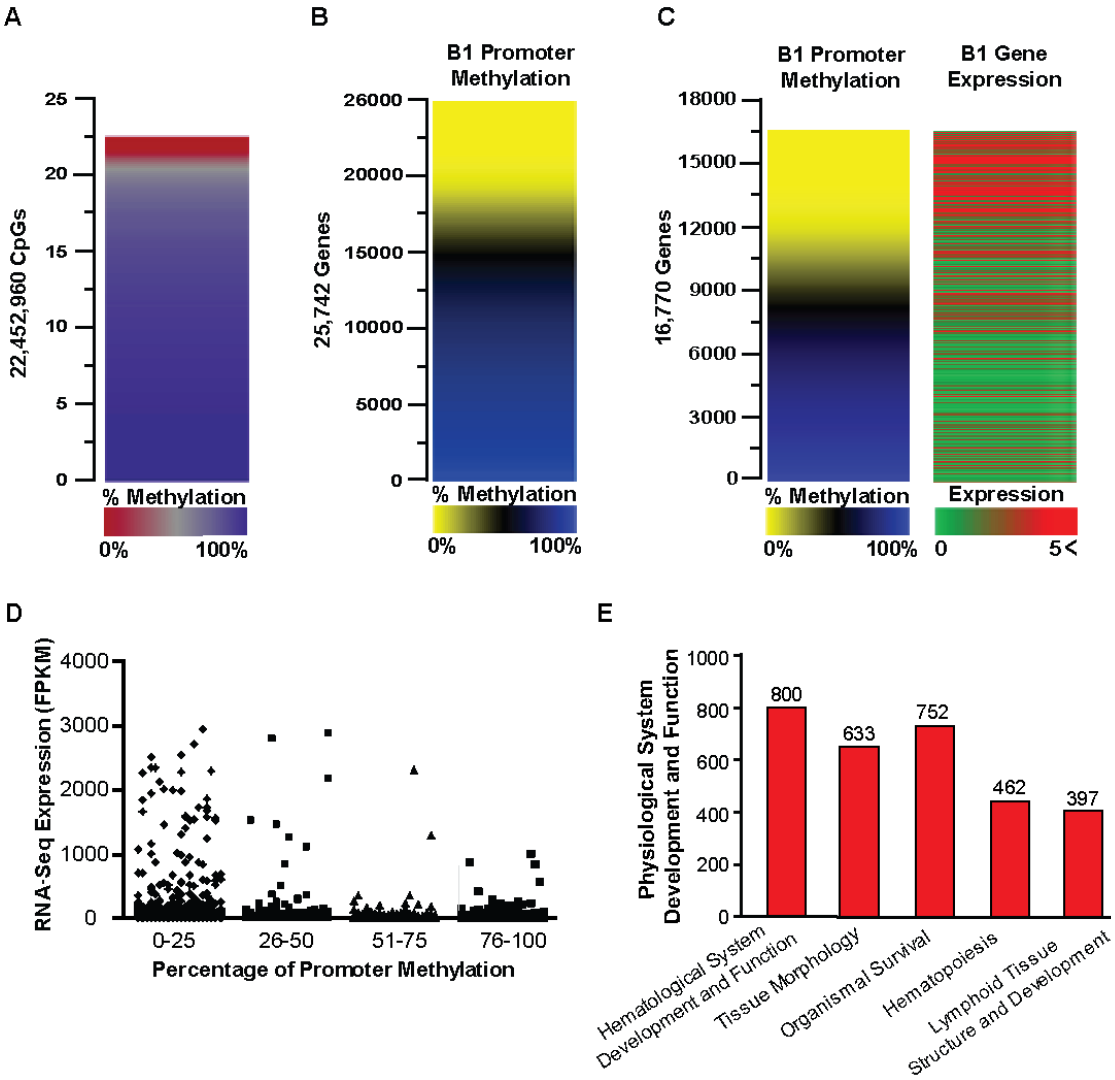

Figure 3. DNA methylome and transcriptome of normal mouse B-1a cells. A. Methylation status of 22,452,960 CpG dinucleotides in normal B-1a cells as determined by whole-genome bisulfite sequencing (WGBS). **B.** A heat map displaying methylation status of 25,742 promoters as determined by WGBS. Methylation percentage for individual CpGs were annotated to the promoter regions -300bp to +150bp relative to the transcription start site (TSS). Methylation percentages for all CpGs across the 450bp region were averaged to give a mean methylation value for each gene promoter. **C.** Heat map presentation of promoter methylation (analyzed as in **Figure 2B**) and corresponding gene expression (average FPKM values from RNA-seq) in mouse splenic B-1a cells for 16,770 genes. Genes with high FPKM values are shown in red and genes with low FPKM values are shown in green. Upper limit for color-coding in gene expression heat map is FPKM ≥ 5 as indicated. Heat maps are organized in the same gene order to match data for methylation and gene expression. **D.** Analysis of promoter (-300 to +150bp) methylation in relation to gene expression in mouse splenic B-1a cells for 16,770 genes. Genes were divided into four groups based on percentage of promoter methylation (0-25%, 26-50%, 51-75% and 76-100%). $P<0.05$ for all pair-wise comparisons except 51-75 to 76-100 group (Bonferroni's multiple comparison test). **E.** Ingenuity Pathway analysis of 3,700 highly expressed genes (FPKM ≥ 10). The top subcategories obtained in “Physiological System, Development and Functions” are shown with the number of genes indicated above individual bars ($P<0.05$, for all subcategories).

DNA methylome of *Dnmt3a*$^{+/\Delta}$ and *Dnmt3a*$^{\Delta/\Delta}$ CLL.

We next performed WGBS on DNA isolated from *Dnmt3a*$^{+/\Delta}$ CLL cells and *Dnmt3a*$^{\Delta/\Delta}$ CLL cells to determine the effects of loss of Dnmt3a on the CLL methylome. Mono-allelic loss of Dnmt3a resulted in a ~1% relative hypomethylation and a 0.1% hypermethylation in individual CpGs relative to B-1a (Figure 4A, Table S3). Bi-allelic loss of Dnmt3a resulted in a substantial 4.1% decrease and a 0.1% increase CpG methylation (Figure 4A, Table S3). Relative to *Dnmt3a*$^{+/\Delta}$ CLL, hypomethylation in the Dnmt3a-deficient CLL genome was most pronounced in repetitive elements and gene bodies (3.5 to 5.5 fold) (Figures 4B, S3A and B). In contrast, the increased incidence of hypomethylated long promoters (-1500 bp to +500 bp relative to TSS) was only 2.2 fold greater in *Dnmt3a*$^{\Delta/\Delta}$ CLL compared to *Dnmt3a*$^{+/\Delta}$ CLL (Figures 4C, S3B, Table S4). This ratio was even smaller (1.9 fold) when analysis was restricted to core promoters (-300 bp to +150 bp) (Figures 4C, S3B, Table S4). These data suggest that Dnmt3a levels are more critical for promoter methylation than other parts of the genome, such as repetitive elements or gene bodies and that 699 hypomethylated promoters in *Dnmt3a*$^{+/\Delta}$ are likely hypersensitive to levels of Dnmt3a (Figure 4C). Overall, 386 hypomethylated promoters and 43 hypermethylated promoters were shared between *Dnmt3a*$^{+/\Delta}$ and *Dnmt3a*$^{\Delta/\Delta}$ CLL (Figure 4D and Table S4). Differentially methylated promoters were equally distributed across the genome, with exception of the X chromosome in which no hypo- or hypermethylated promoters were shared between *Dnmt3a*$^{+/\Delta}$ and *Dnmt3a*$^{\Delta/\Delta}$ CLL cells relative to B-1a control cells (Figure 4D, Table S5). In contrast, chromosome 11 and 19 had the highest number of commonly hypomethylated promoters, with 48 and 23, respectively (Figure 4D, Table S5). Commonly hypomethylated promoters likely represent targets of Dnmt3a maintenance methylation function, whereas

hypermethylated promoters in *Dnmt3a*$^{\Delta/\Delta}$ CLL are likely *de novo* methylated by other Dnmts.

To determine whether the methylation landscape generated by WGBS is specific to the CLL samples profiled or rather represents common changes that occur in Dnmt3a-deficient CLL, we validated hypo- and hypermethylated promoters using locus-specific Combined Bisulfite Restriction Analysis (COBRA) assays, as well as two global methods – methyl sensitive cut counting (MSCC) and reduced representation bisulfite sequencing (RRBS). COBRA analysis of 6 promoters confirmed the hypomethylation identified by WGBS, suggesting that changes in promoter methylation likely represent common events occurring in mouse CLL (Figure 4G, Figure S3C). Next, we validated hypo- and hypermethylated promoters using two global methods – MSCC and RRBS. The choice of two independent approaches was driven by the fact that each method has lower genome-wide coverage and is biased against regions with low-CG content (146). Thus, their concurrent use allowed us to obtain a more comprehensive and complementary methylation dataset. Importantly, were confirmed 53% of hypomethylated and 98% of hypermethyated DMRS in promoters in *Dnmt3a*$^{\Delta/\Delta}$ CLL identified by WGBS using one or both methods (Figure 4G, Table S6). These data demonstrate that methylation changes detected by WGBS on a small sample set likely represent events shared among larger sets of *Dnmt3a*$^{\Delta/\Delta}$ CLL.

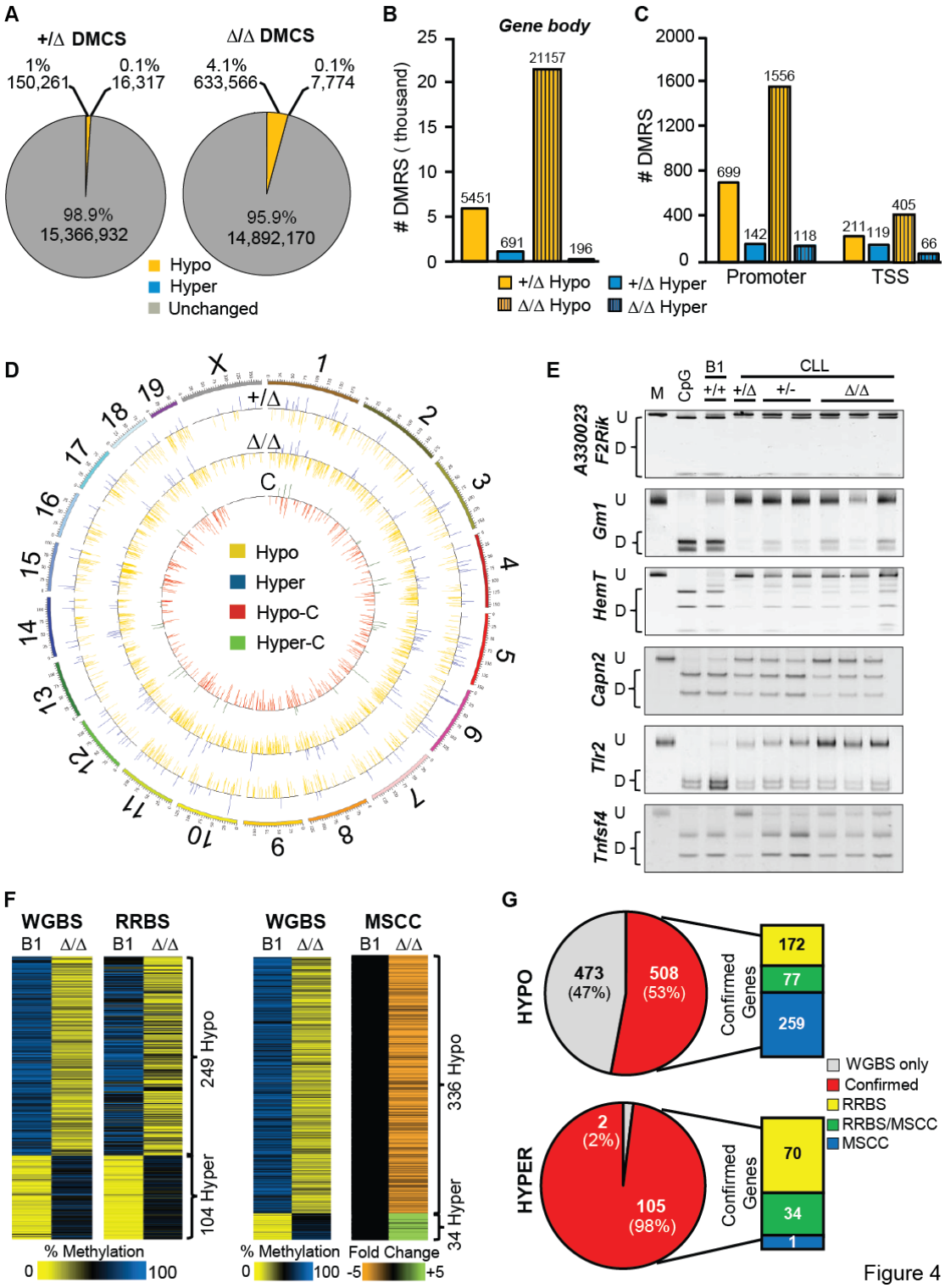
A
+/Δ DMCS
1%
150,261
0.1%
16,317
98.9%
15,366,932
Δ/Δ DMCS
4.1%
633,566
0.1%
7,774
95.9%
14,892,170
Hypo
Hyper
Unchanged
B
Gene body
DMRS (thousand)
5451
691
21157
196
+/Δ Hypo
+/Δ Hyper
Δ/Δ Hypo
Δ/Δ Hyper
C
DMRS
699
142
1556
118
211
119
405
66
Promoter
TSS
D
+/Δ
Δ/Δ
C
Hypo
Hyper
Hypo-C
Hyper-C
E
M
CpG
B1
+/+
CLL
+/Δ
+/-
Δ/Δ
A330023 F2Rik
Gm1
HemT
Capn2
Tlr2
Tnfsf4
U
D
F
WGBS
RRBS
WGBS
MSCC
B1
Δ/Δ
249 Hypo
104 Hyper
336 Hypo
34 Hyper
% Methylation
0
100
Fold Change
-5
+5
G
HYPO
473
(47%)
508
(53%)
Confirmed Genes
172
77
259
HYPER
2
(2%)
105
(98%)
70
34
1
WGBS only
Confirmed
RRBS
RRBS/MSCC
MSCC

Figure 4

Figure 4. DNA methylome of CLL induced by decrease or absence of Dnmt3a. A. A graphical presentation of differentially methylated cytosines (DMCS) in Dnmt3a$^{+/\Delta}$ and Dnmt3a$^{\Delta/\Delta}$ CLL relative to B-1a control. Methylation changes were evaluated in 15,533,510 CpGs and are shown in both absolute numbers and percentages. **B.** The number of differentially methylated regions (DMRS) associated with gene bodies in Dnmt3a$^{+/\Delta}$ and Dnmt3a$^{\Delta/\Delta}$ CLL samples when compared to B-1a control sample. **C.** The number of DMRs associated with long promoters (-1500 to +500 bp relative to the TSS) and core promoters (TSS; -300 to +150bp relative to the TSS) in Dnmt3a$^{+/\Delta}$ and Dnmt3a$^{\Delta/\Delta}$ CLL relative to B-1a control. **D.** Circos plot of DMRs associated with long promoters in Dnmt3a$^{+/\Delta}$ or Dnmt3a$^{\Delta/\Delta}$ CLL. Outer circle is a graphical presentation of mouse chromosomes and inner circles indicate DMRs and their positions on mouse chromosomes observed in Dnmt3a$^{+/\Delta}$ (+/Δ) or Dnmt3a$^{\Delta/\Delta}$ CLL (Δ/Δ) relative to B-1a control. Yellow lines indicate hypomethylated promoters whereas blue lines indicate hypermethylated promoters. Circle 'C' represents hypo- (red lines) and hypermethylated (green lines) promoters commonly observed in both CLL samples. **E.** COBRA analysis of putative Dnmt3a target gene promoters in splenic B-1a cells (B1), Dnmt3a$^{+/\Delta}$ CLL (+/Δ), Dnmt3a$^{+/-}$ CLL (+/-) and Dnmt3a$^{\Delta/\Delta}$ CLL (Δ/Δ) samples. Undigested (U) and digested (D) fragments correspond to unmethylated and methylated DNA, respectively. CpG and M indicates a fully methylated control and undigested PCR fragments, respectively. **F.** (left) Heatmap showing 249 hypomethylated and 104 hypermethylated promoters identified through WGBS and confirmed by RRBS. Data is shown as an average percent methylation for Dnmt3a$^{+/+}$ B-1a (n=2) and Dnmt3a$^{\Delta/\Delta}$ CLL (n=2) for differentially methylated CpGs (minimum 30% change in methylation) annotated to the promoter region (-1500 to +500bp). (right) Heatmap showing 336 hypomethylated and 34 hypermethylated promoters identified through WGBS and confirmed by MSCC. Data is shown as a fold change in methylation for Dnmt3a$^{\Delta/\Delta}$ CLL (n=3) relative to Dnmt3a$^{+/+}$ B-1a (n=2). Differentially methylated CpGs (fold change > 2 and a $P < 0.05$, negative binomial analysis) were annotated to the promoter region. **G.** RRBS and MSCC confirmation of differentially methylated promoters (red) identified through WGBS. The number and percent of confirmed hypomethylated (top) and hypermethylated (bottom) genes by RRBS (yellow), MSCC (blue) or both (green) is shown. Gray represents genes identified through WGBS not confirmed by MSCC or RRBS.

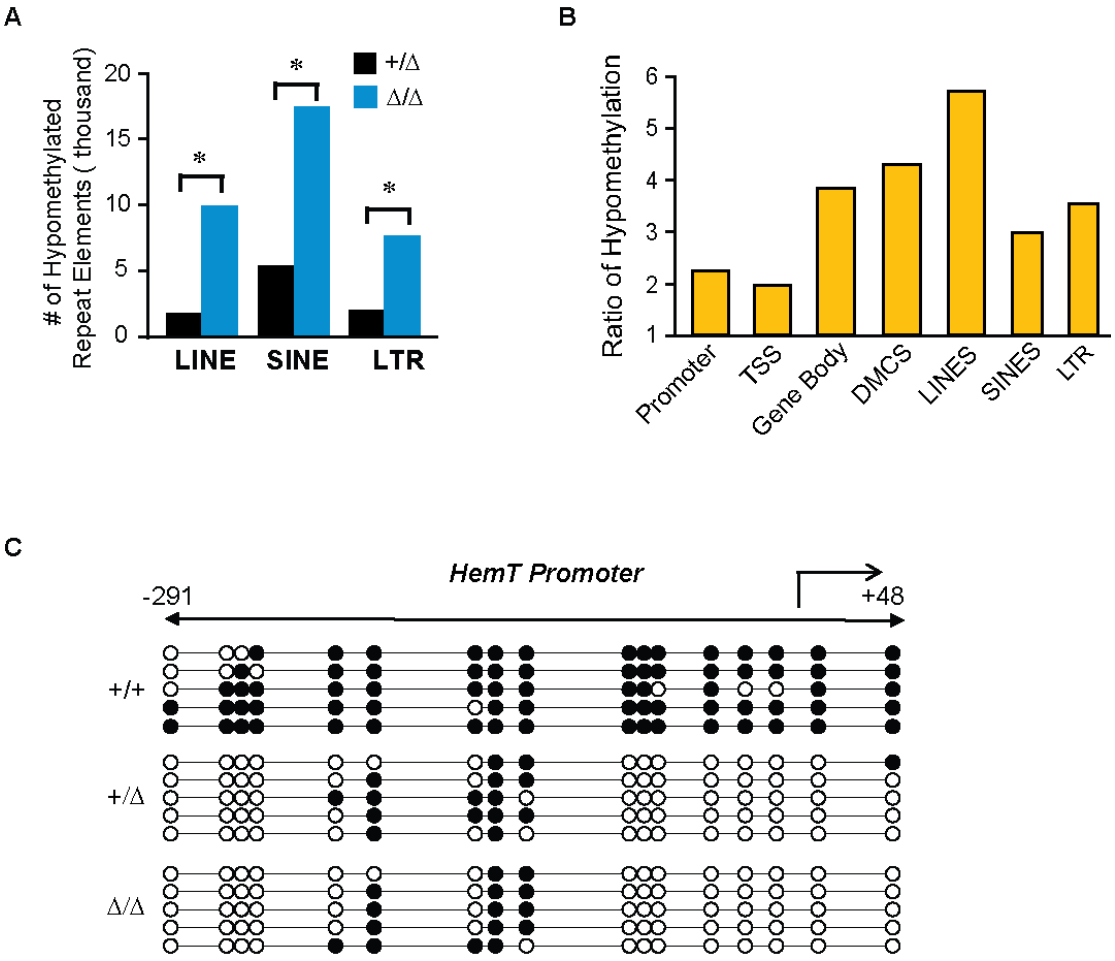

Figure S3. Related to Figure 4. Deregulated methylation in *Dnmt3a*$^{\Delta/\Delta}$ and *Dnmt3a*$^{+/\Delta}$ CLL. A. The number of LINE, SINE and LTR Repeat Elements that are associated with DMRs in *Dnmt3a*$^{+/\Delta}$ and *Dnmt3a*$^{\Delta/\Delta}$ CLL samples when compared to B-1a control. **B.** Ratio between the number hypomethylated genomic elements observed in *Dnmt3a*$^{\Delta/\Delta}$ CLL and in *Dnmt3a*$^{+/\Delta}$ CLL calculated from values in panels A-C of Figure 4 and Figure S3A. **C.** Bisulfite sequencing of the HemT promoter region in normal B-1a , Dnmt3a$^{+/\Delta}$ CLL and Dnmt3a$^{\Delta/\Delta}$ CLL samples. Each line represents the sequence of an individual allele and circles denote individual CpGs, with black showing methylation and white shown lack of methylation.

Promoter hypomethylation in CLL is likely due to the lack of cancer-specific maintenance activity of Dnmt3a and is independent of proliferation.

Promoter hypomethylation observed in *Dnmt3a*$^{+/-}$ and *Dnmt3a*$^{\Delta/\Delta}$ CLL could results from Dnmt3a inactivation in normal B-1a cells, either due to lack of Dnmt3a's *de novo* or maintenance activity. In such a scenario, promoters would be hypomethylated in normal B-1a cells prior to CLL development. To address this, we performed COBRA assays to analyze promoter methylation of 14 genes in normal *Dnmt3a*$^{+/+}$ and *Dnmt3a*$^{+/-}$ B-1a cells. Interestingly, we have not seen any evidence of decreased promoter methylation in any of loci tested in *Dnmt3a*$^{+/-}$ B-1a cells, suggesting that a partial inactivation of Dnmt3a does not affect the methylation status of promoters during the development of normal B-1a cells (Figure 5A). Thus, the decrease in methylation observed in *Dnmt3a*$^{+/-}$ and *Dnmt3a*$^{\Delta/\Delta}$ CLL appears to be tumor-specific.

We next sought to determine if promoter hypomethylation observed in *Dnmt3a*$^{+/-}$ and *Dnmt3a*$^{\Delta/\Delta}$ CLL could be the result of increased proliferation of CLL cells rather than the result of Dnmt3a-deficiency. We therefore examined promoter methylation in selected loci in two independent mouse models of CLL, *IRF4*$^{-/-}$*;Vh11* and *Eμ-TCL1* (147, 148). In *IRF4*$^{-/-}$*;Vh11* CLL samples, no changes in Dnmt3a levels were observed by global gene expression (data not shown). To verify this, we measured transcript levels of Dnmt3a but did not observe changes in Dnmt3a transcript levels in *IRF4*$^{-/-}$*;Vh11* CLL (Figure 5B). Thus, this CLL model likely represent one in which Dnmt3a activity is not altered. In contrast, it has been reported recently, that TCL-1 binds to and inhibits Dnmt3a activity, resulting in suppression of Dnmt3a activity and hypomethylation in the *Eμ-TCL1* mice (65). Thus, *Eμ-TCL1* CLL represents a model in which biochemical inhibition of Dnmt3a occurs. We analyzed promoter methylation of four genes found to be hypomethylated in *Dnmt3a*$^{+/-}$ and *Dnmt3a*$^{\Delta/\Delta}$ CLL using DNA from *IRF4*$^{-/-}$*;Vh11* and

Eμ-TCL1 CLL samples. This analysis revealed that all tested promoters were partially hypomethylated in *Eμ-TCL1* CLL and not hypomethylated in *IRF4*$^{-/-}$*;Vh11* CLL samples (Figure 5C), suggesting that promoter hypomethylation in *Dnmt3a*$^{+/-}$ and *Dnmt3a*$^{\Delta/\Delta}$ CLL is directly linked to the lack of Dnmt3a rather than to increased cellular proliferation. Expression of *Nfam1* correlated with its promoter methylation, as this gene was expressed in *Dnmt3a*$^{+/-}$ and *Dnmt3a*$^{\Delta/\Delta}$ CLL but not in *IRF4*$^{-/-}$*;Vh11* CLL, suggesting that at least some genes that become hypomethylated during CLL development become overexpressed (Figure 5D). These data suggest that Dnmt3a may have a tumor-specific maintenance activity similar to the one we described previously for Dnmt3b in MYC-induced T cell lymphomagenesis (13).

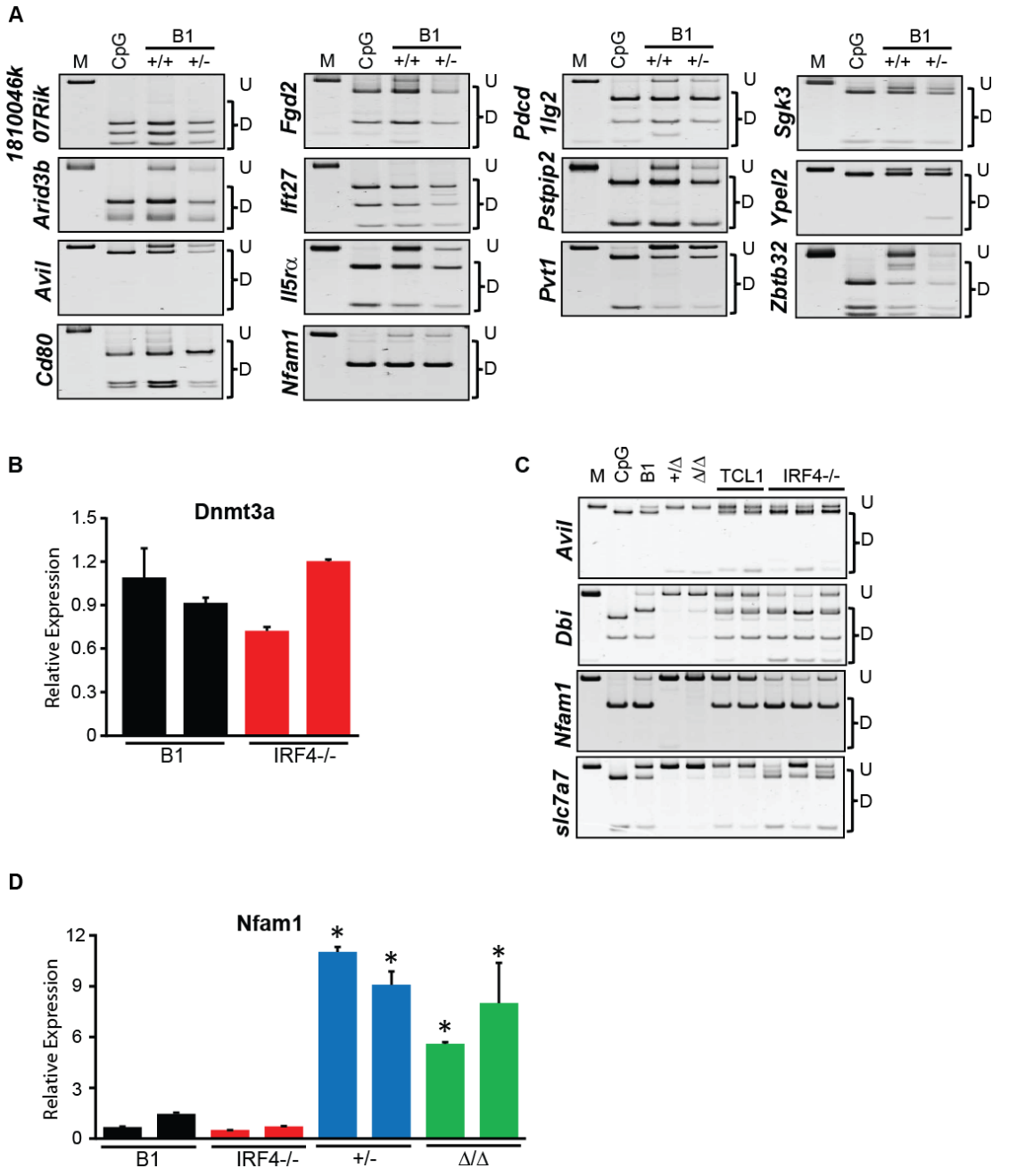

Figure 5. Dnmt3a has a cancer-specific maintenance function. A. COBRA analysis of 14 putative Dnmt3a target gene promoters in splenic Dnmt3a$^{+/+}$ and Dnmt3a$^{+/\Delta}$ B-1a cells. Undigested (U) and digested (D) fragments correspond to unmethylated and methylated DNA, respectively. CpG and M indicates a fully methylated control and undigested PCR fragments, respectively. **B.** qRT-PCR analysis of Dnmt3a expression in normal B-1a and IRF4$^{-/-}$;Vh11 CLL samples. Average of two independent experiments is presented. Error bars represent ± SD. **C.** COBRA analysis of 4 putative Dnmt3a target gene promoters in Dnmt3a$^{+/\Delta}$ (+/Δ), Dnmt3a$^{\Delta/\Delta}$ (Δ/Δ), Eμ-TCL1, and IRF4$^{-/-}$;Vh11 CLL. **D.** qRT-PCR analysis of Nfam1 expression in B-1a, IRF4$^{-/-}$;Vh11, Dnmt3a$^{+/-}$ (+/-), and Dnmt3a$^{\Delta/\Delta}$ (Δ/Δ) CLL. Average of two independent experiments is presented. Error bars represent ± SD.

Gene expression is conserved in *Dnmt3a*$^{+/\Delta}$ and Dnmt3a$^{\Delta/\Delta}$ CLL.

To better understand the molecular basis for CLL development, global gene expression profiles of normal B-1a cells, *Dnmt3a*$^{+/-}$ and *Dnmt3a*$^{\Delta/\Delta}$ CLL cells were determined by RNA-seq. We identified 413 overexpressed and 282 underexpressed genes in *Dnmt3a*$^{+/-}$ CLL relative to B-1a cells (Figure 6A, Table S7). Inactivation of both Dnmt3a alleles in *Dnmt3a*$^{\Delta/\Delta}$ CLL resulted in overexpression of 790 genes and underexpression of 398 genes. Interestingly, the majority of genes upregulated in *Dnmt3a*$^{+/-}$ CLL were also upregulated in *Dnmt3a*$^{\Delta/\Delta}$ CLL cells (67%), whereas downregulated genes were less conserved between the two genetic settings (57%; Figure 6B, Table S7). To gain insight into the nature of deregulated processes in CLL induced by decreased levels of Dnmt3a, we next performed IPA analysis of differentially expressed genes between *Dnmt3a*$^{+/-}$ and *Dnmt3a*$^{\Delta/\Delta}$ CLL relative to control B-1a cells. Notably, the top five subcategories under “Disease and disorder” and “Physiological System Development and Functions” were identical in *Dnmt3a*$^{+/-}$ and *Dnmt3a*$^{\Delta/\Delta}$ CLL (Figure S4A). In addition, three out of five subcategories under “Canonical pathways” were conserved between *Dnmt3a*$^{+/-}$ and *Dnmt3a*$^{\Delta/\Delta}$ CLL. Altogether, this suggests that despite the higher number of differentially expressed genes present in *Dnmt3a*$^{\Delta/\Delta}$ CLL, similar pathways are affected in both settings. However, the physiological relevance of these categories to CLL development is less clear as this analysis did not provide clear links to pathways or molecules driving CLL development.

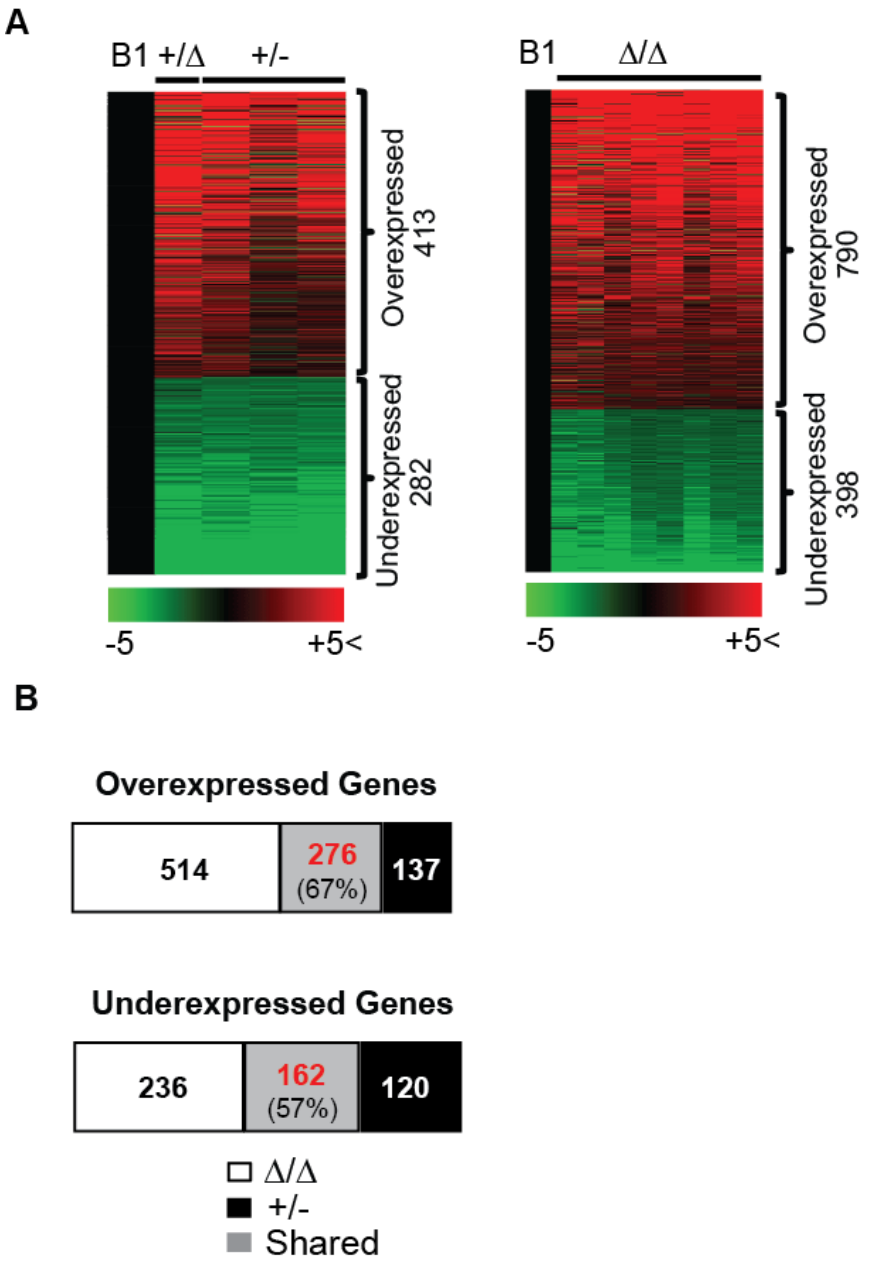

Figure 6. Decreased Dnmt3a levels result in deregulated transcription in Dnmt3a$^{+/\Delta}$ CLL similar to Dnmt3a$^{\Delta/\Delta}$ CLL. A. Heat maps derived from RNA-seq analysis displaying 413 overexpressed and 282 underexpressed genes in Dnmt3a$^{+/\Delta}$ and Dnmt3a$^{+/-}$ CLL (n=4) relative to control B-1a cells (n=2) (left) and 790 overexpressed and 398 underexpressed genes in Dnmt3a$^{\Delta/\Delta}$ CLL (n=8). Only genes with a fold change ≥ 2 and a q-value < 0.05 are shown (CuffDiff analysis). **B.** The number of genes differentially expressed in Dnmt3a$^{\Delta/\Delta}$ CLL (white box), Dnmt3a$^{+/-}$ CLL (black box) and genes common between Dnmt3a$^{\Delta/\Delta}$ and Dnmt3a$^{+/-}$ CLL (grey box).

Genes commonly hypomethylated and overexpressed in *Dnmt3a*$^{+/-}$ and *Dnmt3a*$^{\Delta/\Delta}$ CLL (HOC) are putative drivers of CLL.

Since loss of one allele of Dnmt3a is sufficient to induce CLL, we hypothesized that genes most likely involved in pathogenesis of the disease are those whose promoter methylation affect gene expression in both *Dnmt3a*$^{+/-}$ and *Dnmt3a*$^{\Delta/\Delta}$ CLL. A comparison of promoter methylation and gene expression revealed that 10% of genes in both *Dnmt3a*$^{+/-}$ and *Dnmt3a*$^{\Delta/\Delta}$ CLL were hypomethylated and overexpressed (Figure 7A, Table S8). In contrast, only 3% and 1% of hypermethylated genes showed reduced expression in *Dnmt3a*$^{+/-}$ and *Dnmt3a*$^{\Delta/\Delta}$ CLL, respectively (Figure 7A). We next performed IPA using genes whose expression and methylation was commonly changed in both *Dnmt3a*$^{+/-}$ and *Dnmt3a*$^{\Delta/\Delta}$ CLL. This analysis identified a signature of 26 genes commonly hypomethylated and overexpressed in both *Dnmt3a*$^{+/-}$ and *Dnmt3a*$^{\Delta/\Delta}$ CLL (**H**ypomethylated and **o**verexpressed in **C**LL; HOC genes; Figure 7B). With exception of *Mgmt*, promoter hypomethylation of all HOC genes was confirmed by locus-specific COBRA assay in the vast majority *Dnmt3a*$^{+/-}$ CLL and *Dnmt3a*$^{\Delta/\Delta}$ CLL samples tested, suggesting that HOC promoter hypomethylation is a conserved event in CLL induced by a decrease in Dnmt3a. These genes therefore may play a role in disease development. Consistently, IPA analysis placed twenty-four genes in the category ‘cancer’ (Figure S4B). In contrast to the strong association of HOC genes with the cancer category, IPA analysis of multiple randomly selected groups of 26 overexpressed genes in *Dnmt3a*$^{+/-}$ CLL did not identify the category of ‘cancer’ as top category and failed to yield a single gene associated with cancer (data not shown), further supporting the idea that HOC genes may promote the development of CLL. Thus, combined methylation and gene expression analysis identified genes likely regulated by Dnmt3a maintenance

methylation activity that have strong association to cancer and may contain oncogenic drivers of CLL.

A

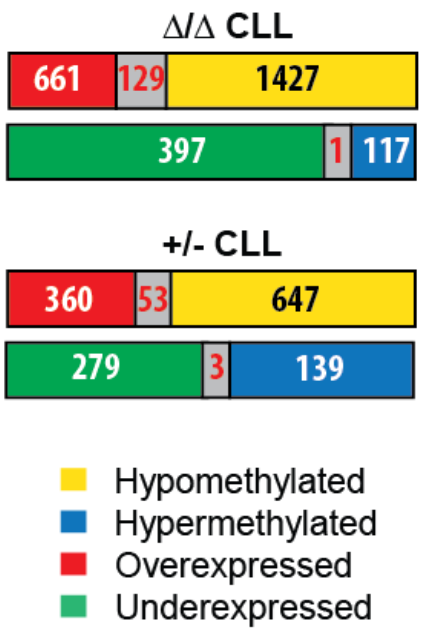

B

Gene	B1 % Meth	+/Δ % Meth	Δ/Δ % Meth	B1 vs +/Δ	B1 vs Δ/Δ
1810046K07Rik	79	4	16	2.3	2.9
Arid3b	80	16	28	2.0	2.2
Cd300ld	88	22	11	15.5	18.3
Cd80	76	14	17	4.0	2.8
Cyth4	87	13	14	2.5	3.3
* Dbi	49	1	2	3.3	2.7
Fgd2	81	20	16	2.2	3.3
Gas7	71	4	17	10.0	13.1
* Hepacam2	77	5	13	7.4	4.8
Ift27	92	18	28	2.4	2.3
Il5rα	82	8	12	4.4	4.0
Krt222	85	26	12	4.2	2.1
Mgmt	95	27	8	4.7	4.5
* Nfam1	85	7	12	5.6	6.5
Nrp2	79	7	10	6.2	3.1
* Pdcd1lg2	87	5	17	4.1	4.7
Plscr1	77	18	12	2.1	4.4
Pon3	81	12	18	4.0	4.0
* Ppil1	61	2	9	2.5	2.8
* Pstpip2	85	6	7	2.0	2.7
Pvt1	80	14	13	3.8	2.9
* Rassf4	76	8	17	3.3	4.6
Sgk3	69	11	16	2.2	2.2
* Slc7a7	80	9	20	2.2	2.3
Ypel2	50	2	5	4.4	2.3
* Zbtb32	59	2	10	11.1	22.2

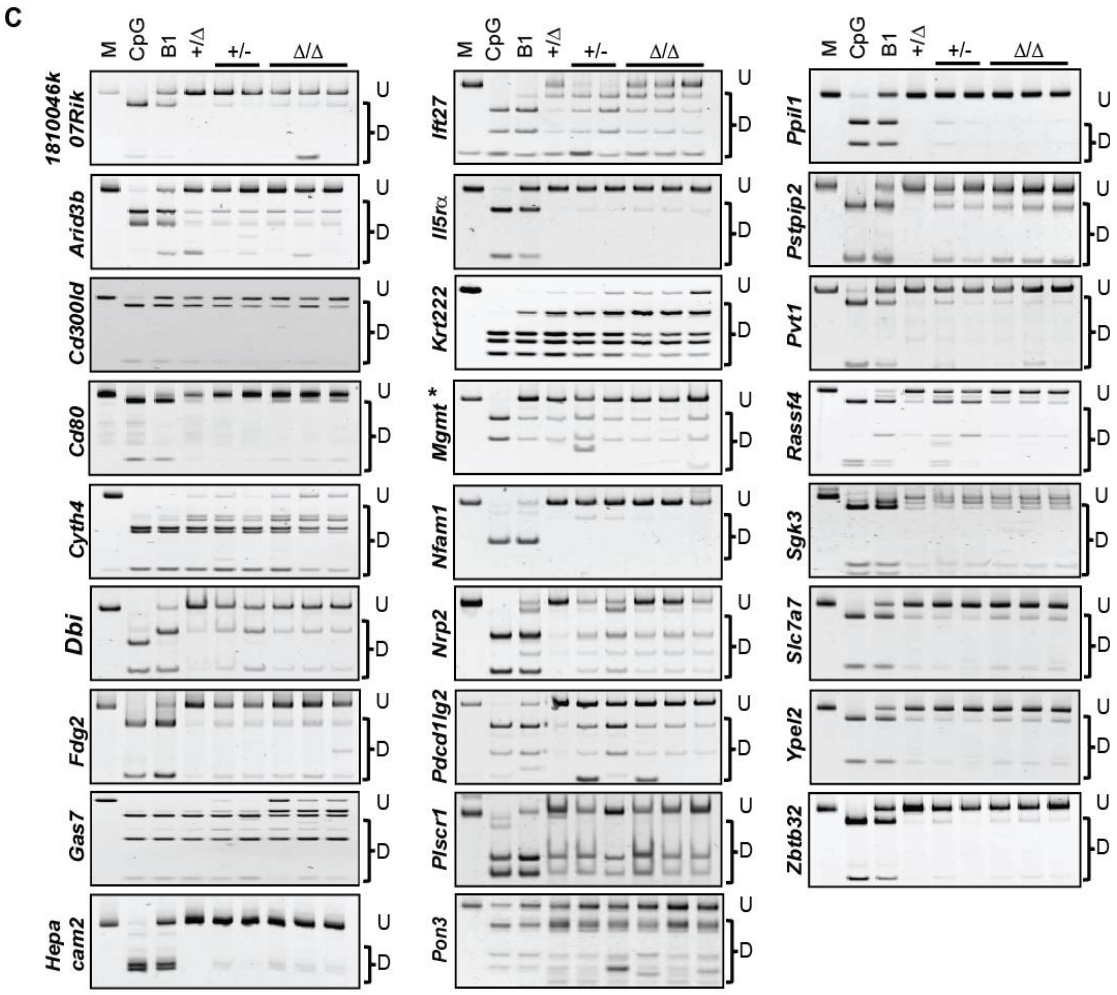

Figure 7. Genes commonly hypomethylated and overexpressed in Dnmt3a$^{+/-}$ and Dnmt3a$^{\Delta/\Delta}$ CLL (HOC) are putative drivers of CLL. A. The number of genes differentially expressed and differentially methylated at the promoter region in Dnmt3a$^{\Delta/\Delta}$ CLL and Dnmt3a$^{+/-}$ CLL. The number of genes with corresponding methylation and expression changes are shown in the grey boxes. **B.** Promoter methylation for HOC genes in B-1a, Dnmt3a$^{+/\Delta}$ CLL**,** and Dnmt3a$^{\Delta/\Delta}$ CLL is shown within boxes. Similarly, fold differences in gene expression between Dnmt3a$^{+/\Delta}$ CLL relative to B-1a and Dnmt3a$^{\Delta/\Delta}$ CLL relative to B-1a is shown. (*) denotes genes overexpressed in human CLL. **C.** COBRA analysis of 26 HOC gene promoters in Dnmt3a$^{+/\Delta}$ CLL (+/Δ), Dnmt3a$^{+/-}$ CLL (+/-) and Dnmt3a$^{\Delta/\Delta}$ CLL (Δ/Δ) samples. Undigested (U) and digested (D) fragments correspond to unmethylated and methylated DNA, respectively. CpG and M indicates a fully methylated control and undigested PCR fragments, respectively. (*) denotes unconfirmed target.

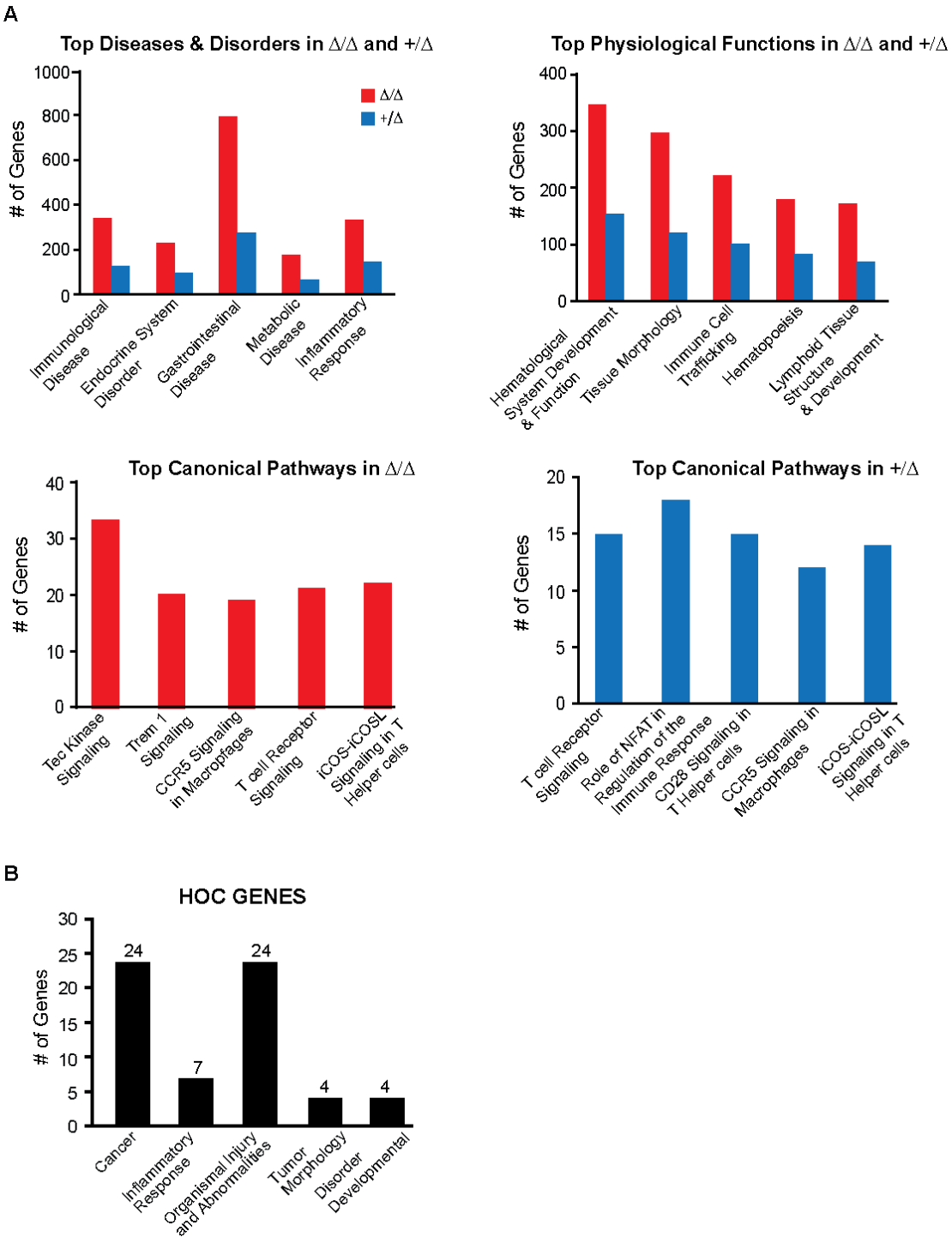

Figure S4. Related to Figures 6 and 7. Ingenuity pathway analysis of differentially expressed genes. A. IPA analysis of genes differentially expressed between Dnmt3a$^{\Delta/\Delta}$ CLL and Dnmt3a$^{+/\square}$ CLL when compared to B-1a cells. Most significant categories and are shown (P<0.05). **B.** IPA analysis of HOC genes. Most significant categories under disease and disorders are shown with a number of genes indicated on the top of the individual bars.

Discussion

Identification of Dnmt3a's molecular targets and understanding how they regulate cellular functions will enrich our understanding of the pathogenesis of human blood cancers given the broad scope of hematologic malignancies in which the function of Dnmt3a is altered. Mouse models represent an invaluable tool in such efforts as they allow us to evaluate the phenotypic and molecular consequences of changes in levels of Dnmt3a in normal and malignant hematopoiesis. Through functional studies in mice, we have previously expanded the known disease spectrum in which Dnmt3a plays a role, as we showed that complete inactivation of Dnmt3a in cells of the hematopoietic system resulted in the development of a CLL-like disease: a malignancy of B cell origin that in humans is not known to harbor genetic alterations of DNMT3A locus. Rather, decreased levels of DNMT3A are a common feature of CLL (34, 63) and wide-spread promoter and gene-body hypomethylation is characteristic of the CLL methylome in humans (64). Similarly, in *Eμ-TCL1* mice Dnmt3a levels are both decreased and inhibited in early stages of CLL development, suggesting a role for Dnmt3a in tumor initiation (65, 149).

In this study, we asked whether a more physiologically relevant setting – a decrease in Dnmt3a, rather than complete deficiency – can drive the development of hematologic malignancies. By analysis of *Dnmt3a*$^{+/-}$ mice, we identified Dnmt3a as a haploinsufficient tumor suppressor gene in the prevention of CLL and MPD. The overall penetrance of disease in Dnmt3a heterozygotes (80%) might be even greater, as the 16 month old healthy *Dnmt3a*$^{+/-}$ mice could have developed disease at a later time. We further demonstrate that *Dnmt3a*$^{+/-}$ CLL cells are fully transformed and capable of inducing disease in wild-type recipient mice, whereas MPD cells fail to engraft in recipients, and appear to represent an expanded population of non-tumorigenic cells.

To gain insight into the pathogenesis of CLL in mice with decreased or completely absent Dnmt3a protein, we analyzed high resolution methylomes and transcriptomes of normal splenic B-1a cells, *Dnmt3a*$^{+/\Delta}$ (or *Dnmt3a*$^{+/-}$), and *Dnmt3a*$^{\Delta/\Delta}$ CLL cells. These analyses resulted in several interesting observations. First, the methylome of normal B-1a cells consisted largely of hypermethylated promoters, most of which were associated with transcriptional repression. This observation could explain why only B-1a cells become fully transformed in Dnmt3a$^{\Delta/\Delta}$ or *Dnmt3a*$^{+/-}$ mice despite the decrease in Dnmt3a levels in all hematopoietic cells. We speculate that B-1a cells have a particularly high base-line level of DNA methylation relative to other normal hematopoietic cells, which is supported by our findings that 60% of promoters are hypermethylated in B-1a cells, as well as our unpublished data showing that normal B-1a cells have higher levels of promoter methylation than normal CD8+ T cells. Thus, the degree of deregulated molecular changes in B-1a cells, in particular, overexpression induced by loss of promoter methylation, upon decrease in Dnmt3a levels can be greater than in other hematopoietic cells, thereby increasing the chance of cellular transformation. Unlike other terminally differentiated hematopoietic cells, B-1a cells are believed to maintain their population through self-renewal. These added cell divisions further increase the chances for the accumulation of epi-mutations over time. This idea is supported by the recently identified maintenance methylation activity for Dnmt3a (14) and findings that all active DNA methyltransferases seem to have cancer-specific maintenance functions (12, 13, 33). Further studies focusing on molecular changes in other B cell subtypes need to be performed to clarify this point.

Second, we observe that promoter methylation appears to be more dependent on high Dnmt3a expression levels than other parts of the genome. Loss of one allele of Dnmt3a induced hypomethylation of 699 2kb-long promoters (-1500 bp to +500 bp

relative to the TSS) in *Dnmt3a*$^{+/\Delta}$ CLL. The number of hypomethylated promoters was increased only 2.2 fold in *Dnmt3a*$^{\Delta/\Delta}$ CLL relative to *Dnmt3a*$^{+/\Delta}$ CLL. In contrast, hypomethylation of CpGs distributed across the genome, gene bodies and repetitive elements was much more pronounced in *Dnmt3a*$^{\Delta/\Delta}$ CLL (3.5-5 fold) relative to *Dnmt3a*$^{+/\Delta}$ CLL. Such data suggest that a select number of promoters are particularly sensitive to Dnmt3a levels and that the complete absence of Dnmt3a is not necessary for hypomethylation to occur at these loci.

Lastly, the number of hypomethylated promoters was 4.9 and 13.2 fold greater than the number of hypermethylated promoters seen in *Dnmt3a*$^{+/\Delta}$ and *Dnmt3a*$^{\Delta/\Delta}$ CLL, respectively. Promoter hypermethylation was somewhat suppressed in *Dnmt3a*$^{\Delta/\Delta}$ CLL, suggesting that Dnmt3a might have tumor specific *de novo* activity. Interestingly, although 3% of hypermethylated promoters were associated with gene down-regulation, these events were not shared in *Dnmt3a*$^{+/\Delta}$ and *Dnmt3a*$^{\Delta/\Delta}$ CLL, suggesting that promoter hypermethylation either contributes to their pathogenesis differently or it does not play a significant role. Unlike hypermethylation, promoter hypomethylation was highly conserved between methylomes of *Dnmt3a*$^{+/\Delta}$ CLL and *Dnmt3a*$^{\Delta/\Delta}$ CLL (60% overlap) and the effects on gene expression were broader, as 10% of hypomethylated promoters were associated with overexpression. These data demonstrate that loss of Dnmt3a in CLL results in genome-wide deregulation of DNA methylation and this is primarily due to hypomethylation.

Based on three simple points - Dnmt3a is a DNA methyltransferase, promoter methylation is associated with gene repression, and loss of one Dnmt3a allele is sufficient to induce CLL - we speculated that genes hypomethylated and overexpressed in both mouse *Dnmt3a*$^{+/-}$ and *Dnmt3a*$^{\Delta/\Delta}$ CLL likely represent oncogenic drivers. Using

statistical approaches, we identified a signature of 26 genes commonly hypomethylated and overexpressed in both mouse *Dnmt3a*$^{+/-}$ and *Dnmt3a*$^{\Delta/\Delta}$ CLL (HOC genes).

The hypomethylation of HOC gene promoters in *Dnmt3a*$^{+/-}$ and *Dnmt3a*$^{\Delta/\Delta}$ CLL could be linked to Dnmt3a inactivation in normal cells either due to lack of Dnmt3a's *de novo* or maintenance activity during normal development of B-1a cells. However, we found that HOC gene promoters are hypermethylated in both normal *Dnmt3a*$^{+/+}$ and *Dnmt3a*$^{+/-}$ B-1a cells, suggesting that loss of one allele of Dnmt3a does not affect the methylation status of promoters in normal B-1a cells. Lack of promoter methylation could also result from increased proliferation of tumor cells without a direct link to Dnmt3a. However, analysis of promoter methylation of several HOC genes revealed while these promoters are hypomethylated in *Dnmt3a*$^{+/-}$ and *Dnmt3a*$^{\Delta/\Delta}$ CLL, they remain hypermethylated in *IRF4*$^{-/-}$*;Vh11* CLL. Such results strongly suggest that the lack of Dnmt3a maintenance methylation activity, rather than proliferation of tumor cells, is responsible for the promoter hypomethylation in HOC genes.

Interestingly, IPA using expression data for the HOC signature placed 24 genes into the category of "cancer". A closer examination of this signature revealed a number of genes with potential to transform cells, including those of hematopoietic origin. For example, *Zbtb32* belongs to a list of genes whose increased expression was recently identified to have positive-predictive value in determining whether patients will develop CLL later in life (150). *Gas7*, a growth arrest–specific gene is overexpressed in hairy cell leukemia, a slow growing malignancy thought to, like CLL, arise from memory B cells (151). *PVT1* gene locus encodes a long non-coding RNA and several microRNA's with predicted oncogenic functions, as it is a target of tumorigenic translocations and retroviral insertions, and its overexpression correlates with upregulation of *MYC*. Specifically, *PVT1* encodes miR-1206 and miR-1204. The former, miR-1206, is

upregulated in tumors of B cell origin such as Burkitt's lymphomas in humans and plasmacytomas in mice (152-154). In mice, miR-1204 is overexpressed in retrovirally induced T cell lymphomas (152). PDCD1LG2 (PD-L2) is aberrantly upregulated in a significant number of patients with AML (155). We also found that several HOC genes were reported to be overexpressed in the *Eμ-TCl1* mouse model as well as other mouse models of CLL. *Slc7a7*, *Pstpip2*, *Pon3*, *Il5ra* and the uncharacterized gene *1810046K07Rik* (C11orf53) are among the Top 25 overexpressed genes in the *Eμ-TCL1* mouse model of CLL (148). *Slc7a7*, *Arid3b* and *Ppil1* are overexpressed in CLL/B cell malignancies that develop in *Eμ-miR-17~92* transgenic mice overexpressing *miR-17~92* polycistronic microRNA (156). Some of these genes or their close relatives show putative oncogenic functions. For example, human PON3 is markedly overexpressed in a variety of human neoplasias and has antiapoptotic function (157). The role of another HOC gene, SLC7A7, is poorly understood but its relative SLC7A5 (LAT1) is associated with high proliferation and poor prognosis in newly diagnosed patients with multiple myeloma – a B cell malignancy (158). Altogether, these data strongly suggest that HOC signature contains oncogenic drivers of CLL that contribute to the transformation of B-1a cells. However, the genes that are oncogenic drivers of CLL do not necessarily need to be limited to only hypomethylated and overexpressed genes. Indeed, other cancer-associated genes are found in gene expression profiles obtained from *Dnmt3a*$^{+/-}$ and *Dnmt3a*$^{\Delta/\Delta}$ CLL. Whatever the case, at a minimum, the HOC signature represents genes likely regulated by Dnmt3a-dependent methylation, providing an opportunity to study the nature of deregulated methylation during disease development and progression. Future functional studies will dissect the potential contribution of these genes to the development of CLL.

DISCUSSION

While Chapters 1-4 represent independent lines of investigation, their results address several fundamental questions posed by the DNA methylation field.

First, we have challenged the canonical *de novo* and maintenance classification for individual Dnmts, while identifying putative targets of Dnmt1 and Dnmt3a. In Chapter 1, our data indicate that even incomplete inactivation of Dnmt1 has a profound effect on the methylation and expression landscape of MTCLs. Using global methylation analysis, we compared the methylation patterns of normal thymocytes, *MYC*;*Dnmt1*$^{flox/flox}$ lymphomas, and *MYC*;*Dnmt1*$^{-/-}$ lymphomas, to identify a subset of 427 putative targets of Dnmt1s *de novo* and maintenance methylation activity. We found 214 gene promoters that are hypomethylation in normal thymocytes and *MYC*; *Dnmt1*$^{-/-}$ lymphomas but hypermethylated in *MYC*; *Dnmt1*$^{flox/flox}$ tumors, indicating that they are likely targets of Dnmt1's cancer-specific *de novo* activity. The remaining putative targets were methylated in normal thymocytes and *MYC*; *Dnmt1*$^{flox/flox}$ lymphomas but hypomethylated in *MYC*; *Dnmt1*$^{-/-}$ lymphomas, suggesting that Dnmt1 is involved in the cancer-specific maintenance methylation of these promoters. Furthermore, comparison of Dnmt1's target genes to those identified in previous studies for Dnmt3b, found very little overlap (3%) in the targets of Dnmt1 and Dnmt3b (13). Similarly, *de novo* methylation of the *H2-Ab1* promoter by Dnmt1 is independent of both Dnmt3a and Dnmt3b, as the *H2-Ab1* promoter is heavily methylated in Dnmt3a and Dnmt3b-deficient lymphomas. The independent targets of Dnmt1 and Dnmt3b are perhaps not surprising given the striking differences in *MYC*;*Dnmt1*$^{-/-}$ and *MYC*;*Dnmt3b*$^{-/-}$ mice, as loss Dnmt3b was found to accelerate tumorigenesis, while loss of Dnmt1 delayed tumorigenesis. Another important finding from these studies is that Dnmt1 appears to have tissue-specific targets. Comparison of promoters hypomethylated in Dnmt1-deficient MTCL to

those identified in Dnmt1-deficient HCT116 colon cancer cell line (88), found very little overlap (2%) in Dnmt1 target genes. This indicates that Dnmt1's role in the establishment and maintenance of methylation patterns is likely cell-type specificity. The tissue specific activity of Dnmt1 is consistent with reports for Dnmt3a, which was found to have unique targets in myeloid versus T-cells (37).

In Chapter 2, using global approaches we analyzed the methylation status of promoters in normal thymocytes, Dnmt3a-deficient thymocytes, and *MYC;Dnmt3a*$^{\Delta/\Delta}$ lymphomas. Out of the 370 promoters hypomethylated in *MYC;Dnmt3a*$^{\Delta/\Delta}$ lymphomas, 353 were also hypomethylated when compared with either normal or *Dnmt3a*$^{\Delta/\Delta}$ thymocytes, implying that Dnmt3a is dispensable for their *de novo* methylation during normal development, but may have a role in the cancer specific maintenance methylation of these loci. In contrast, 17 promoters were specifically hypermethylated in *MYC;Dnmt3a*$^{F/F}$ tumors relative to normal thymocytes, suggesting that they may represent potential targets of Dnmt3a cancer-specific *de novo* methylation. Lastly, 10 promoters were hypomethylated in normal *Dnmt3a* $^{\Delta/\Delta}$ thymocytes, likely due to lack of *de novo* or maintenance activity by Dnmt3a during normal development and thus their hypomethylation in *MYC;Dnmt3a*$^{\Delta/\Delta}$ lymphomas is not tumor-specific. Out of 370 promoters hypomethylated in *MYC;Dnmt3a*$^{\Delta/\Delta}$ lymphomas, only 11 genes were hypomethylated in Dnmt3b-deficient lymphomas. These data indicate that Dnmt3a has distinct targets in MTCL. Collectively, these data show that Dnmt3a contributes to the *de novo* and maintenance methylation of tumor-specific methylation patterns in MTCL.

In Chapter 4 we show that loss of Dnmt3a in HSCs results in the development of CLL in mice which is characterized by genome wide hypomethylation. Furthermore, we show that Dnmt3a is responsible for the cancer-specific maintenance methylation of a subset of 26 genes termed HOC. These genes were specifically hypomethylated in

Dnmt3a$^{\Delta/\Delta}$ and *Dnmt3a*$^{+/-}$ tumors, but were hypermethylated in normal B-1a cells, *Dnmt3a*$^{+/-}$ B-1a cells, and *IRF4*$^{-/-}$*;Vh11* CLL samples. This suggests that Dnmt3a is responsible for the maintenance methylation of these genes in CLL. Furthermore, the 26 HOC genes were not hypomethylated in a Dnmt3a-deficient model of peripheral T cell lymphoma, indicating that HOC genes likely represent B cell specific targets of Dnmt3a. Importantly, the hypomethylation and subsequent over expression of HOC genes may contribute to leukemogenesis in mice, as discussed later on.

Collectively, our data provides a list of putative Dnmt1 and Dnmt3a target genes in T and B cell malignancies. The contribution of Dnmt1 and Dnmt3a to the tumor-specific methylation patterns consists of both *de novo* and maintenance activities. Furthermore, the activity of Dnmts to the establishment and maintenance of normal methylation patterns are likely non-overlapping and cell type specific.

Second, we show that **Dnmt3a can function as both an oncogene and a tumor suppressor in different mouse models.** In Chapter 2 we show that loss of Dnmt3a in MTCL slows tumor cell proliferation and extends the survival of mice. This result is in contrast to our more recent findings that mono- or bi-allelic loss of Dnmt3a induces CLL in mice. We speculate that the opposing roles of Dnmt3a as an oncogene and tumor suppressor stem from Dnmt3a's methylation-independent and methylation-dependent repressor activities, respectively. This is supported by the fact that loss of Dnmt3a in MTCL results in the upregulation of 17 genes whose actions are predicted to suppress lymphomagenesis. Importantly, analysis of MSCC data showed no changes in the promoter methylation of these 17 genes, suggesting they may be regulated through Dnmt3a's methylation independent function. These genes have been implicated as tumor suppressor in several relevant settings, including spontaneous B- and T-cell lymphomagenesis (*Brca2*, *Dna2*, *Exo1*, *Prdm2*, *Smurf2* and *Ssbp2* (99, 114-117)), p53-

deficient or oncogene-provoked lymphomagenesis (*Bcl2l11*, *E2f1*, *Xrcc2*, *Recql4* and *Tyk2* (118-122)), including MTCL (*Pten*, *E2f2 and Dnmt3b* (13, 87, 123)), or other aspects of lymphomagenesis (*Nqo1*, *Irf1 and Irf8 (124-126))*. Whether upregulation of any of these genes play a causative role in the delayed lymphomagenesis observed in *MYC;Dnmt3a*$^{\Delta/\Delta}$ mice remains to be seen; however, individual inactivation of E2f2, Dnmt3b and Pten accelerated MTCL in mice (13, 87, 123). The methylation independent repressor activity is further supported by evidence that both wild-type and catalytically dead Dnmt3a protein can inhibit the expression of Dnmt3b in MTCL cell lines. The inhibition of Dnmt3b is likely partially responsible for the delayed lymphomagenesis in Dnmt3a-deficient lymphomas, as concomitant deletion of Dnmt3b accelerated disease development in DKO mice, further illustrating Dnmt3b's role as a tumor suppressor. While we do not yet know how Dnmt3a inhibits Dnmt3b expression, we speculate that Dnmt3a may recruit repressor proteins to the Dnmt3b locus to block gene transcription. Alternatively, Dnmt3a may inhibit transcription factor binding to the Dnmt3b promoter. The exact mechanism by which catalytically dead Dnmt3a inhibits Dnmt3b's expression remains to be determined.

Third, we show that **Dnmt3a functions as a tumor suppressor gene in the prevention of B-cell transformation.** Loss of Dnmt3a in the hematopoietic compartment results in the development of CLL around 1 year of age with 100% penetrance. Furthermore, leukemogenesis can be accelerated by concomitant deletion of Dnmt3b, further illustrating its tumor suppressor properties**.** In Chapter 4 we show that Dnmt3a is a haplo-insufficient tumor suppressor, as loss of a single allele is sufficient to induce CLL and MPD in mice by 16 months of age. The study presented in Chapter 4 is perhaps more physiologically relevant to human disease, as Dnmt3a activity is likely reduced but not entirely eliminated in human tumors. In patients, mutations in Dnmt3a

are commonly observed in myeloid and T-cell malignancies (138). Interestingly, we only observed the development of MPD in 15% of *Dnmt3a*$^{+/-}$ mice, and never in the *Dnmt3a*$^{-/-}$ mice, despite the fact we have conditionally deleted Dnmt3a in all hematopoietic lineages and that DNMT3A mutations present at high frequency in the myeloid compartment (39). In addition, the myeloid derived tumors that developed in *Dnmt3a*$^{+/-}$ mice could not be serially transplanted into wild-type recipients, suggesting that these cells do not contain leukemia initiating potential. It is possible that the preferential presence of Dnmt3a mutations in human AML may reflect a necessity for tight collaboration with commonly co-mutated genes, such as *NPM1*, *FLT3* and *IDH1* (136). Alternatively, mutations observed in human AML may have gain of function activity, and not loss of function. In addition, we have observed the development of T-cell lymphomas in both *Dnmt3a*$^{\Delta/\Delta}$ and *Dnmt3a*$^{+/-}$ mice, albeit at a lower frequency than CLL (data not shown). This result is consistent with human T-cell lymphomas in which DNMT3A is mutated at a frequency of ~11% (42) and indicate that Dnmt3a is critical for the prevention of T cell transformation.

In studies performed by Mayle et al., and Celik et al., it was reported that Dnmt3a loss in the hematopoietic compartment results in the development of primarily myeloid malignancies, followed by T cell malignancies, and lastly by B cell malignancies which occur infrequently (36, 37). There are several reasons for the differences in disease spectrum observed in our Dnmt3a-deficient mice. First, the Dnmt3a phenotypes may be strain specific, as they use mice on a C57BL/6 background, while we use FVB/N. Second, differences may stem from variations in experimental approaches, such as design of the knockout allele or differences in the strategy which by Dnmt3a is deleted. In our system we use primary *Dnmt3a*$^{-/-}$ mice whereby Cre mediated excision of the Dnmt3a loci occurs very early in hematopoietic development. In their model, HSCs

isolated from *Mx-Cre;Dnmt3a*$^{F/F}$ mice are used for bone marrow adoptive transfer with subsequent pIpC injections to delete Dnmt3a. It is possible that such differences in experimental design could alter disease development in Dnmt3a-deficient mice. Despite differences in our studies, for the first time we provide evidence that Dnmt3a functions as tumor suppressor genes in the prevention of B cell malignancies in mice. This mouse model may serve as a particularly useful tool for studying the contribution of aberrant DNA methylation to CLL pathogenesis.

Despite the lack of observable mutations in DNMT3A and DNMT3B in B cell malignancies, the tumor suppressor function of Dnmt3a and Dnmt3b in the prevention of CLL is supported by several studies. Analysis of available expression data derived from microarray on 448 human CLL samples revealed that Dnmt3a and Dnmt3b are both in the top 1% of underexpressed genes (63). Furthermore, WGBS of the CLL methylome revealed massive genome-wide hypomethylation (64). Such loss of methylation may be attributable to a decrease in Dnmt3a or Dnmt3b maintenance activity in tumors, although such causal link has not been established. One study using the *Eμ-TCL1* CLL mouse model, found that the Tcl1 protein binds to and inhibits Dnmt3a and Dnmt3b activity, resulting in hypomethyation at the early stages of tumorigenesis (65). These studies, along with our own demonstrating that loss of Dnmt3a is sufficient to induce CLL in mice, which is characterized by large-scale genome-wide hypomethylation, suggest that CLL to a large extent may be an epigenetic disease. Further evaluation of the tumor suppressor properties of Dnmt3a and Dnmt3b in the prevention of CLL are needed to fully understand the enzymes role in disease pathogenesis. In particular, functional studies investigating the oncogenic potential of genes hypomethylated and overexpressed in Dnmt3a-deficient CLL will need to be performed.

Lastly, **for the first time using whole genome bisulfite sequencing we provide a high resolution DNA methylome for normal B-1a and CLL cells in mice.** Given the broad scope of hematologic malignancies in which the activity of Dnmt3a is altered, identification of Dnmt3a's molecular targets and understanding how they regulate cellular functions will enhance our understanding of the pathogenesis of human blood cancers. In Chapter 4 we pose the question, can reduction in Dnmt3a levels induce cellular transformation in mice? We show that loss of a single allele of Dnmt3a is sufficient to induce CLL in 65% of mice and MPD in 15% of mice. It is important to note that the lower penetrance of disease may be due to the time frame of our mouse studies and that perhaps the remaining 20% of *Dnmt3a*$^{+/-}$ would have developed disease at a later age. While cells derived from myeloid tumors were incapable of engrafting, we show that CLL cells can induce leukemia following multiple rounds of injection, suggesting they are fully transformed cells. To understand the changes in the molecular landscape of Dnmt3a-deficient tumors we performed WGBS and RNA-seq on normal B-1a cell, *Dnmt3a*$^{+/-}$ CLL and *Dnmt3a*$^{\Delta/\Delta}$ CLL samples.

Analysis of high resolution methylomes and transcriptomes from B-1a cells revealed that the majority of promoters were hypermethylated and repressed. We speculate that B-1a cells may be more sensitive to changes in the activity of Dnmt3a due to their high baseline levels of methylation. In fact, our unpublished data show that B-1a cells have significantly higher levels of methylation than CD8+ T cells. This observation could explain why B-1a cells are preferentially transformed upon loss or decrease in Dnmt3a levels, despite simultaneous inactivation in other hematopoietic lineages. Thus, the degree of deregulated molecular changes in B-1a cells, in particular, overexpression induced by loss of promoter methylation, upon decrease in Dnmt3a levels can be greater than in other hematopoietic cells, thereby increasing the chance of cellular

transformation. Furthermore, unlike other fully differentiated hematopoietic cells, B-1a cells are believed to maintain their population through self-renewal. Perhaps these additional rounds of cell divisions further increase the chances of acquiring epi-mutations with time.

Overall, using WGBS we found that *Dnmt3a*$^{+/-}$ and *Dnmt3a*$^{\Delta/\Delta}$ tumors were characterized by genome wide hypomethylation, with very little hypermethylation observed. Promoters were uniquely sensitive to Dnmt3a levels, as mono-allelic loss of Dnmt3a was sufficient to induce the hypomethylation of 699 promoters in heterozygous mice. While full inactivation of Dnmt3a increased the number of hypomethylated promoters observed, the effect was minimal. These data indicate that a subset of gene promoters are sensitive to changing levels of Dnmt3a, as complete ablation of Dnmt3a is not necessary for hypomethylation to occur at these loci. Unlike hypermethylation, there was a high 60% overlap in promoter hypomethylation between *Dnmt3a*$^{+/\Delta}$ and *Dnmt3a*$^{\Delta/\Delta}$ methylomes. Also, the effects of hypomethylation on gene expression were broader, as 10% of hypomethylated promoters were associated with overexpression, whereas only 2% of hypermethylated promoters were silenced. These results lead us to investigate genes that were hypomethylated and overexpressed in both *Dnmt3a*$^{+/-}$ and *Dnmt3a*$^{\Delta/\Delta}$ CLL (termed HOC genes), with the hypothesis that such genes likely play a role in oncogenesis. We identified 26 genes with hypomethylated DMRS in their promoter region that were also overexpressed in tumors. To gain insight into the biological function of HOC genes we performed Ingenuity Pathways Analysis. Interestingly, 24 out of 26 HOC genes were places in the category of “Cancer”, demonstrating they may play a role in CLL development in Dnmt3a-deficient mice.

In fact, reports from the literature support the oncogenic functions of many HOC genes. For example, overexpression of *Zbtb32* was found to have a positive-predictive

value in determining whether patients will develop CLL later in life (150). The growth arrest–specific gene, *Gas7*, is highly overexpressed in hairy cell leukemia, which like CLL is a slow growing malignancy that arises from memory B cells (151). PDCD1LG2 (PD-L2) is aberrantly upregulated in a significant number of patients with AML (155). Likewise, PON3 is overexpressed in a variety of human neoplasias and has antiapoptotic function (157). *PVT1* gene locus encodes a long non-coding RNA and several microRNA's with predicted oncogenic functions, as it is a target of tumorigenic translocations and retroviral insertions, and its overexpression correlates with upregulation of *MYC*. Specifically, *PVT1* encodes miR-1206 and miR-1204. miR-1206 is upregulated in tumors of B cell origin such as Burkitt's lymphomas in humans and plasmacytomas in mice (152-154). In mice, miR-1204 is overexpressed in retrovirally induced T cell lymphomas (152). In the *Eμ-TCl1* mouse model of CLL, we found that *Slc7a7*, *Pstpip2*, *Pon3*, *Il5ra* and *1810046K07Rik* were reported to be in the top 25 highly overexpressed genes (148). Similarly, *Slc7a7*, *Arid3b* and *Ppil1* are overexpressed in CLL/B cell malignancies that develop in *Eμ-miR-17~92* transgenic mice overexpressing *miR-17~92* polycistronic microRNA (156). Collectively, these reports support the notion that HOC genes contain oncogenic modifiers that contribute to CLL pathogenesis in Dnmt3a-deficient mice. Furthermore, the HOC signature represents genes likely regulated by Dnmt3a-dependent methylation, providing an opportunity to study the nature of deregulated methylation during disease development and progression. Future functional studies will need to be done to address the oncogenic properties of these genes. However, putative oncogenic drivers of CLL do not need to be fully restricted to those that are hypomethylated and overexpressed in tumors. Indeed, IPA analysis of all genes differentially expressed in $Dnmt3a^{+/-}$ and $Dnmt3a^{\Delta/\Delta}$ tumors identified numerous cancer-associated genes that likely contribute to tumorigenesis. Additional work with be needed to fully dissect the potential contribution of these genes

to the development of CLL. Specifically, we could simultaneously overexpress all 26 HOC genes in wild-type hematopoietic stem and progenitor cells that would then be used for adoptive transfer experiments into lethally irradiated FVB/N mice. Recipient mice would then be monitored for signs of hematological disease to determine if HOC genes, either alone or in combination, have transforming potential in any hematopoietic lineage.

Hypomethylation of HOC genes could be attributed to passive demethylation that arose as a results of tumor cell hyper-proliferation. In order to determine if HOC gene hypomethylation was a result of Dnmt3a inactivation in tumors, we analyzed the promoter methylation of HOC genes in two independent mouse models of CLL. Analysis of promoter methylation of several HOC genes revealed while these promoters are hypomethylated in *Dnmt3a*$^{+/-}$ and *Dnmt3a*$^{\Delta/\Delta}$ CLL, they remain hypermethylated in *IRF4*$^{-/-}$*;Vh11* CLL. Interestingly, these promoters were only partially hypomethylated in *Eμ-TCL1* CLL, which is consistent with recent findings that Dnmt3a is partially inhibited by Tcl1. Furthermore, COBRA analysis of normal pre-malignant B-1a cells isolated from *Dnmt3a*$^{+/-}$ mice revealed no changes in promoter methylation of 14 HOC genes, indicating that a lack of maintenance or *de novo* methylation event during development is not responsible for promoter hypomethylation in tumors. These results indicate that lack of Dnmt3a's cancer-specific maintenance function is responsible for the hypomethylation of HOC genes.

Collectively, these studies use relevant in vivo models to provide insight into the activities of Dnmts in cancer. In brief, we have shown that Dnmt1 is critical for T cell development and is required for tumor cell maintenance in MTCL. In addition, we identified putative *de novo* and maintenance targets for Dnmt1. We show that Dnmt3a functions as an oncogene in MTCL, likely through the methylation-independent

repression of several tumor suppressor genes, including Dnmt3b. Lastly, we demonstrate that mono- or bi-allelic loss of Dnmt3a alone is sufficient to induce CLL in mice, suggesting that Dnmt3a has tumor suppressor properties in B cells. Using comprehensive WGBS techniques, we found that the Dnmt3a-deficient CLL methylome is largely hypomethylated, and loss of methylation at promoter regions is associated with the upregulation of a subset of genes normally silenced in B-1a cells. This result is of importance to the CLL field because it provides evidence that epimutations, in particular promoter hypomethylation, likely plays a role in CLL pathogenesis. Altogether, the work presented in this dissertation demonstrate critical roles for Dnmt1 and Dnmt3a in mouse malignant hematopoiesis.

BIBLIOGRAPHY

1. Jones PA, Liang G. Rethinking how DNA methylation patterns are maintained. Nature reviews Genetics. 2009;10(11):805-11.

2. You JS, Jones PA. Cancer genetics and epigenetics: two sides of the same coin? Cancer cell. 2012;22(1):9-20.

3. Yang X, Han H, De Carvalho Daniel D, Lay Fides D, Jones Peter A, Liang G. Gene Body Methylation Can Alter Gene Expression and Is a Therapeutic Target in Cancer. Cancer cell. 2014;26(4):577-90.

4. Li E, Bestor TH, Jaenisch R. Targeted mutation of the DNA methyltransferase gene results in embryonic lethality. Cell. 1992;69(6):915-26.

5. Okano M, Bell DW, Haber DA, Li E. DNA methyltransferases Dnmt3a and Dnmt3b are essential for de novo methylation and mammalian development. Cell. 1999;99(3):247-57.

6. Liang G, Chan MF, Tomigahara Y, Tsai YC, Gonzales FA, Li E, et al. Cooperativity between DNA methyltransferases in the maintenance methylation of repetitive elements. Molecular and cellular biology. 2002;22(2):480-91.

7. Pradhan S, Bacolla A, Wells RD, Roberts RJ. Recombinant human DNA (cytosine-5) methyltransferase. I. Expression, purification, and comparison of de novo and maintenance methylation. The Journal of biological chemistry. 1999;274(46):33002-10.

8. Chuang LS, Ian HI, Koh TW, Ng HH, Xu G, Li BF. Human DNA-(cytosine-5) methyltransferase-PCNA complex as a target for p21WAF1. Science (New York, NY). 1997;277(5334):1996-2000.

9. Feltus FA, Lee EK, Costello JF, Plass C, Vertino PM. Predicting aberrant CpG island methylation. Proceedings of the National Academy of Sciences. 2003;100(21):12253-8.

10. Vertino PM, Yen RW, Gao J, Baylin SB. De novo methylation of CpG island sequences in human fibroblasts overexpressing DNA (cytosine-5-)-methyltransferase. Molecular and cellular biology. 1996;16(8):4555-65.

11. Arand J, Spieler D, Karius T, Branco MR, Meilinger D, Meissner A, et al. In vivo control of CpG and non-CpG DNA methylation by DNA methyltransferases. PLoS genetics. 2012;8(6):e1002750.

12. Haney SL, Hlady RA, Opavska J, Klinkebiel D, Pirruccello SJ, Dutta S, et al. Methylation-independent repression of Dnmt3b contributes to oncogenic activity of Dnmt3a in mouse MYC-induced T-cell lymphomagenesis. Oncogene. 2015;34(43):5436-46.

13. Hlady RA, Novakova S, Opavska J, Klinkebiel D, Peters SL, Bies J, et al. Loss of Dnmt3b function upregulates the tumor modifier Ment and accelerates mouse lymphomagenesis. The Journal of clinical investigation. 2012;122(1):163-77.

14. Jeong M, Sun D, Luo M, Huang Y, Challen GA, Rodriguez B, et al. Large conserved domains of low DNA methylation maintained by Dnmt3a. Nature genetics. 2014;46(1):17-23.

15. Fernandez AF, Huidobro C, Fraga MF. De novo DNA methyltransferases: oncogenes, tumor suppressors, or both? Trends in genetics : TIG. 2012;28(10):474-9.

16. Fuks F, Burgers WA, Godin N, Kasai M, Kouzarides T. Dnmt3a binds deacetylases and is recruited by a sequence-specific repressor to silence transcription. The EMBO journal. 2001;20(10):2536-44.

17. Datta J, Majumder S, Bai S, Ghoshal K, Kutay H, Smith DS, et al. Physical and functional interaction of DNA methyltransferase 3A with Mbd3 and Brg1 in mouse lymphosarcoma cells. Cancer research. 2005;65(23):10891-900.

18. Wang YA, Kamarova Y, Shen KC, Jiang Z, Hahn MJ, Wang Y, et al. DNA methyltransferase-3a interacts with p53 and represses p53-mediated gene expression. Cancer biology & therapy. 2005;4(10):1138-43.

19. Hervouet E, Vallette FM, Cartron PF. Dnmt3/transcription factor interactions as crucial players in targeted DNA methylation. Epigenetics. 2009;4(7):487-99.

20. Herman JG, Civin CI, Issa JP, Collector MI, Sharkis SJ, Baylin SB. Distinct patterns of inactivation of p15INK4B and p16INK4A characterize the major types of hematological malignancies. Cancer research. 1997;57(5):837-41.

21. Roman-Gomez J, Castillejo JA, Jimenez A, Gonzalez MG, Moreno F, Rodriguez Mdel C, et al. 5' CpG island hypermethylation is associated with transcriptional silencing of the p21(CIP1/WAF1/SDI1) gene and confers poor prognosis in acute lymphoblastic leukemia. Blood. 2002;99(7):2291-6.

22. Kantarjian HM, O'Brien S, Huang X, Garcia-Manero G, Ravandi F, Cortes J, et al. Survival advantage with decitabine versus intensive chemotherapy in patients with higher risk myelodysplastic syndrome: comparison with historical experience. Cancer. 2007;109(6):1133-7.

23. Wang Q, Williamson M, Bott S, Brookman-Amissah N, Freeman A, Nariculam J, et al. Hypomethylation of WNT5A, CRIP1 and S100P in prostate cancer. Oncogene. 2007;26(45):6560-5.

24. Pakneshan P, Tetu B, Rabbani SA. Demethylation of urokinase promoter as a prognostic marker in patients with breast carcinoma. Clin Cancer Res. 2004;10(9):3035-41.

25. Pulukuri SM, Estes N, Patel J, Rao JS. Demethylation-linked activation of urokinase plasminogen activator is involved in progression of prostate cancer. Cancer research. 2007;67(3):930-9.

26. Ehrlich M. DNA hypomethylation in cancer cells. Epigenomics. 2009;1(2):239-59.

27. Bestor TH, Tycko B. Creation of genomic methylation patterns. Nature genetics. 1996;12(4):363-7.

28. Howard G, Eiges R, Gaudet F, Jaenisch R, Eden A. Activation and transposition of endogenous retroviral elements in hypomethylation induced tumors in mice. Oncogene. 2008;27(3):404-8.

29. Schulz WA, Elo JP, Florl AR, Pennanen S, Santourlidis S, Engers R, et al. Genomewide DNA hypomethylation is associated with alterations on chromosome 8 in prostate carcinoma. Genes, Chromosomes and Cancer. 2002;35(1):58-65.

30. Wong N, Lam WC, Lai PB, Pang E, Lau WY, Johnson PJ. Hypomethylation of chromosome 1 heterochromatin DNA correlates with q-arm copy gain in human hepatocellular carcinoma. The American journal of pathology. 2001;159(2):465-71.

31. Broske AM, Vockentanz L, Kharazi S, Huska MR, Mancini E, Scheller M, et al. DNA methylation protects hematopoietic stem cell multipotency from myeloerythroid restriction. Nature genetics. 2009;41(11):1207-15.

32. Gaudet F, Hodgson JG, Eden A, Jackson-Grusby L, Dausman J, Gray JW, et al. Induction of tumors in mice by genomic hypomethylation. Science (New York, NY). 2003;300(5618):489-92.

33. Peters SL, Hlady RA, Opavska J, Klinkebiel D, Novakova S, Smith LM, et al. Essential role for Dnmt1 in the prevention and maintenance of MYC-induced T-cell lymphomas. Molecular and cellular biology. 2013;33(21):4321-33.

34. Peters SL, Hlady RA, Opavska J, Klinkebiel D, Pirruccello SJ, Talmon GA, et al. Tumor suppressor functions of Dnmt3a and Dnmt3b in the prevention of malignant mouse lymphopoiesis. Leukemia. 2014;28(5):1138-42.

35. Vasanthakumar A, Lepore JB, Zegarek MH, Kocherginsky M, Singh M, Davis EM, et al. Dnmt3b is a haploinsufficient tumor suppressor gene in Myc-induced lymphomagenesis. Blood. 2013;121(11):2059-63.

36. Celik H, Mallaney C, Kothari A, Ostrander EL, Eultgen E, Martens A, et al. Enforced differentiation of Dnmt3a-null bone marrow leads to failure with c-Kit mutations driving leukemic transformation. Blood. 2015;125(4):619-28.

37. Mayle A, Yang L, Rodriguez B, Zhou T, Chang E, Curry CV, et al. Dnmt3a loss predisposes murine hematopoietic stem cells to malignant transformation. Blood. 2015;125(4):629-38.

38. Ley TJ, Ding L, Walter MJ, McLellan MD, Lamprecht T, Larson DE, et al. DNMT3A mutations in acute myeloid leukemia. The New England journal of medicine. 2010;363(25):2424-33.

39. Walter MJ, Ding L, Shen D, Shao J, Grillot M, McLellan M, et al. Recurrent DNMT3A mutations in patients with myelodysplastic syndromes. Leukemia. 2011;25(7):1153-8.

40. Abdel-Wahab O, Pardanani A, Rampal R, Lasho TL, Levine RL, Tefferi A. DNMT3A mutational analysis in primary myelofibrosis, chronic myelomonocytic leukemia and advanced phases of myeloproliferative neoplasms. Leukemia. 2011;25(7):1219-20.

41. Roller A, Grossmann V, Bacher U, Poetzinger F, Weissmann S, Nadarajah N, et al. Landmark analysis of DNMT3A mutations in hematological malignancies. Leukemia. 2013;27(7):1573-8.

42. Couronne L, Bastard C, Bernard OA. TET2 and DNMT3A mutations in human T-cell lymphoma. The New England journal of medicine. 2012;366(1):95-6.

43. Corces-Zimmerman MR, Hong W-J, Weissman IL, Medeiros BC, Majeti R. Preleukemic mutations in human acute myeloid leukemia affect epigenetic regulators and persist in remission. Proceedings of the National Academy of Sciences. 2014;111(7):2548-53.

44. Shlush LI, Zandi S, Mitchell A, Chen WC, Brandwein JM, Gupta V, et al. Identification of pre-leukaemic haematopoietic stem cells in acute leukaemia. Nature. 2014;506(7488):328-33.

45. Challen GA, Sun D, Jeong M, Luo M, Jelinek J, Berg JS, et al. Dnmt3a is essential for hematopoietic stem cell differentiation. Nature genetics. 2012;44(1):23-31.

46. Yang L, Rau R, Goodell MA. DNMT3A in haematological malignancies. Nature reviews Cancer. 2015;15(3):152-65.

47. Russler-Germain DA, Spencer DH, Young MA, Lamprecht TL, Miller CA, Fulton R, et al. The R882H DNMT3A mutation associated with AML dominantly inhibits wild-type DNMT3A by blocking its ability to form active tetramers. Cancer cell. 2014;25(4):442-54.

48. Xu J, Wang YY, Dai YJ, Zhang W, Zhang WN, Xiong SM, et al. DNMT3A Arg882 mutation drives chronic myelomonocytic leukemia through disturbing gene expression/DNA methylation in hematopoietic cells. Proc Natl Acad Sci U S A. 2014;111(7):2620-5.

49. Qu Y, Lennartsson A, Gaidzik VI, Deneberg S, Karimi M, Bengtzen S, et al. Differential methylation in CN-AML preferentially targets non-CGI regions and is dictated by DNMT3A mutational status and associated with predominant hypomethylation of HOX genes. Epigenetics. 2014;9(8):1108-19.

50. Comprehensive molecular characterization of human colon and rectal cancer. Nature. 2012;487(7407):330-7.

51. Genomic and epigenomic landscapes of adult de novo acute myeloid leukemia. The New England journal of medicine. 2013;368(22):2059-74.

52. Grasso CS, Wu YM, Robinson DR, Cao X, Dhanasekaran SM, Khan AP, et al. The mutational landscape of lethal castration-resistant prostate cancer. Nature. 2012;487(7406):239-43.

53. Kanai Y, Ushijima S, Nakanishi Y, Sakamoto M, Hirohashi S. Mutation of the DNA methyltransferase (DNMT) 1 gene in human colorectal cancers. Cancer letters. 2003;192(1):75-82.

54. Dolnik A, Engelmann JC, Scharfenberger-Schmeer M, Mauch J, Kelkenberg-Schade S, Haldemann B, et al. Commonly altered genomic regions in acute myeloid leukemia are enriched for somatic mutations involved in chromatin remodeling and splicing. Blood. 2012;120(18):e83-e92.

55. Andersson A, Ritz C, Lindgren D, Eden P, Lassen C, Heldrup J, et al. Microarray-based classification of a consecutive series of 121 childhood acute leukemias: prediction of leukemic and genetic subtype as well as of minimal residual disease status. Leukemia. 2007;21(6):1198-203.

56. Ramaswamy S, Tamayo P, Rifkin R, Mukherjee S, Yeang C-H, Angelo M, et al. Multiclass cancer diagnosis using tumor gene expression signatures. Proceedings of the National Academy of Sciences of the United States of America. 2001;98(26):15149-54.

57. Morey Kinney SR, Moser MT, Pascual M, Greally JM, Foster BA, Karpf AR. Opposing Roles of Dnmt1 in Early- and Late-Stage Murine Prostate Cancer. Molecular and cellular biology. 2010;30(17):4159-74.

58. Yamada Y, Jackson-Grusby L, Linhart H, Meissner A, Eden A, Lin H, et al. Opposing effects of DNA hypomethylation on intestinal and liver carcinogenesis. Proceedings of the National Academy of Sciences of the United States of America. 2005;102(38):13580-5.

59. Trowbridge JJ, Sinha AU, Zhu N, Li M, Armstrong SA, Orkin SH. Haploinsufficiency of Dnmt1 impairs leukemia stem cell function through derepression of bivalent chromatin domains. Genes & development. 2012;26(4):344-9.

60. Wijmenga C, Hansen RS, Gimelli G, Bjorck EJ, Davies EG, Valentine D, et al. Genetic variation in ICF syndrome: evidence for genetic heterogeneity. Human mutation. 2000;16(6):509-17.

61. Shen H, Wang L, Spitz MR, Hong WK, Mao L, Wei Q. A novel polymorphism in human cytosine DNA-methyltransferase-3B promoter is associated with an increased risk of lung cancer. Cancer research. 2002;62(17):4992-5.

62. Kn H, Bassal S, Tikellis C, El-Osta A. Expression analysis of the epigenetic methyltransferases and methyl-CpG binding protein families in the normal B-cell and B-cell chronic lymphocytic leukemia (CLL). Cancer biology & therapy. 2004;3(10):989-94.

63. Haferlach T, Kohlmann A, Wieczorek L, Basso G, Kronnie GT, Bene MC, et al. Clinical utility of microarray-based gene expression profiling in the diagnosis and subclassification of leukemia: report from the International Microarray Innovations in

Leukemia Study Group. Journal of clinical oncology : official journal of the American Society of Clinical Oncology. 2010;28(15):2529-37.

64. Kulis M, Heath S, Bibikova M, Queiros AC, Navarro A, Clot G, et al. Epigenomic analysis detects widespread gene-body DNA hypomethylation in chronic lymphocytic leukemia. Nature genetics. 2012;44(11):1236-42.

65. Palamarchuk A, Yan PS, Zanesi N, Wang L, Rodrigues B, Murphy M, et al. Tcl1 protein functions as an inhibitor of de novo DNA methylation in B-cell chronic lymphocytic leukemia (CLL). Proc Natl Acad Sci U S A. 2012;109(7):2555-60.

66. Roll JD, Rivenbark AG, Jones WD, Coleman WB. DNMT3b overexpression contributes to a hypermethylator phenotype in human breast cancer cell lines. Molecular cancer. 2008;7:15.

67. Rhee I, Bachman KE, Park BH, Jair K-W, Yen R-WC, Schuebel KE, et al. DNMT1 and DNMT3b cooperate to silence genes in human cancer cells. Nature. 2002;416(6880):552-6.

68. Poetsch AR, Plass C. Transcriptional regulation by DNA methylation. Cancer treatment reviews. 2011;37 Suppl 1:S8-12.

69. Shenker N, Flanagan JM. Intragenic DNA methylation: implications of this epigenetic mechanism for cancer research. British journal of cancer. 2012;106(2):248-53.

70. Jones PA, Baylin SB. The epigenomics of cancer. Cell. 2007;128(4):683-92.

71. McCabe MT, Brandes JC, Vertino PM. Cancer DNA Methylation: Molecular Mechanisms and Clinical Implications. Clinical cancer research : an official journal of the American Association for Cancer Research. 2009;15(12):3927-37.

72. Portela A, Esteller M. Epigenetic modifications and human disease. Nature biotechnology. 2010;28(10):1057-68.

73. Robertson KD. DNA methylation and human disease. Nature reviews Genetics. 2005;6(8):597-610.

74. Borgel J, Guibert S, Li Y, Chiba H, Schubeler D, Sasaki H, et al. Targets and dynamics of promoter DNA methylation during early mouse development. Nature genetics. 2010;42(12):1093-100.

75. Robert MF, Morin S, Beaulieu N, Gauthier F, Chute IC, Barsalou A, et al. DNMT1 is required to maintain CpG methylation and aberrant gene silencing in human cancer cells. Nature genetics. 2003;33(1):61-5.

76. Fuks F, Burgers WA, Brehm A, Hughes-Davies L, Kouzarides T. DNA methyltransferase Dnmt1 associates with histone deacetylase activity. Nature genetics. 2000;24(1):88-91.

77. Robertson KD, Ait-Si-Ali S, Yokochi T, Wade PA, Jones PL, Wolffe AP. DNMT1 forms a complex with Rb, E2F1 and HDAC1 and represses transcription from E2F-responsive promoters. Nature genetics. 2000;25(3):338-42.

78. Rountree MR, Bachman KE, Baylin SB. DNMT1 binds HDAC2 and a new co-repressor, DMAP1, to form a complex at replication foci. Nature genetics. 2000;25(3):269-77.

79. Mao X, Fujiwara Y, Chapdelaine A, Yang H, Orkin SH. Activation of EGFP expression by Cre-mediated excision in a new ROSA26 reporter mouse strain. Blood. 2001;97(1):324-6.

80. Perl AK, Wert SE, Nagy A, Lobe CG, Whitsett JA. Early restriction of peripheral and proximal cell lineages during formation of the lung. Proc Natl Acad Sci U S A. 2002;99(16):10482-7.

81. Ball MP, Li JB, Gao Y, Lee JH, LeProust EM, Park IH, et al. Targeted and genome-scale strategies reveal gene-body methylation signatures in human cells. Nature biotechnology. 2009;27(4):361-8.

82. Langmead B, Trapnell C, Pop M, Salzberg SL. Ultrafast and memory-efficient alignment of short DNA sequences to the human genome. Genome biology. 2009;10(3):R25.

83. Robinson MD, McCarthy DJ, Smyth GK. edgeR: a Bioconductor package for differential expression analysis of digital gene expression data. Bioinformatics (Oxford, England). 2010;26(1):139-40.

84. Song L, James SR, Kazim L, Karpf AR. Specific method for the determination of genomic DNA methylation by liquid chromatography-electrospray ionization tandem mass spectrometry. Analytical chemistry. 2005;77(2):504-10.

85. Baldi P, Long AD. A Bayesian framework for the analysis of microarray expression data: regularized t -test and statistical inferences of gene changes. Bioinformatics (Oxford, England). 2001;17(6):509-19.

86. Li LC, Dahiya R. MethPrimer: designing primers for methylation PCRs. Bioinformatics (Oxford, England). 2002;18(11):1427-31.

87. Opavsky R, Wang SH, Trikha P, Raval A, Huang Y, Wu YZ, et al. CpG island methylation in a mouse model of lymphoma is driven by the genetic configuration of tumor cells. PLoS genetics. 2007;3(9):1757-69.

88. Rhee I, Jair KW, Yen RW, Lengauer C, Herman JG, Kinzler KW, et al. CpG methylation is maintained in human cancer cells lacking DNMT1. Nature. 2000;404(6781):1003-7.

89. Stables MJ, Shah S, Camon EB, Lovering RC, Newson J, Bystrom J, et al. Transcriptomic analyses of murine resolution-phase macrophages. Blood. 2011;118(26):e192-208.

90. Trowbridge JJ, Snow JW, Kim J, Orkin SH. DNA methyltransferase 1 is essential for and uniquely regulates hematopoietic stem and progenitor cells. Cell stem cell. 2009;5(4):442-9.

91. Laurenti E, Varnum-Finney B, Wilson A, Ferrero I, Blanco-Bose WE, Ehninger A, et al. Hematopoietic stem cell function and survival depend on c-Myc and N-Myc activity. Cell stem cell. 2008;3(6):611-24.

92. Wilson A, Murphy MJ, Oskarsson T, Kaloulis K, Bettess MD, Oser GM, et al. c-Myc controls the balance between hematopoietic stem cell self-renewal and differentiation. Genes & development. 2004;18(22):2747-63.

93. Lee PP, Fitzpatrick DR, Beard C, Jessup HK, Lehar S, Makar KW, et al. A critical role for Dnmt1 and DNA methylation in T cell development, function, and survival. Immunity. 2001;15(5):763-74.

94. Ginsberg AM, Raffeld M, Cossman J. Inactivation of the retinoblastoma gene in human lymphoid neoplasms. Blood. 1991;77(4):833-40.

95. Sherr CJ. Cancer Cell Cycles. Science (New York, NY). 1996;274(5293):1672-7.

96. Iozzo RV, Chakrani F, Perrotti D, McQuillan DJ, Skorski T, Calabretta B, et al. Cooperative action of germ-line mutations in decorin and p53 accelerates lymphoma tumorigenesis. Proceedings of the National Academy of Sciences. 1999;96(6):3092-7.

97. Nepal RM, Zaheen A, Basit W, Li L, Berger SA, Martin A. AID and RAG1 do not contribute to lymphomagenesis in Emu c-myc transgenic mice. Oncogene. 2008;27(34):4752-6.

98. Wang Y, Klumpp S, Amin HM, Liang H, Li J, Estrov Z, et al. SSBP2 is an in vivo tumor suppressor and regulator of LDB1 stability. Oncogene. 2010;29(21):3044-53.

99. Connor F, Bertwistle D, Mee PJ, Ross GM, Swift S, Grigorieva E, et al. Tumorigenesis and a DNA repair defect in mice with a truncating Brca2 mutation. Nature genetics. 1997;17(4):423-30.

100. Martin-Caballero J, Flores JM, Garcia-Palencia P, Serrano M. Tumor susceptibility of p21(Waf1/Cip1)-deficient mice. Cancer research. 2001;61(16):6234-8.

101. Silva FP, Morolli B, Storlazzi CT, Anelli L, Wessels H, Bezrookove V, et al. Identification of RUNX1/AML1 as a classical tumor suppressor gene. Oncogene. 2003;22(4):538-47.

102. Hidaka T, Nakahata S, Hatakeyama K, Hamasaki M, Yamashita K, Kohno T, et al. Down-regulation of TCF8 is involved in the leukemogenesis of adult T-cell leukemia/lymphoma. Blood. 2008;112(2):383-93.

103. Putz G, Rosner A, Nuesslein I, Schmitz N, Buchholz F. AML1 deletion in adult mice causes splenomegaly and lymphomas. Oncogene. 2006;25(6):929-39.

104. Clements EG, Mohammad HP, Leadem BR, Easwaran H, Cai Y, Van Neste L, et al. DNMT1 modulates gene expression without its catalytic activity partially through its interactions with histone-modifying enzymes. Nucleic Acids Research. 2012;40(10):4334-46.

105. Colaneri A, Staffa N, Fargo DC, Gao Y, Wang T, Peddada SD, et al. Expanded methyl-sensitive cut counting reveals hypomethylation as an epigenetic state that highlights functional sequences of the genome. Proceedings of the National Academy of Sciences. 2011;108(23):9715-20.

106. Odejide O, Weigert O, Lane AA, Toscano D, Lunning MA, Kopp N, et al. A targeted mutational landscape of angioimmunoblastic T-cell lymphoma. Blood. 2014;123(9):1293-6.

107. Neumann M, Heesch S, Schlee C, Schwartz S, Gokbuget N, Hoelzer D, et al. Whole-exome sequencing in adult ETP-ALL reveals a high rate of DNMT3A mutations. Blood. 2013;121(23):4749-52.

108. Kim SJ, Zhao H, Hardikar S, Singh AK, Goodell MA, Chen T. A DNMT3A mutation common in AML exhibits dominant-negative effects in murine ES cells. Blood. 2013;122(25):4086-9.

109. Weng AP, Millholland JM, Yashiro-Ohtani Y, Arcangeli ML, Lau A, Wai C, et al. c-Myc is an important direct target of Notch1 in T-cell acute lymphoblastic leukemia/lymphoma. Genes & development. 2006;20(15):2096-109.

110. Thorns C, Bastian B, Pinkel D, Roydasgupta R, Fridlyand J, Merz H, et al. Chromosomal aberrations in angioimmunoblastic T-cell lymphoma and peripheral T-cell lymphoma unspecified: A matrix-based CGH approach. Genes, chromosomes & cancer. 2007;46(1):37-44.

111. Felsher DW, Bishop JM. Reversible tumorigenesis by MYC in hematopoietic lineages. Molecular cell. 1999;4(2):199-207.

112. Robinson MD, Smyth GK. Moderated statistical tests for assessing differences in tag abundance. Bioinformatics (Oxford, England). 2007;23(21):2881-7.

113. Wu H, Coskun V, Tao J, Xie W, Ge W, Yoshikawa K, et al. Dnmt3a-dependent nonpromoter DNA methylation facilitates transcription of neurogenic genes. Science (New York, NY). 2010;329(5990):444-8.

114. Lin W, Sampathi S, Dai H, Liu C, Zhou M, Hu J, et al. Mammalian DNA2 helicase/nuclease cleaves G-quadruplex DNA and is required for telomere integrity. The EMBO journal. 2013;32(10):1425-39.

115. Schaetzlein S, Chahwan R, Avdievich E, Roa S, Wei K, Eoff RL, et al. Mammalian Exo1 encodes both structural and catalytic functions that play distinct roles in essential biological processes. Proceedings of the National Academy of Sciences. 2013;110(27):E2470-E9.

116. Steele-Perkins G, Fang W, Yang XH, Van Gele M, Carling T, Gu J, et al. Tumor formation and inactivation of RIZ1, an Rb-binding member of a nuclear protein-methyltransferase superfamily. Genes & development. 2001;15(17):2250-62.

117. Ramkumar C, Kong Y, Cui H, Hao S, Jones SN, Gerstein RM, et al. Smurf2 regulates the senescence response and suppresses tumorigenesis in mice. Cancer research. 2012;72(11):2714-9.

118. Shang Q, Zhang D, Guo C, Lin Q, Guo Z, Deng C. Potential synergism of Bim with p53 in mice with Mycinduced lymphoma in a mouse lymphoma model. Molecular medicine reports. 2012;5(6):1401-8.

119. Baudino TA, Maclean KH, Brennan J, Parganas E, Yang C, Aslanian A, et al. Myc-mediated proliferation and lymphomagenesis, but not apoptosis, are compromised by E2f1 loss. Molecular cell. 2003;11(4):905-14.

120. Orii KE, Lee Y, Kondo N, McKinnon PJ. Selective utilization of nonhomologous end-joining and homologous recombination DNA repair pathways during nervous system development. Proc Natl Acad Sci U S A. 2006;103(26):10017-22.

121. Mann MB, Hodges CA, Barnes E, Vogel H, Hassold TJ, Luo G. Defective sister-chromatid cohesion, aneuploidy and cancer predisposition in a mouse model of type II Rothmund-Thomson syndrome. Human molecular genetics. 2005;14(6):813-25.

122. Schuster C, Berger A, Hoelzl MA, Putz EM, Frenzel A, Simma O, et al. The cooperating mutation or "second hit" determines the immunologic visibility toward MYC-induced murine lymphomas. Blood. 2011;118(17):4635-45.

123. Opavsky R, Tsai SY, Guimond M, Arora A, Opavska J, Becknell B, et al. Specific tumor suppressor function for E2F2 in Myc-induced T cell lymphomagenesis. Proc Natl Acad Sci U S A. 2007;104(39):15400-5.

124. Iskander K, Barrios RJ, Jaiswal AK. Disruption of NAD(P)H:quinone oxidoreductase 1 gene in mice leads to radiation-induced myeloproliferative disease. Cancer research. 2008;68(19):7915-22.

125. Liu J, Xiang Z, Ma X. Role of IFN regulatory factor-1 and IL-12 in immunological resistance to pathogenesis of N-methyl-N-nitrosourea-induced T lymphoma. Journal of immunology (Baltimore, Md : 1950). 2004;173(2):1184-93.

126. Li H, Kaminski MS, Li Y, Yildiz M, Ouillette P, Jones S, et al. Mutations in linker histone genes HIST1H1 B, C, D, and E; OCT2 (POU2F2); IRF8; and ARID1A underlying the pathogenesis of follicular lymphoma. Blood. 2014;123(10):1487-98.

127. Gao Q, Steine EJ, Barrasa MI, Hockemeyer D, Pawlak M, Fu D, et al. Deletion of the de novo DNA methyltransferase Dnmt3a promotes lung tumor progression. Proc Natl Acad Sci U S A. 2011;108(44):18061-6.

128. Weis B, Schmidt J, Maamar H, Raj A, Lin H, Toth C, et al. Inhibition of intestinal tumor formation by deletion of the DNA methyltransferase 3a. Oncogene. 2015;34(14):1822-30.

129. Puto LA, Reed JC. Daxx represses RelB target promoters via DNA methyltransferase recruitment and DNA hypermethylation. Genes & development. 2008;22(8):998-1010.

130. Li H, Rauch T, Chen ZX, Szabo PE, Riggs AD, Pfeifer GP. The histone methyltransferase SETDB1 and the DNA methyltransferase DNMT3A interact directly and localize to promoters silenced in cancer cells. The Journal of biological chemistry. 2006;281(28):19489-500.

131. Kim MS, Kim YR, Yoo NJ, Lee SH. Mutational analysis of DNMT3A gene in acute leukemias and common solid cancers. APMIS : acta pathologica, microbiologica, et immunologica Scandinavica. 2013;121(2):85-94.

132. Li KK, Luo LF, Shen Y, Xu J, Chen Z, Chen SJ. DNA methyltransferases in hematologic malignancies. Seminars in hematology. 2013;50(1):48-60.

133. Shah MY, Vasanthakumar A, Barnes NY, Figueroa ME, Kamp A, Hendrick C, et al. DNMT3B7, a truncated DNMT3B isoform expressed in human tumors, disrupts embryonic development and accelerates lymphomagenesis. Cancer research. 2010;70(14):5840-50.

134. Nguyen S, Meletis K, Fu D, Jhaveri S, Jaenisch R. Ablation of de novo DNA methyltransferase Dnmt3a in the nervous system leads to neuromuscular defects and shortened lifespan. Developmental dynamics : an official publication of the American Association of Anatomists. 2007;236(6):1663-76.

135. Ji H, Ehrlich LI, Seita J, Murakami P, Doi A, Lindau P, et al. Comprehensive methylome map of lineage commitment from haematopoietic progenitors. Nature. 2010;467(7313):338-42.

136. Ding L, Ley TJ, Larson DE, Miller CA, Koboldt DC, Welch JS, et al. Clonal evolution in relapsed acute myeloid leukaemia revealed by whole-genome sequencing. Nature. 2012;481(7382):506-10.

137. Kaneda M, Okano M, Hata K, Sado T, Tsujimoto N, Li E, et al. Essential role for de novo DNA methyltransferase Dnmt3a in paternal and maternal imprinting. Nature. 2004;429(6994):900-3.

138. Yang L, Rau R, Goodell MA. DNMT3A in haematological malignancies. Nature reviews Cancer. 2015;15(3):152-65.

139. Challen GA, Sun D, Mayle A, Jeong M, Luo M, Rodriguez B, et al. Dnmt3a and Dnmt3b have overlapping and distinct functions in hematopoietic stem cells. Cell stem cell. 2014;15(3):350-64.

140. Chang YI, You X, Kong G, Ranheim EA, Wang J, Du J, et al. Loss of Dnmt3a and endogenous Kras(G12D/+) cooperate to regulate hematopoietic stem and progenitor cell functions in leukemogenesis. Leukemia. 2015;29(9):1847-56.

141. Gao XN, Yan F, Lin J, Gao L, Lu XL, Wei SC, et al. AML1/ETO cooperates with HIF1alpha to promote leukemogenesis through DNMT3a transactivation. Leukemia. 2015;29(8):1730-40.

142. Krueger F, Andrews SR. Bismark: a flexible aligner and methylation caller for Bisulfite-Seq applications. Bioinformatics (Oxford, England). 2011;27(11):1571-2.

143. Assenov Y, Muller F, Lutsik P, Walter J, Lengauer T, Bock C. Comprehensive analysis of DNA methylation data with RnBeads. Nature methods. 2014;11(11):1138-40.

144. Wu H, Xu T, Feng H, Chen L, Li B, Yao B, et al. Detection of differentially methylated regions from whole-genome bisulfite sequencing data without replicates. Nucleic Acids Res. 2015;43(21):e141.

145. Krzywinski M, Schein J, Birol I, Connors J, Gascoyne R, Horsman D, et al. Circos: an information aesthetic for comparative genomics. Genome research. 2009;19(9):1639-45.

146. Hirst M, Marra MA. Next generation sequencing based approaches to epigenomics. Briefings in Functional Genomics. 2010;9(5-6):455-65.

147. Shukla V, Ma S, Hardy RR, Joshi SS, Lu R. A role for IRF4 in the development of CLL. Blood. 2013;122(16):2848-55.

148. Nganga VK, Palmer VL, Naushad H, Kassmeier MD, Anderson DK, Perry GA, et al. Accelerated progression of chronic lymphocytic leukemia in Emu-TCL1 mice expressing catalytically inactive RAG1. Blood. 2013;121(19):3855-66, s1-16.

149. Chen SS, Sherman MH, Hertlein E, Johnson AJ, Teitell MA, Byrd JC, et al. Epigenetic alterations in a murine model for chronic lymphocytic leukemia. Cell cycle (Georgetown, Tex). 2009;8(22):3663-7.

150. Chadeau-Hyam M, Vermeulen RC, Hebels DG, Castagne R, Campanella G, Portengen L, et al. Prediagnostic transcriptomic markers of Chronic lymphocytic leukemia reveal perturbations 10 years before diagnosis. Annals of oncology : official journal of the European Society for Medical Oncology / ESMO. 2014;25(5):1065-72.

151. Dunphy CH. Gene expression profiling data in lymphoma and leukemia: review of the literature and extrapolation of pertinent clinical applications. Archives of pathology & laboratory medicine. 2006;130(4):483-520.

152. Beck-Engeser GB, Lum AM, Huppi K, Caplen NJ, Wang BB, Wabl M. Pvt1-encoded microRNAs in oncogenesis. Retrovirology. 2008;5:4.

153. Guan Y, Kuo WL, Stilwell JL, Takano H, Lapuk AV, Fridlyand J, et al. Amplification of PVT1 contributes to the pathophysiology of ovarian and breast cancer. Clin Cancer Res. 2007;13(19):5745-55.

154. Huppi K, Volfovsky N, Runfola T, Jones TL, Mackiewicz M, Martin SE, et al. The identification of microRNAs in a genomically unstable region of human chromosome 8q24. Molecular cancer research : MCR. 2008;6(2):212-21.

155. Yang H, Bueso-Ramos C, DiNardo C, Estecio MR, Davanlou M, Geng QR, et al. Expression of PD-L1, PD-L2, PD-1 and CTLA4 in myelodysplastic syndromes is enhanced by treatment with hypomethylating agents. Leukemia. 2014;28(6):1280-8.

156. Sandhu SK, Fassan M, Volinia S, Lovat F, Balatti V, Pekarsky Y, et al. B-cell malignancies in microRNA Emu-miR-17~92 transgenic mice. Proc Natl Acad Sci U S A. 2013;110(45):18208-13.

157. Schweikert EM, Devarajan A, Witte I, Wilgenbus P, Amort J, Forstermann U, et al. PON3 is upregulated in cancer tissues and protects against mitochondrial superoxide-mediated cell death. Cell death and differentiation. 2012;19(9):1549-60.

158. Isoda A, Kaira K, Iwashina M, Oriuchi N, Tominaga H, Nagamori S, et al. Expression of L-type amino acid transporter 1 (LAT1) as a prognostic and therapeutic indicator in multiple myeloma. Cancer science. 2014;105(11):1496-502.